UPDATES IN COMPUTATIONAL CIVIL ENGINEERING

IN COMPUTATIONAL
CIVIL ENGINEERING

UPDATES

C. IONESCU, R. SCÎNTEIE

editors

UPDATES
IN COMPUTATIONAL CIVIL ENGINEERING

editors
C. Ionescu, R. Scînteie

Editura Societăţii Academice "Matei - Teiu Botez"
Iaşi   2009

Proceedings of the seventh International Symposium

" Computational Civil Engineering 2009"
Iaşi, Romania, May 22, 2009

THE VII th INTERNATIONAL SYMPOSIUM
"COMPUTATIONAL CIVIL ENGINEERING 2009"

ORGANIZERS

Academic Society "Matei - Teiu Botez"
Academy of Romanian Scientists
Faculty of Civil Engineering and Installations

Co-ordination committee

Prof. Eng. Constantin Ionescu - president
Prof. Eng. Nicolae Ţăranu
Prof. Eng. Horia Alexandru Barbat
Prof. Eng. Mihai Budescu

Scientific commission

Dr. Eng. Rodian Scînteie - co-ordinating
Prof. Eng. Elena Axinte
Prof. Eng. Andrei Radu
Prof. Eng. Maria Urmă
Prof. Eng. Irina Lungu
Prof. Eng. Marinela Bărbuţă
Secretary - Drd. Eng. Cristian Ciobanu

Organizing commission

Dr. Eng. Ionică Modoi - co-ordinating
Drd. Arh. Tudor Grădinaru
Drd. Eng. Gabriela Covatariu
Drd. Eng. Cristian Blejeru
Drd. Eng. Gheorghiţă Boacă
Drd. Eng. Costel Pleşcan
Drd. Eng. Andrei Jantea
Secretary – Eng. Nicoleta Peşehonov

Table of Contents

A probabilistic model for seismic risk assessment of buildings

A. Aguilar [1], L.G. Pujades [2], A. H. Barbat [3] and N. Lantada [4]

[1] Dept. of Geotechnical Engineering and Geosciences, Technical University of Catalonia
Jordi Girona 1-3. Edificio D2. UPC Campus Nord. Barcelona. 08034,
armando.aguilar.melendez@upc.edu

[2] Dept. of Geotechnical Engineering and Geosciences, Technical University of Catalonia
Jordi Girona 1-3. Edificio D2. UPC Campus Nord. Barcelona. 08034,
lluis.pujades@upc.edu

[3] Dept. of Structural Mechanics, Technical University of Catalonia
Jordi Girona 1-3. Edificio C1. UPC Campus Nord. Barcelona. 08034
alex.barbat@upc.edu

[3] Dept. of Geotechnical Engineering and Geosciences, Technical University of Catalonia
Jordi Girona 1-3. Edificio D2. UPC Campus Nord. Barcelona. 08034,
nieves.lantada@upc.edu

Summary

A probabilistic model to estimate seismic risk is presented. The main elements of this model are the seismic hazard, the vulnerability, and the structural response. These elements are evaluated through a probabilistic point of view, in order to compute the seismic risk. In order to illustrate the application of the proposed model a new method, mLM1, is used to estimate the expected physical damage of the buildings located in a block of Barcelona. Most of the buildings in this block are unreinforced masonry buildings. In this new method the vulnerability of each building is modelled through probability density functions that describe the variation of a vulnerability index. The uncertainties related to the data of each building, and the uncertainties associated to the estimation of the vulnerability by means of a simplified method, are considered in the process used to estimate the seismic vulnerability of each building. In order to compute the seismic risk in the mLM1 method, the seismic hazard is obtained through a probabilistic seismic hazard assessment and it is expressed in terms of annual probability of exceedance of an intensity parameter. The seismic risk computed is ex-pressed in terms of annual exceedance rate of damage states.

KEYWORDS: Seismic risk, seismic hazard, seismic vulnerability, annual exceedance rates, seismic damage.

1. INTRODUCTION

The knowledge of the seismic risk in buildings allows to take decisions about the way in which this risk will be faced. In the context of the seismic risk management the possible decisions that can be taken about the seismic risk in buildings are showed in the figure 1.

The results of any study of seismic risk are useful if they contribute to answer questions like the following examples: When will a specific building be damaged by the occurrence of a seismic motion? What will be the magnitude of this seismic damage? What is the probability that a specific seismic damage will occur in a building in the next 50 years? Which is the damage that has a probability of occurrence of 10% in the next 50 years? Which is the damage that has a probability of occurrence of 2% in the next 50 years?
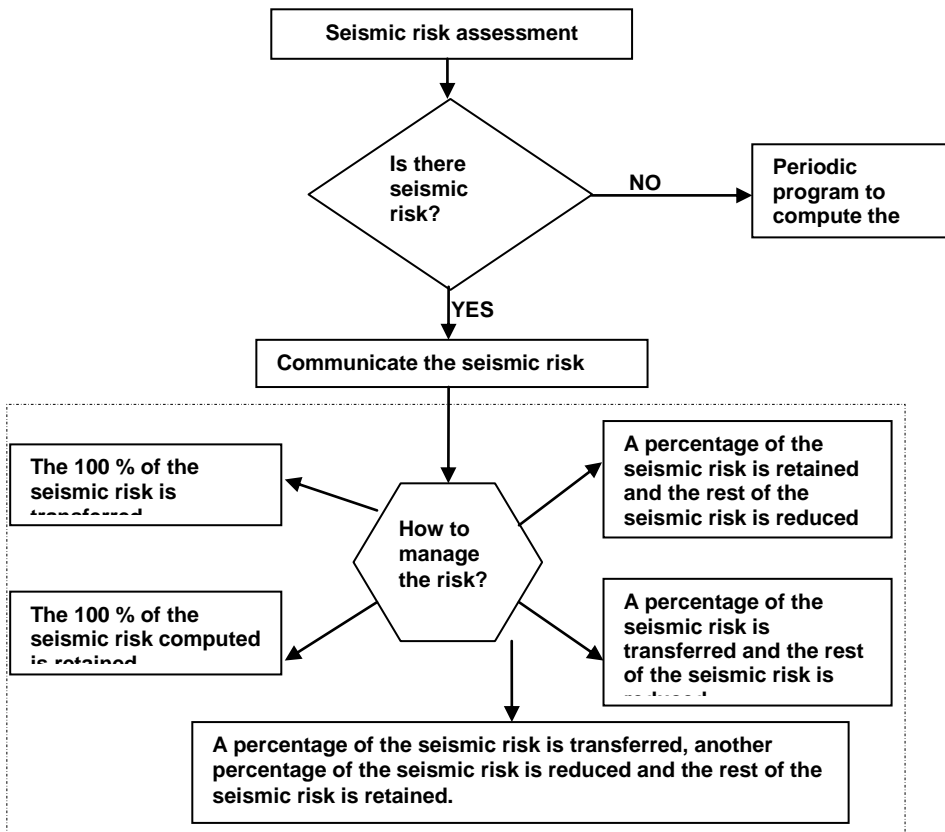
Figure 1. Main steps of the seismic risk management

2. SEISMIC RISK MODEL

The main elements that usually are considered to estimate the seismic risk are the seismic hazard, the seismic vulnerability and the damage functions (McGuire, 2004). These three elements are considered into a probabilistic point of view in the present seismic risk model (figure 2).
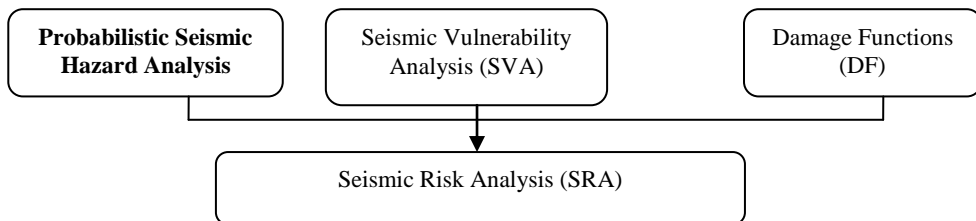
Figure 2. Basic elements of a Seismic Risk Analysis

Conceptually, the present approach is represented by the Eqn. 1.1 which can be used to estimate the annual probability that the earthquake damage D exceeds d, as a function of the seismic vulnerability of the studied building, and the seismic intensity that can affect to the studied building:

$$P[D > d] \simeq \iint P[D > d \mid I, V] \gamma'[I] P[V] dV dI \qquad (1.1)$$

where γ' [I] is the frequency of occurrence of the seismic intensity I, P [V] is the probability of occurrence of the seismic vulnerability V and P [D > d | I, V] is the probability that the earthquake damage D exceeds d for a given seismic intensity I and a given building with vulnerability V. Equation 1.1 applies the total probability theorem, taking into account that the seismic vulnerability V and the seismic intensity I are independent random variables (Aguilar et al., 2008). Two relevant characteristics of this method are that it allows consider the main uncertainties that are present in the elements required to estimate seismic risk and it allows represent inherent uncertainty to the seismic risk results.

The seismic vulnerability is a variable that indicate the probable structural response that a building will have when it will be excited by earthquake motions. Then, estimate the seismic vulnerability is at the same time estimate the probable structural capacity that a building has to resist earthquake motions. There are many procedures to estimate the probable seismic capacity of a building. Each one of these procedures requires different quantity and quality of data about the building and about the environment where the building is located. The data available is one of the several variables that usually are taken into account to decide, which procedure will be used to compute the seismic vulnerability of a building. Other examples of variables usually considered to choose a procedure to estimate seismic

vulnerability are the main objective to estimate the seismic capacity of the studied building, the time available to obtain results and the total resources available to realize the seismic vulnerability study. In any case it is important to recognize that the seismic vulnerability results obtained by any procedure have uncertainties associated. In the present model the vulnerability is considered as a variable with its uncertainty related.

The seismic hazard is other basic element of the present model to compute seismic risk. There are different ways to compute the seismic hazard, but in most of the cases there is coincidence in the important uncertainties associated to the main elements that generate the seismic hazard (Mc-Guire, 2004). In the present model, the seismic hazard estimated through a probabilistic seismic hazard assessment (McGuire, 2004) is expressed in terms of annual probability of exceedance of an intensity parameter.

Given the uncertainties that are present in the seismic vulnerability estimation and in the seismic hazard, there is no doubt that any procedure used to estimate the seismic risk, must capture and represent the probabilistic character of the seismic vulnerability and the seismic hazard.

3. APPLICATION

The model summarized in the expression 1.1 can be used to generate particular methodologies to estimate seismic risk. An example of these methodologies is the modified LM1 (mLM1) method (Aguilar et al., 2008). This new method allows estimate the exceedance rate of physical damage states of buildings. The mLM1 method is essentially a method oriented to the estimation of the seismic risk of buildings in an urban scale.

In order to illustrate the application of the mLM1 method, the annual probability of exceedance of different damage states is computed, for the total number of buildings that exist in a block located in the Eixample district of the city of Barcelona.

3.1. The data

The main sources of the data about the buildings used to compute the seismic risk in this work are: a) The government data and b) The information generated in a study of seismic risk scenarios for the Barcelona City (Barbat et al., 2006; Lantada, 2007)

In the present project the studied block has 10 buildings and it is identified by the code "B1". The figure 3a shows a satellite picture of the block B1 in a plan view

and the figure 3b shows a geometric representation of a plan view of the same block. In the figure 4 two pictures of some of the buildings located in the block B1 are showed.

3.2. The seismic vulnerability analysis

The seismic vulnerability is estimated for each building and it is represented through three vulnerability curves (lower, mean and upper). These curves describe the variation of a vulnerability index in a range between 0 and 1. Values near to zero represent low seismic vulnerability, whereas values near to 1 represent high seismic vulnerability.

The quantity and quality of data available about buildings that can be used to estimate its seismic vulnerability is variable. However, it is desirable that in the method mLM1, during the estimation of the intrinsic vulnerability will be considered at least the following parameters: a) Structural type, b) Plan geometric irregularity, c) Vertical mass irregularity, d) Vertical geometric irregularity, e) Conservation state, f) Year of construction, g) Seismic code, h) Height. The extrinsic vulnerability can be considered in the vulnerability analysis through different parameters like the relative position of the building in the block, and the possible seismic pounding between buildings (Aguilar et al., 2008).

<table>
<tr><td>(a)</td><td>(b)</td></tr>
</table>

Figure. 3 (a) Satellite picture of the block B1 (Google, 2008) and; (b) image of the geometric representation of a plan view of the block B1.

The buildings in the block B1 are classified into some of the building typologies defined in the RISK-UE project (Milutinovic and Trendafiloski, 2003). According with this classification in the block B1 there are only two different structural types: 1) M33 - Masonry structure. Unreinforced masonry bearing walls with composite

steel and masonry slabs; 2) RC32 – Reinforced concrete structure. Concrete frames with unreinforced masonry infill walls. Irregularly frames.
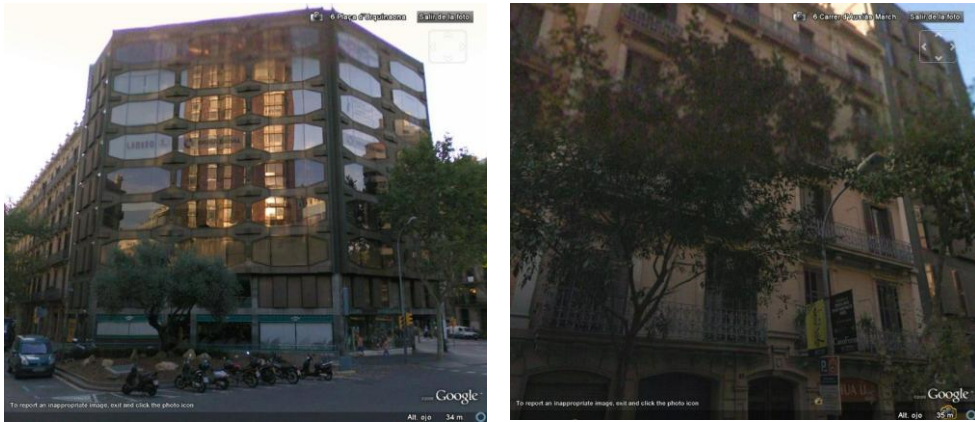
Figure. 4. Pictures of buildings in the block B1 in the Eixample district of the city of Barcelona (Google, 2008).

The quantity and quality of the data related to each building and its environment are also considered when the probability density functions that define to the seismic vulnerability curves are computed.

In order to identify the quality of the data, a confidence value must be estimated for each one of the main data used to compute the seismic vulnerability. This confidence value is a number between 1 and 10. Values near to 1 represent that there is low confidence in the data, whereas values near to 10 are used when there is high confidence in the data. For example, the data used in the present study to estimate the structural type for the buildings in the block B1 of the city of Barcelona, were obtained in most of the cases through a visual field inspection which in sometimes were realized only outside of the buildings. Additionally, these inspections were not part of a specific work to evaluate the structural safety or the seismic vulnerability of each building (Lantada, 2007). For these reasons, a confidence value for the datum of the structural type was estimated.

The uncertainties associated to the seismic vulnerability of each building are due mainly to the quality of the data (a confidence value for each datum), the quantity of the data (number of data available with its respective importance level) and the inherent uncertainty to the use of a simplified method to estimate the seismic vulnerability.

According with the results of this study, the building No. 3 is one of the buildings that have the lower seismic vulnerability in the block B1. The figure 3b shows the location of the building No. 3 in the block B1.

Figure 5 shows the curves that describe the seismic vulnerability of the building No. 3 (figure 3b).These vulnerability curves correspond to beta cumulative probability functions (CDF). The canonical parameters *a* and *b* for each beta cumulative probability function were computed according with the procedure indicated in the mLM1 method (Aguilar et al., 2008).
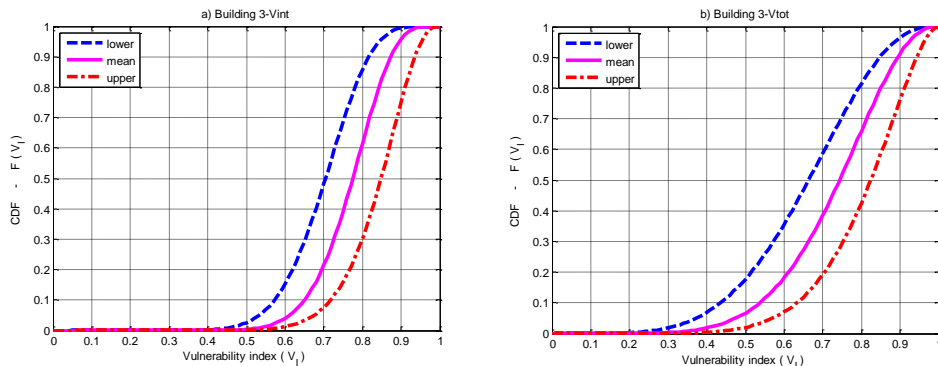
Figure 5. (a) Seismic vulnerability curves obtained considering only the intrinsic vulnerability of the building No. 3; (b) Seismic vulnerability curves obtained considering simultaneously the intrinsic and the extrinsic vulnerability of the building No. 3.

The results also indicate that the building No. 3 has an intrinsic seismic vulnerability (figure 5a) greater than the total seismic vulnerability (figure 5b). The total seismic vulnerability is obtained when the intrinsic vulnerability and the extrinsic vulnerability, are simultaneously considered. According with the results of this work, the building No.8 is one of the buildings that have the higher seismic vulnerability in the block B1. Figure 3b shows the location of the building No. 8 in the block B1. Figure 6 shows the curves that describe the seismic vulnerability of the building No.8.
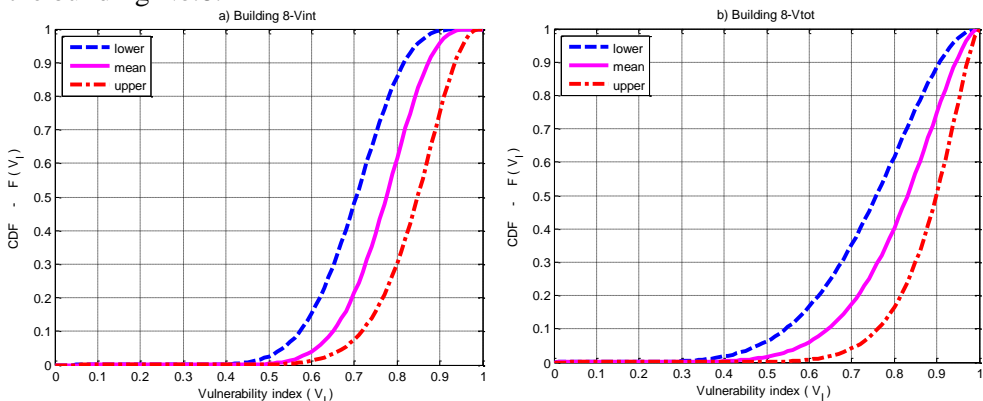
Figure 6. (a) Seismic vulnerability curves obtained considering only the intrinsic vulnerability of the building No. 8; (b) Seismic vulnerability curves obtained considering simultaneously the intrinsic and the extrinsic vulnerability of the building No. 8.

3.3. The seismic hazard

In the method mLM1 the seismic hazard is expressed in terms of exceedance rates of intensity parameters. Figure 7 shows the seismic hazard curve of Barcelona (Secanell et al., 2004) that is used in this study. According with these seismic hazard results, the maximum macroseismic intensity that can occur in Barcelona corresponds to the degree 8.
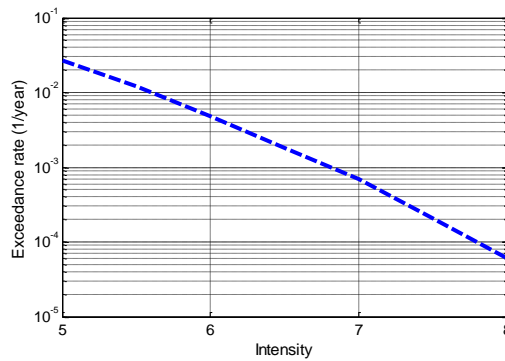
Figure 7. Exceedance rates of macroseismic intensities for the city of Barcelona.

3.4. The damage function

In the mLM1 method a known semi-empirical function is applied in order to estimate damage. Ac-cording with this relationship, the damage is in function of a macroseismic intensity and a vulnerability index grade (Milutinovic and Trendafiloski, 2003; Giovinazzi, 2005). This relationship is based on damage grades, which are defined in the EMS-98 scale (Grüntal, 1998).

3.4. The seismic risk results

In order to compute the exceedance rate of the physical damage states, the model that is summa-rized in the expression 1.1 is used. The seismic risk results indicate that the building No. 8 (figure 8b) has in average a seismic risk higher than the building No.3 (figure 8a). For example, in the building No. 3 the moderate damage grade has an exceedance rate between 0.00078 and 0.001933, whereas in the building No. 8, the

moderate damage grade has an exceedance rate be-tween 0.001345 and 0.002916. These results also mean that there is a probability between 3.8% and 9.2% that in the building No. 3 the moderate damage grade will be reached or exceeded in the next 50 years; and that there is a probability between 6.5% and 13.6% that in the building No. 8 the moderate damage grade will be reached or exceeded in the next 50 years.
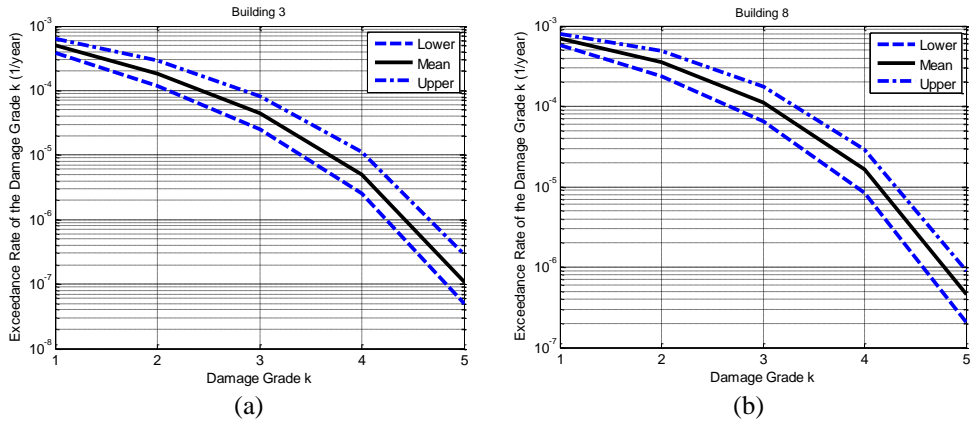
Figure 8. Damage curves, presented as annual probability of exceedance as a function of damage grade k, for the building No.3 (a) and for the building No. 8 (b).

The results showed in the figure 9 allow compare the seismic risk obtained for the buildings No.3 and No.8. In order to take decisions the seismic risk results can be expressed in terms of damage grade as a function of the return period (figure 9b).
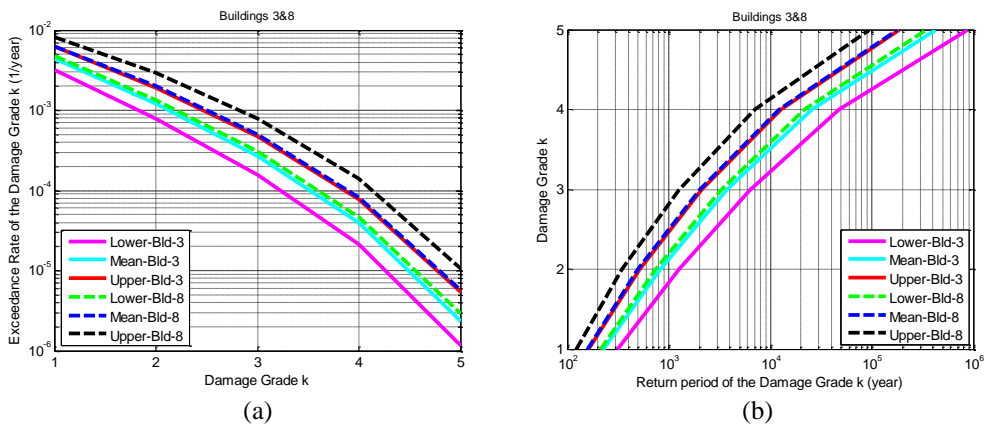
Figure 9. Damage curves for the buildings No. 3 and No. 8 presented as both annual probability of ex-ceedance as a function of damage grade k (a) and damage grade k as a function of the return period (b).

The figure 10 shows an example of the seismic risk results obtained in this study for the 10 build-ings located in the block B1.

(a)   (b)
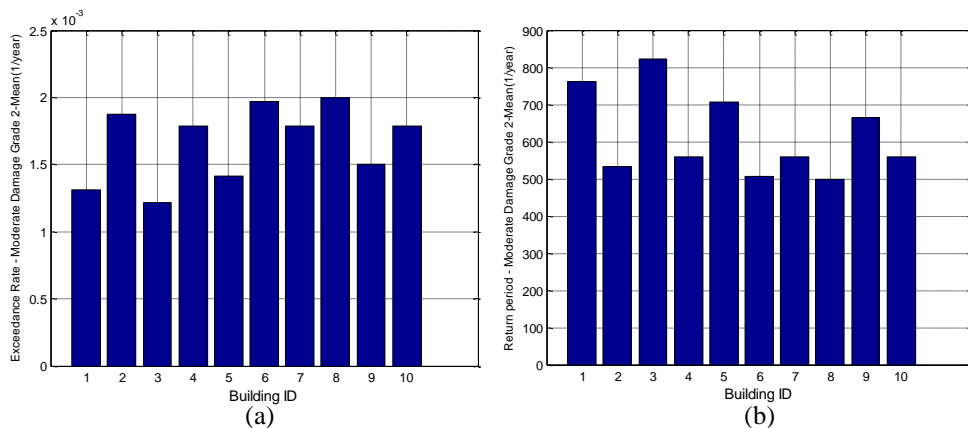
Figure 10. Mean estimation of the exceedance rates of the moderate damage grade for the 10 buildings lo-cated in the block B1 (a) and mean estimations of the return period of the moderate damage grade for the same buildings (b).

4. CONCLUSIONS

The probabilistic seismic risk approach that is presented in this paper, can be successfully applied in a simplified method as the mLM1 procedure, which allows to estimate the seismic risk of buildings in an urban scale.

The damage curves obtained in the present study contain useful information, for instance, they de-scribe numerous damage scenarios with its respective return period. This information about the seismic damage is fundamental to take decisions about the management of the seismic risk in buildings.

According with the results obtained in the present work, the seismic risk could be important in some buildings in the Eixample district of Barcelona, due to the combination of buildings with a high seismic vulnerability that are located in a place with low to moderate seismic hazard.

Acknowledgements

acknowledges the big support of the University of Veracruz in México, the CONACYT (National Council for Research and Technology of Mexico) and the Technical University of Catalonia.

References

Aguilar A., Pujades L., Barbat A. & Ordaz M. (2008), "Probabilistic assessment of seismic risk in urban areas", Proceedings of the 14th World Conference on Earthquake Engineering, Paper No. 09_01_0158, Beijing, 8 pages.

Barbat, A., Lagomarsino, S. & Pujades, L. (2006). Vulnerability assessment of dwelling buildings. In C. Sousa, A. Roca, & X. Goula (Ed.), *Assessing and Managing Earthquake Risk* (pages: 115-134). Netherlands: Springer.

Giovinazzi, S. (2005). The vulnerability assessment and the damage scenario in seismic risk analysis. Dottore di Ricerca in Risk Management on the Built Enviroment Dissertation. Technical University Carolo-Wilhelmina at Braunschweig, Braunschweig and University of Florence, Florence, Italy, 210 pages.

Google (2008). Google Earth software 4.3.7289.3916 (beta).http://earth.google.com/

Grüntal, G. (1998). European Macroseismic Scale 1998. Centre Européen de Géodynamique et de Séismologie, Luxemburg. 99 pages.

Lantada, N. (2007). Evaluación del riesgo sísmico mediante métodos avanzados y técnicas GIS. Aplicación a la ciudad de Barcelona. Tesis doctoral. Universitat Politécnica de Catalunya. 338 pages.

McGuire, R. K. (2004). Seismic Hazard and Risk Analysis, Earthquake Engineering Research Institute, Oakland, CA. 221 pages.

Milutinovic Z. & Trendafiloski G. (2003). *WP4: Vulnerability of current buildings*. RISK-UE. "An advanced approach to earthquake risk scenarios with applications to different European towns". Contract: EVK4-CT-2000-00014. 109 pages.

Secanell, R., Goula, X., Susagna, T., Fleta, J. & Roca, A. (2004) Seismic hazard zonation of Catalonia, Spain, integrating random uncertainties. Journal of Seismology. 8:, 25-40

Evaluation of the seismic safety of RC framed buildings designed according to EC-2 and EC-8

Alex H. Barbat[1], Juan C. Vielma[2] and Sergio Oller[3]

[1] Technical University of Catalonia, Departamento de Resistencia de Materiales y Estructuras en la Ingeniería, E.T.S. de Ingenieros de Caminos Canales y Puertos, Edificio C1, Campus Norte, Jordi Girona 1-3, Barcelona, 08034, Spain e-mail: alex.barbat@upc.edu
[2] Lisandro Alvarado University, Av. La Salle entre Av. Las industrias y Av. Benítez, Decanato de Ingeniería Civil, Departamento de Estructuras. Barquisimeto, Venezuela e-mail: jcvielma@ucla.edu.ve

Abstract

One of the main objectives of the design of earthquake resistant structures is to ensure that these do not collapse when subjected to the action of strong motions. Modern codes include prescriptions in order to guarantee that the behavior of the elements and the whole structure is ductile. It is especially important for the designer to know the extent of damage that the structure will suffer under a specific seismic action, described by the design spectrum. To achieve this damage there are several static and dynamic nonlinear procedures. This paper presents a procedure for nonlinear static analysis in which the maximum displacements are determined based on the condition of satisfying a minimum value of a finite element based damage index. This procedure is validated by applying incremental dynamic analysis, and is used in the assessment of the response of a set of regular reinforced concrete buildings designed according to the EC-2/EC-8 prescriptions for high seismic hazard level. The results of nonlinear analysis allows the formulation of a new seismic damage index and of damage thresholds associated with five Limit States, which are used to calculate fragility curves and damage probability matrices for the performance point of the studied buildings. The results show that the design of earthquake resistant buildings according to the prescriptions of EC-2/EC-8 not only ensures that the collapse is not reached, but also that the structural damage does not exceed the irreparable damage limit state.

KEYWORDS: ductility, over strength, behavior factor, non-linear analysis, fragility curves, objective damage index

1. INTRODUCTION

The main objective of the earthquake resistant design is to produce structures capable to sustain a stable response under strong ground motions. Some of the aspects of the current seismic analysis procedure allow adapting the characteristics of the non-linear structural behavior to the equivalent elastic analysis. Obviously, the formulation of these characteristics is an important task in order to obtain a satisfactory design.

Recent advances and developments in the computational tools enabled to develop and to apply more realistic analysis models to new or existent buildings and to take into account main features of the non-linear seismic behavior of structures, like constitutive laws (plasticity and damage) or large deformations. The non linear analysis has been used in the assessment of buildings designed according to specific design codes [1, 2, 3].

Among the characteristics studied in past works, some examples can be provided: displacement ductility, overstrength and behavior factor. The assessment of these characteristics is possible by applying deterministic procedures in analyzing the non-linear response of the structures subjected to static or dynamic loads. The static non-linear analysis is usually performed by using a predefined lateral load distribution which corresponds to the first mode shape. The dynamic analysis is applied using a suitable set of records obtained from the existing strong ground motion databases or from design spectrum-compatible synthetic accelerograms.

Recently, the application of the Performance-Based Design concepts required the definition of a set of Limit States, usually starting from engineering demand parameters, such as the interstory drift, the global drift or the global structural damage. These parameters allow defining damage thresholds associated with the Limit States which are applied to the calculation of the fragility curves and of the damage probability matrices used in the seismic safety assessment of the buildings.

In this paper, the seismic safety of regular framed buildings is studied using static and dynamic non-linear analysis. The static analysis is performed by means of pushover procedures while the dynamic analysis is performed using the Incremental Dynamic Analysis (IDA). For this purpose, a set of 16 reinforced concrete framed buildings was designed according to EC-2 [4] and EC-8 [5]. The buildings are regular in plan and elevation. The analysis was performed using the PLCd program [6] which allows incorporating the main characteristics of the reinforcement and of the confinement provided to the structure members. The results of the non-linear analysis allow calculating the displacement ductility, the overstrength and the behavior factors of the structures. The latter are compared with those prescribed by EC-8. The global performance of the buildings is evaluated using an objective damage index, formulated starting from the capacity

curve. Finally, for the predefined damage thresholds, fragility curves and damage probability matrices are calculated.

2. DESCRIPTION AND DESIGN OF THE STUDIED BUILDINGS

A set of regular reinforced concrete moment-resisting framed buildings (MRFB), designed according to EC-2 and EC-8, characterized by the number of stories (3, 6, 9 and 12) and of spans (3, 4, 5 and 6) was used in the paper. These buildings cover a low to medium structural period range and also and relevant range of structural redundancy. The structural members of are analyzed, designed and detailed according to the EC-2 and EC-8 prescriptions for high ductility class (behavior factor equal to 5.85). The seismic demand is obtained for the B Soil type design spectrum (stiff soil) and for a peak ground acceleration of 0.3g. The geometric characteristics of the studied buildings are shown in figures 1 and 2.
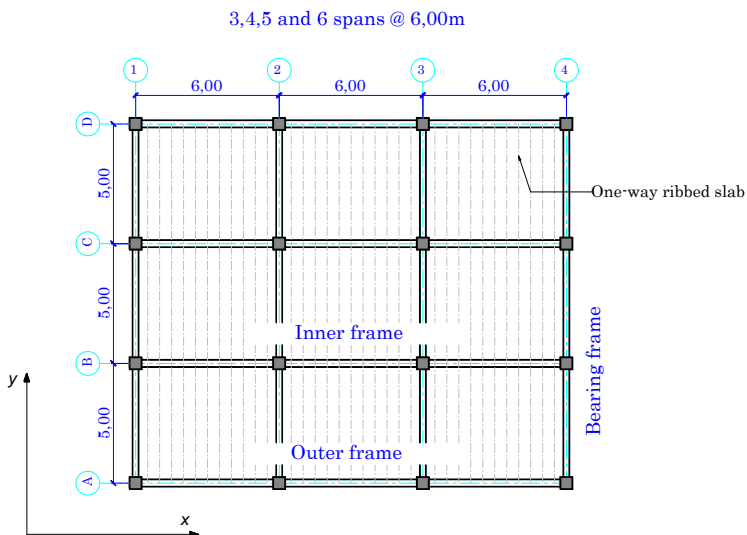
Figure 1. Plan view of the framed buildings

3 story framed buildings

6 story framed buildings

9 story framed buildings

12 story framed buildings
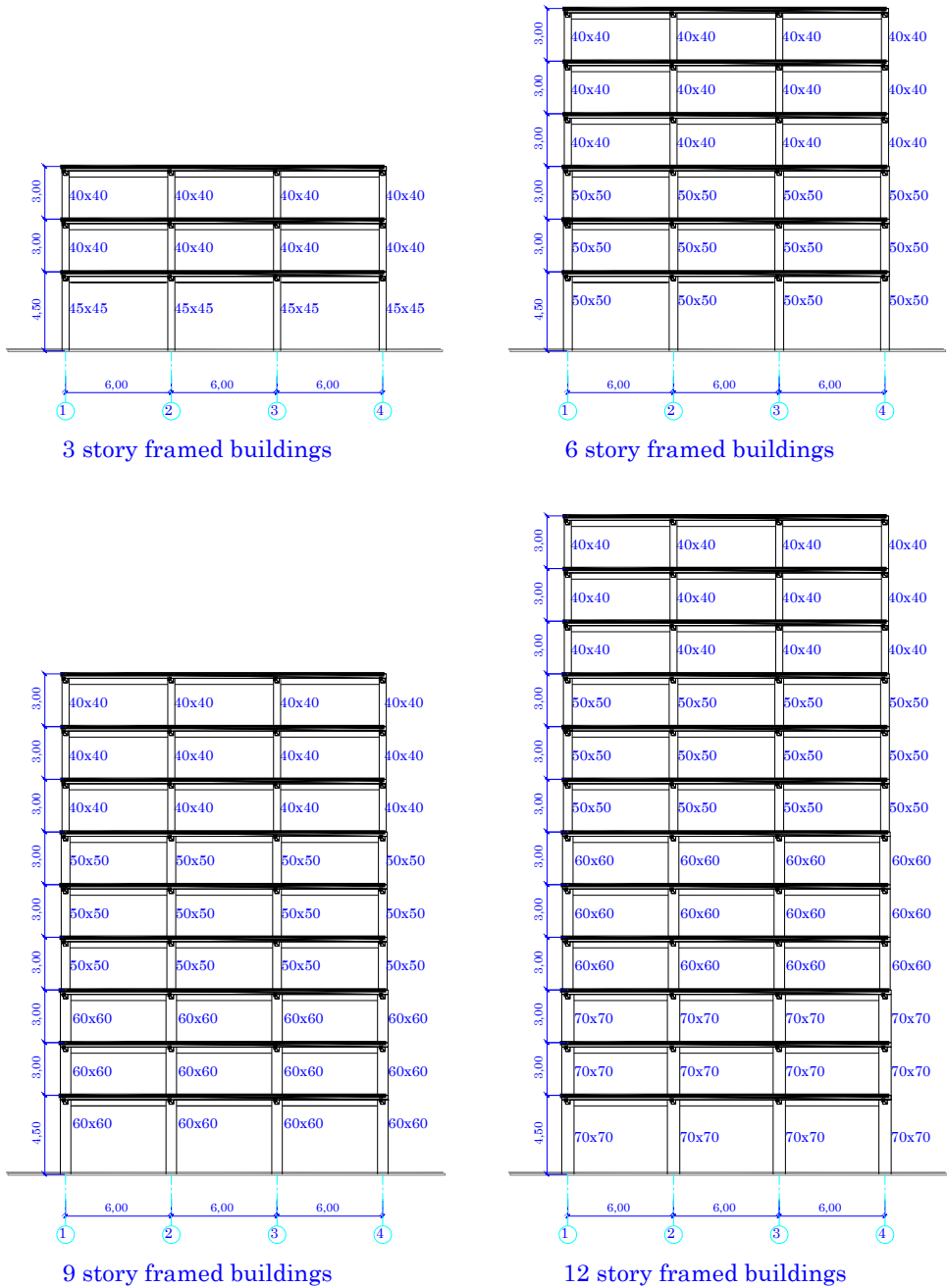
Figure 2. Elevation of the framed buildings

3. NON-LINEAR ANALYSIS OF THE BUILDINGS

3.1. Characteristics of the computational model

The non-linear static analysis with force control was performed using the PLCd finite element code [7, 8] which allows using two and three-dimensional solid elements as well as prismatic, reduced to one-dimensional, members. This code provides a solution combining both numerical precision and reasonable computational costs [9, 10]. It can deal with kinematics and material nonlinearities. It uses various 3-D constitutive laws to predict the material behavior (elastic, visco-elastic, damage, damage-plasticity, etc. [11]) with different yield surfaces to control its evolution (Von-Mises, Mohr–Coulomb, improved Mohr–Coulomb, Drucker–Prager, etc. [12]). Newmark's method [13] is used to perform the dynamic analysis. A more detailed description of the code can be found in Mata *et al.* [9,10]. The main numerical features included in the code to deal with composite materials are: 1) Classical and serial/parallel mixing theory used to describe the behavior of composite components [14]. 2) Anisotropy Mapped Space Theory enables the code to consider materials with a high level of anisotropy, without the associated numerical problems [15]. 3) Fiber–matrix debonding which reduces the composite strength due to the failure of the reinforced–matrix interface [16].

Experimental evidence shows that inelasticity in beam elements can be formulated in terms of crossectional quantities [17] and, therefore, the beam's behavior can be described by means of concentrated models, sometimes called plastic hinge models, which localize all the inelastic behaviour at the ends of the beam by means of ad-hoc force–displacement or moment–curvature relationships [18]. But, in the formulation used in this computer program, the procedure consists of obtaining the constitutive relationship at cross-sectional level by integrating on a selected number of points corresponding to fibers directed along the beam's axis [19]. Thus, the general nonlinear constitutive behavior is included in the geometrically exact nonlinear kinematics formulation for beams proposed by Simo [20], considering an intermediate curved reference configuration between the straight reference beam and the current configuration. The displacement based method is used for solving the resulting nonlinear problem. Plane cross sections remain plane after the deformation of the structure; therefore, no cross sectional warping is considered, avoiding to include additional warping variables in the formulation or iterative procedures to obtain corrected cross sectional strain fields. An appropriated cross sectional analysis is applied for obtaining the cross sectional forces and moments and the consistent tangential tensors in the linearized problem. Thermodynamically consistent constitutive laws are used in describing the material behavior for these beam elements, which allows obtaining a more rational estimation of the energy dissipated by the structures. The simple mixing rule for composition of the materials is also considered in modeling materials for these elements, which are

composed by several simple components. Special attention is paid to obtain the structural damage index capable of describing the load carrying capacity of the structure.

According to the Mixing Theory, in a structural element coexist N different components, all of them subject to the same strain; therefore, strain compatibility is forced among the material components. Free energy density and dissipation of the composite are obtained as the weighted sum of the free energy densities and dissipation of the components, respectively. Weighting factors k_q are the participation volumetric fraction of each compounding substance, $k_q=V_q/V$, which are obtained as the quotient between the q-th component volume, V_q, and the total volume, V [7, 8, 9, 10].

Discretization of frames was performed with finite elements whose lengths vary depending on the column and beam zones with special confinement requirements. These confinement zones were designed according to the general dimensions of the structural elements, the diameters of the longitudinal steel, the clear of the spans and the story heights. Frame elements are discretized into equal thickness layers with different composite materials, characterized by their longitudinal and transversal reinforcement ratio (see Figure 3). Transversal reinforcement benefits are included by means of the procedure proposed by Mander *et al.* [21].
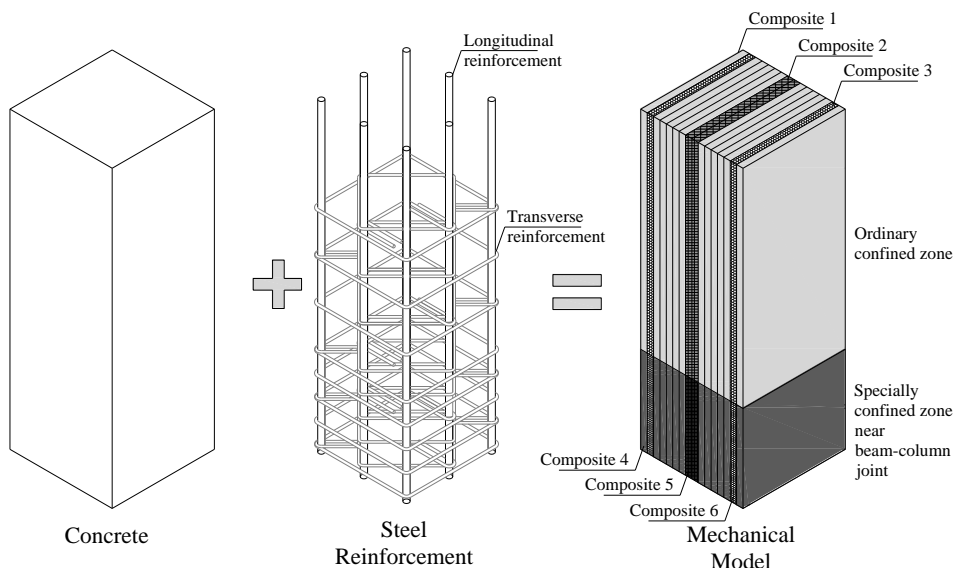
Figure 3. Discretization of the RC frame elements

3.2. Non-linear static analysis

To evaluate the inelastic response of the four structures, pushover analysis was performed applying a set of lateral forces representing seismic actions corresponding to the first vibration mode. The lateral forces are gradually increased starting from a zero value, passing through the value which induces the transition from elastic to plastic behavior and, eventually, reaching the value which corresponds to the ultimate drift (*i.e.* the point at which the structure can no longer support any additional load and collapses). Before the structure is subjected to the lateral loads simulating seismic action, it is first subjected to the action of gravity loads, in agreement with the combinations applied in the elastic analysis. The method applied does not allow evaluating the effect of torsion, being the used structural model a 2D one.

Although it is difficult to find a method to obtain the global yield and ultimate displacements [22] in this work a simplified procedure is applied. The non-linear static response obtained via finite element techniques is used to generate the idealized bilinear shaped capacity curve shown in Figure 4, which has a secant segment from the origin to a point on the capacity curve that corresponds to a 75% of the maximum base shear [23]. The second segment, which represents the branch of plastic behavior, was obtained by finding the intersection of the aforementioned segment with another, horizontal segment which corresponds to the maximum base shear. The use of the compensation procedure guarantees that the energies dissipated by both nonlinear models are equal.
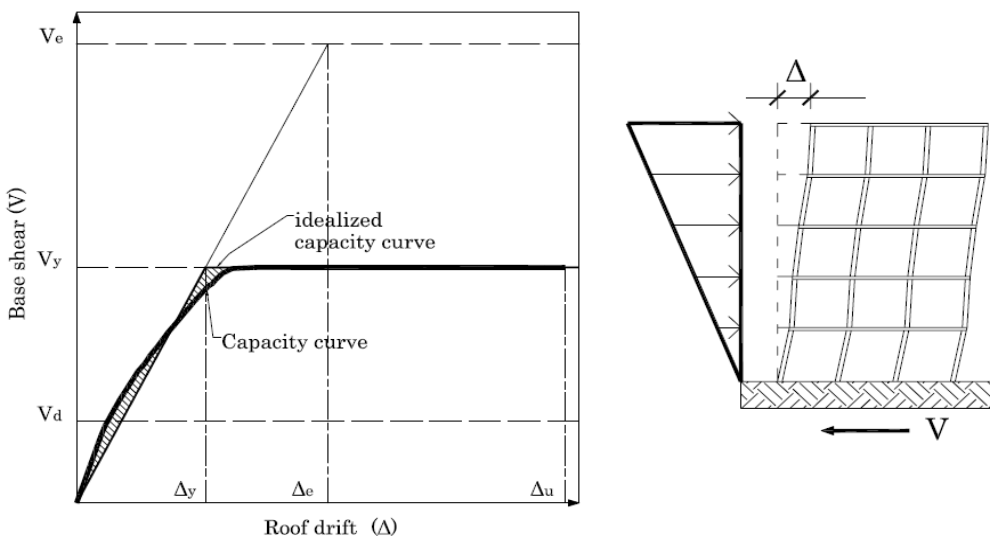
Figure 4. Scheme for determining the displacement ductility and the overstrength
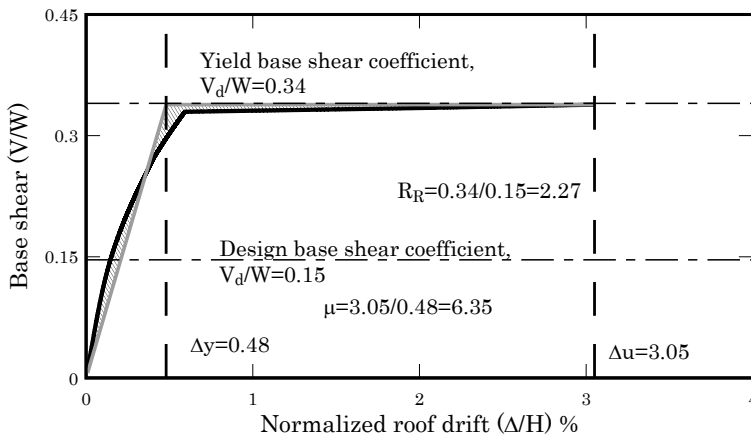
Figure 5. Idealized capacity curve of the MRFB

For simplified non-linear analysis there are two variables that characterize the quality of the seismic response of buildings. The first is the displacement ductility μ, defined as

$$\mu = \frac{\Delta_u}{\Delta_y} \tag{1}$$

and calculated based on the values of the yield drift Δy, and ultimate drift Δu, from the idealized capacity curve shown in Figure 5. The second variable is the overstrength R_R of the building, which is defined as the ration of the design base shear V_d to the yielding base shear V_y, both of which are shown in Figure 5

$$R_R = \frac{V_y}{V_d} \tag{2}$$

The overstrength R_R is like a safety factor applied in design and evaluation of the buildings.

Figure 5 shows the capacity curve of the outer frame of the 9 story building. The curve clearly illustrates how this structural type is capable to sustain stable ductile response, which is reflected in the high value for the final drift. Based on the idealized bilinear curve of this figure, a displacement ductility of 6.35 is obtained; this is a higher value than that specified in the EC-8 seismic design code, which is 5.85. In the same figure, the overstrength is also calculated, which has a value of 2.27. This means that the moment resisting buildings designed according to EC-2 and EC-8 have a ductile response to seismic forces, and also an adequate overstrength.
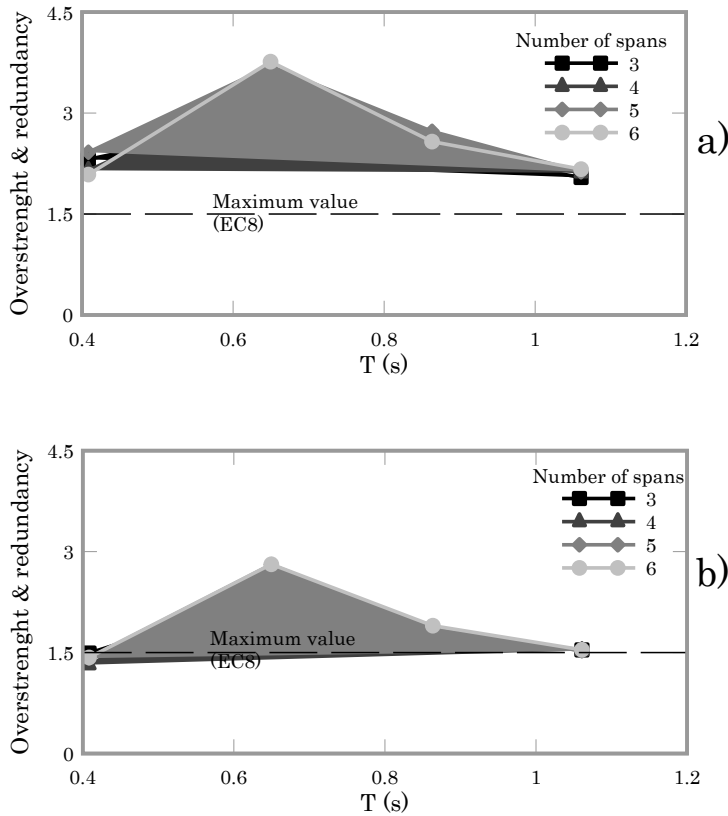
Figure 6. Overstrength and redundancy spectrum of the a) outer frames and b) inner frames

Figures 6a and 6b shows computed values of the overstrength for the outer and inner frames of the studied buildings, plotted versus the periods of the first mode, respectively. The results demonstrate clearly that influence of increasing the number of spans, which is equivalent to consider various defense lines, is very low, excepting the case of the 6 story buildings. For the other buildings, the values of the overstrength are closer. It is also seen that the computed values of the combined overstrength factors are greater than the value that EC-8 prescribes for the design of ductile framed buildings.

3.3. Damage index

A local damage index *D* is calculated using the finite element program PLCd with a damage and plasticity constitutive model that enables correlation of damage with lateral displacements [24, 25]

$$D = 1 - \frac{\left\| P^{in} \right\|}{\left\| P_0^{in} \right\|}$$

where $\left\| P^{in} \right\|$ and $\left\| P_0^{in} \right\|$ are the norm of current and elastic values of the internal forces vectors, respectively. Initially, the material remains elastic and $D=0$ but, when all the energy of the material is dissipated $\left\| P^{in} \right\| \rightarrow 0$ and $D \rightarrow 1$. Figure 7 shows the distribution of the damage index to the members of the studied frames corresponding to the collapse displacement. In this figure, each rectangle represents the magnitude of the damage reached by the finite element. It is important to observe that, for low rise buildings (N=3), the maximum values of the damage occurs at the extremities of the columns of the first story; this damage concentration is characteristic for a soft-story mechanism. Instead, high rise buildings (N= 6, 9 and 12) show maximum damage values at the extremities of the beams of the stories. This is the desired objective of the conceptual design: to produce a structure with weak beams and strong columns.

It is important to know the level which the damage reaches when a structure suffers a certain demand. This is possible if the damage index is normalized respecting the maximum damage which can occur in the structure. Vielma *et al.* [26] proposed a capacity curve-based damage index D_{obj}^P which allows assessing the damage level for a specific roof displacement. This objective damage index $0 \leq D_{obj}^P \leq 1$ reached by a structure for a given drift corresponding to a point *P* of the capacity curve is defined as

$$D_{obj}^P = D_P \frac{1-\mu}{\mu} = \frac{(1 - K_P / K_0)\mu}{\mu - 1} \tag{4}$$

For example, *P* might be the performance point resulting from intersection between the inelastic demand spectrum and the capacity curve; the stiffness K_P corresponds to this point. Other parameters are the initial stiffness K_0 and the displacement ductility μ, calculated with the yield displacement Δ_y^* which corresponds to the intersection of the initial stiffness with the maximum shear value (see Figure 8).

Figure 9 shows the evolution of the objective damage index with respect to the normalized roof drift, computed for all the frames of the studied buildings.
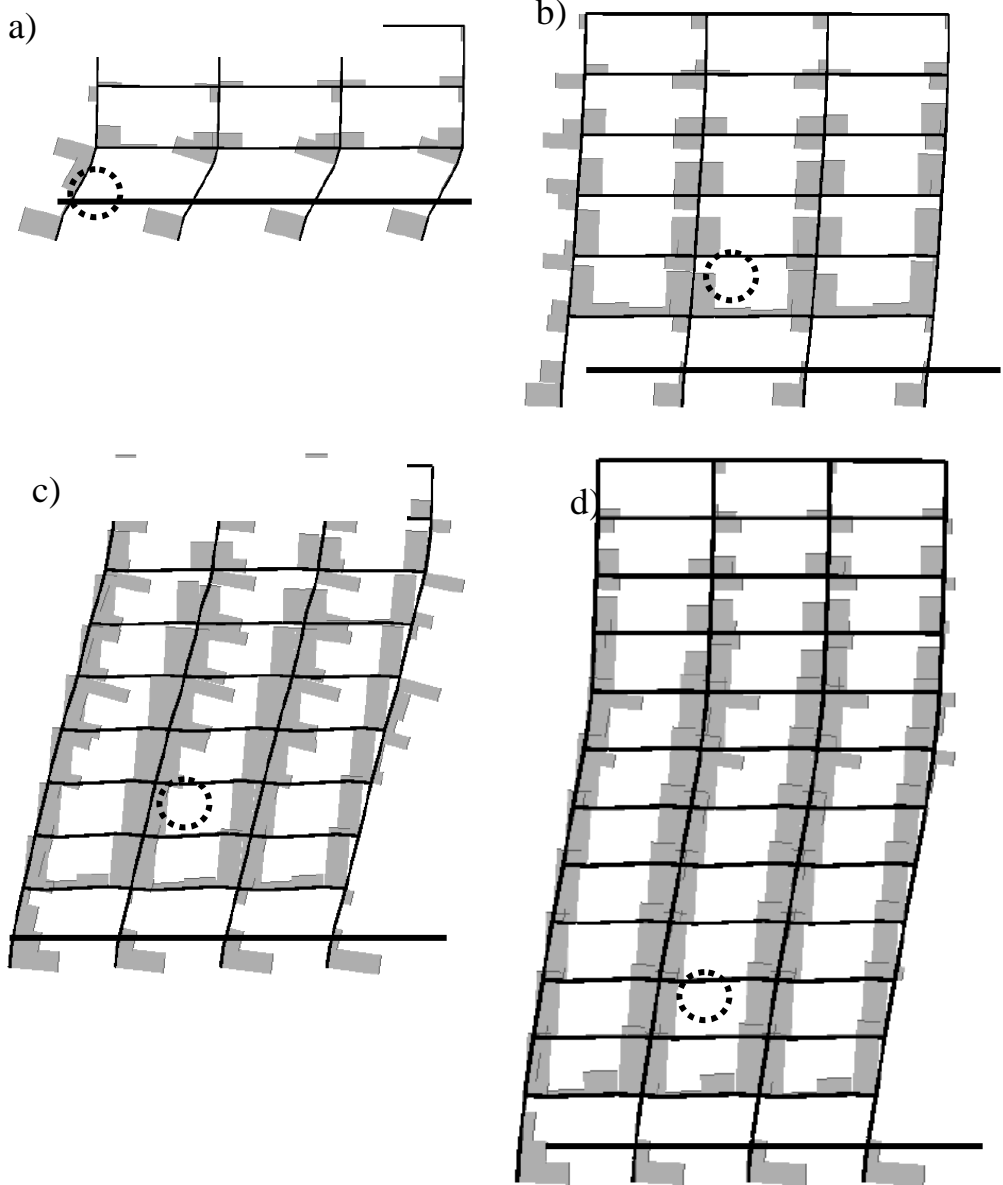
Figure 7. Distribution of the local damage index at collapse displacement
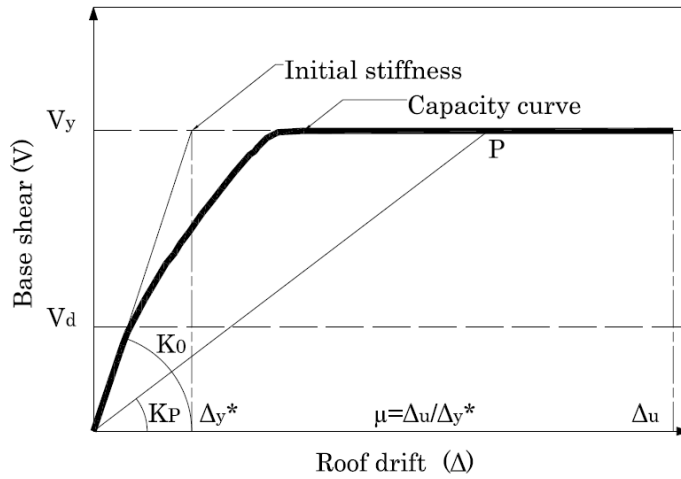
Figure 8. Parameters used in the calculation of the objective damage index
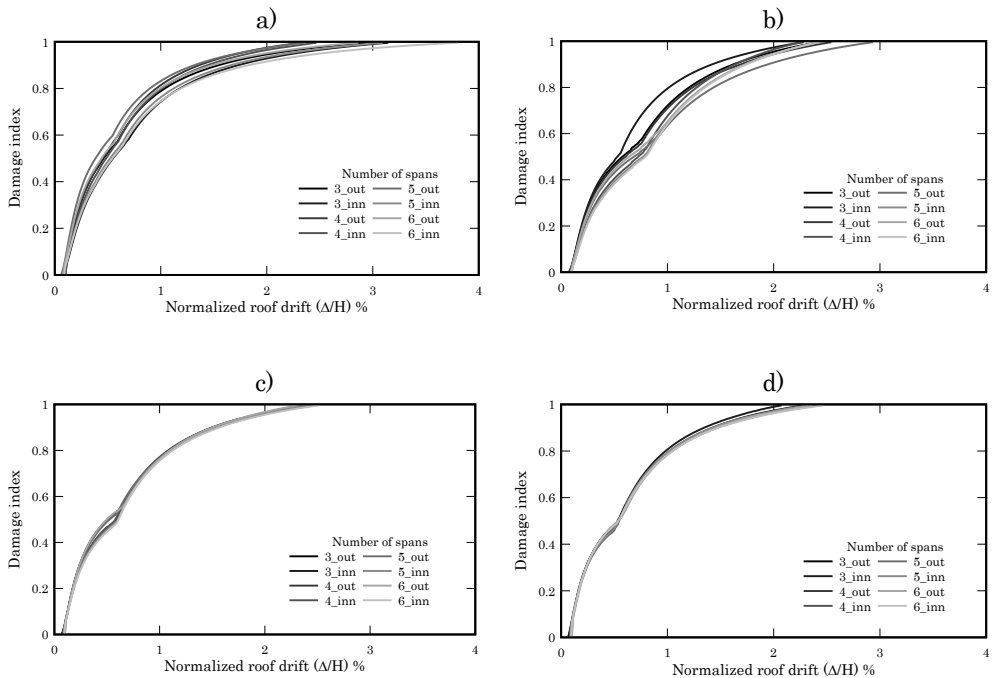
Figure 9. Evolution of the damage index of the a) 3 story, b) 6 story, c) 9 story and d) 12 story building

3.4. Incremental Dynamic Analysis

In order to evaluate the dynamic response of the buildings, the Incremental Dynamic Analysis (IDA) [27] was applied. This procedure consists in performing time-history analyses using real or artificial accelerograms, which are scaled each time in order to induce increasing levels of inelasticity in the structural model. A set of six artificial accelerograms compatible with soil type B of the EC-8 design spectrum were generated. Figure 10 shows the design spectrum and the 5% damping response spectra obtained for the set of synthetic accelerograms.

The IDA response curves are obtained plotting the ground motion intensity versus demand parameters which, in this study, are the spectral accelerations of the 5% damped spectra and the roof drifts, respectively. The collapse point is reached when the capacity of the structure drops [28]. A usual criterion is to consider the slope of the curve less than the 20% of the elastic slope [27, 29]. Figure 8 shows the IDA curves computed from the 3-spans outer frames of the 3, 6, 9 and 12 story buildings. Note that the collapse points of the frames are closer to the values of the capacity curves.

Table 2 summarizes the average values of the collapse points for all the studied cases, computed by means of the performed dynamic analysis. Dynamic analysis is useful in assessing the collapse point of the buildings and, for obtaining the values of the behavior factors q, the following equation has been proposed [2]

$$q = \frac{a_{g(collapse)}}{a_{g(design\_yield)}}$$

(5)

where $a_{g(collapse)}$ and $a_{g(design\_yield)}$ are the collapse and the yield design peak ground acceleration, respectively. $a_{g(collapse)}$ is obtained from the IDA curves and $a_{g(design\_yield)}$ is calculated from the elastic analysis of the building. Average values of the computed behavior factor q of the studied buildings are show in Table 2; these values correspond to the dynamic response of the buildings subjected to the set of synthetic accelerograms and are compared with the behavior factors prescribed by the design codes.

The computed behavior factors show that the applied seismic design allows designing structures with satisfactory lateral capacity when they are subjected to strong ground motions, regardless of the building height. The relationship between the calculated and the prescribed behavior factors is close to three for the case of low rise buildings.

a)

b)
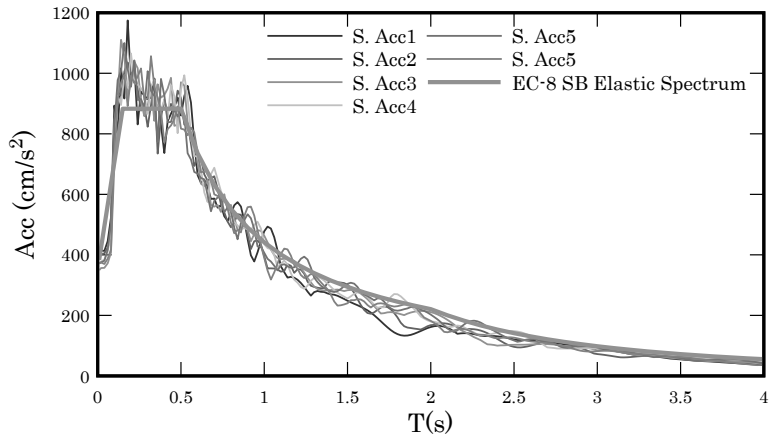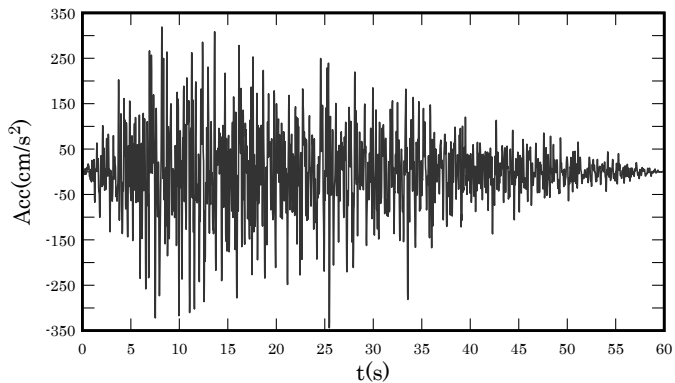
Figure 10. a) Sinthesized accelerogram b) EC-8 soil type B, elastic design spectrum and response spectra

4. SEISMIC SAFETY OF THE BUILDINGS

4.1. Calculation of the performance point

As the main objective of this paper is to study the seismic safety of buildings designed according to the Eurocodes, it is necessary to define a measure of the engineering demand. The global drift of the structure corresponding to the performance point has been selected herein to assess the seismic safety of the buildings.
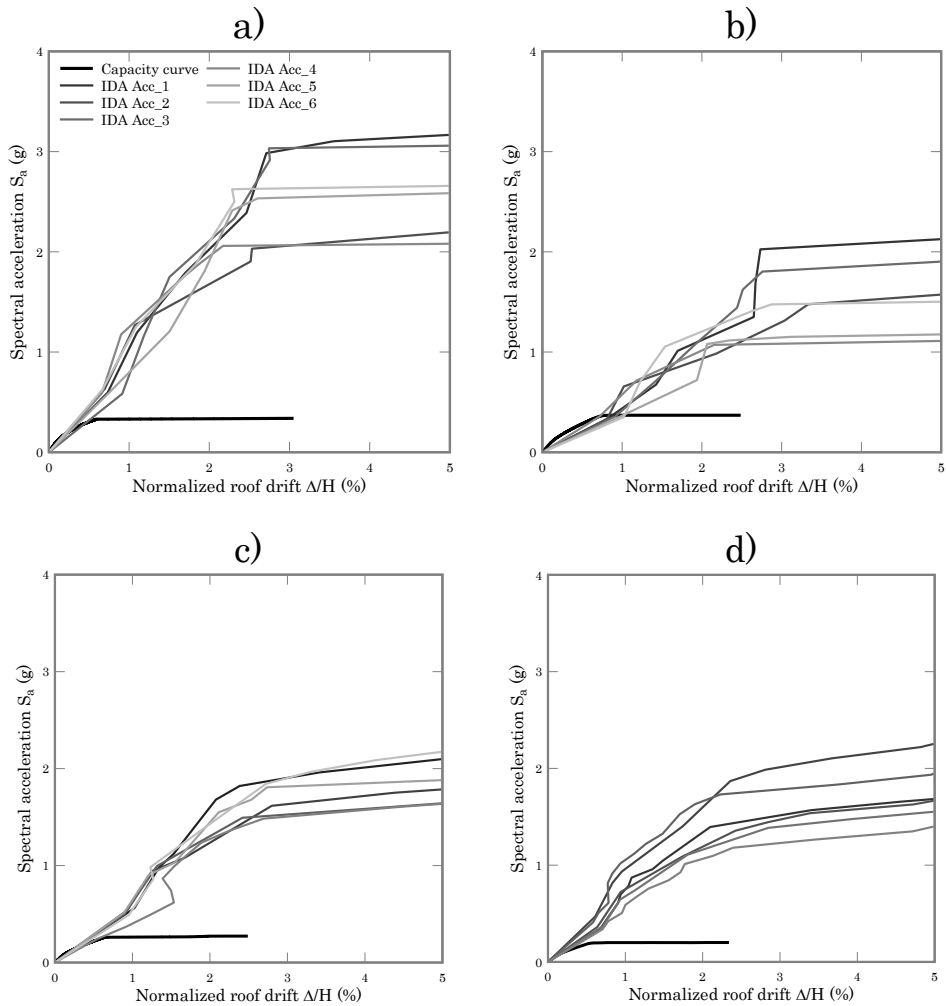
Figure 11. IDA curves of the a) WSB b) FBFB c) MRFB (EHE) and d) MRFB (EC)

Table 1. Normalized roof displacement (%) at the collapse of the structures

	Static analysis	Dynamic analysis (average)
3	2.51	2.51
6	2.63	2.63
9	2.48	2.62
12	2.35	2.39

Table 2. Behavior factors of the buildings

	$q_{equation}$ (Average)	q_{code}	$q_{equation}/q_{code}$
3	17.40	5.85	2.97
6	10.79	5.85	1.84
9	15.07	5.85	2.57
12	15.12	5.85	2.58

The performance point permits establishing the point of maximum drift of an equivalent single degree of freedom model induced by the seismic demand. It is determined in the paper by using the N2 procedure [30] which N2 requires transforming the capacity curve into a capacity spectrum expressed in terms of the spectral displacements S_d and of the spectral acceleration S_a; S_d is obtained by

$$S_d = \frac{\delta_c}{MPF} \tag{6}$$

where δ_c is the roof displacement and *MPF* the modal participation factor obtained from the response of the first mode of vibration

$$MPF = \frac{\sum_{i=1}^{n} m_i \phi_{1,i}}{\sum_{i=1}^{n} m_i \phi_{1,i}^2} \tag{7}$$

In this equation, m_i is the mass *I* and $\phi_{1,I}$ is the spectral ordinate. The spectral acceleration S_a is given by

$$S_a = \frac{V/W}{\alpha} \tag{8}$$

where *V* is the base shear, *W* is the seismic weight α and is the coefficient

$$\alpha = \frac{\left(\sum_{i=1}^{n} m_i \phi_{1,i}\right)^2}{\sum_{i=1}^{n} m_i \phi_{1,i}^2} \tag{9}$$

Figure 12 shows the capacity spectra for the outer frame of the building with 3 stories and 3 spans, crossed with the corresponding demand elastic spectra. The idealized bilinear form of the capacity spectrum is also shown in the figure.
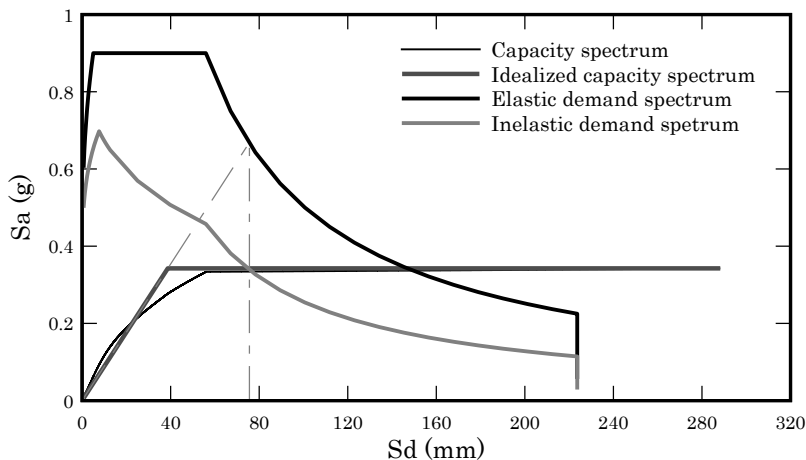
Figure 12. Capacity and demand spectra allowing the determination of the performance point of the outer frame of the building with 3 spans and 3 stories

The values of the spectral displacements corresponding to the performance point are shown in Table 3. An important feature in the non linear response of the buildings is the ratio between the performance point displacement and the ultimate displacement. This ratio indicates whether the behavior of a structure is ductile or fragile. The lower values of this ratio correspond to the 12 story building, which has a weak-beam strong-column failure mechanism.

Table 3. Roof drift of performance points for the studied buildings

Story number	Normalized roof drift (%)			Ratio	
	Performance point %)	Static analysis	Dynamic analysis (average)	Static analysis	Dynamic analysis (average)
3	0.80	3.02	2.51	0.26	0.32
6	0.51	2.48	2.63	0.20	0.19
9	0.39	2.48	2.62	0.16	0.15
12	0.21	2.34	2.39	0.09	0.09

4.2. Fragility curves and damage probability matrices

The damage thresholds are determined using the VISION 2000 procedure [31] which expresses the thresholds in function of the interstory drift. In this work, five damage states thresholds are defined using both the interstory drift curve and the capacity curve. The *slight* damage state corresponds to the roof drift for which the first plastic hinge appears. The *moderate* damage state corresponds to the roof drift

for which an interstory drift of 1% is reached in all the stories of the structure. The *repairable* damage state is defined by a interstory drift of 2%. The *severe* damage state is identified by a roof drift producing a 2,5% of interstory drift at each of the levels of the structure. Finally, the total damage state (collapse) corresponds to the ultimate roof displacement obtained from the capacity curve. Mean values and standard deviation were computed from the non linear response of buildings having the same geometry and structural type, by varying the number of spans from 3 to 6 in the *x* direction [32, 33].

The fragility curves are obtained by using the spectral displacements determined for the damage thresholds and considering a lognormal probability density function for the spectral displacements which define the damage states [34]

$$F(S_d) = \frac{1}{\beta_{ds} S_d \sqrt{2\pi}} \exp\left[-\frac{1}{2}\left(\frac{1}{\beta_{ds}} \ln \frac{S_d}{\overline{S}_{d,ds}}\right)^2\right] \tag{10}$$

where $\overline{S}_{d,ds}$ is the mean value of the spectral displacement for which the building reaches the damage state threshold d_s and β_{ds} is the standard deviation of the natural logarithm of the spectral displacement for the damage state d_s. The conditional probability $P(S_d)$ of reaching or exceeding a particular damage state d_s, given the spectral displacement S_d, is defined as

$$P(S_d) = \int_0^{S_d} F(S_d) d(S_d) \tag{11}$$

Figure 13 shows the fragility curves calculated for the four different heights of buildings considered in the analysis.
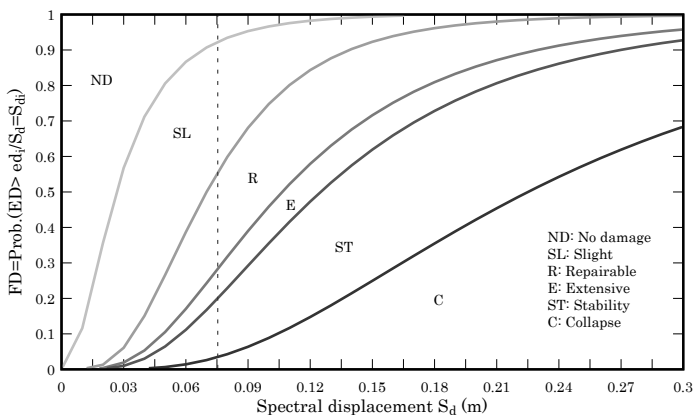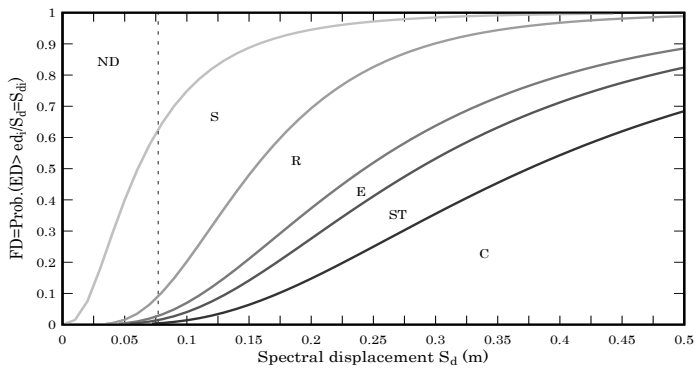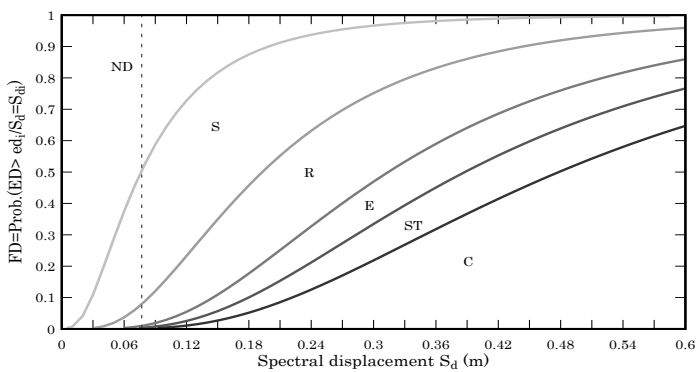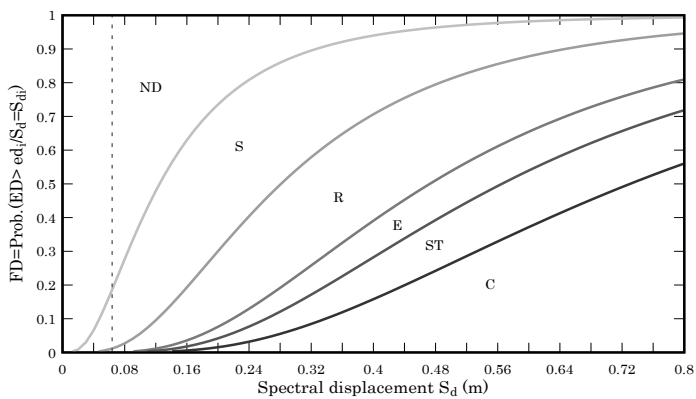
Figure 13. Fragility curves of the a) 3 story, b) 6 story, c) 9 story and d) 12 story buildings

Figure 14 shows the damage probability matrices calculated for the performance points corresponding to all the studied cases. It is worth to observe that the probabilities are not sensitive to the variation of the span number. It is also important to note that for the frames of the same building, the probabilities vary according to the load ratio (seismic load/gravity load).
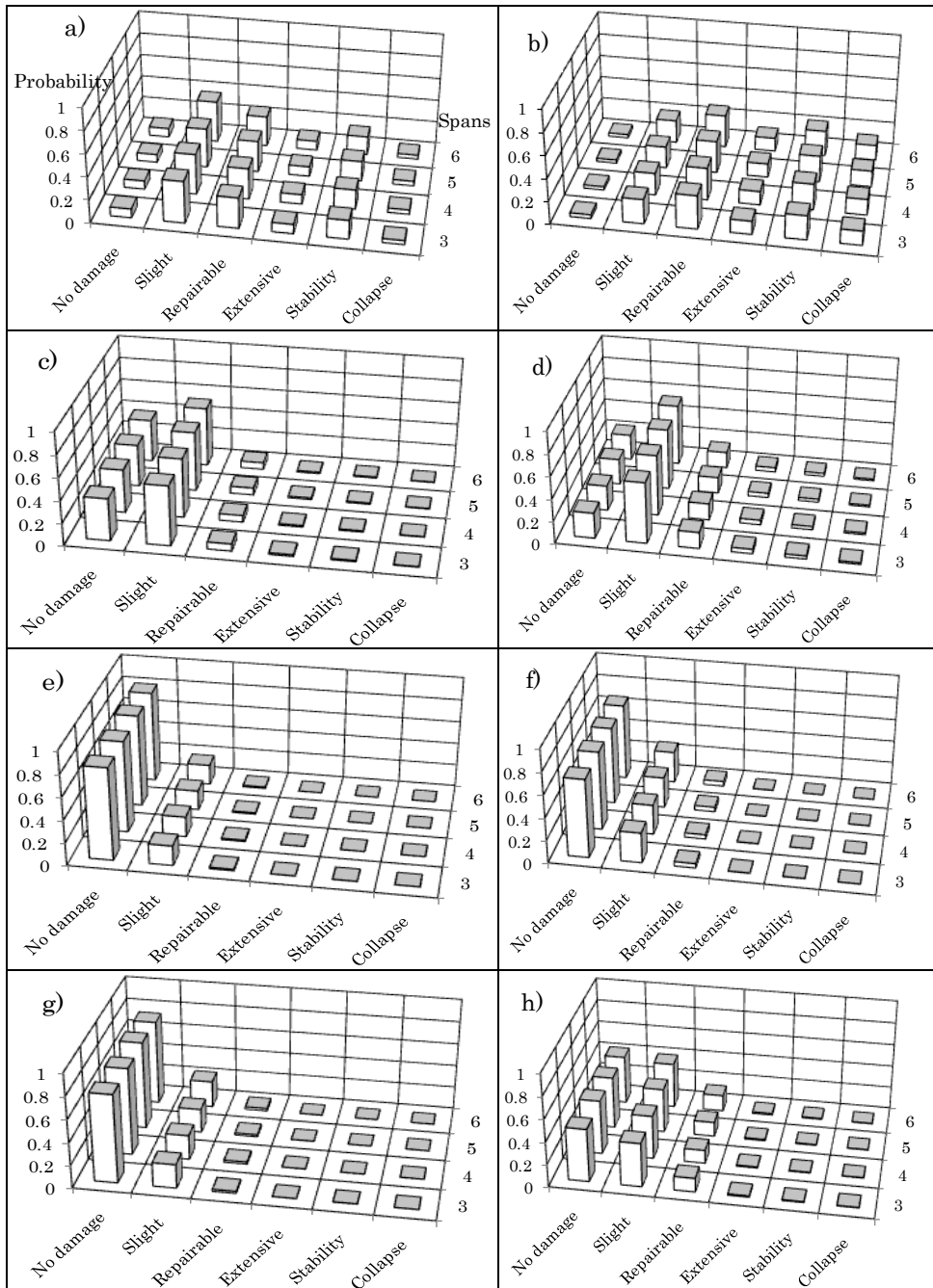
Figure 14. Damage probability matrices of a) outer and b) inner frames of 3 story buildings, c) outer and d) inner frames of 6story buildings, e) outer and f) inner frames of 9 story buildings and g) outer and h) inner frames of 12 story buildings

Another important feature which can be observed in the obtained results is the increase of the probability values that correspond to the higher damage states for low rise buildings, for which the collapse is associated to the soft-storey mechanism as discussed in previous sections. For example, in the case of the inner frames of the 3 levels building, the probability to reach the *collapse* is four times higher than in the case of the outer frames of the same building. In contrast, the 6, 9 and 12 story buildings show very low probabilities to reach more severe damage states regardless of the load ratio and of the span number. For these buildings, the predominant damage states are the *non-damage* and the *slight* damage.
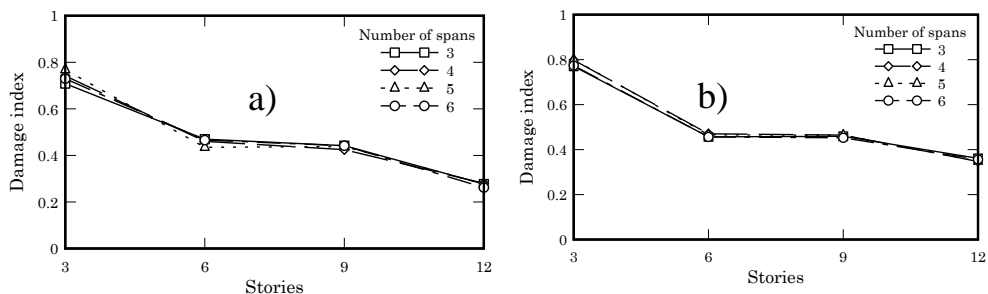
Figure 14. Damage index computed for the a) outer frames and b) inner frames

Figure 14 shows the values of the damage index correspondingto the performance point of the different frames. These values were obtained using Eq. 3. First of all, it is possible to observe that low rise buildings (3 levels) reach high values of the damage index than the other buildings; this is a consequence of the failure mechanism which occurs for this kind of buildings (soft story mechanism). In contrast, the 12 levels buildings exhibits damage index about 0.3 to 0.35 for the outer frames, values that are consistent with the failure mechanism (strong columns-weak beams) and with the probabilities obtained from the fragility curves. Finally it is important to observe that the values of the damage index of the outer frames are lower than the values of the damage index of the inner frames, indicating that the damage index depends on the load type ratio.

5. CONCLUSIONS

- The Incremental Dynamic Analysis is useful in order to assess the collapse threshold of the frames. The dynamic analysis, which is also suitable for the evaluation of the behavior factor q, confirms the values obtained by means of the pushover analysis.
- The local damage distribution of the buildings corresponding to the collapse threshold shows that low rise buildings have a failure mechanism associated to the formation of the soft storey mechanism. Medium rise buildings (6, 9

and 12 story) exhibit a failure mechanism associated to the weak-beam and strong-column conceptual design objective.

- Reinforced concrete framed buildings, designed according to the Eurocodes for a high ductility class, exhibit adequate values of overstrength which are greater than the value prescribed in the code (1.5). Behavior factors obtained by means of the dynamic analysis are also adequate and are twice the code values. In the procedure applied to evaluate such factors, no influence of the structural redundancy was detected.
- Generally speaking, the studied buildings show adequate ductility behavior, as it is evidenced by the displacement ductility values and by the ratio between the performance point and the ultimate displacement.
- The nonlinear response of the buildings depends on the ratio between the seismic and gravity loads. The inner frames which are designed for lower ratios have lower overstrength values. Consequently, the seismic safety of the different frames is influenced by this ratio.
- The assessment of the seismic safety of the buildings demonstrates that low rise buildings reach higher damage states than the other studied buildings, when they are subjected to the demand prescribed by the elastic design spectrum. This fact is a consequence of the failure mechanism of the low rise buildings. The probability of damage is not sensitive to the span number of the frames.
- The proposed objective damage index predicts adequately the state of damage that is achieved by the frames for a specific seismic demand value (displacement of the performance point).

Acknowledgements

References

1. Mwafi, A.M. Elnashai, A. Overstrength and force reduction factors of multistory reinforced-concrete buildings, *Structural design of tall buildings*, **11**, 329-351, 2002.
2. Mwafi AM, Elnashai A. Calibration of force reduction factors of RC buildings, *Journal of Earthquake Engineering*, **6(2)**, 239-273, 2002
3. Sanchez, L. Plumier, A. Parametric study of ductile moment-resisting steel frames: a first step towards Eurocode 8 calibration, *Earthquake engineering and structural dynamics*, **37**, 1135-1155, 2008.
4. Comité Européen de Normalisation (CEN). *Eurocode 2: Design of concrete structures. BS EN 1992*, Brussels, 2001.
5. Comité Européen de Normalisation (CEN). *Eurocode 8: Design of Structures for Earthquake Resistance. EN 2004-1-1*, Brussels, 2003.
6. PLCd Manual. Non-linear thermo mechanic finite element oriented to PhD student education, code developed at CIMNE, Barcelona, Spain, 2009.
7. Oller, S. and Barbat, A. H. (2006). Moment-curvature damage model for bridges subjected to seismic loads, *Computer Methods in Applied Mechanics and Engineering*, **195**, 4490-4511, 2006.
8. Car, E., Oller, S. and Oñate, E. A large strain plasticity for anisotropic materials: Composite material application, *International Journal of Plasticity*, **17(11)**, 1437-1463, 2001.
9. Mata, P., Oller, S. and Barbat, A.H. Static analysis of beam structures under nonlinear geometric and constitutive behaviour, *Computer Methods in Applied Mechanics and Engineering*, **196**, 4458-4478, 2007
10. Mata, P., Oller, S. and Barbat, A. H. Dynamic analysis of beam structures under nonlinear geometric and constitutive behaviour, *Computer Methods in Applied Mechanics and Engineering*, **197**, 857-878, 2008.
11. Oller S, Onate E, Oliver J, Lubliner J. Finite element non-linear analysis of concrete structures using a plastic-damage model, *Engineering Fracture Mechanics*, **35(1–3)**, 219–31, 1990.
12. Lubliner, J. Oliver, J. Oller, S. Oñate, E. A plastic-damage model for concrete, *International Journal of Solids & Structures*, **25(3)**, 299–326, 1989
13. Barbat, A.H. Oller, S. Onate, E. Hanganu, A. Viscous damage model for Timoshenko beam structures, *International Journal of Solids & Structures*, **34(30)**, 3953–76, 1997.
14. Faleiro, J. Oller, S. Barbat, A.H. Plastic-damage seismic model for reinforced concrete frames, *Computer and Structures*, **86**, 581–97, and 2008.
15. Oller S., Car E., Lubliner J. Definition of a general implicit orthotropic yield criterion, *Computer Methods in Applied Mechanics and Engineering*, **192(7–8)**, 895–912, 2003.
16. Martinez, X. Oller, S. Rastellini, F. Barbat, A.H. A numerical procedure simulating RC structures reinforced with FRP using the serial/parallel mixing theory, *Computers and Structures*, **86**, 1604–1618, 2008.
17. Bayrak O., Sheikh SA. Plastic hinge analysis, *Journal of Structural Engineering*; **127**, 1092–100, 2004.
18. Spacone E, El-Tawil S. Nonlinear analysis of steel–concrete composite structures: State of the art, *Journal of Structural Engineering,* **126**, 159–68, 2000.
19. Shao Y, Aval S, Mirmiran A. Fiber–element model for cyclic analysis of concrete-filled fiber reinforced polymer tubes, *Journal of Structural Engineering,* **131**, 292–303, 2005.
20. Simo, J.C. A finite strain beam formulation. The three-dimensional dynamic problem. Part I. *Computer Methods in Applied Mechanic and Engineering*, 49:55–70, 1985.
21. Mander, J. B., Priestley, M.J. N. y Park, R. Observed stress-strain behaviour of confined concrete, *Journal of Structural Engineering*, **114**, 1827-1849, 1988.
22. Priestley, M.J.N. Calvi, G.M. Kowalsky, M.J. *Displacement-based seismic design of structures*. IUSS Press. Pavia, Italy, 2007.
23. Park, R. State-of-the-art report: ductility evaluation from laboratory and analytical testing, *Proceedings 9th WCEE, IAEE*, Tokyo-Kyoto, Japan, 605-616, 1988.

24. Barbat, A. H. Oller, S. Oñate, E. Hanganu, A. Viscous damage model for Timoshenko beam structures, *International Journal of Solids and Structures*, **34(30)**, 3953-3976, 1997.
25. Car, E., Oller, S. and Oñate, E. An anisotropic elastoplastic constitutive model for large strain analysis of fiber reinforced composite materials, *Computer Methods in Applied Mechanics and Engineering*, **185(2-4)**, 5-277, 2000.
26. Vielma, J. C. Barbat, A. H. Oller, S. Un índice de daño objetivo para la evaluación de los edificios de hormigón armado. *Hormigón y acero*. **248**, 53-64, 2007.
27. Vamvatsikos. D, Cornell, C.A. Incremental dynamic analysis, *Earthquake Engineering and Structural Dynamics*, **31(3)**, 491-514, 2002.
28. Kunnath, S. *Performance-based seismic design and evaluation of buildings structures. In: Chen W and Lui E (ed). Earthquake engineering for structural design*, CRC Press. Boca Raton, 2005.
29. Han, S.W. Chopra, A. Approximate incremental dynamic analysis using the modal pushover analysis procedure, *Earthquake Engineering and Structural Dynamics*, 35(3): 1853-1873, 2006.
30. Fajfar, P. A. Nonlinear Analysis Method for Performance Based Seismic Design, *Earthquake Spectra*, **16(3)**, 573-591, 2000.
31. SEAOC. *Vision 2000 Report on Performance Based Seismic Engineering of Buildings*, Structural Engineers Association of California, Volume I, Sacramento, California, 1995.
32. Vielma, J. C., Barbat, A. H. y Oller, S. Umbrales de daño para estados límite de edificios porticados de concreto armado diseñados conforme al ACI-318/IBC-2006, *Revista Internacional de Desastres Naturales, Accidentes e Infraestructura*, 8(2), 119-133, 2008.
33. Vielma, J. C. *Caracterización de la respuesta sísmica de edificios de hormigón armado mediante la respuesta no lineal*, PhD Thesis, Barcelona, **ISBN**: 978-84-691-3475-7, 2008.
34. Pinto, P.E. Giannini, R. Franchin, P. Seismic reliability analysis of structures. IUSS Press, Pavia, Italy. 2006.

Use of the disaster deficit index in the evaluation of the fiscal impact of future earthquakes

O.D. Cardona[1], M.G. Ordaz[2], M.C. Marulanda[3] and A.H. Barbat[4]

[1] *Professor, Instituto de Estudios Ambientales, Universidad Nacional de Colombia, Manizales, Colombia Email:* odcardonaa@unal.edu.co

[2] *Professor, Instituto de Ingeniería, Universidad Nacional Autónoma de México (UNAM), México DF. Email:* mors@pumas.iingen.unam.mx

[3] *Research Assistant, PhD. Student, Universidad Politécnica de Cataluña (UPC), Barcelona, Spain. Email:* mmarulan@cimne.upc.edu

[4] *Professor, Technical University of Catalonia, UPC, Barcelona, Spain Email:* barbat@cimne.upc.edu

ABSTRACT

The Disaster Deficit Index (DDI) measures disaster country risk from a macroeconomic and financial perspective, according to possible future catastrophic events. The DDI captures the relationship between the demand for contingent resources to cover the maximum probable losses and the public sector's economic resilience; that is, the availability of internal and external funds for restoring affected inventories. For calculating potential losses, the model follows the insurance industry in establishing a probable loss, based on the critical impacts during a given period of exposure, and for the economic resilience the model computes the country's financial ability to cope with the situation taking into account: the insurance and reinsurance payments; the reserve funds for disasters; the funds that may be received as aid and donations; the possible value of new taxes; the margin for budgetary reallocations; the feasible value of external credit; and the internal credit the country may obtain. Access to these resources has limitations and costs that must be taken into account as feasible values according to the macroeconomic and financial conditions. This paper presents the model of DDI and the results for fourteen countries of the Americas to design appropriate risk evaluation tools to guide the governmental decision making.

KEYWORDS: Disaster deficit, contingent liabilities, fiscal sustainability, seismic vulnerability.

1. INTRODUCTION

Disaster risk management requires measuring risk to take into account not only the expected physical damage, victims and economic equivalent loss, but also social, organizational and institutional factors. The difficulty in achieving effective disaster risk management has been, in part, the result of the lack of a comprehensive conceptual framework of disaster risk to facilitate a multidisciplinary evaluation and intervention. Most existing indices and evaluation techniques do not adequately express risk and are not based on a holistic approach that invites intervention. The various planning agencies dealing with the economy, the environment, housing, infrastructure, agriculture, or health, to mention but a few relevant areas, must be made aware of the risks that each sector faces. In addition, the concerns of different levels of government should be addressed in a meaningful way. For example, risk at the local level is very different from risk at the national level. Risk is most detailed at a micro-social or territorial scale. As we work at more macro scales, details are lost. However, decision making and information needs at each level are different, as are the social actors and stakeholders. If risk is not presented and explained in a way that attracts stakeholders' attention, it will not be possible to make progress in reducing the impact of disasters. This means that appropriate evaluation tools are necessary to make it easy to understand the problem and guide the decision-making process. It is fundamentally important to understand how vulnerability is generated, how it increases and how it builds up. Performance benchmarks are also needed to facilitate decision makers' access to relevant information as well as the identification and proposal of effective policies and actions.

A system of indicators is proposed to meet this need and to enable the depiction of disaster risk at the national level, allowing the identification of key issues by economic and social category. It also makes possible the creation of national risk management performance benchmarks in order to establish performance targets for improving management effectiveness. Four components or composite indicators were designed to represent the main elements of vulnerability and show each country's progress in managing risk. This paper presents one of them related to the macroeconomic potential impact: the *Disaster Deficit Index* (DDI). These indicators were developed by the Institute of Environmental Studies (IDEA in Spanish) of the National University of Colombia, in Manizales, for the Inter-American Development Bank, in the framework of its Program of Indicators for Disaster Risk and Risk Management in the Americas. Program reports, technical details and the application results for the countries in the Americas can be consulted at the following web page: http://idea.unalmzl.edu.co (Cardona 2005, IDEA 2005, Carreño et al. 2007a/b).

2. DISASTER DEFICIT INDEX

The DDI measures country risk from a macroeconomic and financial perspective according to possible catastrophic events. It requires the estimation of critical impacts during a given period of exposure, as well as the country's financial ability to cope with the situation. This index measures the economic loss that a particular country could suffer when a catastrophic event takes place, and the implications in terms of resources needed to address the situation. Construction of the DDI requires undertaking a forecast based on historical and scientific evidence, as well as measuring the value of infrastructure and other goods and services that are likely to be affected. The DDI captures the relationship between the demand for contingent resources to cover the losses, L_R^P, caused by the Maximum Considered Event (MCE),[1] and the public sector's economic resilience, R_E^P, that is, the availability of internal and external funds for restoring affected inventories[2]. Thus, DDI is calculated using Eqn 2.1, as follows:

$$DDI = \frac{L_R^P}{R_E^P} \qquad (2.1)$$

where

$$L_R^P = \varphi \, L_R \qquad (2.2)$$

L_R^P represents the maximum direct economic impact in probabilistic terms on public and private stocks that are governments' responsibility. The value of public sector capital inventory losses is a fraction φ of the loss of all affected goods, L_R, which is associated with an MCE of intensity I_R, and whose annual exceedance rate (or return period, R) is defined in the same way for all countries (i.e. return periods of 50, 100 and 500 years, whose probability during any 10 years exposure period is 18 percent, 10 percent and 2 percent, respectively). This total loss L_R, can be estimated as follows:

$$L_R = E \, V(I_R C_S) \, K \qquad (2.3)$$

where, E is the economic value of all the property exposed; $V(\ )$ is the *vulnerability function*; I_R is the intensity associated to the selected return period; C_S is a

---

[1] This model follows the insurance industry in establishing a reference point for calculating potential losses (ASTM, 1999) or the common concept of Probable Maximum Loss, PML, broadly used for risk evaluation of portfolios of buildings (Ordaz and Santa-Cruz, 2003).
[2] A similar approach estimating the resource gap has been proposed by Freeman et al. (2002b). In this report they say that being able to quickly access sufficient funds for reconstruction after a disaster is critical to a country's ability to recover with minimal long-term consequences.

coefficient that corrects intensities to account for local site effects; and K is a factor that corrects for uncertainty in the vulnerability function.

Economic resilience, R_E^P (the denominator of the index), is defined in the following equation:

$$R_E^{\ P} = \sum_{i=1}^{n} F_i^{\ P}$$

(2.4)

where F_i^P represents the possible internal and external resources that were available to the government, in its role as a promoter of recovery and as owner of affected goods, when the evaluation was undertaken. Access to these resources has limitations and costs that must be taken into account as feasible values according to the macroeconomic and financial conditions of the country. Figure 1 shows a diagram illustrating the way to obtain the DDI.
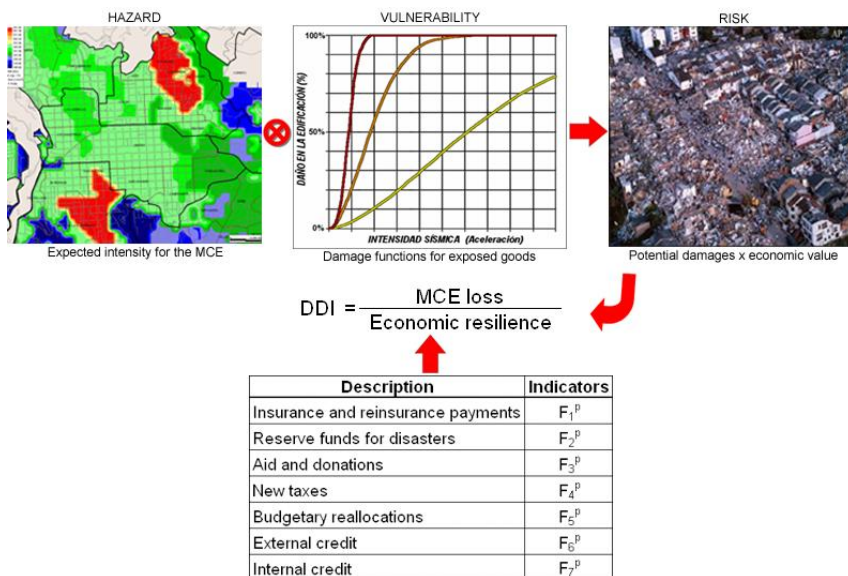
Figure 1 Diagram for DDI calculation

A DDI greater than 1.0 reflects the country's inability to cope with extreme disasters even by going into as much debt as possible. The greater the DDI, the greater the gap between losses and the country's ability to face them. If constrictions for additional debt exist, this situation implies the impossibility to recover. To help place the DDI in context, we have developed a complementary indicator, DDI', to illustrate the portion of a country's annual Capital Expenditure, E_C^P, that corresponds to the expected annual loss, Ly^P, or the pure risk premium.

That is, DDI' shows the percentage of the annual investment budget that would be needed to pay for future disasters.

$$DDI' = \frac{L_y^P}{E_C^P}$$

(2.5)

The pure premium value is equivalent to the annual average investment or saving that a country would have to make in order to approximately cover losses associated with major future disasters. Other DDI' was also estimated with respect to the amount of sustainable resources due to inter-temporal surplus, S_i^P. That is to say, the percentage the technical premium of potential savings at present values represents as expressed:

$$DDI' = \frac{L_y^P}{S_I^P}$$

(2.6)

The sustainable amount of resources due to inter-temporal surplus, S_i^P, is the saving which the government can employ, calculated over a ten year period, in order to best attend the impacts of disasters (IDEA 2005). What we need to know is if the government, from an orthodox perspective, complies with its inter-temporal budgetary restriction. That is to say, if the flows of expenditures and incomes guarantee –in present value terms– that current and future primary surpluses allow a canceling of the present stock of debt. In other words, financial discipline requires that government action be limited and that the financial capacity to deal with disasters must comply with the inter-temporal restriction of public finances. In the case that annual losses exceed the amount of resources available in the surplus it is predicted that over time there will be a debt due to disasters that inevitably increase the overall debt levels. That is to say, the country does not have sufficient resources to attend future disasters. In the case that restrictions to additional indebtedness should exist, this situation would signify that recovery is impossible. In general, if inter-temporal surplus is negative, premium payment would increase the existent deficit.

3. ESTIMATING PROBABLE LOSSES

The computation of losses during future natural hazard events (index numerator) is always a very complex problem. Due to the uncertainties of this process, losses must be regarded as random variables, which can only be known in a probabilistic sense, i.e. through their probability distributions. Consequently, this approach has been adopted in this model (Ordaz and Santa-Cruz, 2003). Given existing

knowledge, it is clearly theoretically impossible to predict the times of occurrence and magnitudes of all future natural hazard events. In view of the uncertain nature of the processes involved, our second best choice is to estimate the probability distribution of the times of occurrence and impacts of all future disasters. In general, however, this estimation is also a titanic task. A convenient way of describing the required probability distributions (those of the occurrence times and the sizes of the physical impact) is the use of the exceedance rate curve of the physical losses (Loss Exceedance Curve). This curve relates the value of the loss with the annual frequency with which this loss value is exceeded; the inverse of the exceedance rate is the return period. The PML curve is equivalent to the LEC. An example of this risk metric is depicted in the Figure 2.
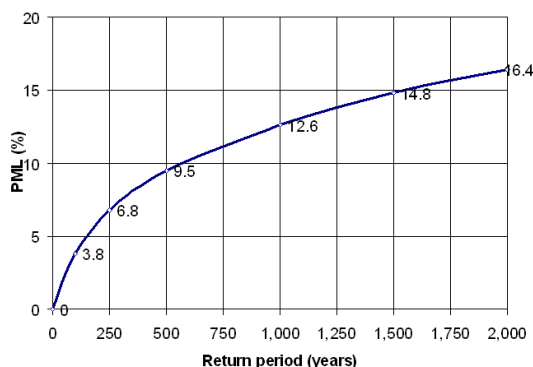
Figure 2 Example of a PML curve with the results for several return periods

There is a large body of work in the past decades on earthquake loss estimation and more recently with GIS; e.g. the ATC-13 (Applied Technology Council, 1985) and the HAZUS (FEMA, 1999) that have been considered outstanding methods. See also Coburn and Spence (1992) and the EERI Earthquake Spectra Loss Estimation Theme Issue (1997). See details of risk model in "Probabilistic seismic risk assessment for comprehensive risk management: Modeling for innovative risk transfer and loss financing mechanisms" by Cardona et al. in these proceedings.

3.1. Hazard

In this context, *intensity* is defined as a local measure of the disturbance produced by a natural event in those physical characteristics of the environment relevant to the phenomenon under study. For all types of hazards, it is almost impossible to describe the intensity with a single parameter. For instance, when dealing with earthquake hazards, the peak ground acceleration gives some general information about the size of the ground motion, but does not give indications about its

frequency content. This is crucial for an accurate estimation of structural response. In view of this, it is understood that a single-parameter description of intensity will always be incomplete. However, a multi-variable description of intensity is far too complex for our goals (actually, very few, if any risk studies undertaken in the past, have considered multi-variable descriptions of intensity). We propose to use a single measure of intensity for each type of hazard that correlates well with damage and for which hazard measures are relatively easy to obtain. It should be noted that since we are mainly interested in disasters that have an economic impact at the national level, we have restricted ourselves to those hazards that produce large, immediate economic losses, like earthquakes or hurricanes. Other hazards, like landslides, are extremely important at local level, and historically have produced many victims. However, their economic impact has been very limited. Slow on-set disasters, like drought, are also very important, but their economic impacts are deferred over time. As these do not have immediate effects, they are beyond the scope of the proposed estimation model.

In many cases, hazard estimations are obtained from regional studies, or by assuming average environmental conditions. For example, seismic hazard maps are usually produced assuming average firm soil conditions, i.e. assuming that there are no significant amplifications of seismic intensity due to soft soils. Also, wind velocity maps are generally produced assuming average exposure conditions, that is, velocities are not obtained for sites on hills, but for reference sites. However, for each type of hazard, particular environmental characteristics may exist in the cities under study that cause intensities to be larger or smaller than the intensities in the neighborhood. In other words, environmental characteristics may exist that differ from those corresponding to the standard characteristics used in hazard evaluation. These characteristics are known as *local site conditions*, and they give rise to *local site effects*. In the framework of the present project, the local site effects in all cities and for all types of hazards are impossible to take into account in any accurate manner. Our first rough approach would be to simply ignore the site effects. However, there are cases in which the local site effects cannot be disregarded. Since by definition these site effects are local, it would be impossible for us to give general rules for values of C_S for all cities and types of hazard. In our view, appropriate values would have to be assigned by the local experts who participate in the loss estimations for different countries. Once an appropriate intensity is chosen for each type of phenomenon, a probabilistic hazard description must be given. Usually, the hazard is expressed in terms of the exceedance rates of intensity values. It must be noted that, for our purposes, we require *local* indications of hazard, that is, exceedance rates of intensity at the points or cities of interest (one of our assumptions is that all property in a city is concentrated in a point or in a geographical area of limited size). In principle, a hazard curve must be constructed for every type of hazard and every city under study. However, recalling Eqn 2.3, it

is needed just a few points of this curve, namely those intensities associated to the selected return periods. In the case of seismic hazard the intensity is calculated taking into account the sum of effects of all seismic sources located in a certain influence area. Hazard expressed in terms of exceedance rates of the peak accelerations for firm soil, a, is calculated through the following expression (Esteva 1970):

$$v(a) = \sum_{i=1}^{i=N} \int_{M_0}^{M_u} -\frac{\partial \lambda}{\partial M} \Pr(A > a \,|\, M, R_i) dM$$

(3.1)

where the sum includes all the seismic sources, N, and $Pr(A>a|M,R_i)$ is the probability of the intensity exceeding a certain value, given the earthquake's magnitude, M, and the distance between the ith source and the site, R_i. The $\lambda(M)$ function represents the activity rates of the seismic sources. The integration is done from M_0 to M_u, which indicates that the contribution of all magnitudes is taken into account for each seismic source. It is important to note that the previous equation would be exact if the seismic sources were points. In reality, they are volumes, therefore the epicenters cannot only occur in the centers of the sources, but can also occur, with equal probability, in any point inside the corresponding volume. Supposing that the intensity variable has a lognormal distribution given the magnitude and distance, the probability $Pr(A>a|M, R_i)$ is calculated in the following way:

$$\Pr(A > a \,|\, M, R) = \Phi\left[\frac{1}{\sigma_{\ln a}} \ln \frac{MED(A \,|\, M, R)}{a}\right]$$

(3.2)

being $\Phi(\cdot)$ the standard normal distribution, $MED(A/M, R_i)$ the median value of the intensity variable (given by the corresponding attenuation law) and σ_{Lna} the standard deviation of the natural logarithm of a. In Eqn 3.1and Eqn 3.2 both the attenuation law and its uncertainty are included. The seismic hazard is expressed in terms of the exceedance rates of given values of seismic intensity. The seismic intensity, a, refers to the pseudo acceleration response spectra ordinates for a 5% of critical camping for a given structural period, T. Once the attenuation laws are calculated for different structural periods, it is possible to determine uniform hazard spectra for a specific site, based on the calculated intensity value (acceleration) for a fixed return period.

3.2. Vulnerability

As indicated in Eqn 2.3, $V(I)$ is the vulnerability function, which relates the intensity of the event, I, with the expected fraction of the value that is lost if an event of such intensity takes place.
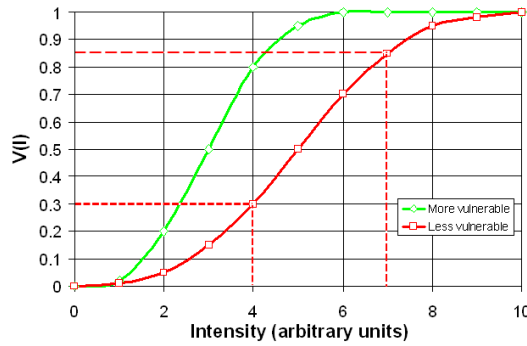
Figure 3. Representation of vulnerability functions

Vulnerability functions usually have shapes like that shown in Figure 3. A building is said to be *more vulnerable* than another if greater damage is expected in the former than in the latter given similar hazard intensities. Vulnerability functions are highly hazard-specific. In other words, in the same city, buildings and infrastructure might be very vulnerable to a certain hazard and much less vulnerable to another. As defined, vulnerability functions might change depending on technological, educational, cultural and social factors. For instance, for the same seismic intensity, buildings in a city might be more vulnerable than buildings in another city due to higher dissemination of construction technology or application of seismic-resistant design in the latter. In rigor, vulnerability functions should be expressed in the following way:

$$V(I) = V(I; \phi) \tag{3.3}$$

where ϕ is a set of parameters that will be denoted as vulnerability factors. In fact, it is through these factors that the effects of prevention can be appreciated, and their economic impact can be assessed. Consider, for instance, that the vulnerability curves correspond to earthquake hazard. Here it is conceivable that the application of seismic-resistant design in a city (a change in one of the vulnerability factors) could move the vulnerability function from the "more vulnerable" to the "less vulnerable" case of Figure 3. Usually, the costs of development, implementation and enforcement of seismic regulations would be much less than the amount saved by reducing the vulnerability, so improving the design practices would be a sound decision even from the economic point of view. A discussion about probabilistic benefit-cost ratio is presented in the paper "Probabilistic seismic risk assessment for comprehensive risk management: modeling for innovative risk transfer and loss financing mechanisms" of Cardona et al. of these proceedings.

As it may be noted in the preceding paragraphs, we always refer to $V(I; \phi)$ as being related to the *expected* damage, that is, to the expected value (in the

probabilistic sense) of the damage. Due to the uncertainties involved, it is impossible to deterministically predict the damage resulting from an event with a given intensity. Thus, we try to predict its expected damage with $V (I; \phi)$, keeping in mind that there are uncertainties that cannot be neglected. There are, of course, rigorous probabilistic ways to account for this uncertainty. One way of solving this problem is to find a factor, that we call K (Eqn 2.3), which relates the loss estimator that would be obtained accounting for the uncertainty with the loss estimators obtained disregarding this uncertainty. Factor K depends on several things: the uncertainty in the vulnerability relation, the shape of the intensity exceedance rate curve, and the return period. We have found that, under reasonable hypotheses, a factor of $K=1.2\sim1.3$ is reasonable for our goals.[3] The vulnerability functions can be expressed analytically using:

$$V(I) = 1 - \exp\left\{ \ln 0.5 \left(\frac{I}{\gamma} \right)^{\alpha} \right\}$$

(3.4)

where α and γ are parameters that define the shape of the function. Table 3.1 shows some values of α and γ for some building constructions (Ordaz and Santa-Cruz, 2003).

Table 3.1 Parameters for some vulnerability functions

Construction class	α	γ
Non reinforced masonry	5.0	0.25
Confined masonry	5.5	0.50
Reinforced concrete frames	3.0	0.40

So far, our analysis has been restricted to estimate losses in cities or regions of limited geographical size. The key to the definition of "limited geographical size" is our hypothesis that everything within the city is affected simultaneously by the event under study. In reality, damage during disasters varies, sometimes widely, even within a city, so our hypothesis hardly, if ever, holds. But, this assumption has to be made for the sake of simplicity. However, for extensive regions, comprising several cities, perhaps hundreds of kilometers apart, it would be extremely risky to assume that everything is affected simultaneously. In view of this, we have to derive ways to combine the computed loss estimators for each city in order to obtain a reasonable combined estimator for the whole country. We shall call these

---

[3] Note that if a constant factor $K=1.2$ is used for all countries, cities and types of hazard then it becomes irrelevant for comparison purposes. However, we prefer to deal with K explicitly for two reasons. The first is of symbolic nature: it helps to keep in mind that our estimation process is uncertain and that we must account for uncertainty in a formal way. The second reason is that, as defined, our loss estimators have a clear meaning: they are economic losses, measured in monetary units. Thus, their scale is relevant.

rules the *aggregation rules*. IDEA (2005) presents details about the mathematical relations between the exceedance rates and other interesting and useful measures of risk; the rigorous probabilistic ways to account for the vulnerability uncertainty and the derivation on the loss-aggregation rules proposed.

4. RESOURCES POTENTIALLY AVAILABLE

Economic resilience (the denominator of the index, see Eqn. 2.4) represents internal and external resources that were available to the government when the evaluation was undertaken. Seven constraints are explicitly taken into consideration in this study: *Insurance and reinsurance payments* (F_1^P) that the country would approximately receive for goods and infrastructure insured by government; *Disaster reserve funds* (F_2^P) that the country has available during the evaluation year; public, private, national or international *aid and donations* (F_3^P); *New taxes* (F_4^P) that the country could collect in case of disasters; *Budgetary reallocations* (F_5^P) which usually corresponds to the margin of discretional expenses available to the government; *External credit* (F_6^P) that the country could obtain from multilateral organisms and in the capital market; and *Internal credit* (F_7^P) the country may obtain from commercial banks as well as the central bank. IDEA (2005) presents a method for estimating taxes on financial transactions. In addition, it presents a model for calculating the external financial situation of a country and the access to internal credit taking into account the associated uncertainties. It is important to indicate that this estimation is proposed considering restrictions or feasible values and without considering possible associated costs of access to some of these funds and opportunity costs which could be important. Figures 4 and 5 present the application results for some countries in the Americas (Cardona 2005; Carreño et al. 2005, IDEA 2005).
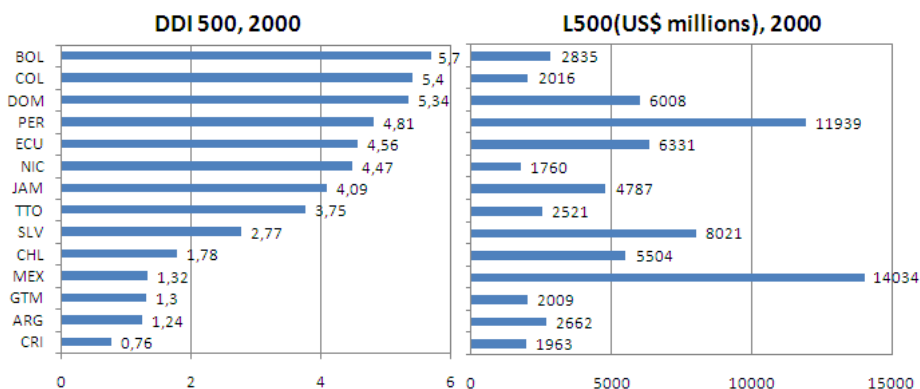
Figure 4 DDI and Probable Maximum Loss in 500 Years
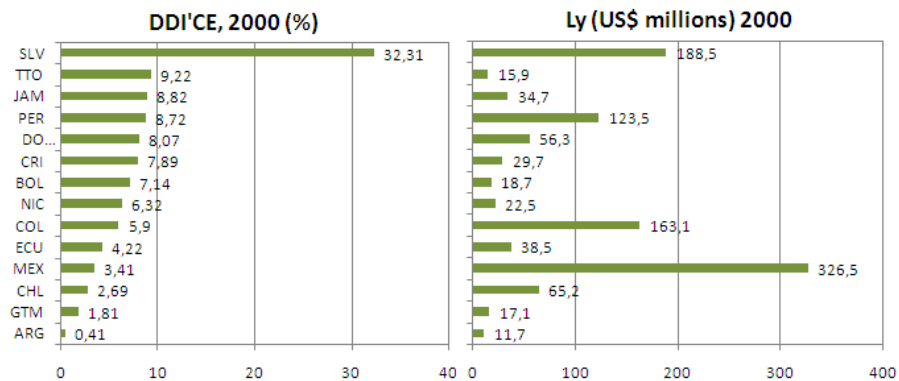
Figure 5 DDI$_{CE}$' and Annual Probable Loss

5. CONCLUSIONS

These indicators provide a simple way of measuring a country's fiscal exposure and potential deficit (or contingency liabilities) in case of an extreme disaster. They allow national decision makers to measure the budgetary implications of such an event and highlight the importance of including this type of information in financial and budgetary processes. These results substantiate the need to identify and propose effective policies and actions such as, for example, using insurance and reinsurance (transfer mechanisms) to protect government resources or establishing reserves based on adequate loss estimation criteria. Other such actions include contracting contingency credits and, in particular, the need to invest in structural retrofitting and rehabilitation, and nonstructural prevention and mitigation, to reduce potential damage and losses as well as the potential economic impact of disasters. The approach proposed here is fundamentally a probabilistic risk model similar to those used for loss transfer and retention aims. Due to this, it is substantially different to that used by UNDP (2004), to estimate the Disaster Risk Index, DRI, or at *Hot Spots* project of World Bank (2004), and to those applied in the majority of the models proposed for estimating the impact of disasters on economic growth. The present approach was chosen given that serious theoretical controversies still exist in terms of whether disasters cause a significant impact on economic development. According to the results obtained by Albala-Bertrand (1993, 2002) disasters usually affect the less productive capital and unskilled labor. Therefore, while leading to profound social consequences, they have little effect on the macro economy of a country. Similar models have been formulated by IIASA and Freeman et al. (2002a/b). Benson et al. (2003) and ECLAC (2003) amongst others, argue that in the long run such impacts may be important for certain economies. IDEA (2005) presents an analytical approach

about growth and disasters. It concludes that disasters may reduce the savings level in society and thus the amount of capital and product per person in the stationary state, i.e. recurrent and random disasters affect per capita income and growth rates in the long term.

REFERENCES

1. Albala-Bertrand, J.M. (1993) "Natural Disaster Situations and Growth: A Macroeconomic Model for Sudden Disasters Impacts", *World Development* **21:9**, 1417-1434.
2. Albala-Bertrand, J.M (2002) Urban Disasters and Globalization, in *The Future of Disaster Risk: Building Safer Cities.* Conference organized by the ProVention Consortium. DMF, World Bank. Available   at:
   http://www.proventionconsortium.org/conferences/washington_agenda.htm
3. ASTM (1999) Standard Guide for the Estimation of Building Damageability in Earthquakes, E 2026-99.
4. ATC (1985) Earthquake Damage Evaluation Data for California, ATC-13 (FEMA), Applied Technology Council, Redwood City, CA.
5. Benson, C. (2003) The Economy-wide Impact of Natural Disasters in Developing Countries, London University.
6. Cardona, O.D. (2005) Indicators of Disaster Risk and Risk Management: Program for Latin America and the Caribbean, Summary Report, IDB/IDEA Program of Indicators for Disaster Risk Management, National University of Colombia, Manizales. Available at:
   http://idea.unalmzl.edu.co
7. Carreño, M.L, Cardona, O.D., Barbat, A.H. (2005) *Sistema de indicadores para la evaluación de riesgos*, Monografía CIMNE IS-52, Universidad Politécnica de Cataluña, Barcelona.
8. Carreño, M.L, Cardona, O.D., Barbat, A.H. (2007a) A disaster risk management performance index, *Journal of Natural Hazards*, **41:1**, 1-20, The Netherlands: Springer.
9. Carreño, M.L, Cardona, O.D., Barbat, A.H. (2007b) Urban Seismic Risk Evaluation: A Holistic Approach, *Journal of Natural Hazards* **40:1**, 137-172, The Netherlands: Springer.
10. Coburn, A. & Spence, R. (1992) *Earthquake Protection* (John Wiley & Sons Ltd, Chichester, UK.)
11. ECLAC (2003) Manual para la estimación de los efectos socio-económicos y ambientales de los desastres. Economic Commission for Latin American and the Caribbean and World Bank, four volumes, Washington.
12. EERI (1997) *Earthquake Spectra, Theme issue: Loss Estimation*, **13:4**, Oakland.
13. Esteva, L. (1970) *Regionalización sísmica de México para fines de ingeniería*, Serie Azul 246, Instituto de Ingeniería, UNAM, México.
14. FEMA (1999) *Earthquake Loss Estimation Methodology, HAZUS*, National Institute of Building Science for Federal Emergency Management Agency, Washington.
15. Freeman, P.K., Martin, L.A., Mechler, R., & Warner, K. (2002a) "Catastrophes and Development: Integrating Natural Catastrophes into Development Planning", *Disaster Risk Management Working Paper Series No. 4.* World Bank, Washington.
16. Freeman, P.K., Martin, L.A., Linneroot-Bayer, J., Mechler, R., Pflug G. & Warner, K. (2002b) Disaster Risk Management: National Systems for the Comprehensive Management of Disaster Financial Strategies for Natural Disaster Reconstruction, SDD/IRPD, Regional Policy Dialogue, Inter-American Development Bank, IDB, Washington.
17. IDEA (2005) System of Indicators for Disaster Risk Management: Program for Latin American and the Caribbean, Main Technical Report, IDB/IDEA Program of Indicators for Disaster Risk Management, National University of Colombia, Manizales. Available at: http://idea.unalmzl.edu.co

18. Ordaz, M. & Santa-Cruz, S. (2003) <u>Computation of physical damage to property due to natural hazard events, IDB/IDEA Program of Indicators for Risk Management, National University of Colombia, Manizales. Available at: http://idea.unalmzl.edu.co</u>

19. UNDP (2004) International Patterns of Risk, the Disaster Risk Index, DRI Reducing, in *Disaster Risk: A Challenge for Development. A Global Report*, Geneva. Available at: <u>http://www.undp.org/bcpr/disred/rdr.htm</u>

20. World Bank (2004) *Identification of global natural disaster risk hotspots*, Center for Hazard and Risk Research at University of Columbia, Washington.

Holistic evaluation of the seismic urban risk using the fuzzy sets theory

M.L. Carreño[1], O.D. Cardona[2] and A.H. Barbat[3]

[1]International Center of Numerical Methods in Engineering, Barcelona, Spain
[2]National University of Colombia, Manizales
[3]Technical University of Catalonia, Barcelona, Spain

Abstract

Risk is defined, for management purposes, as the potential economic, social and environmental consequences of hazardous events that may occur in a specified period of time. From the perspective of this paper, risk requires a multidisciplinary evaluation that takes into account not only the expected physical damage, the number and type of casualties or economic losses, but also the conditions related to social fragility and lack of resilience conditions, which favour the second order effects when a hazard event strike an urban centre. The proposed general method of urban risk evaluation uses the fuzzy sets theory in order to manage qualitative concepts and variables involved in the evaluation. Finally, the method is applied in its single hazard version to the holistic seismic risk evaluation for the cities of Barcelona (Spain) and Bogotá (Colombia).

KEYWORDS: holistic approach, risk evaluation, seismic risk, socio-economic vulnerability.

1. INTRODUCTION

For management purposes, risk can be defined as the potential economic, social and environmental consequences of hazardous events that may occur in a specified period of time. However, in the past, in many cases the concept of risk has been defined in a fragmentary way, according to each scientific discipline involved in its appraisal [1]. Based on the formulation of the disaster risk [2] several methodologies for risk assessment have been developed from different perspectives in the last decades. From a holistic perspective, risk requires a multidisciplinary evaluation that takes into account not only the expected physical damage, the number and type of casualties or economic losses (first order impact), but also the conditions related to social fragility and lack of resilience conditions, which favour the second order effects (indirect impact) when a seismic hazard event strikes an urban centre [3,4,5] (see Figure 1).

Cardona in 2001 [6] developed a conceptual framework and a model for risk analysis of a city from a holistic perspective. It considers both "hard" and "soft" risk variables of the urban centre, taking into account exposure, socio-economic characteristics of the different localities (units) of the city and their disaster coping capacity or degree of resilience. One of the objectives of the model was to guide the decision-making in risk management, helping to identify the critical zones of the city and their vulnerability from different professional disciplines. Carreño in 2006 [7], developed an alternative method for Urban Risk Evaluation, starting from Cardona's model [6,8], in which urban risk is evaluated using composite indicators or indices. Expected building damage and losses in the infrastructure, obtained from loss scenarios, are basic information for the evaluation of a physical risk index in each unit of analysis. Often, when historical information is available, the seismic hazard can be usually identified and thus the most potential critical situation for the city. This paper proposes a new method using the fuzzy sets theory in order to have a more flexible tool in cases were the information is not available or incomplete.

The holistic evaluation of risk is achieved affecting the physical risk with an aggravation coefficient, obtained from contextual conditions, such as the socio-economic fragility and the lack of resilience, that aggravate initial physical loss scenario. Available data for these conditions at urban level are necessary to apply the method. Figure 1 shows the theoretical framework of the model.
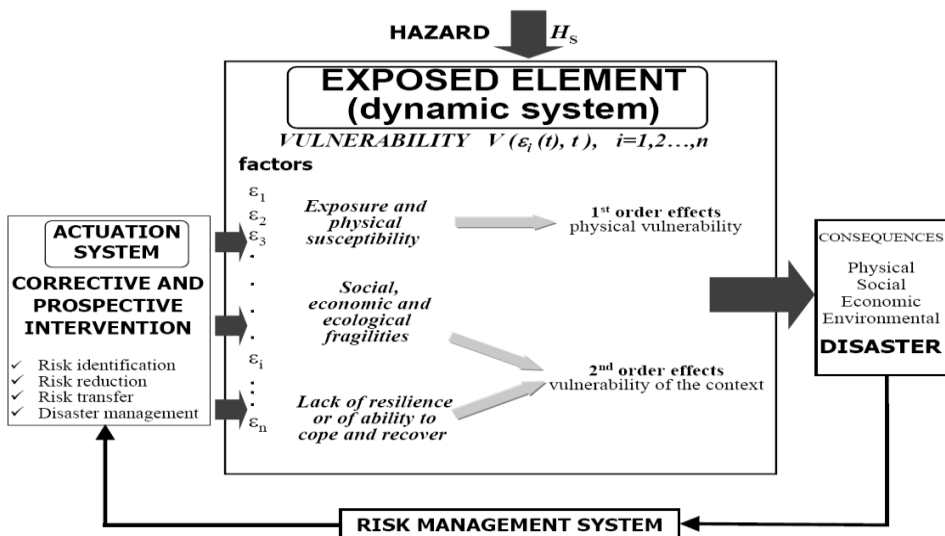
Figure 1: Theoretical Framework and Model for a Holistic Approach to Disaster Risk Assessment and Management. Adapted from [3,9,10,11]. Where, i is the severity of the event, V is the vulnerability, and ε_i are the vulnerability factors.

Using the meta-concepts of the theory of control and complex system dynamics, to reduce risk it is necessary to intervene in a corrective and prospective way the vulnerability factors. Then risk management requires a system of control (institutional structure) and an actuation system (public policies and actions) to implement the changes needed on the exposed elements or complex system where risk is a socio-environmental process.

2. HOLISTIC EVALUATION METHODOLOGY

The main objective of the proposed methodology is to measure seismic risk from an integrated and comprehensive perspective and to guide decision-making identifying the main multidisciplinary factors of vulnerability to be reduced or intervened. The first step of the method is the evaluation of the potential physical damage as the convolution of the seismic hazard and the physical vulnerability of buildings and infrastructure. Subsequently, a set of social context conditions that aggravate the physical effects are also considered. According to this procedure, a physical risk index and level are obtained, for each unit of analysis, from the existing loss scenarios, whereas the total risk index is obtained affecting the physical risk by aggravation conditions based on variables associated with the socio-economic conditions of each unit of analysis.

The proposed holistic evaluation method of risk uses a set of input variables, herein denominated descriptors. They reflect the physical risk and the aggravating conditions that contribute to the potential impact. Those descriptors are obtained from the loss scenarios and from socio-economic and coping capacity information of the exposed context [12].

Figure 2 shows the process of calculation of the total risk R_T for the units of analysis, starting from the descriptors of physical risk, X_{RFi}, and the descriptors of the aggravating coefficient F, X_{FSi} and X_{RFi}, using the weights w_{RFi}, w_{FSi} and w_{FRi} of each descriptor. These weights take values according to the expert opinion for each studied city applying the Analytic Hierarchical Process (AHP) [7,13].

The process is reflected in the following equation

$$R_T = R_F(1 + F)$$

(1)

expression known as the Moncho's Equation in the field of disaster risk indicators, where R_T is the total risk index, R_F is the physical risk index and F is the aggravating coefficient. This coefficient, F, depends on factors related to the socio-economic fragility, FS, and the lack of resilience of the exposed context, FR.

A qualification for each descriptor is obtained by means of fuzzy sets (L_{RFi} or L_{Fi}) (see reference [14]). Membership functions for five levels of physical risk and

aggravation are defined for each physical risk and aggravation descriptor, based on expert opinion. Figure 3 shows the membership functions for the fuzzy sets corresponding to the predefined physical risk levels of the *damaged area*. Using this type of functions, a physical risk index and qualification is obtained by means of the union and subsequent defuzzification, applying the method of the centroid of area (COA) of the group of descriptors (see Equations 2 and 3).

$$\mu_{RF}\left(X_{RFi}\right) = \max\left(w_{RF1} \times \mu_{LRFi}\left(L_{RF1}\right),...,w_{RFi} \times \mu_{LRF_i}\left(L_{RFi}\right)\right) \tag{2}$$

$$R_F = \left\lfloor \max\left(w_{RF1} \times \mu_{LRFi}\left(L_{RF1}\right),...,w_{RFi} \times \mu_{LRF_i}\left(L_{RFi}\right)\right)\right\rfloor_{centroid} \tag{3}$$

The aggravation factor, *F*, is evaluated by means of a similar process (see Equations 3 and 4); Figure 4 and 5 show examples of the membership functions used for the social fragility and lack of resilience descriptors corresponding to the aggravation level of *mortality rate* and *hospital beds*.

$$\mu_F\left(X_{FSi}, X_{FRi}\right) = \max\left(w_{FSi} \times \mu_{LF1}\left(L_{Fi}\right),...,w_{FRi} \times \mu_{LF_i}\left(L_{Fi}\right)\right) \tag{3}$$

$$F = \left\lfloor \max\left(w_{FSi} \times \mu_{LF1}\left(L_{F1}\right),...,w_{FRi} \times \mu_{LFi}\left(L_{Fi}\right)\right)\right\rfloor_{centroid} \tag{4}$$

X_{RF1}	Damaged area	w_{RF1}
X_{RF2}	Dead people	w_{RF2}
X_{RF3}	Injured people	w_{RF3}
X_{RF4}	Damage in water mains	w_{RF4}
X_{RF5}	Damage in gas network	w_{RF5}
X_{RF6}	Fallen lengths on HT power lines	w_{RF6}
X_{RF7}	Electricity substations affected	w_{RF7}
X_{RF8}	Electricity substations affected	w_{RF8}

➡ R_F Physical risk

➡ R_T Total risk

X_{FS1}	Slums-squatter neighbourhoods	w_{FS1}
X_{FS2}	Mortality rate	w_{FS2}
X_{FS3}	Delinquency rate	w_{FS3}
X_{FS4}	Social disparity index	w_{FS4}
X_{FS5}	Population density	w_{FS5}
X_{FR1}	Hospital beds	w_{FR1}
X_{FR2}	Health human resources	w_{FR2}
X_{FR3}	Public space	w_{FR3}
X_{FR4}	Rescue and firemen manpower	w_{FR4}
X_{FR5}	Development level	w_{FR5}
X_{FR6}	Emergency planning	w_{FR6}

➡ F Aggravation

Figure 2: Descriptors of the physical risk, social fragility and lack of resilience and their weights.

Finally, the total risk is calculated applying a fuzzy rule base to the obtained qualifications of physical risk and aggravation. The used fuzzy rule base is shown in Table 1.

This method has the advantage that in case of unavailable or incomplete information, this can be replaced by the opinion of local experts of the studied city.

The proposed methodology has been applied to the cities of Barcelona, Spain and Bogotá, Colombia. The following section shows the obtained results.

Table 1: Fuzzy rule base used to evaluate the Total Risk.

Aggravation / Physical risk	Low	Medium-low	Medium-high	High	Very high
Low	Low	Low	Medium-low	Medium-low	Medium-low
Medium-low	Medium-low	Medium-low	Medium-high	Medium-high	Medium-high
Medium-high	Medium-high	Medium-high	High	High	Very high
High	High	High	Very high	Very high	Very high
Very high	Very high	Very high	Very high	Very high	Very high
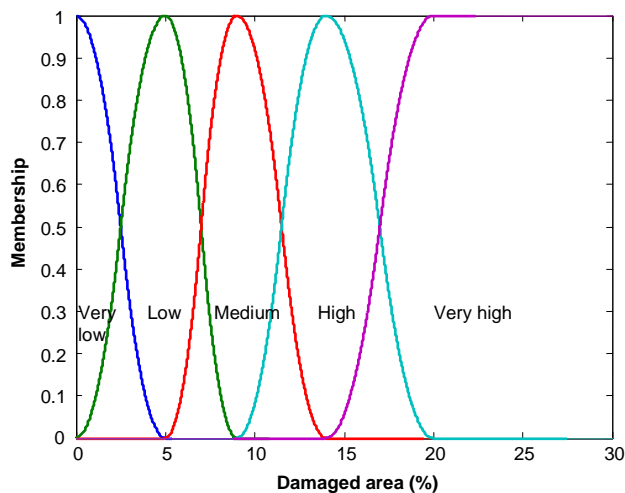
Figure 3: Membership functions for physical risk levels by *damaged area*.
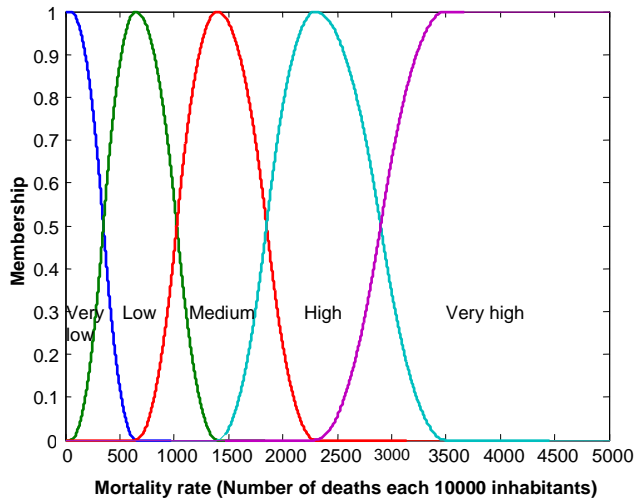
Figure 4: Membership functions for different aggravation levels by *mortality rate*.
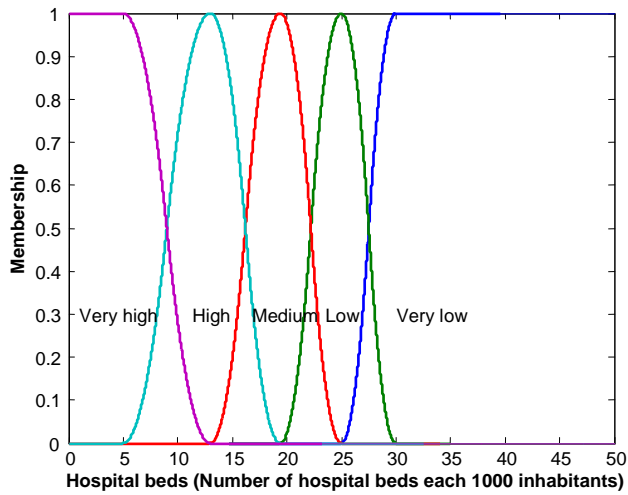
Figure 5: Membership functions for the aggravation levels by *hospital beds*.

3. CASES OF STUDY

3.1 Barcelona, Spain

The city of Barcelona, Spain, is subdivided in ten districts (see Figure 6), which are directed by a Mayor. The districts have management competences in subjects like urbanism, public space, infrastructure maintenance, etc. They are: Ciutat Vella, Eixample, Sants-Montjuïc, Les Corts, Sarrià-Sant Gervasi, Gràcia, Horta-Guinardó, Nou Barris, Sant Andreu and Sant Martí. The districts are subdivided in 38 neighbourhoods or large statistical zones. Barcelona is also subdivided in 248 small statistical zones (ZRP). The physical risk index was calculated from a probabilistic risk scenario developed in the framework of the Risk-UE project [15,16,17,18,19]. This scenario was calculated considering the 248 small ZRP zones. The impact factor was calculated by district, due to the availability of data at this level only.

Figure 7 shows the obtained physical risk levels obtained for the 248 ZRP of Barcelona, were the most part of the city has a medium-low physical risk level, and the rest has a medium-high physical risk level. Figure 8 shows the results of the aggravating coefficient for each district of Barcelona. Figures 9 and 10 show the results of the aggravating coefficient and the corresponding aggravation level for the district of the city of Barcelona.

The total risk levels obtained are shown in Figure 11, were the areas of Barcelona correspond to high and medium-high level of total risk.
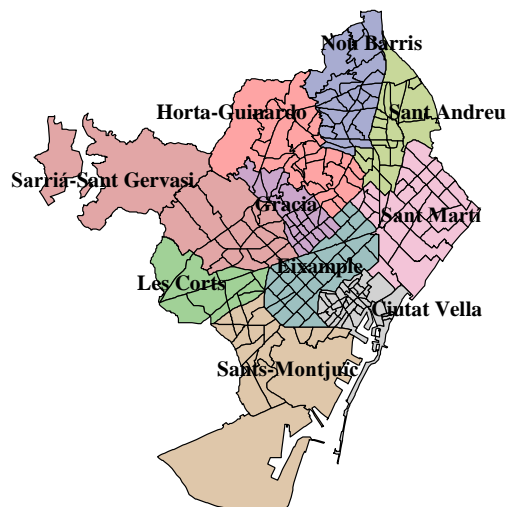
Figure 6: Territorial division of Barcelona.
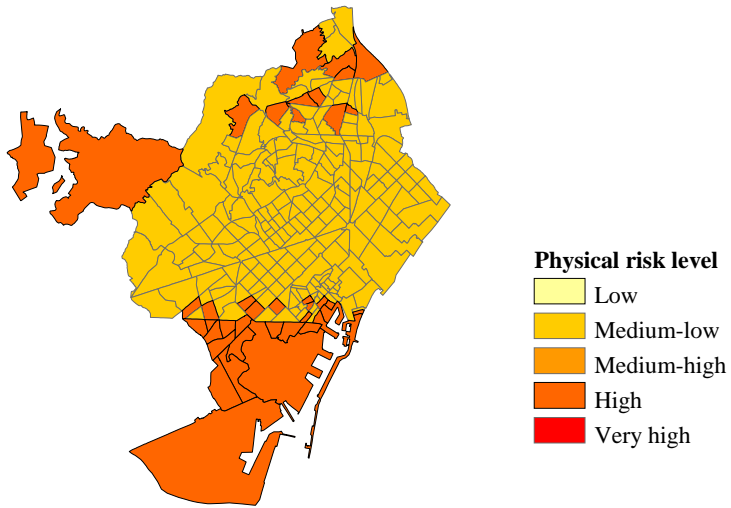
Figure 7: Physical risk levels of Barcelona
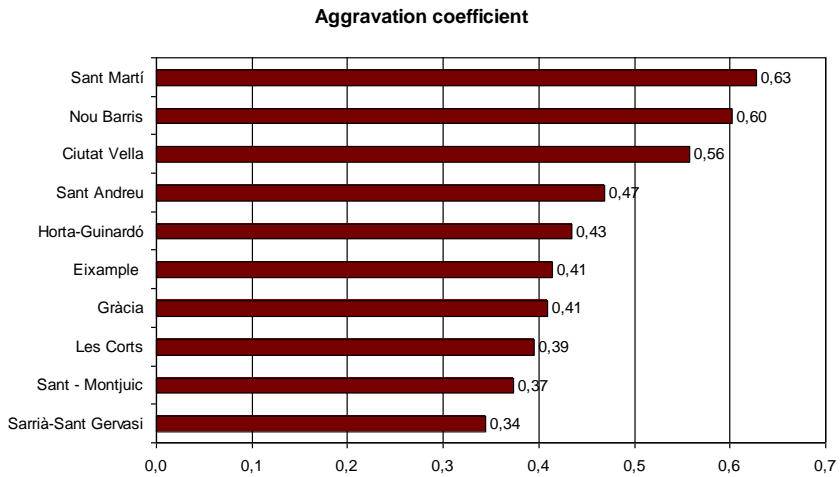
Figure 8: Aggravation coefficient of Barcelona's districts
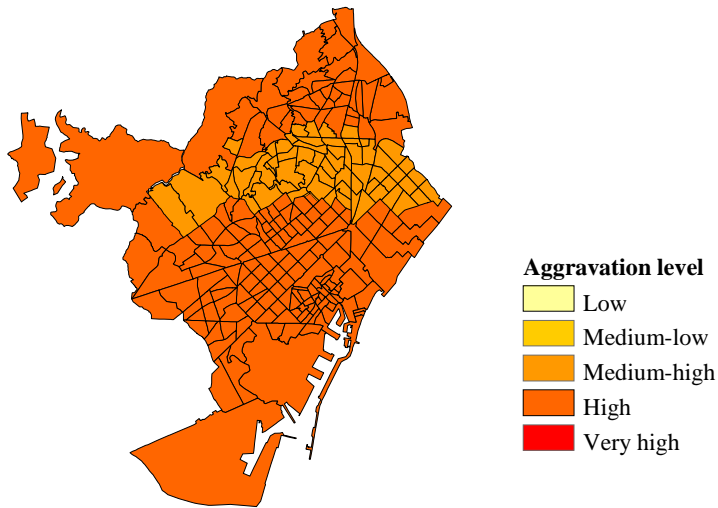
Figure 9: Aggravation level of the districts of Barcelona.
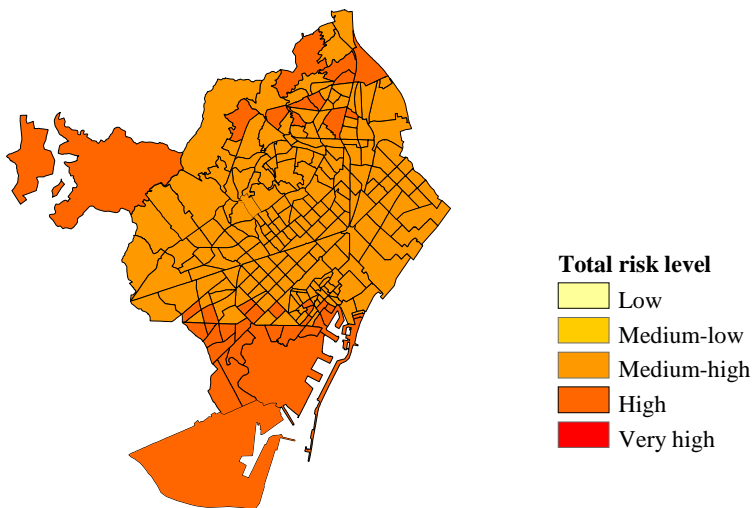
Figure 10: Total risk levels of Barcelona.

3.2 Bogota, Colombia

In Bogotá, the capital of Colombia, the localities are political-administrative subdivisions of the urban territory, with clear competences in financing and application of resources. They were created with the objective of attending in an effective way the necessities of the population of each territory. Since 1992,

Bogotá has 20 localities which can be seen in Figure 11: Usaquén, Chapinero, Santafé, San Cristóbal, Usme, Tunjuelito, Bosa, Ciudad Kennedy, Fontibón, Engativa, Suba, Barrios Unidos, Teusaquillo, Mártires, Antonio Nariño, Puente Aranda, Candelaria, Rafael Uribe, Ciudad Bolívar y Sumapaz. In this study, only 19 of these localities are considered, because the locality of Sumapaz corresponds to the rural area.

Figure 12 shows the obtained physical risk levels obtained for the 117 UPZs of Bogota beased on an existent scenario [20]. Figure 13 shows the results of the aggravating coefficient for each locality of Bogota. The obtained results of the aggravation coefficient for the localities of Bogota correspond to the high level of aggravation; this means that although the localities have several differences, in average, the aggravation due to the lack of resilience and the social fragilities is similar. Figure 14 shows the results of total risk.
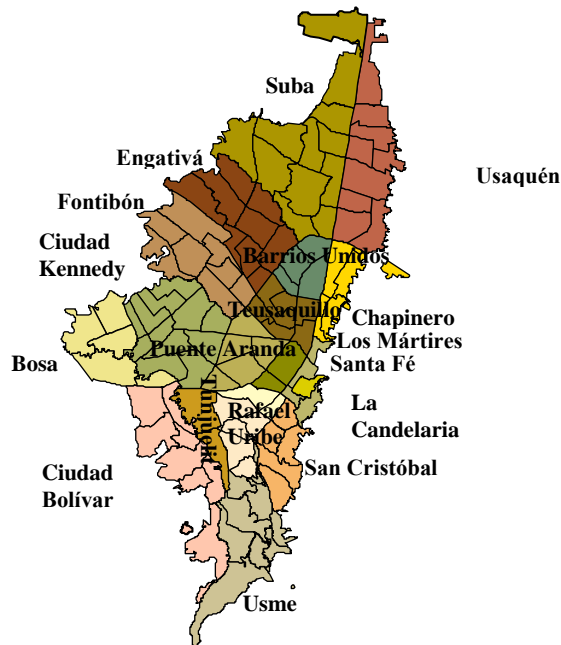
Figure 11: Political-administrative division of Bogotá, Colombia.
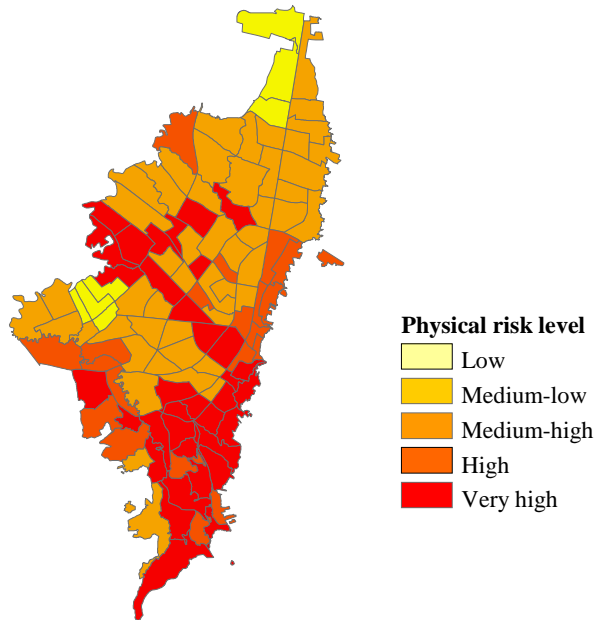
Figure 12: Physical risk levels for Bogota.
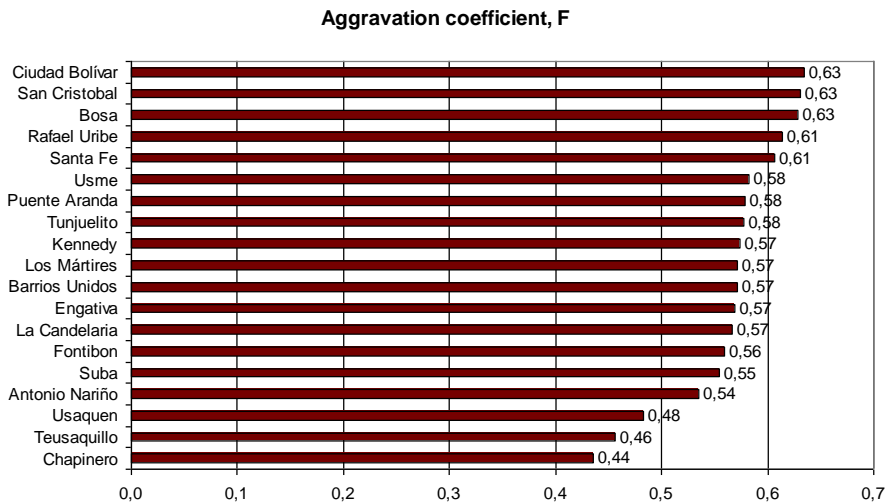
Figure 13: Aggravation coefficient of Bogota's localities.
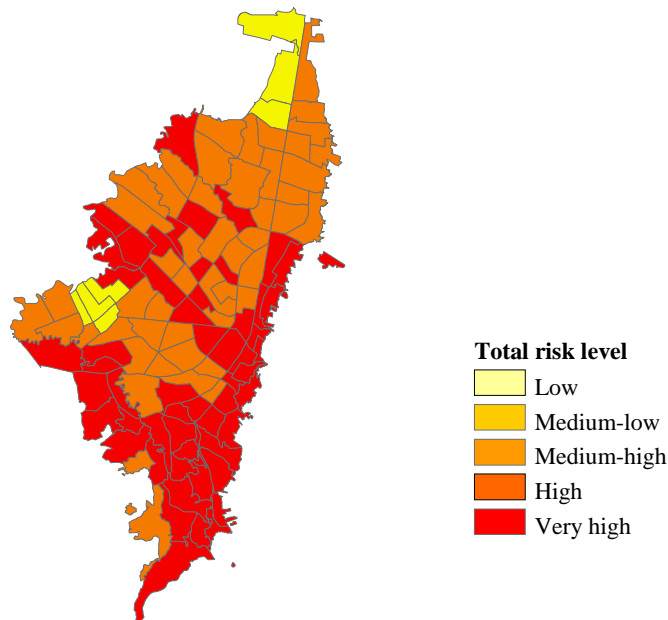
Figure 14: Total risk levels of Bogota.

4. CONCLUSIONS

A simplified but multidisciplinary model of the urban seismic risk has been proposed in this paper, based on the parametric use of variables that reflect different aspects of such risk. This model is formulated in the most realistic possible manner using the fuzzy sets theory, to which corrections or alternative figures may be continuously introduced. The consideration of physical aspects allowed the construction of a physical risk index. Also, the contextual variables (social, economic, etc.) allowed the construction of an aggravation coefficient. The former is built from the information about the seismic scenarios of physical damage (direct effects) and the latter is the result from the estimation of aggravating conditions (indirect effects) based on descriptors and factors related to the social fragility and the lack of resilience of the exposed elements. the application of fuzzy sets is proposed for the case in which the necessary information is not available, starting from this can be replaced by experts opinion.

This new fuzzy model for holistic evaluation of risk facilitates the integrated risk management by the different stakeholders involved in risk reduction decision-making. The proposed method has been applied to the cities of Barcelona (Spain) and Bogota (Colombia), proved to be robust, and allowed to identify the most

relevant aspects of the total risk index, with no need for further analysis and interpretation of results.

Acknowledgements

References

1. Cardona, O.D., "The need for rethinking the concepts of vulnerability and risk from a holistic perspective: a necessary review and criticism for effective risk management", in G. Bankoff, G. Frerks, D. Hilhorst (eds.), *Mapping Vulnerability: Disasters, Development and People,* Earthscan Publishers, London, UK. 2004.
2. UNDRO, Natural Disasters and Vulnerability Analysis, Report of Experts Group Meeting, UNDRO, Geneva. 1980.
3. Cardona, O.D. and Hurtado J.E.:, "Holistic seismic risk estimation of a metropolitan center", in Proceedings of 12th World Conference of Earthquake Engineering, Auckland, New Zeland, 2000.
4. Masure, P., "Variables and indicators of vulnerability and disaster risk for land-use and urban or territorial planning", IDB/IDEA Programa de Indicadores para la Gestión de Riesgos, http://idea.unalmzl.edu.co, Universidad Nacional de Colombia, Manizales, 2003.
5. Carreño, M.L., Cardona, O.D. and Barbat, A.H, "Urban Seismic Risk Evaluation: A Holistic Approach", Journal of Natural Hazards Vol 40 Num 1. DOI 10.1007/s11069-006-0008-8, 2007.
6. Cardona, O. D., Holistic evaluation of the seismic risk using complex dynamic systems (in Spanish), PhD Thesis, Technical University of Catalonia, Barcelona, Spain, 2001.
7. Carreño, M.L., Técnicas innovadoras para la evaluación del riego sísmico y su gestión en centros urbanos: Acciones ex ante y ex post. PhD Thesis, Technical University of Catalonia, Barcelona, Spain, Departamento de Ingeniería del Terreno, cartografía y geofísica, 2006.
8. Barbat, A. H. and Cardona O. D., "Vulnerability and disaster risk indices from engineering perspective and holistic approach to consider hard and soft variables at urban level", IDB/IDEA Program on Indicators for Disaster Risk Management, http://idea.unalmzl.edu.co, Universidad Nacional de Colombia, Manizales, 2003.
9. Cardona, O. D. and Barbat, A. H., El Riesgo Sísmico y su Prevención, Cuaderno Técnico 5, Calidad Siderúrgica, Madrid. 2000.
10. IDEA, System of indicators for disaster risk management: Main technical report. IDB/IDEA Programme of Indicators for Disaster Risk Management (Manizales: UNC), 2005.
11. Cardona, O.D., "Disaster Risk and Vulnerability: Notions and Measurement of Human and Environmental Insecurity" in Coping with Global Environmental Change, Disasters and Security - Threats, Challenges, Vulnerabilities and Risks, Editors: H.G. Brauch, U. Oswald Spring, C. Mesjasz, J. Grin, P. Kameri-Mbote, B. Chourou, P. Dunay, J. Birkmann: Springer-Verlag (in press), Berlin - New York, 2009.

12. Carreño, M.L., Cardona, O.D. and Barbat, A.H.:, System of Indicators for the risk evaluation (in Spanish), Monographs of Earthquake Engineering, IS-52, Editor A.H. Barbat, International Center for Numerical Methods in Engineering (CIMNE), Barcelona, España, 2005.
13. Saaty, T.L. and Vargas, L.G., Prediction, Projection, and Forecasting: Applications of the Analytical Hierarchy Process in Economics, Finance, Politics, Games, and Sports, Kluwer Academic Publishers, Boston, USA, 1991.
14. Carreño M. L., Cardona O. D. and Barbat A. H., "Disaster risk management performance index", Journal of Natural Hazards, 41, 2007, 1-20, 2007.
15. ICC/CIMNE, An Advanced Approach to Earthquake Risk Scenarios with Applications to Different European Towns, WP08, Application to Barcelona, RISK-UE Project, 2004.
16. Barbat A. H., Mena U. y Yépez F., "Evaluación probabilista del riesgo sísmico en zonas urbanas", Revista internacional de métodos numéricos para cálculo y diseño en ingeniería, 14(2), 1998, 247-268.
17. Barbat A. H., Pujades L. G. and Lantada N., "Performance of buildings under earthquakes in Barcelona, Spain", Computer-Aided Civil and Infrastructure Engineering, 21, 2006, 573-593.
18. Barbat A. H., Pujades L. G. and Lantada N., "Seismic damage evaluation in urban areas using the capacity spectrum method: application to Barcelona", Soil Dynamics and Earthquake Engineering, 28, 2008, 851–865.
19. Lantada N., Pujades L. G. and Barbat A. H., "Vulnerability index and capacity spectrum based methods for urban seismic risk evaluation. A comparison", Natural Hazards, 2009 (in press).
20. Universidad de los Andes, Escenarios de riesgo y pérdidas por terremoto para Bogota, D.C, Centro de Estudios sobre Desastres y Riesgos CEDERI, Alcaldía Mayor de Bogotá, Dirección de Prevención y Atención de Emergencias, DPAE, Bogota, Colombia, 2005.

EBBEF2p - A Computer Code for Analysing Beams on Elastic Foundations

Iancu Bogdan Teodoru

Department of Transportation Infrastructure and Foundations,
"Gh. Asachi" Technical Univesity, Iaşi, 700050, România

Summary

The development of a finite element computer code for the static structural analysis of beams on elastic foundation is described. Called EBBEF2p (Euler-Bernoulli Beams on Two-Parameter Elastic Foundationis) this code is written in the computer programme package MATLAB and can handle a wide range of static loading problems involving a one-dimensional beam supported by elastic foundation. The theoretical basis for the code, its computer implementation, and its use to solve example problems are discussed too.

KEYWORDS: Beams; Elastic Foundations; Winkler Foundation; Two-Parameter Elastic Foundation; Vlasov Foundation; Finite Elements; Static Structural Analysis; Computer Program.

1. INTRODUCTION

The concept of beams on elastic foundations it is extensively used by geotechnical, pavement and railroad engineers for foundation design and analysis.

Currently, the analysis of beams on elastic foundation is performed by using special computer programs based on numerical methods, such as Finite Difference Method (FDM) and Finite Element Method (FEM). However, these programs are limited in their application, most of them being developed only for a very simple subgrade model, Winkler's Hypothesis. They cannot be used for other soil models such as Two-Parameter, Elastic Half-Space or Elastic Layer and others.

This paper describes a finite element computer program, as a toolbox to MATLAB, developed to analyse the interaction between a beam and its two-parameter elastic foundation. By considering a linear variation of both foundation parameter, EBBEF2p can account in a consistent way for the bearing soil inhomogeneity. It can be used for any practical static loading and support condition including prescribed displacement.

The numerical model uses a cubic Hermitian polynomial to interpolate nodal values of the displacements field for a two-node beam elements. The elemental stiffness matrix and load vector are obtained by using Galerkin's Residual Method with adding the contribution of the foundation as element foundation stiffness matrices to the regular flexure beam element.

2. BEAM-SOIL SYSTEM MODELLING

Generally, the analysis of bending of beams on an elastic foundation is developed on the assumption that the reaction forces of the foundation are proportional at every point to the deflection of the beam at that point. The vertical deformation characteristics of the foundation are defined by means of identical, independent, closely spaced, discrete and linearly elastic springs. The constant of proportionality of these springs is known as the modulus of subgrade reaction, k_s. This simple and relatively crude mechanical representation of soil foundation was first introduced by Winkler, in 1867 [1], [2].
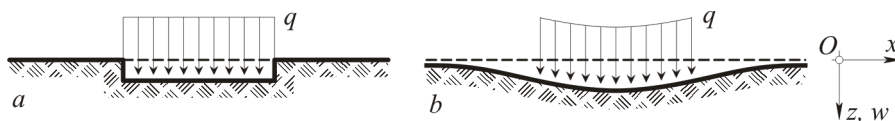
Figure 1. Deflections of elastic foundations under uniform pressure: a – Winkler foundation; b – practical soil foundations.

The Winkler model, which has been originally developed for the analysis of railroad tracks, is very simple but does not accurately represents the characteristics of many practical foundations. One of the most important deficiencies of the Winkler model is that a displacement discontinuity appears between the loaded and the unloaded part of the foundation surface. In reality, the soil surface does not show any discontinuity (Figure 1).

Historically, the traditional way to overcome the deficiency of Winkler model is by introducing some kind of interaction between the independent springs by visualising various types of interconnections such as flexural elements (beams in one-dimension (1-D), plates in 2-D), shear-only layers and deformed, pretensioned membranes [1]. The foundation model proposed by Filonenko and Borodich in 1940 [1] acquires continuity between the individual spring elements in the Winkler model by connecting them to a thin elastic membrane under a constant tension. In the model proposed by Hetényi in 1950 [1], interaction between the independent spring elements is accomplished by incorporating an elastic plate in three-dimensional problems, or an elastic beam in two-dimensional problems, that can deforms only in bending. Another foundation model proposed by Pasternak in 1954

acquires shear interaction between springs by connecting the ends of the springs to a layer consisting of incompressible vertical elements which deform only by transverse shearing [1].

This class of mathematical models have another constant parameter which characterizes the interaction implied between springs and hence are called *two-parameter models* or, more simply, *mechanical models* (Figure 2).
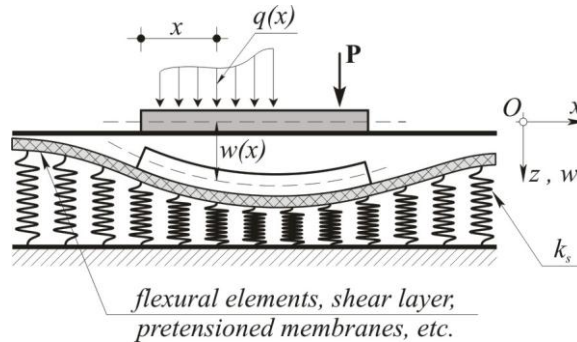
Figure 2. Beam resting on two-parameter elastic foundation.

Another approach to developing, and also to improve foundation models, starts with the three complex sets of partial-differential equations (compatibility, constitutive, equilibrium) governing the behavior of the soil as a semi-infinite continuum, and then introduce simplifying assumptions with respect to displacements or/and stresses in order to render the remaining equations fairly easy to solve in an exact, closed-form manner. These are referred to as *simplified-continuum models*.

Vlasov, in 1960, adopted the simplified-continuum approach based on the variational principle and derived a two parameter foundation model [3]. In his method the foundation was treated as an elastic layer and the constraints were imposed by restricting the deflection within the foundation to an appropriate mode shape, $\phi(z)$. The two parameter Vlasov model (Figure 3) accounts for the effect of the neglected shear strain energy in the soil and shear forces that come from surrounding soil by introducing an arbitrary parameter, γ, to characterize the vertical distribution of the deformation in the subsoil [3]; the authors did not provide any mechanism for the calculation of γ. Jones and Xenophontos [3] established a relationship between the parameter γ and the displacement characteristics, but did not suggest any method for the calculation of its actual value. Following Jones and Xenophontos, Vallabhan and Das [4] determined the parameter γ as a function of the characteristic of the beam and the foundation, using an iterative procedure. They named this model a *modifed Vlasov model* [4], [5].
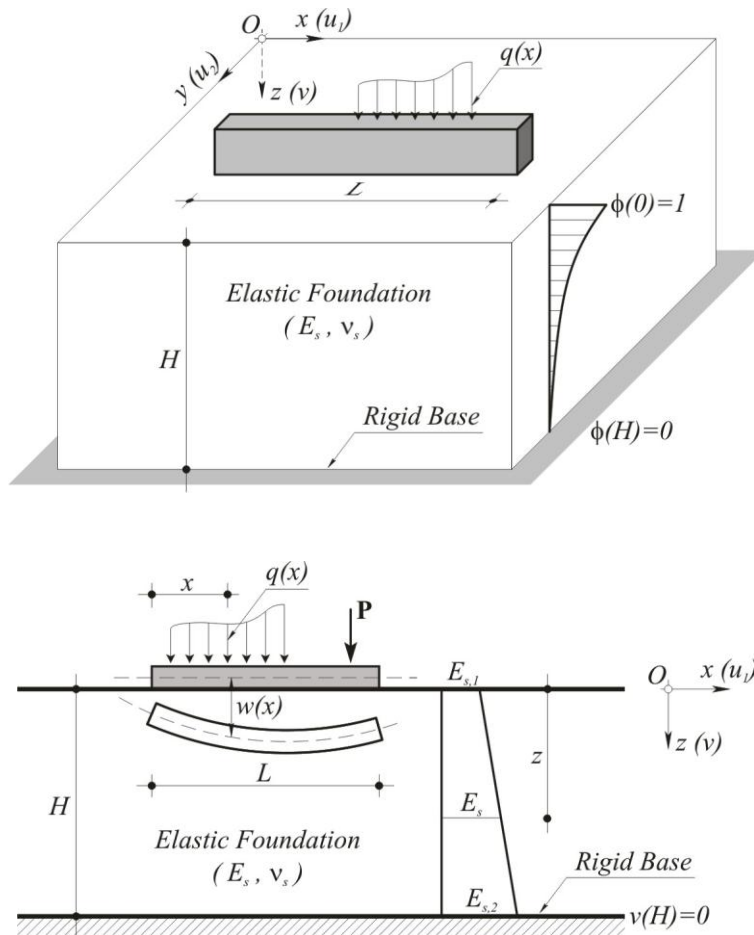
Figure 3. Beam resting on two-parameter Vlasov foundation.

3. FINITE ELEMENT MODELLING

All foundation models shown foregoing lead to the same differential equation. Basically, all these models are equivalent and differ only in the definition of its parameters [6].

3.1. Governing Differential Equation

The various two-parameter elastic foundation models define the reactive pressure of the foundation $p(x)$, as [6]

$$p(x) = k_s B w(x) - k_1 B \frac{\mathrm{d}^2 w(x)}{\mathrm{d}x^2} = k w(x) - \bar{k}_1 \frac{\mathrm{d}^2 w(x)}{\mathrm{d}x^2}, \tag{1}$$

where: B is the width of the beam cross section; w – deflection of the centroidal line of the beam and k_1 is the second foundation parameter with a different definition for each foundation model. As a special case, if the second parameter k_1 is neglected, the mechanical modelling of the foundation converges to the Winkler formulation. For the case of a (linear) variable subgrade coefficients, Equation (1) may be written as

$$\begin{aligned} p(x) &= k_s(x) B w(x) - k_1(x) B \frac{\mathrm{d}^2 w(x)}{\mathrm{d}x^2} = \\ &= k(x) w(x) - \bar{k}_1(x) \frac{\mathrm{d}^2 w(x)}{\mathrm{d}x^2} \end{aligned}. \tag{2}$$

Using the last relation and beam theory, one can generate the governing differential equations for the centroidal line of the deformed beam resting on two-parameter elastic foundation as [6]

$$EI \frac{\mathrm{d}^4 w(x)}{\mathrm{d}x^4} + k(x) w(x) - \bar{k}_1(x) \frac{\mathrm{d}^2 w(x)}{\mathrm{d}x^2} = q(x), \tag{3}$$

where: E is the modulus of elasticity for the constitutive material of the beam; I – the moment of inertia for the cross section of the beam and $q(x)$ is the distributed load on the beam.

3.1.1. Parameters estimation

It is difficult to interpret exactly what subgrade material properties or characteristics are reflected in the various mechanical elements (springs, shears layers, etc.) thus evaluation on a rational, theoretical basis is cumberstome. The advantage of simplified-continuum approach is the elimination of the necesity to determine the values of the foundation parameters, arbitrarily, because these values can be computed from the material properties (deformation modulus E_s, Poisson number v_s and depth of influence zone H along the beam) for the soil. Thus there is insight into exactly what each model assumes and implies in terms of subgrade behavior.

With the assumptions of

vertical displacement,

$$v(x, z) = w(x)\phi(z) \text{ and} \tag{4}$$

horizontal displacement,

$$u_1(x,z)=0, \tag{5}$$

and using variational calculus, Vlasov model parameters are expressed as [3], [4], [5]

$$k_s = \int_0^H \frac{E_s(1-v_s)}{(1+v_s)(1-2v_s)}\left(\frac{d\phi}{dz}\right)^2 dz, \quad k_1 = \int_0^H \frac{E_s}{2(1+v_s)}\phi^2 dz, \tag{6}$$

were

$$\phi(z) = \frac{\sinh\gamma\left(1-\dfrac{z}{H}\right)}{\sinh\gamma}, \tag{7}$$

is a function defining the variation of the deflection $v(x, z)$ in the z direction, which satisfy the boundary condition shown in Figure 3, and

$$\left(\frac{\gamma}{H}\right)^2 = \frac{1-2v_s}{2(1-v_s)}\frac{\displaystyle\int_{-\infty}^{+\infty}\left(\frac{dw}{dx}\right)^2 dx}{\displaystyle\int_{-\infty}^{+\infty} w^2\, dx}. \tag{8}$$

Since γ is not known apriory, the solution technique for parameters evaluation is an iterative process which is dependent upon the value of the parameter γ. Therefore, by assuming an approximate value of γ initially, the values of k and k_1 are evaluated using (6). From the solution of the deflection of the beam, the value of γ is computed using (8). The new γ value is again used to compute new values of k and k_1. The procedure is repeated until two succesive values of γ are approximately equal [4], [5].

3.2. Finite Element Formulation

The assumptions and restrictions underlying the development are the same as those of elementary beam theory with the addition of [7], [8]
- the element is of length l and has two nodes, one at each end;
- the element is connected to other elements only at the nodes;
- element loading occurs only at the nodes.

Figure 4. shows a finite element of a beam on a two-parameter elastic foundation were $\{d_e\} = \{w_1\ \theta_1\ w_2\ \theta_2\}^T$ are the degrees of freedom of the element and $\{S_e\} = \{Q_1\ M_1\ Q_2\ M_2\}^T$ are loads applied to the nodes [7], [8].
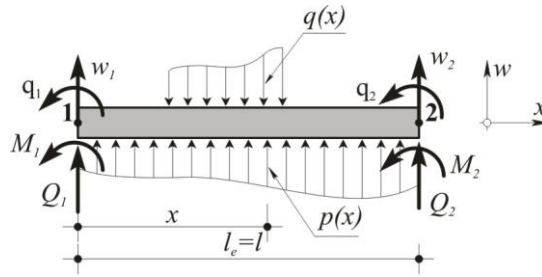
Figure 4. Nodal degrees of freedom and corresponding nodal forces on a beam element on a two-parameter foundation.

It must note that Q_1 and Q_2 from the load vector $\{S_e\}$ are not simply the transverse shear forces in the beam; they includes also the shear resistance associated with modulus of the two-parameter foundation [6]. Force Q_i (i = 1, 2), is a generalized shear force defined by

$$Q_i = V_i + V_i^* , \tag{9}$$

were: $V_i = EI\dfrac{\mathrm{d}^3w(x)}{\mathrm{d}x^3}$ is the usual shear contribution from elementary beam theory; $V_i^* = -\bar{k}_1\dfrac{\mathrm{d}w(x)}{\mathrm{d}x}$ – the shear contribution from two-parameter elastic foundation (negative sign arises because a positive slope requires opposite shear forces in the foundation) [6].

Considering the four boundary conditions and the one-dimensional nature of the problem in terms of the independent variable, we assume the displacement function in the form [7], [8]:

$$w_e(x) = a_0 + a_1 x + a_2 x^2 + a_3 x^3 , \tag{10}$$

For the both foundation parameters a linear variation is considered [8],

$$k(x) = k_{(1)} + \frac{k_{(2)} - k_{(1)}}{l}x, \quad \bar{k}_1(x) = \bar{k}_{1,(1)} + \frac{\bar{k}_{1,(2)} - \bar{k}_{1,(1)}}{l}x . \tag{11}$$

The choice of a cubic function to describe the displacement is not arbitrary. With the specification of four boundary conditions, we can determine no more than four constants in the assumed displacement function. The second derivative of the assumed displacement function, $w_e(x)$ is linear; hence, the bending moment varies linearly, at most, along the length of the element. This is in accord with the assumption that loads are applied only at the element nodes [7].

Applying the boundary conditions and solving the constants from (10) and then substituting the results back into (10) we can obtain the interpolation form of the displacement as [7], [8]

$$w_e(x) = N_1(x)w_1 + N_2(x)\theta_1 + N_3(x)w_2 + N_4(x)\theta_2 = [N_i]^T\{d_e\}, \quad (12)$$

where $N_i(x)$, $(i = 1, ..., 4)$ are the well-known shape functions of Hermite type that describe the distribution of displacement in terms of nodal values in the nodal displacement vector $\{d_e\}$:

$$\begin{cases} N_1(x) = 1 - 3\dfrac{x^2}{l^2} + 2\dfrac{x^3}{l^3}, \ N_2(x) = x - 2\dfrac{x^2}{l} + \dfrac{x^3}{l^2} \\ N_3(x) = 3\dfrac{x^2}{l^2} - 2\dfrac{x^3}{l^3}, \ N_4(x) = -\dfrac{x^2}{l} + \dfrac{x^3}{l^2} \end{cases}. \quad (13)$$

As the polynomial (12) represents an approximate solution of the governing Equations (3), it result the residuum (error or discrepancy):

$$\varepsilon(x) = EI\frac{d^4 w_e(x)}{d x^4} - \overline{k}_1(x)\frac{d^2 w_e(x)}{dx^2} + k(x)w_e(x) - q(x) \neq 0. \quad (14)$$

The minimizing of this residuum means to the annulment of Galerkin balanced functional where the weight is considered for each of the four functions, $N_i(x)$. So the element stiffness matrix resulting are [6]…[11]:

$$[k_e] = \frac{EI}{l^3}\begin{bmatrix} 12 & 6l & -12 & 6l \\ 6l & 4l^2 & -6l & 2l^2 \\ -12 & -6l & 12 & -6l \\ 6l & 2l^2 & -6l & 4l^2 \end{bmatrix}; \quad (15)$$

$$[k_w] =$$
$$= \frac{l}{840}\begin{bmatrix} 24(10k_{(1)} + 3k_{(2)}) & 2l(15k_{(1)} + 7k_{(2)}) & 54(k_{(1)} + k_{(2)}) & -2l(7k_{(1)} + 6k_{(2)}) \\ 2l(15k_{(1)} + 7k_{(2)}) & l^2(5k_{(1)} + 3k_{(2)}) & 2l(6k_{(1)} + 7k_{(2)}) & -3l^2(k_{(1)} + k_{(2)}) \\ 54(k_{(1)} + k_{(2)}) & 2l(6k_{(1)} + 7k_{(2)}) & 24(3k_{(1)} + 10k_{(2)}) & -2l(7k_{(1)} + 15k_{(2)}) \\ -2l(7k_{(1)} + 6k_{(2)}) & -3l^2(k_{(1)} + k_{(2)}) & -2l(7k_{(1)} + 15k_{(2)}) & l^2(3k_{(1)} + 5k_{(2)}) \end{bmatrix}; \quad (16)$$

$$[k_t] = \frac{1}{30l}\begin{bmatrix} 3(11\overline{k}_{1(1)} + \overline{k}_{1(2)}) & -3l(\overline{k}_{1(1)} - 2\overline{k}_{1(2)}) & -3(11\overline{k}_{1(1)} + \overline{k}_{1(2)}) & 3l(2\overline{k}_{1(1)} - \overline{k}_{1(2)}) \\ 3l\overline{k}_{1(1)} & l^2(3\overline{k}_{1(1)} + \overline{k}_{1(2)}) & -3l\overline{k}_{1(1)} & -l^2\overline{k}_{1(2)} \\ -3(\overline{k}_{1(1)} + 11\overline{k}_{1(2)}) & 3l(\overline{k}_{1(1)} - 2\overline{k}_{1(2)}) & 3(\overline{k}_{1(1)} + 11\overline{k}_{1(2)}) & -3l(2\overline{k}_{1(1)} - \overline{k}_{1(2)}) \\ 3l\overline{k}_{1(2)} & -l^2\overline{k}_{1(1)} & -3l\overline{k}_{1(2)} & l^2(\overline{k}_{1(1)} + 3\overline{k}_{1(2)}) \end{bmatrix}, \quad (17)$$

were,

$$(\ [k_e]+[k_w]+[k_t] \ )\{d_e\}=\{S_e\}-\{R_e\} \tag{18}$$

is the matrix notation of the governing differential equation (3) and $[k_e]$ is the stiffness matrix of the flexure beam element; $[k_w]$ is the stiffness matrix of the first subgrade parameter (springs layer); $[k_t]$ is the stiffness matrix of the second subgrade parameter.

The vector $\{R_e\}$ depends on the distributed load on the element and, for $q(x) = q = const.$, it result

$$\{R_e\}=\left\{\frac{ql}{2} \ \frac{ql^2}{12} \ \frac{ql}{2} \ -\frac{ql^2}{12}\right\}^T . \tag{19}$$

4. PROGRAM GENERAL DESCRIPTION

A typical finite element program consists of the following sections [12] (Figure 5):
  1. Preprocessing section.
  2. Processing section.
  3. Post-processing section.

In the preprocessing section the data and structures that describe the particular problem statement are defined. These include the finite element discretization, material properties, solution parameters, etc.

The processing section is where the finite element objects (*e.g.* stiffness matrices, force vectors, etc.) are computed, boundary conditions are enforced and the system is solved.

The post-processing section is where the results from the processing section are analyzed. Here stresses may be calculated and data might be visualized.

The Graphical User Interface (GUI) of the EBBEF2p lets the user to interactively enter the operations from the above sections. Although many pre and post-processing operations are already programmed in MATLAB, the EBBEF2p environment have build-functions that come to answer to a particular problem statement. The procedure used to obtain a complet solution for a beam resting on two-parameter foundation is indicated below.

A EBBEF2p work session is started with calling the main function file *input.m*, from the MATLAB prompt. The functions that are integrated here (*draw*, *write* and user interface controls – *mnu* function) aids the user in generating data defining the finite element model, for a given problem, with taking advantage of a fully functional GUI (Figure 6).
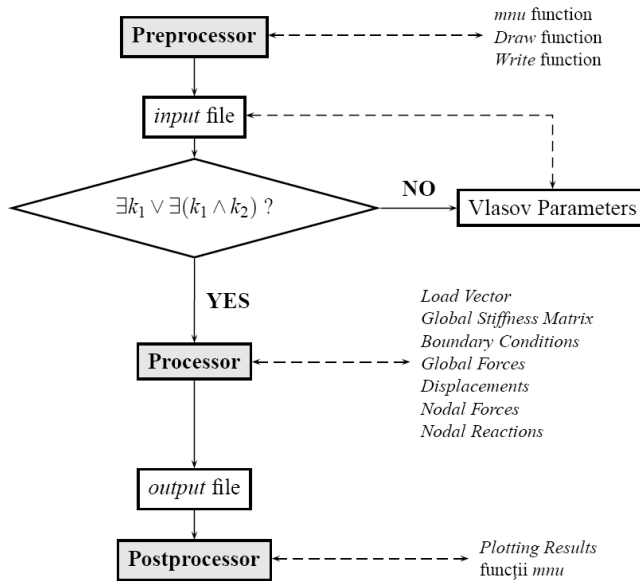
Figure 5. Flow chart for EBBEF2p.

All the finite element data (geometry, material properties, loads, supports, soil parameters and generated FE mesh) are write in a binary data file *input.mat*.

Before EBBEF2p solver (processor) initialization (*ebbef2p.m* function file) are checked the subgrade conditions:
- if exist k_s or (k_s and k_1) values, the finite element model is analysed with these one;
- in this case, the user is required to put in distributions of the deformation modulus E_s, the Poisson number v and a depth of influence zone H along a beam (if these are not introduced apriory). The program then exploits these parameters to compute values k_s and k_1 using the iterative procedure described foregoing.

In the locations where there is no subsoil, the user can simply set to zero k_s and k_1 parameters (or E_s).

By collecting element data from the input file, development of the elements stiffness matrices, which are assembling into the global stiffness matrix by using the direct stiffness approach, is done. Partitioning the global stiffness matrix by applying boundary condition (forces, displacements, supports), the remain matrix equation is solved by using Gaussian elimination. With the obtained solution, the displacements, global and nodal forces are calculated and saved to the binary data file *output.mat*.

Finaly, the data stored in *output* file are visualized by the help of MATLAB build-in plot function.
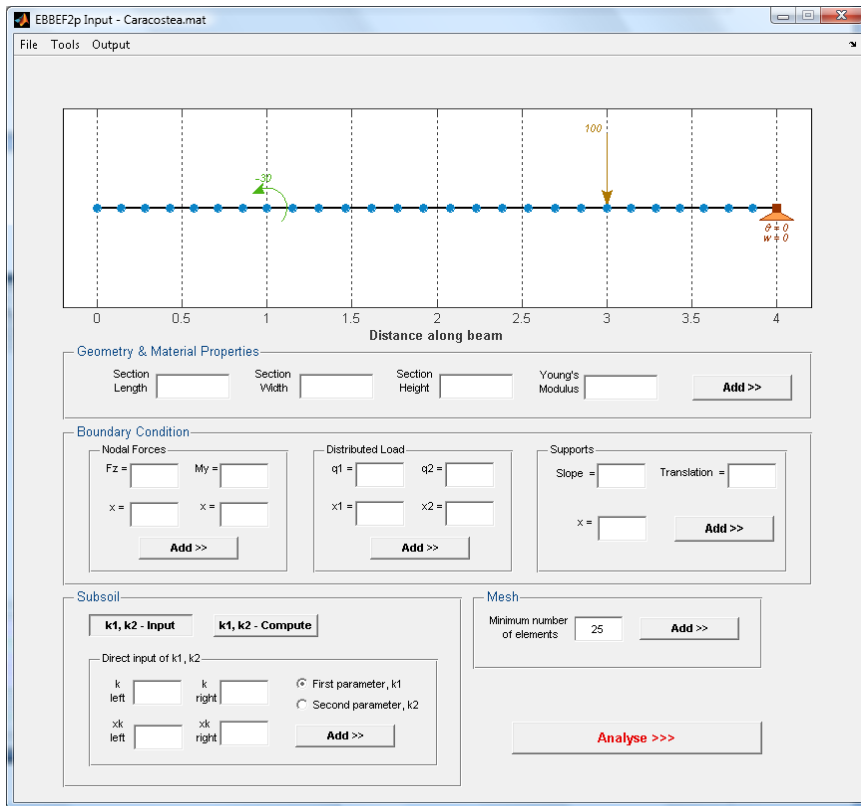
Figure 6. Sample input screen of EBBEF2p.

5. EXAMPLE PROBLEMS. BENCHMARKING

In order to give a comparison between the EBBEF2p solution and the other solution from theory of beams on elastic foundation, a few example problems are presented below.

5.1. Beam on Winkler Foundation

With the general footing and load data shown in Figure 7 (after [13]), the correponding EBBEF2p model is given in Figure 8.
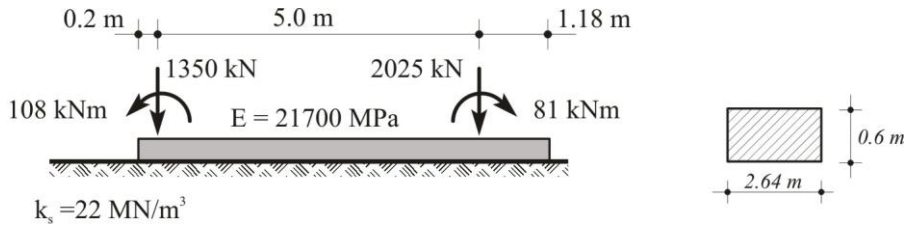
Figure 7. Geometry and load data for the considered example.
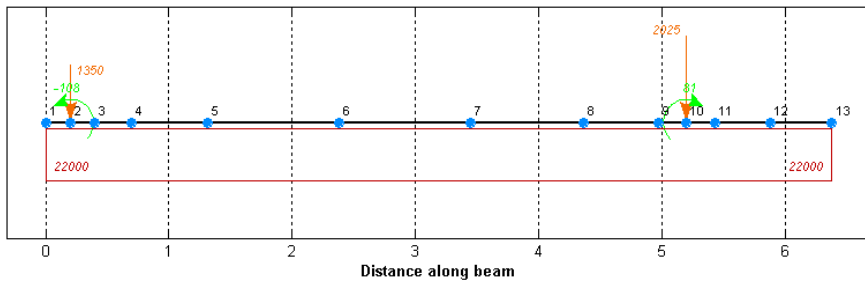
Figure 8. EBBEF2p finite element model.
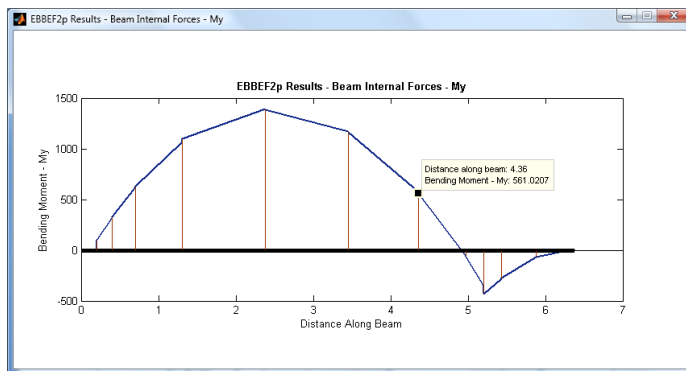
Figure 9. Sample EBBEFp output screen for bending moment.

The results of the numerical analyses have been summarized in Table 1 (maximum values) and a typical EBBEFp output for bending moment pattern is shown in Figure 9.

Table 1. Comparison between EBBEF2p and Bowles solution.

	EBBEF2p	Bowles [13]
Rotation (at node 1), [rad]	0.00269	0.00253
Vertical displacement (at node 1), [mm]	12.3	11.8
Bending moment (at node 6), [kNm]	1387.1	1223.3
Shearing force (at node 10, left), [kN]	1236.7	1190.7
Soil pressure (at node 1), [kN/m]	271.3	260.1

5.2. Fixed-End Beam on Winkler Foundation

The example problem shown in Figure 10 is solved in [14] by the Umanski's method, only for the bending moment.
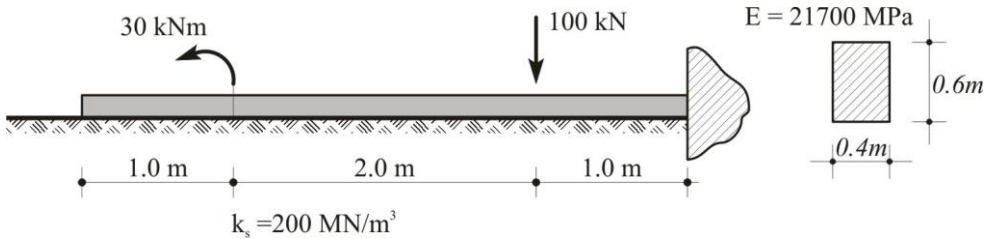
Figure 10. Fixed-end beam on Winkler foundation.

A total of 27 two-node beam element were used to define the corresponding EBBEF2p finite element mesh shown in Figure 11.
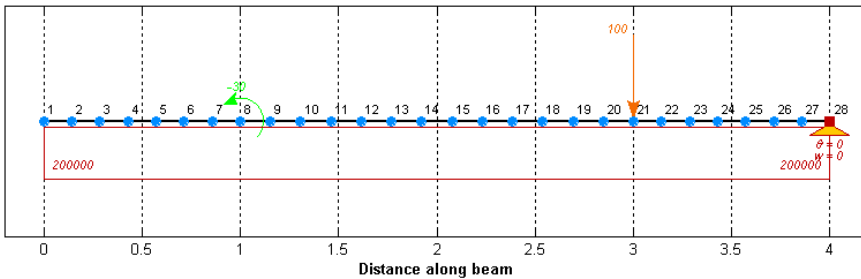
Figure 11. EBBEF2p finite element model.

The computed bending moment pattern is shown in Figure 12. It can be noted that the obtained solution is fairly close to those by Umanski's method.
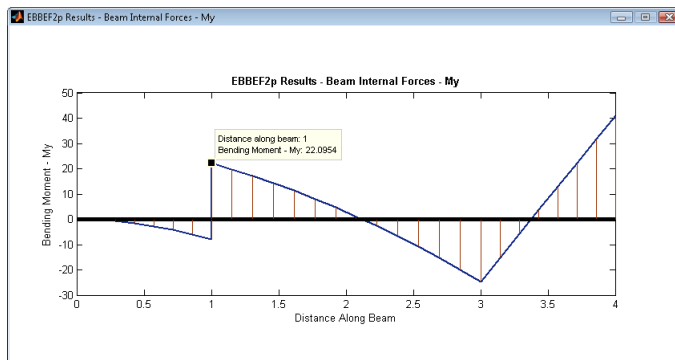
Figure 12. EBBEFp output for bending moment.

5.3. Beam on Modified Vlasov Foundation

As numerical example, a beam of length L = 20 m, width b = 0.5 m and height h = 1.0 m with modulus of elasticity E = 27000 MPa is considered to be suported by foundation having depth H = 5 m, deformation modulus E_s = 20 MPa and Poissons ratio v_s = 0.25 (Figure 13). A concentrated load P = 500 kN applied at the center of the beam, is assumed. The results of this example problem are compared with solutions obtained by two-dimensional finite element plane strain analyses (2D FEM).

A total of 905, 15-noded triangular elements with a fourth order interpolation for displacements and twelve Gauss points for the numerical integration were used to define the mesh for the 2D FEM model.
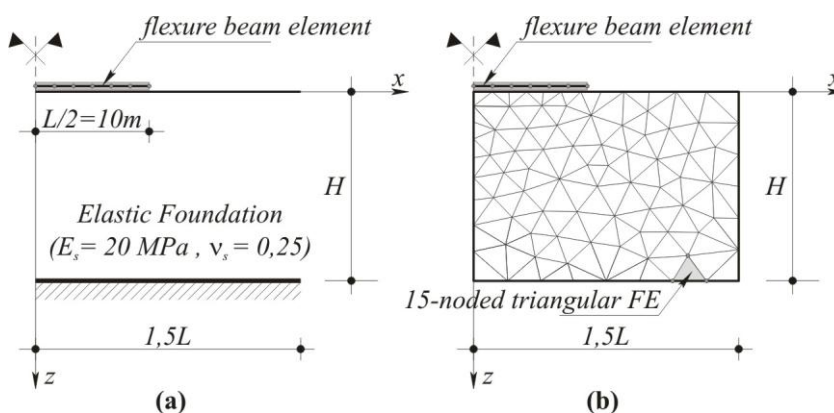
Figure 13. Geometry of the considered example: (**a**) – EBBEF2p; (**b**) – 2D FEM.

In both EBBEF2p and 2D FEM models, the beam is modeled with flexure beam element (Table 2).

Table 2. Beam modelling.

	EBBEF2p model	2D FEM model
Element type	linear with 2 nodes	linear with 5 nodes
Total number of nodes	35	469
Total number of elements	34	117

The results from both 2D FEM and EBBEF2p technique are shown for comparison in Figure 14. It can be noted that both solution have almost the same shape and they are in good agreement. However, a full comparison between these two technique is not fair, because in the 2D finite element solution, complete compatibility of displacements at the beam-soil interface is assumed, but only vertical displacement compatibility exists in Vlasov model [5].
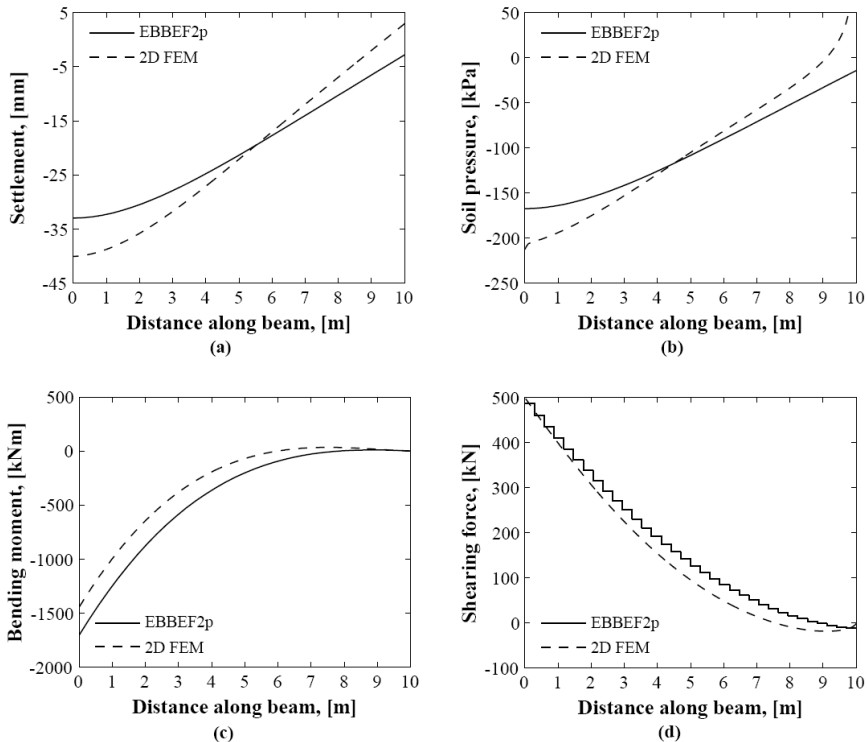
Figure 14. EBBEF2p *vs.* 2D FEM solution: (**a**) – settlement; (**b**) – soil pressure; (**c**) – bending moment; (**d**) – shearing force.

The results of the final computed values of the soil parameters are presented in Table 3. This demonstrate the versatility of the modified Vlasov foundation model, programmed in EBBEF2p: solve beam on elastic foundation problems without having a need to establish the values of foundation parameters.

Table 3. The obtained values of Vlasov foundation parameters.

k , [kN/m^2]	$\bar{k}_1$, [kN]	γ	Number of iterations
2401.57	6515.22	0.418	3

6. CONCLUSIONS

A computer program called EBBEF2p has been developed in MATLAB environment in order to performs complete static structural analysis of beams which rests on one or two-parameter elastic foundation for any loading and boundary condition. By considering a linear variation of both foundation parameter, EBBEF2p can account in a consistent way for the bearing soil inhomogeneity.

The performance and accuracy of EBBEF2p has been carefully tested by carrying out analyses of problems with known solution or comparing results with solutions obtained on numerical model more complex. As a general observation, the obtained EBBEF2p solution are reasonably close to those from theory of beams on elastic foundation and also in good agreement with more sophisticated finite element solutions.

References

1. Kerr, A. D., Elastic and Viscoelastic Foundation Models, *Journal of Applied Mechanics*, vol. 31, No. *3*, p. 491–498, 1964.
2. Hetényi, M., *Beams on elastic foundation: theory with applications in the fields of civil and mechanical engineering,* University of Michigan Press, Ann Arbor, Michigan, 1964.
3. Jones, R., Xenophontos, J., The Vlasov Foundation Model, *International Journal of Mechanical Science*, vol. 19, No. *6*, p. 317–323, 1977.
4. Vallabhan, C. V. G., Das, Y. C., A Parametric Study of Beams on Elastic Foundations, *Journal of Engineering Mechanics Division*, vol. *114*, No. *12*, p. 2072-2082,1988.
5. Vallabhan, C. V. G., Das, Y. C., Modified Vlasov Model for Beams on Elastic Foundations, *Journal of Geotechnical Engineering*, vol. *117*, No. *6*, p. 956–966, 1991.
6. Zhaohua, F., Cook, D. R., Beam Elements on Two-Parameter Elastic Foundation, *Journal of Engineering Mechanics*, vol. 109, No. *6*, p. 1390-1402, 1983.
7. Hutton, D. V., *Fundamentals of Finite Element Enalysis,* McGraw Hill, New York, 2004.
8. Jerca, Şt., Ungureanu, N., Diaconu, D., *Metode numerice în proiectarea construcţiilor*, Universitatea Tehnică „Gh. Asachi", Iaşi, 1997. (in Romanian)

9.   Teodoru, I. B., Muşat, V., Beam Elements on Linear Variable Two-Parameter Elastic Foundation, *Buletinul Institutului Politehnic din Iaşi*, Tomme LIV (LVIII), Fasc. *2*, s. Constr., Archit., p. 69-78, 2008.

10. Teodoru, I. B., Muşat, V., Vrabie, M., A Finite Element Study of the Bending Behavior of Beams on Two-Parameter Elastic Foundation, *Buletinul Institutului Politehnic din Iaşi*, Tomme LII (LVI), Fasc. *3-4*, s. Constr., Archit., p. 7-18, 2006.

11. Jerca, Şt., Vrabie, M., Răileanu, P., *et al.*, Static Analysis of Beams on Elastic Foundation With Variable Coefficient of Soil Reaction Using the Finite Element Method, *Buletinul Institutului Politehnic din Iaşi*, Tomme XLVI (*L*), Fasc. *1-2*, s. Constr., Archit., p. 13-21, 2000.

12. Kwon, Y. W., Bang, H., *The Finite Element Method Using MATLAB*, 2nd edition, CRC Press Boca Raton, Florida, 1996.

13. Bowles, J. E., *Foundation Analysis and Design*, 5th edition, McGraw-Hill, New York, 1996.

14. Caracostea, A. D., *Manual pentru calculul construcţiilor*, Editura Tehnică, Bucuresti, 1977. (in Romanian)

The shaping for the mixed structures evaluation

Ioan Buliga[1], Constantin Amariei[2]

[1]S.C. BULCON GRUP S.R.L. Constanta, 900312, Romania
[2]Structural Mechanics Department, T.U. "Gh. Asachi", Iasi, 708050, Romania

Summary:

Some aspects regarding the possibilities of shaping the mixed structures are presented (structural frames and walls), in a view to use automatic usual evaluation programs, made for bar structures. The paper also contains an example of evaluation that draws several useful conclusions regarding different adopted evaluation models.

KEY WORDS: mixed structures, structural frames and walls, evaluation models, comparative results, efforts, movements.

1. INTRODUCTION:

The mixed structures made of structural ferro-concrete frames and walls are used on a large scale in socio-cultural and administrative buildings.

An important step in designing theses structures is establishing the evaluation model that depends on the available means of solving and that determines the accuracy of the obtained results. Some shaping possibilities are presented in the paper regarding the mixed structures made of structural frames and walls with holes.

A case study referring to a mixed structure, in which three evaluation models have been taken into account, allowed some interesting and useful conclusions and results concerning the effort states from the elements pertaining to the structures and the corresponding movements.

2. CASE STUDY

2.1. General issues

A mixed structure was taken into consideration, made of a frame with two openings and a structural wall with symmetrical large holes. The structure was shaped in three ways, to which three loading plans were taken into consideration, determining the maximum efforts from the structure elements and the entire lateral movements. The structure elements have been pre-dimensioned maintaining the established dimensions in the three shaping version.

In order to determine the efforts and movements the automatic evaluation program SCIA.ESA.PT was used . The purpose of the case study was to determine some comparative data about the efforts and movements for the suggested shaping version. The resulting conclusions are gathered in the final part of the study.

In fig. 1 the analyzed structure is presented (the first model of evaluation):
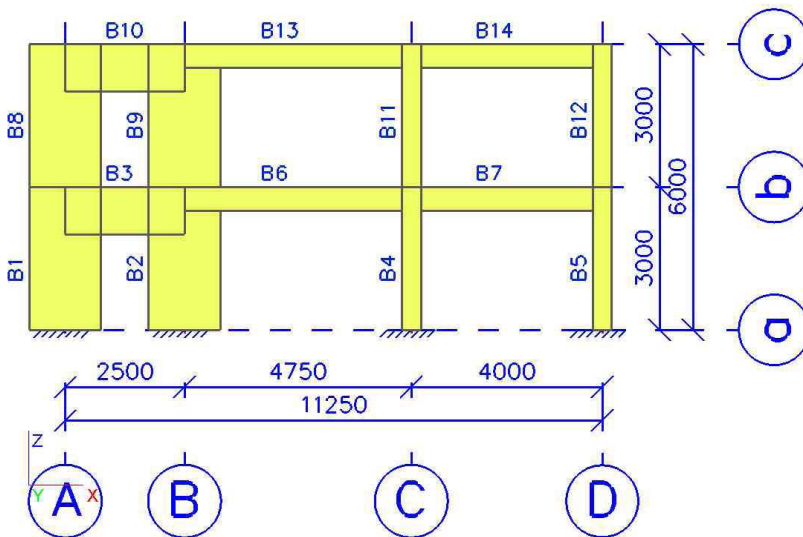
Fig. 1 The first model of evaluation
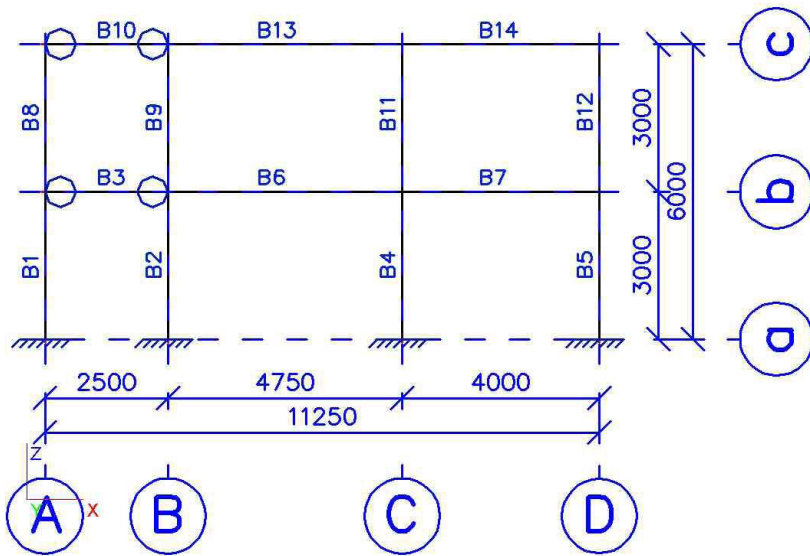
Fig. 2 The second model of evaluation
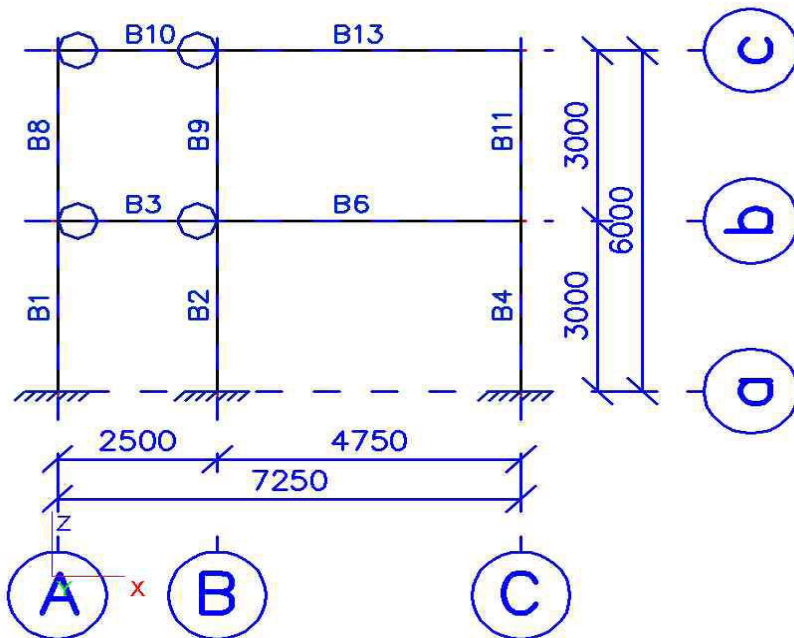
Fig. 3 The third model of evaluation

2.2. Considered models of evaluation

The first model of evaluation is the real structure (fig.1). The second model of evaluation (fig.2) keeps the real frame, but assimilates the coupling bars of the structural wall with articulated bars at the ends. The third model of evaluation maintains the structural wall plan and replaces the real frame with an equivalent frame with one opening.

2.3. Geometrical features of the structure elements

They are presented in table 1 for the model 1 (for exemplification)
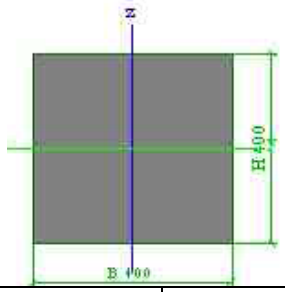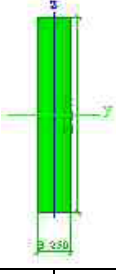
2.4. Loading plans

These are presented as follows in table 1, containing:
- Loadings from their own weight
- Loadings from the snow
- Loadings from the wind
- Seismic loadings
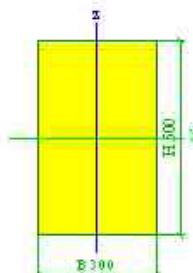
In the same table the loading groups and combinations are exhibited, considered for all the three models of evaluation.
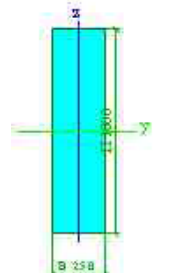
Tab.1. Cross-sections

Name	PILLAR FOR FRAME		Name	WALL VERTICAL	
Detailed	400; 400		Detailed	1500; 250	
Material	C12/15		Material	C12/15	
Buckling y-y,z-z	b, b		Buckling y-y, z-z	b, b	
FEM analysis	x		FEM analysis	x	
Picture			Picture		
Material	C12/15		Material	C12/15	
A [m2]	1,6000e-001		A [m2]	3,7500e-001	

Ay,z [m2]	1,3333e-001	1,3333e-001
Iy,z [m4]	2,1333e-003	2,1333e-003
It [m4], w [m6]	3,5994e-003	0,0000e+000
alpha [deg]	0,00	
Wel y, z [m3]	1,0667e-002	1,0667e-002
Wpl y,z [m3]	1,6000e-002	1,6000e-002
cYLCS, ZLCS [mm]	200	200
d y,z [mm]	0	0
AL [m2/m]	1,6000e+000	

Ay,z [m2]	3,1250e-001	3,1250e-001
Iy,z [m4]	7,0313e-002	1,9531e-003
It [m4], w [m6]	6,9277e-003	0,0000e+000
alpha [deg]	0,00	
Wel y, z [m3]	9,3750e-002	1,5625e-002
Wpl y,z [m3]	1,4063e-001	2,3438e-002
cYLCS, ZLCS [mm]	125	750
d y,z [mm]	0	0
AL [m2/m]	3,5000e+000	

	BEAM FOR FRAME	
Name		
Detailed	500; 300	
Material	C12/15	
Fabrication	concret	
Buckling y-y,z-z	b,b	
FEM analysis	x	
Desen		
Material	C12/15	
A [m2]	1,5000e-001	
Ay,z [m2]	1,2500e-001	1,2500e-001
Iy,z [m4]	3,1250e-003	1,1250e-003
It [m4], w [m6]	2,7913e-003	0,0000e+000
alpha [deg]	0,00	
Wel y, z [m3]	1,2500e-002	7,5000e-003
Wpl y,z [m3]	1,8750e-002	1,1250e-002

	WALL ORIZONTAL	
Name		
Detailed	1000; 250	
Material	C12/15	
Fabrication	concret	
Buckling y-y,z-z	b,b	
FEM analysis	x	
Desen		
Material	C12/15	
A [m2]	2,5000e-001	
Ay,z [m2]	2,0833e-001	2,0833e-001
Iy,z [m4]	2,0833e-002	1,3021e-003
It [m4], w [m6]	4,3336e-003	0,0000e+000
alpha [deg]	0,00	
Wel y, z [m3]	4,1667e-002	1,0417e-002
Wpl y,z [m3]	6,2500e-002	1,5625e-002

cYLCS, ZLCS [mm]	150	250
d y,z [mm]	0	0
AL [m₂/m]	1,6000e+000	

cYLCS, ZLCS [mm]	125	500
d y,z [mm]	0	0
AL [m₂/m]	2,5000e+000	

Tab. 2 - Load cases

NAME	DESCRIPTION	ACTION TYPE	LOAD GROUP	LOAD TYPE	SPEC	DIRECTION	DURATION	MASTER LOAD CASE
LC1	Weight proprie	Permanently	LG1	Weight proprie		-Z		
LC2	Snow	Variable	LG2	Static	Standard		Short	None
LC3	Wind crosswise	Variable	LG3	Static	Standard		Short	None
LC4	Wind longitudinal	Variable	LG4	Static	Standard		Short	None
LC5	Seism	Variable	LG5	Dynamic	Seismicity			None
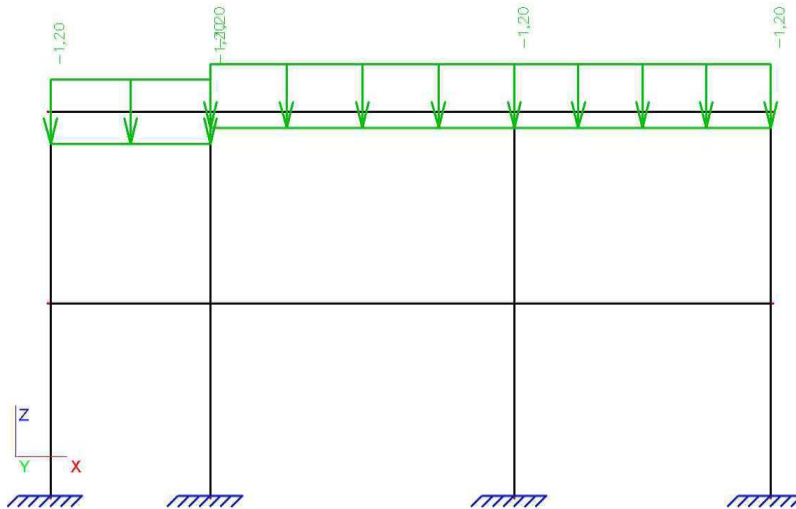
Fig. 4 Loading from snow
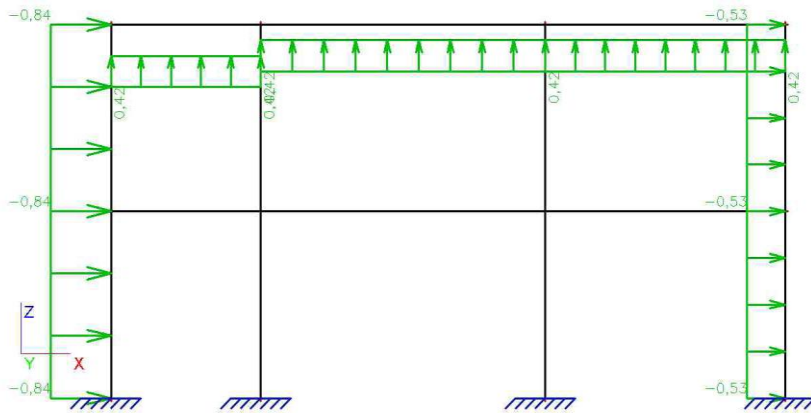
Fig.5 Loading from wind transversely
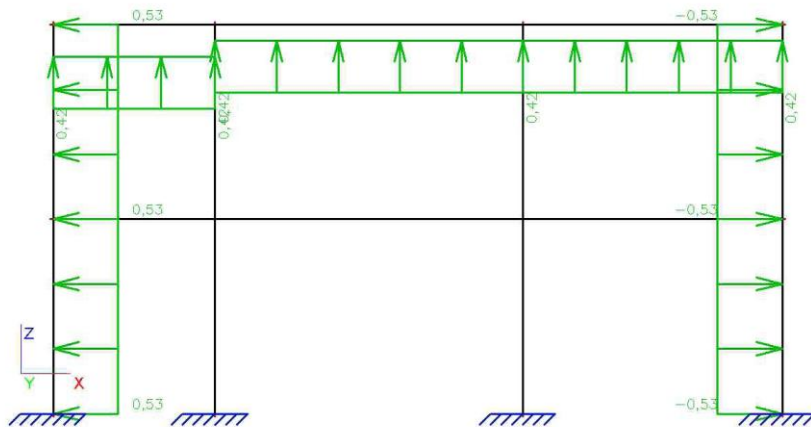
Fig.6 Loading from wind longitudinal

Tab. 3 Loads groupe

Name	Incarcari	Relatii	Coef. 2
LG1	Permanent		Snow load H<1000m a.s.l. Wind
LG2	Variable	Standard	
LG3	Variable	Exclusive	
LG4	Seismic	Together	

Tab. 4 Combinations

Nume	Description	Type	cases of loading	coef.1
Co1	Usl Str	En-Usl	lc1- own weight	1.00
			lc2-snow	1.00
			lc3-wind transverse	1.00
			lc4-wind longitudinal	1.00
Co2	Seism 1	Liniar-Ultimate	lc1- own weight	1.00
			lc2-snow	1.00
			lc5-seism	1.00
Co3	Seism 2	Liniar-Ultimate	lc1- own weight	1.00
			lc2-snow	1.00
			lc5-seism	1.00

2.5. Obtained results

The efforts and the movements for the three models of evaluation are gathered in table 2.

Tab. 5 Centralizing with efforts with values in the section three cases analyzed

Name Elements	Hypothesis 1								
	Type Of Loading								
	Uls			Seism			Total		
	N_x (kN)	T_z (kN)	M_y (kNm)	N_x (kN)	T_z (kN)	M_y (kNm)	N_x (kN)	T_z (kN)	M_y (kNm)
B2	-129	2,06	-7,84	-86,1	4,92	11,79	-129	17,35	42,82
B6	4,03	11,99	-9,62	8,56	9,94	-4,44	8,56	9,94	-4,44
B13	-3,48	-15,8	-11,8	-0,34	-11,1	-7,97	-3,48	17,35	42,82
B3				4,15	23,21	17,11	4,15	23,21	17,11
B1									
B10									
B9									

Name Elements	Hypothesis 2								
	Type Of Loading								
	Uls			Seism			Total		
	N_x (kN)	T_z (kN)	M_y (kNm)	N_x (kN)	T_z (kN)	M_y (kNm)	N_x (kN)	T_z (kN)	M_y (kNm)
B2	-125,5	-1,2	-3,25	-91	17,25	70,86	-91	17,25	70,86
B6	4,55	11,54	-8,4	10,89	11,16	-0,71	10,89	11,16	-0,071
B13	-3,82	16,14	-12,5	-1,57	-10,9	-7,48	-1,57	-10,9	-7,48
B3									

B1	-95,5	5,98	-18,2						
B10	1,28	0	7,87						
B9				-20,1	-0,47	-8,18	-20,1	-0,47	-8,18

	Hypothesis 3								
	Type Of Loading								
Name Elements	Uls			Seism			Total		
	Nx (kN)	Tz (kN)	My (kNm)	Nx (kN)	Tz (kN)	My (kNm)	Nx (kN)	Tz (kN)	My (kNm)
B2	-127,2	-1,09	-3,85	-92,4	3,6	15,75	-127	14,09	59,01
B6	5,17	11,69	-8,46	6,55	11,35	-1,25	6,55	11,35	-1,25
B13	-4,36	17,7	-14,5	-2,59	-15	-4,28	-4,36	17,7	-14,54
B3									
B1	-95,53	6,28	-19,9				-95,5	6,28	-19,85
B10									
B9				-21,2	-1,21	-9,94			

2.6. Conclusions and comments

From comparing the obtained results for the three shaping version, the following conclusions may be drawn:

2.6.1 The efforts dimension

Compared to the values resulted from the version 1 (the real structure) the following effort variations can be noticed for the special loading version (permanent, quasi-permanent and seism):

A. Axial force

a) The structural wall pillars:
- In shaping version 2, 40% lower axial forces resulted;
- In shaping version 3, the axial forces were relatively the same;

b) In the coupling girders between the frame and the structural wall, the axial forces have low values and their comparison is not significant.

B. Cutter forces from the structural wall pillars have close values in the three shaping versions.

C. The flexion moments

a) The structural wall pillars:

- For the structural wall pillars in the shaping version 2, the moments are approximately 65% higher, while in shaping version 3 they are only about 15% higher.

b)The frame shafts do not have significant values for the flexion moments.

c)In the coupling girders between the frame and the structural wall, the flexion moments have important values in the real structure, while in shaping versions 2, 3 the flexion moments have much lower values.

2.6.2. The maximum lateral movements

For the loading version 3, (permanent loading, quasi-permanent and seism) the maximum lateral movements are close regarding the values to all three shaping versions.

3. CONCLUSIONS

1. The analyzed case study emphasizes the importance of the evaluation model adopted as far as the effort dimensions from the structure elements are concerned.

2. As far as lateral movements are concerned, they are not significantly different in comparison to the chosen evaluation model.

3. Similar studies have been made also for mixed structures with several levels having significant differences both regarding the effort dimension and the movement dimension. These studies are included in the paper [4].

Bibliography:

1. AGENT R., POSTELNICU T. – The evaluation of ferro-concrete membrane structures, Technical Publishing House, Bucharest, vol. I (1982), vol. II (1983)
2. AMARIEI C., DUMITRAS AL. – Elements of structure matrix analysis, Publishing House of "Matei-Tezu Botez" Academy, Iasi, 2003.
3. BRANZAN I., BARBAIANI M., The evaluation and composition of multiple level and membrane structures, Technical Publishing House, Bucharest, 1976.
4. BULIGA I., - The improvement of structural wall structures and mixed structures taking into account the elastic and plastic qualities of materials, Doctor degree thesis.
5. IFRIM M., - Dynamic analysis of structures and seismic engineering, Didactical and pedagogical Publishing House, Bucharest, 1973.
6. xxx CR2-1-1/2005 – Code of designing ferro-concrete structural walls buildings, M.T.C.T., 2006.

Individual Dimension Styles an Efficient Tool in Civil Engineering Computer Aided Design

Andrei Slonovschi, Liviu Prună and Ion Antonescu

Department of Descriptive Geometry and Technical Drawing,
Technical University "Gh. Asachi" Iasi, 70005, Romania

Summary

In this paper the authors make a critical analysis of the problems that appears in the technical drawing for construction's dimensioning process when the AutoCAD computer program is used. Then, they suggest solutions allowing the dimensioning process to be develop rapidly, with respect of the dimensioning standards and in a complete concordance with the units that are used to carry out the drawing.

KEYWORDS: Computer Graphical Communication, Technical Drawing, Computer Graphics, AutoCAD.

1. INTRODUCTION

The AutoCAD's users knows the fact that in the process of carrying out technical drawing for construction, the time needed for the dimensioning process represent an average of 50% from the duration required for carrying out the all drawing.

At first sight, using specific commands, the technical drawing for construction's dimensioning process is very simple, because the user must specify only the particular points that are required for achieving the dimensioning process. In fact this task is very complex because the user is forced to modify the dimensioning variables values so the dimensions are drawn accordingly to the standards from these countries. Thus, a set of specifications must be done:
- the way of limiting the dimension lines (arrows, ticks or dots);
- dimension text high;
- the size of delimiting elements of dimension lines (extension lines);
- the distance between dimension text and dimension lines;
- the distance from the ends of the dimensioned elements and the starts of the extension lines;
- the distance on witch the extension lines exceeded the dimension line;
- dimension text placement according with the dimension line;
- scaling of the dimension text values;
- dimension text precision (number of decimal places).

2. ANALISIS OF ARISING PROBLEMS IN THE ESTABLISHING PROCESS OF DIMENSIONING VARIABLES

Some of the problems arising in realizing of the previously presented settings are linked by:
- the way of limiting the dimension lines (arrows, ticks or dots);
- variants of leader limiting as function of the indicated element (arrows or dots);
- the size of limiting elements of the dimension lines;
- the size of limiting elements for the leaders.

2.1. The Way of Limiting the Dimension Lines (Arrows, Ticks or Dots)

According with the up the date technical drawing standards, the way of limiting the dimension lines differs as function of the specific elements represented in the drawing, thus:

- generally the limiting of dimension lines is made by ticks sloped at 45° (figure 1);
- in case of dimensioning of circles, arcs, and angles the limiting elements for dimension lines are arrows (figure 1);
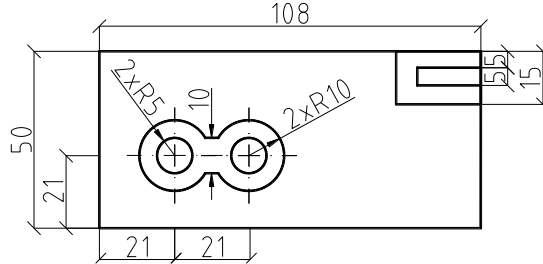
Figure 1. The dimensioning of an element according with the technical drawing standards

- in case of metal structure drawings the limiting elements for dimension lines are arrows (figure 2);
- in case that the dimensions text are small and cant' be written down the dimension text value it is possible to use the arrows in combination with dots or ticks sloped at 45° (figure 2).
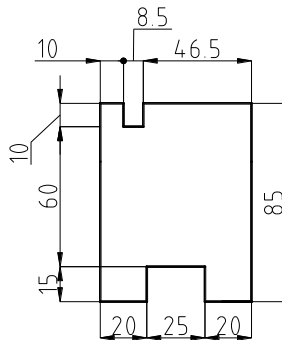
Figure 2. Part dimensioning according to the technical drawing standards

In figure 3 e.g. the dimensioning, using the AutoCAD computer program, of a metal structure detail is presented. As we see al the dimensions have arrows as delimiters. This fact is disadvantaging for the dimension texts that have the values 10 and 8.5 (figure 4), because:
- the right delimiter of the dimension 10 is overlapping on the dimension 8.5 space;
- the left delimiter of the dimension 8.5 is overlapping on the dimension 10.

If some one tries to modify from the *Modify Dimension Style → Symbols and Arrows* dialog box (figure 5), the shape of delimiter that are not correctly represented (e.g. the right delimiter's shape of the dimension 10 from arrow to dot, figure 6), he noticed that this is not correctly done, because:
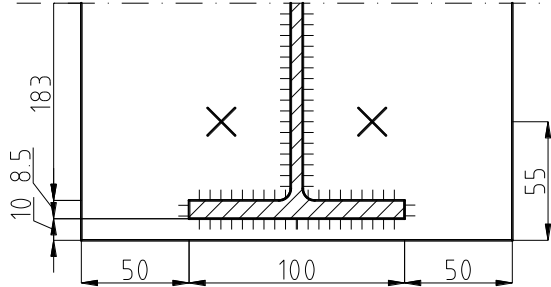
Figure 3. Metal structure; the dimension line's delimiters representation
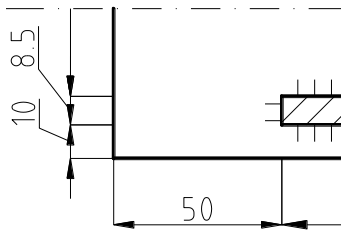
Figure 4. Dimensions' 10 and 8.5 delimiters positioning
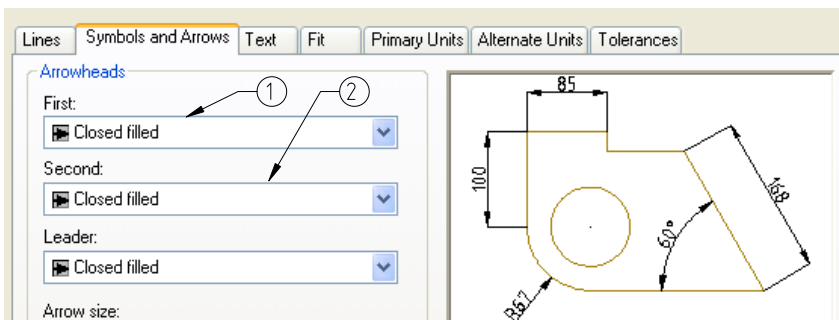
Figure 5. *Modify Dimension Style* dialog box;
1 – left side delimiter; 2 – right side delimiter
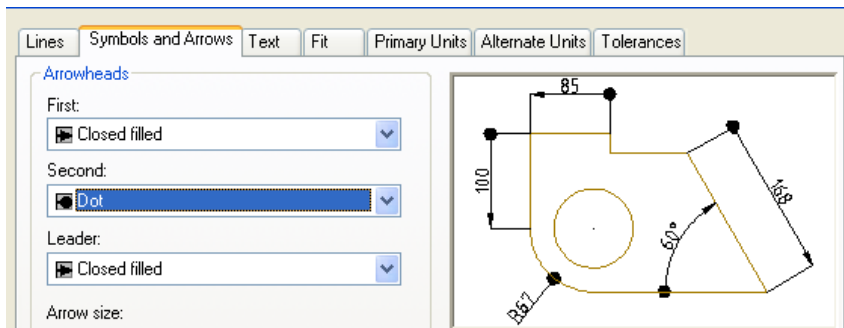
Figure 6. *Modify Dimension Style* dialog box; dimension's 10 right side delimiter was modified from arrow to dot

- by modifying any of the delimiters, the program automatically changes for the all the dimension lines the shape of the delimiters (figure 7).
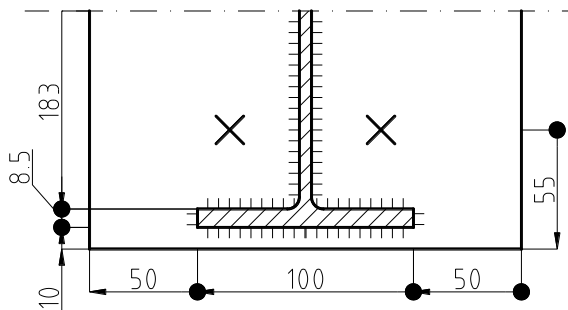
Figure. 7 Metal structure; The dimension lines' delimiters representation after the modify of dimension's 10 right side delimiter from arrow to dot

2.2. Delimiting Variants of a Leader as Function of Indicated Element (Arrows or Dots)

According to technical drawing for construction up to date standards, the way of leader delimiting differs as function of the indicated element thus:
- the leaders indicating a surface end with dots (figure 8);
- leaders indicating the contour end with arrows (figure 8).
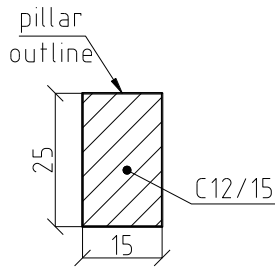
Figure 8. Leaders representation

As we notice from figure 9, in *Modify Dimension Style → Symbols and Arrows* dialog box, the AutoCAD computer program doesn't allow distinct change of delimiters shape for leaders. In case if it establishes that the shape of the delimiters is a dot (figure 10), the drawing from figure 8 looks like in figure 11.
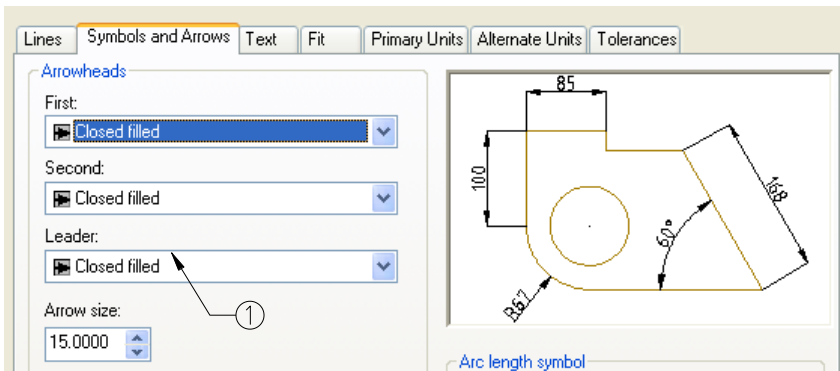
Figure 9. *Modify Dimension Style* dialog box; 1 – tile allowing to modify the shape of leaders delimiter
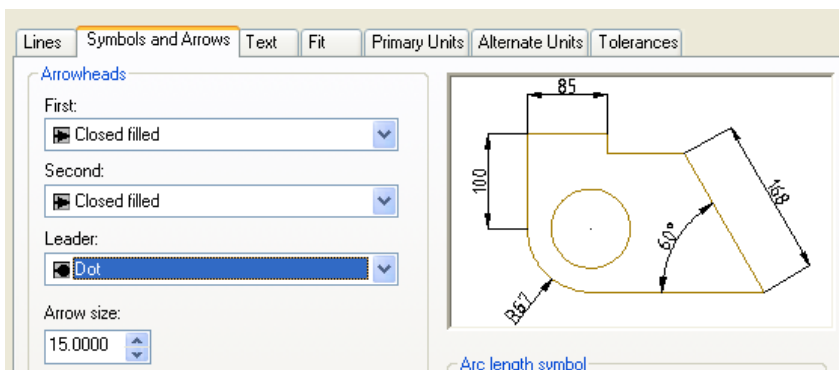
Figure 10. The leaders' delimiters have dot shape

As we notice, in figure 11, the rules regarding leaders' representation are not respected.
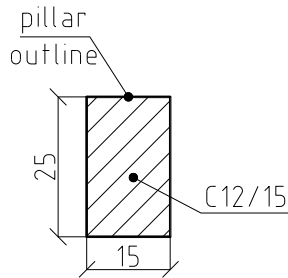
Figure 11. Leaders representation

2.3. The Dimension Lines Delimiters' Size

For the dimension lines' delimiters to be visible they must be appreciatively equal with the dimension text's high. In case that on the same drawing are used different types of delimiters (ticks sloped at 45° and dots or arrows and dots) must be established different size for dots delimiters in comparison with arrow or ticks delimiters.

As we notice in figure 12, in *Modify Dimension Style → Symbols and Arrows* dialog box, the AutoCAD code doesn't allow distinct change of the dimension lines' delimiters high, dimensioning of a drawing using different delimiters with shapes been presented in figure 7.
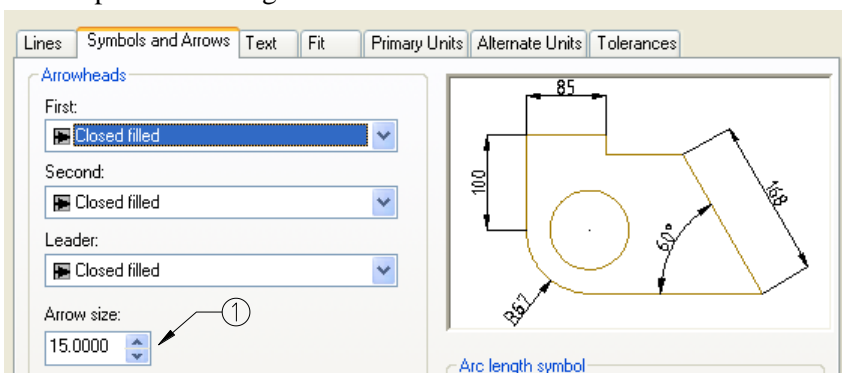
Figure 12. *Modify Dimension Style* dialog box; 1 – the dialog box allowing to modify the dimension lines' delimiters high

As we can see in figure 7, because the delimiters sizes weren't distinctively modified, the dot delimiters are much greater than the arrow delimiters, which have a proper size.

2.4. Leader Delimiters Sizes

To be visible the delimiters for leader lines must be near equal with the dimension text high. In case that on the same drawing different kinds of delimiters are used (dots and arrows) different sizes must be established for dot delimiters in comparison with arrow delimiters.

As we notice in figure 12, in *Modify Dimension Style → Symbols and Arrows* dialog box, the AutoCAD computer program doesn't allow distinctively modifying of delimiters high for leaders, the results of a drawing dimensioning using different shape of delimiters with same high being presented in figure 13.
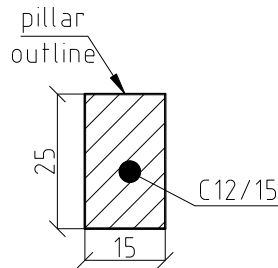
Figure 13 Leaders representation with the
same high for delimiters

According with the previously presented ideas it seems that the AutoCAD computer program is useless for dimensioning of technical drawing for constructions according with the up to day standards witch, is totally false because the program allows the dimensioning to be rapidly done if different dimensioning styles are created allowing individual settings for dimension text, dimension lines, leaders an so on.

3. CREATION AND USING OF INDIVIDUAL DIMENSION STYLES

For explaining the logic at the basis of constructing individual dimension styles we will use two examples (figure 14). The first example refers to the correct making of the dimension lines' delimiters and the second one for the leaders. As we notice in

neither of the two examples the rules referring to the technical drawing for constructions are not respected.
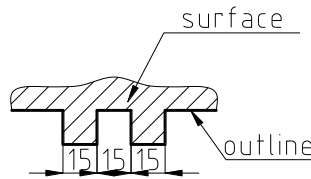
Figure 14. Sample for creation of individual dimension styles

3.1. Creation and Using of Individual Dimension Styles for Correct Representation of Dimension Lines Delimiters

If we try to separate the three assemblies (dimension text, dimension line and extension line) having the dimension text of value 15, we would noticed that each of them have arrows as delimiters (figure 15).
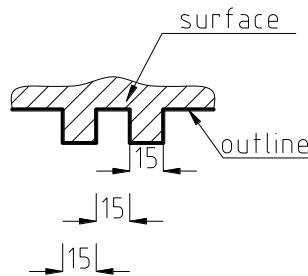
Figure 15. Assemblies' separation for visualizing of the delimiting way of dimension lines

As we can see in figure 15:
- the right side delimiter of the first dimension with value 15 should be replaced with a dot;
- the left side delimiter of the third dimension with value 15 should be replaced with a dot ;
- the two delimiters for the second dimension with value 15 should be replaced with dots.

For making possible the replacing of the delimiters individual dimension styles are created. Individual dimension styles creation is realized from *Dimension Style Manager* dialog box, pushing button *New* (figure 16).
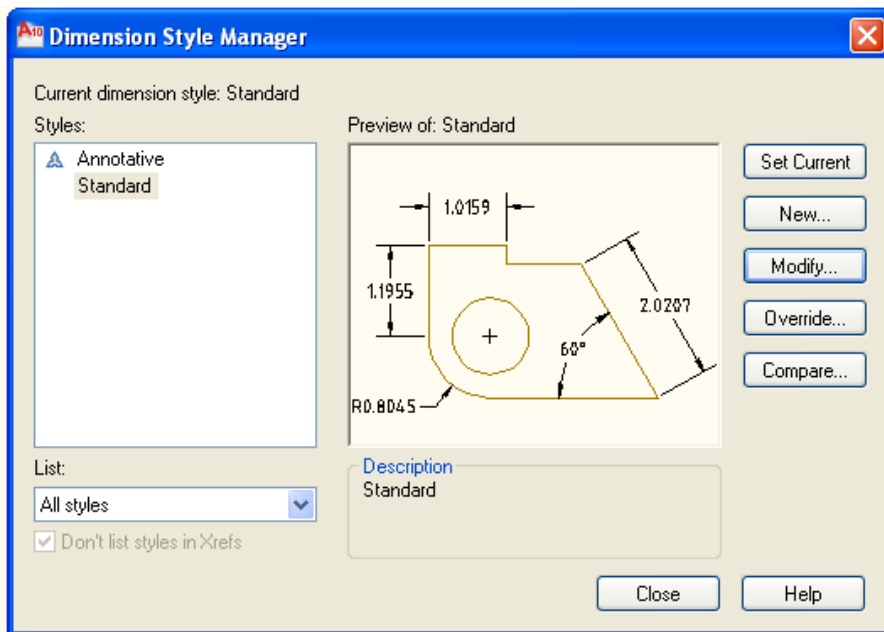
Figure 16. *Dimension Style manager* dialog box
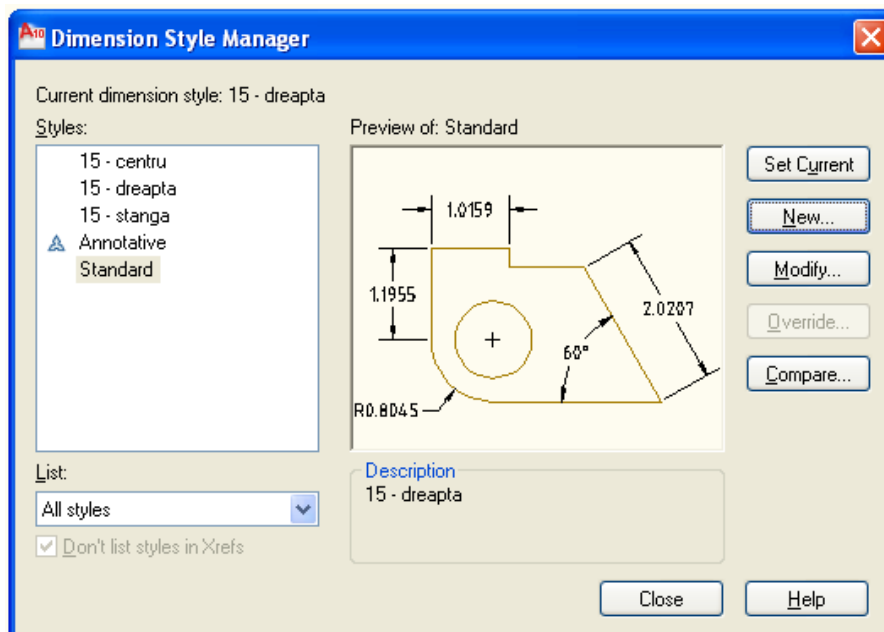
Figure 17. Presentation of the created dimension styles

By pushing the button *New*, the computer program opens the *Create New*

Dimension Style dialog box. The created styles were named *15 – stânga*, *15 – centru* şi *15 – dreapta* for each of the assembly that that must be modified (figure 17).

Next the style *15 – stânga* is selected, e.g., and the shape of the dimension line's right side delimiter is modified (figure 18).
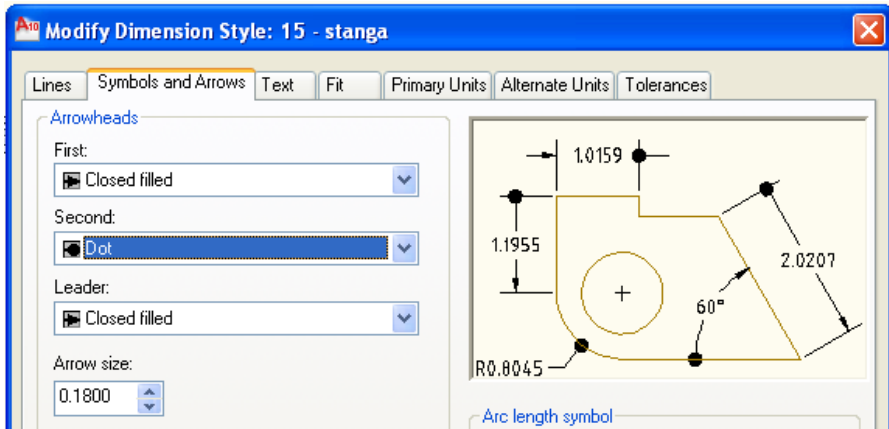
Figure 18. Modifying the right side delimiter for the dimension style *15 - stânga*

It is notice that no change appears in the delimiters representation, because the dimensions were created with base dimension style named *Standard* witch exist before the creation of the three new styles. For the dot delimiters to appear in place of the arrow delimiters two variants exist:
- the dimension represented with *Standard* dimension style is erased and drawing is dimensioned with the newly created style *15 – stânga*;
- the left side dimension is selected and the associated dimension style is change from the *STYLE* tool box (figure 19 and 20).
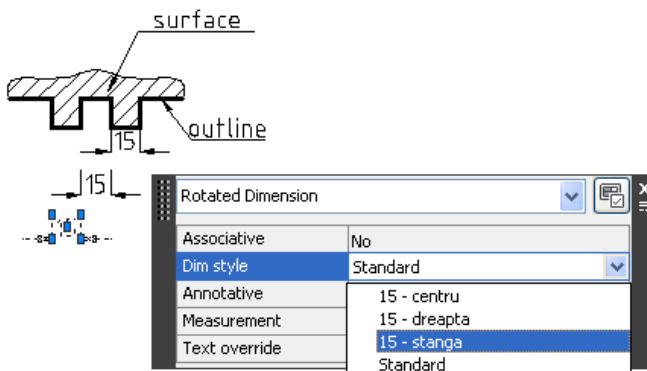
Figure 19. Modifying of dimension style from *STANDARD* to *15 - stânga*
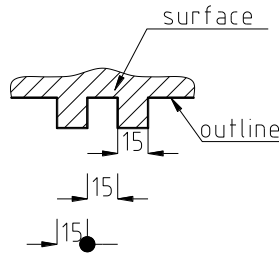
Figure 20. Results of changing the dimension style from *STANDARD* to *15 - stânga*

As we can see in figure 20 the dot delimiter's size is much bigger than the arrow delimiter's size. Because for a dimension line can't be established different size for delimiters (figure 18) follows that the must convenient way for creating the delimiters for those three dimension line is:

- the first dimension line's left delimiter from *CLOSED FILLED* (arrow) changes in *NONE* (without delimiter) (figure 21);
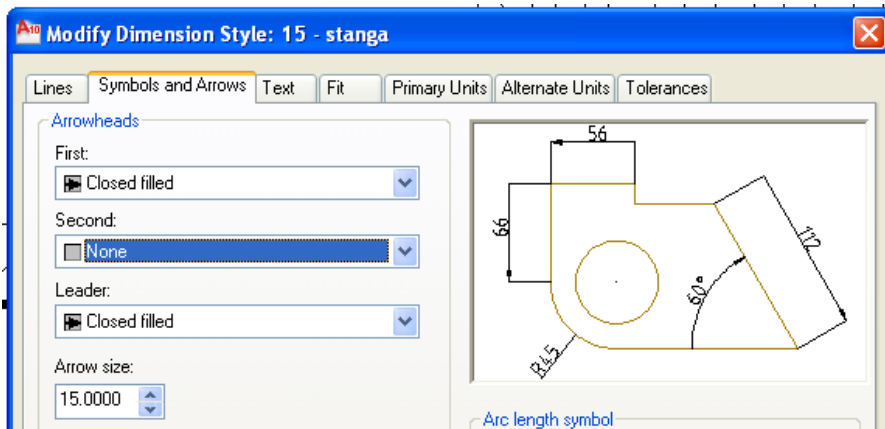
Figure 21. Modification of the first dimension's right side delimiter

- the second dimension line's delimiters change in *DOT*, by reducing to the half the size of these in comparison with the arrow delimiters' size (fig 22);
- the third dimension line's left delimiter from *CLOSED FILLED* (arrow) changes in *NONE* (without delimiter) (figure 23);
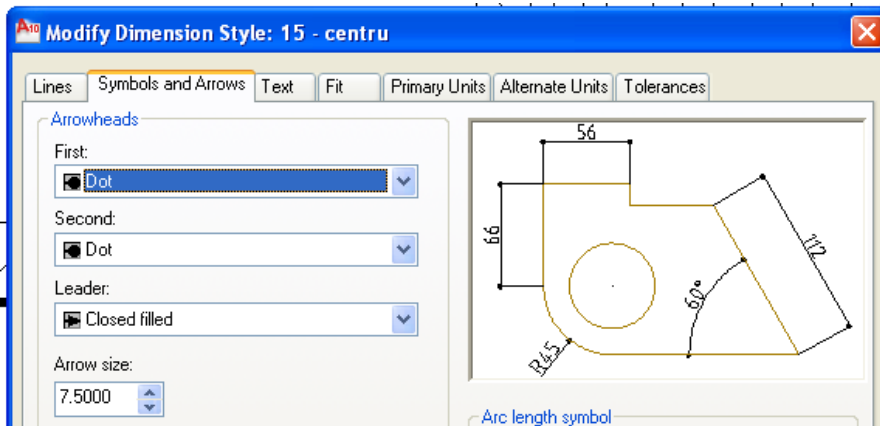
Figure 22. Modification of shapes and sizes of the second dimension's delimiters
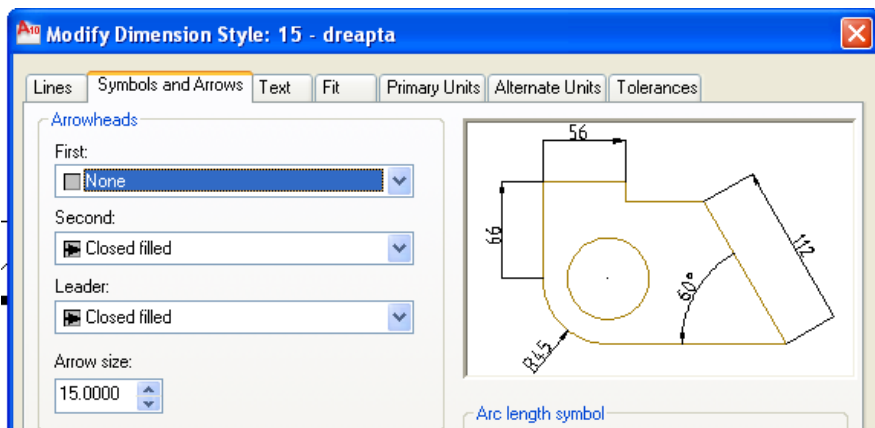
Figure 23. Shape modification of the third dimension's right side delimiter

After the change of the delimiters' representations for those tree dimension lines, the dimension are selected one by one and changing dimension styles, from *STYLE* button bar, the result being presented in figure 24.

3.2. Creation and Using of the Individual Dimension Styles for the Correct Achieving of the Leaders' Delimiters

As we can see in figure 24 in case that aren't using different dimension's styles, the AutoCAD computer program doesn't allows the different representation of the delimiters for leaders. The individual dimension styles creation is realized from *Multileader Style Manager* dialog box, pushing button *New* (figure 25).

By pushing the *New* button, the computer program opens the *Create New Multileader Style* dialog box. The style that is created was named *punct*.
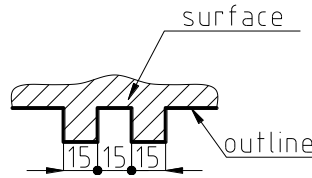
Figure 24. Dimensioning representation using individual
dimension styles
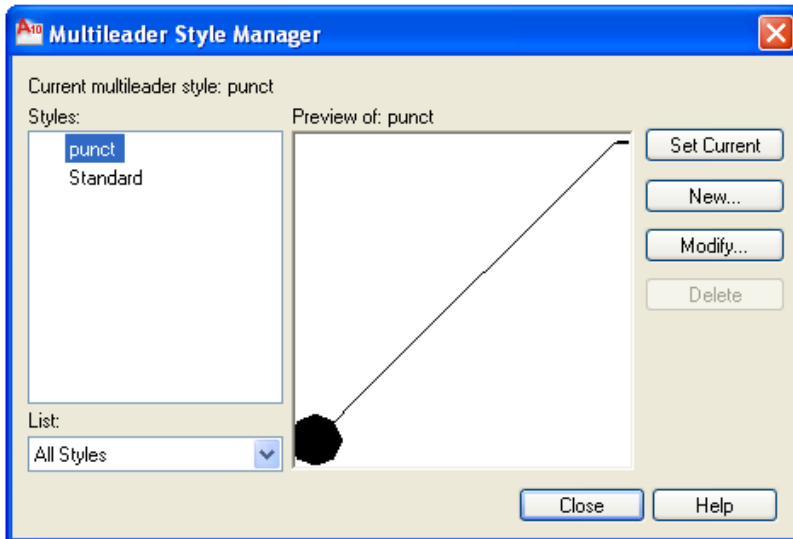
Figure 25. The presentation of the created dimension individual style

Then the *punct* style is selected and the delimiter's size and the shape are changed from *CLOSED FILLED* (arrow) in *DOT* (figure 26).

We can observe once again that any change in delimiter's representation doesn't appear, because the two leaders were drawn with the basis *Standard* style that exists before the creation of *punct* style. For the dot delimiter to appear in place of the arrow delimiter two variants exist:
   - deleting the leader that indicates a surface and that should have a dot for delimiter's shape and drawing it again using the style named *punct*.
   - Selecting the leader that indicates a surface and changing the dimension style from *STYLE* tool bar (figure 27 and 28).
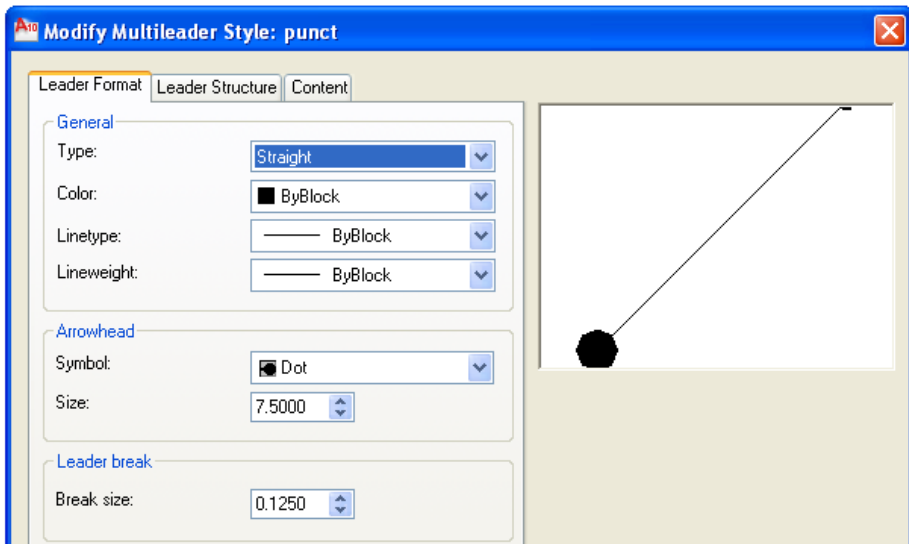
Figure 26. Modifing of size and shape of the delimiter for the created dimension style
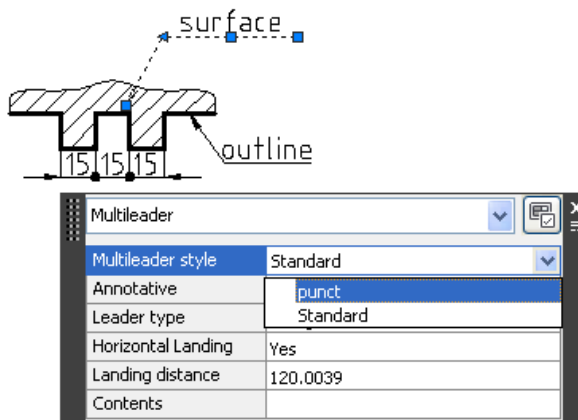
Figure 27. Modifying of dimension style from *STANDARD* to *punct*
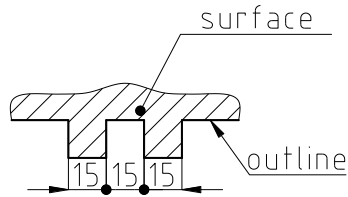
Figure 28 Dimensioning representation using the dimension
styles for dimesnion lines and leaderss

4. CONCLUSIONS

Creation and using the individual dimension styles allows the solving of the drawing problems that refer to the respect of technical drawing for construction's dimensioning standards from each country. More than that, if these are built in a unitary way, the time needful for accomplish the dimensioning operation may be reduce.

We notice that it is possible to build libraries with a sufficient number of individual dimension styles that could be used from one to another technical drawing. Doing so, the effort that is necessary to achieve the technical drawings for construction will reduce in a significant way.

Finally, we underline the fact that the person's skill that built such a library can be evaluated in concordance with the way that she think out an optimum number of individual dimension styles. We affirm that because a too little number of individual dimension styles won't totally cover the dimension's problems that could be meet on technical drawing for construction and a too large number can create confusion.

Flexural behavior of short reinforced concrete hybrid beams – experiment and numerical simulations

Marinela Bărbuță[1], Constantin Gavriloaia[2] and Ionuț Ovidiu Toma[3]

[1]*Departmen of Civil Engineering, Technical University "Gheorghe Asachi" of Iasi, Iasi, 700050, Romania*

[2] *Departmen of Civil Engineering, Technical University "Gheorghe Asachi" of Iasi, Iasi, 700050, Romania*

[3] *Departmen of Civil Engineering, Technical University "Gheorghe Asachi" of Iasi, Iasi, 700050, Romania*

Summary

The paper presents the experimental results on the influence of the longitudinal reinforcement ratio on the flexural behavior of the short reinforced concrete hybrid beams. The beams are made of two materials: high strength concrete (HSC) in the upper part (in order to take over compressive stresses) and polymer concrete at the bottom part (in order to withstand tensile stresses). Different longitudinal reinforcement ratios and reinforcement placing on the cross-section were used in order to study its influence on the overall flexural behavior of the beams.

A finite element nonlinear analysis was performed using the LUSAS program. The high strength concrete and the polymer concrete were modeled using linear plane stress elements. The reinforcement was considered as bar type with embedded functions in the plane stress elements. The complete bonding between the reinforcement and the polymer concrete was considered during the initial stages of the simulation.

The contribution of the longitudinal reinforcement to the peak resisted load is negligible once a certain value of ρ is attained. The midspan deflection corresponding to the peak load decreases with the increase in the longitudinal reinforcement ratio. The arrangement of the reinforcement on the cross-section has an important influence both on the load carrying capacity and on the maximum midspan deflection of the beams.

KEYWORDS: polymer concrete, hybrid beams, flexural behavior, FEM analysis

1. INTRODUCTION

Since the early times, engineers have been looking for ways to combine two or more materials in a structural element in order to take advantage of their strong features. This is how the so called hybrid structural elements were born. A very common type of hybrid structural element is the reinforced concrete made from the combination of concrete, which is good in compression, and steel, as reinforcement, which behaves very well in tension. This gave the engineers the possibility to build new structures with larger spans than before. Reinforced concrete is so widely spread and utilized today that it isn't even considered a hybrid material anymore.

The present paper brings its contribution to a better understanding of the flexural behavior of short reinforced concrete hybrid beams. The beams consist of a high strength concrete (HSC) part in the compression zone and a polymer concrete part (PoC) in the tensile zone. As it was first reported by Snell et al. in 1972 [1], polymer concrete is characterized by high tensile strength (2.92 times higher than the normal or high strength concrete), improved freeze-thaw durability and negligible water durability. A few decades later, the ACI Committee 548 in 2003 [2] issued a report in which the same properties were listed for the polymer concrete.

To the normal process of cement hydration, polymer modifications add a process of coalescence. As cement hardens, there form small spaces between the aggregate particles. These spaces are what allow water to penetrate, and do damage in freezing conditions. Polymer particles coalesce to fill these voids. That is why the concrete becomes less permeable and better protected against freezing [3]. Interestingly, polymer concrete does not produce bleed water. It makes an excellent overlay because it needs very little finishing. It is more accurate to say that it dries, than to call it curing. The polymer bonds not only to the concrete and the aggregate in the mix but also in the underlying concrete. It is for that reason that it is used to resurface concrete, Park et al. [4]. The patch method used to repair deteriorated reinforced concrete structures should produce patches that are dimensionally and electrochemically stable, resistant against penetration of deterioration factors, and mechanically strong. Today, the patch repair materials that are widely used contain admixtures, such as silica fume and polymers, to improve the performance of cement mortar [5].

The main objective of this research work is to assess the structural behavior of the polymer concrete. There has been quite extensive research done in the field of using polymers in construction materials [6-7]. However, the experimental research on different types of materials and elements is very seldomly completed by numerical models. The combination of the two materials with different properties such as high strength concrete and polymer concrete was used for obtaining short

reinforced hybrid beams. In the present paper both the experimental results and the finite element (FEM) analysis of the behavior of short hybrid beams are presented.

2. MATERIALS AND EXPERIMENTAL PROCEDURE

2.1. Concrete

The mix proportion of the high strength concrete used in the compression zone of the beams is presented in Table 1. The mechanical properties of the HSC were

Table 1. Mix proportion for the high strength concrete

HSC	Cement [kg/m³]	Aggregates [kg/m³]			Water [l/m³]	W/C W/C+SF	Super-plasticizer [l/m³]	Silica fume [kg/m³]
		0–4 mm	4–8 mm	8–16 mm				
	550	457	359	815	159.5	0.295 0.264	6.6	55

Table 2. Mechanical properties of the high strength concrete

HSC	Density [kg/m³]	Young's modulus [GPa]	f_c' [MPa]	f_{ti} [MPa]	f_{td} [MPa]
	2506	30	90.3	5.53	4.01

Table 3. Mix proportion for the polymer concrete

Polymer Concrete	Epoxy resin [%]	Fly ash [%]	Aggregate [%]	
			0–4 mm	4–8 mm
	12.4	12.8	37.4	37.4

determined experimentally and are summarized in Table 2.

The tension zone of the beams was cast out of polymer concrete. The mix proportion of the polymer concrete is given in Table 3. Fly ash was used as filler instead of Portland cement. Even though the mechanical properties of concrete using fly ash are tremendously improved [8], there are still concerns about the radioactivity levels of fly ashes [9].

2.2. Reinforcement

The reinforcement used in the experimental procedure was with smooth surface, made of mild steel, OB37 type. The mechanical properties of the longitudinal reinforcement were determined experimentally by means of the uniaxial tensile test on 10 mm diameter steel bars. The obtained yield strength was $f_y = 318$ MPa and the ultimate tensile strength was $f_u = 484$ MPa.

Figure 1a shows the reinforcement layout of the hybrid concrete beams. The shear reinforcement consisted of Φ6 smooth stirrups made out of OB37 steel. The stirrups are located in both shear spans so that to prevent the occurrence of the shear failure. Depending on the specimen, the longitudinal reinforcement consisted of 2 or 3 bars of different diameters. Their distribution is shown in Figure 1b for HBS029, HBS049 and HBS077 and in Figure 1c for HBS041 and HBS074. Figure 1d presents the geometry of a Φ6 longitudinal reinforcing bar. Its characteristics were the same for all other longitudinal reinforcing bars.

Each specimen was denoted in the form HBS029 where HB stands for hybrid beam, S stands for smooth (smooth longitudinal reinforcement) and 029 stands for the longitudinal reinforcement ration (which in this case is 0.29%).

2.3. Hybrid beams

Five hybrid beams with the dimensions of 600 × 150 × 150 mm (L × b × h) were cast in two stages. First, the high strength concrete part was cast and, after its hardening, the polymer concrete was cast. This procedure was chosen due the high

a) Beam geometry and reinforcement layout   b) Cross-section (2 bars)

d) Geometry of the longitudinal reinforcement   c) Cross-section (3 bars)
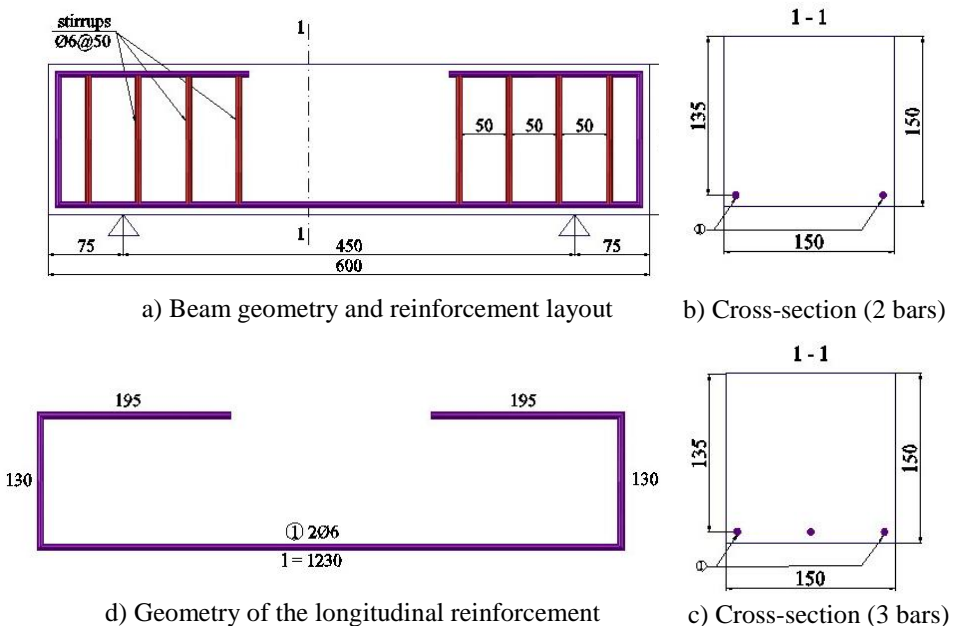
Figure 1. Beam geometry and reinforcement layout

bonding capacity of the polymer concrete [4].

The main parameter was the longitudinal reinforcement ratio ρ. Its values varied from 0.29% to 0.77%. In order to reach the above mentioned values of the longitudinal reinforcement ratio, the flexural reinforcement was distributed as shown in Figure 1b and 1c. The specimens together with their longitudinal reinforcement ratio ρ as well as the number to bars forming the tensile reinforcement are presented in Table 4. After 28 days, the beams were subjected to a three point loading test, Figure 2, in order to determine their flexural strength.

A total number of five hybrid beams were cast and tested in order to assess the flexural behavior of such types of elements. Concrete surface strains were measured both at the top fiber and at the bottom fiber of the specimens. The beams

Table 4. Longitudinal reinforcement ratio ρ

Specimen	No. of bars	Diameter [mm]	Area of the reinforcement [mm^2]	Longitudinal reinforcement ratio [%]
HSB029	2	6	56.55	0.29
HSB049	2	8	100.53	0.49
HSB077	2	10	157.08	0.77
HSB041	3	6	84.82	0.41
HSB074	3	8	150.79	0.74
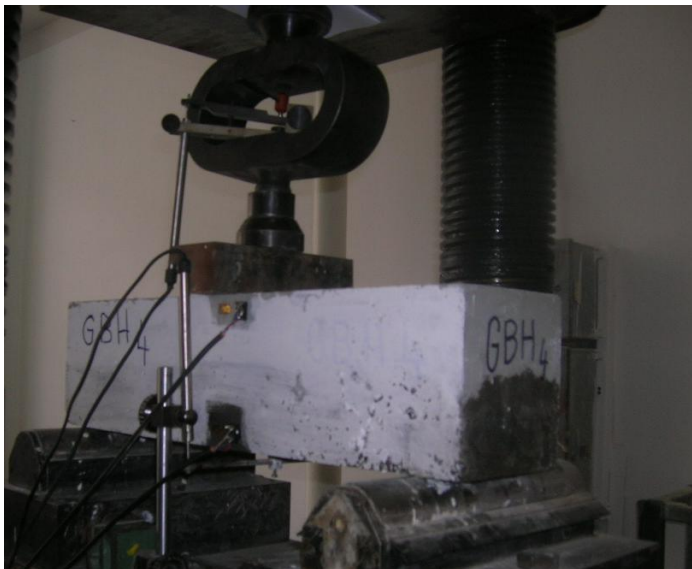
Figure 2. Three point loading test of the hybrid beams

were also instrumented with LVDT's located at the midspan in order to record the deflection during the loading (Figure 2).

The experimental results were accompanied by numerical simulations using the FEA program Lusas.

3. RESULTS AND DISCUSSIONS

3.1. Modes of failure

All beams failed in flexure tension mode of failure by yielding of the longitudinal reinforcement. The post-peak behavior of the specimens was characterized by a brittle formation of a single major crack at the midspan.

It should be pointed out that for all specimens, with the exception of HSB041, the bond between the high strength concrete part and the polymer concrete was not destroyed. For the HSB041 beam, a parallel crack with the longitudinal axis of the specimen was formed at the interface between the two materials. This crack, however, was observed only on one side of the beam.

Specimen HSB077 exhibited three flexural cracks. The major crack propagated to the compression zone. The other two cracks developed only within the polymer concrete part, one of them reaching the interface zone between the two materials. Once the interface zone was reached, the crack propagated longitudinally.

The width of the critical flexural crack was measured for all beams and its opening was 1 mm. It can be concluded, based on the recorded data, that the variation of the longitudinal reinforcement ratio does not influence the width of the critical crack in hybrid beams. This is somehow in contradiction with the general practice in reinforced concrete design where the reinforcement is used both for taking over the tensile stresses and to limit the width of the opening cracks. Further research is deemed necessary by the authors with respect to this particular behavior of the polymer hybrid beams.

3.2. Load – deflection curves

Figure 3 shows the load – deflection curves for all the specimens. It can be seen that the higher the longitudinal reinforcement ratio was, the higher the initial stiffness of the beams. However, the peak resisted load did not follow the same trend. The HSB049 (2 bars of Φ8 diameter) resisted a slightly larger load than the HSB077 (2 bars of Φ10 diameter). It can, therefore, be concluded that the contribution of the longitudinal reinforcement to the peak resisted load is negligible

once a certain value of ρ is attained. However, it can be observed that the midspan deflection corresponding to the peak load decreases with the increase in the longitudinal reinforcement ratio. This observation is strongly related to the initial stiffness of the specimens with the same arrangement of the reinforcing bars on the cross-section (Figure 1b, specimen HSB029, HSB049, HSB077).
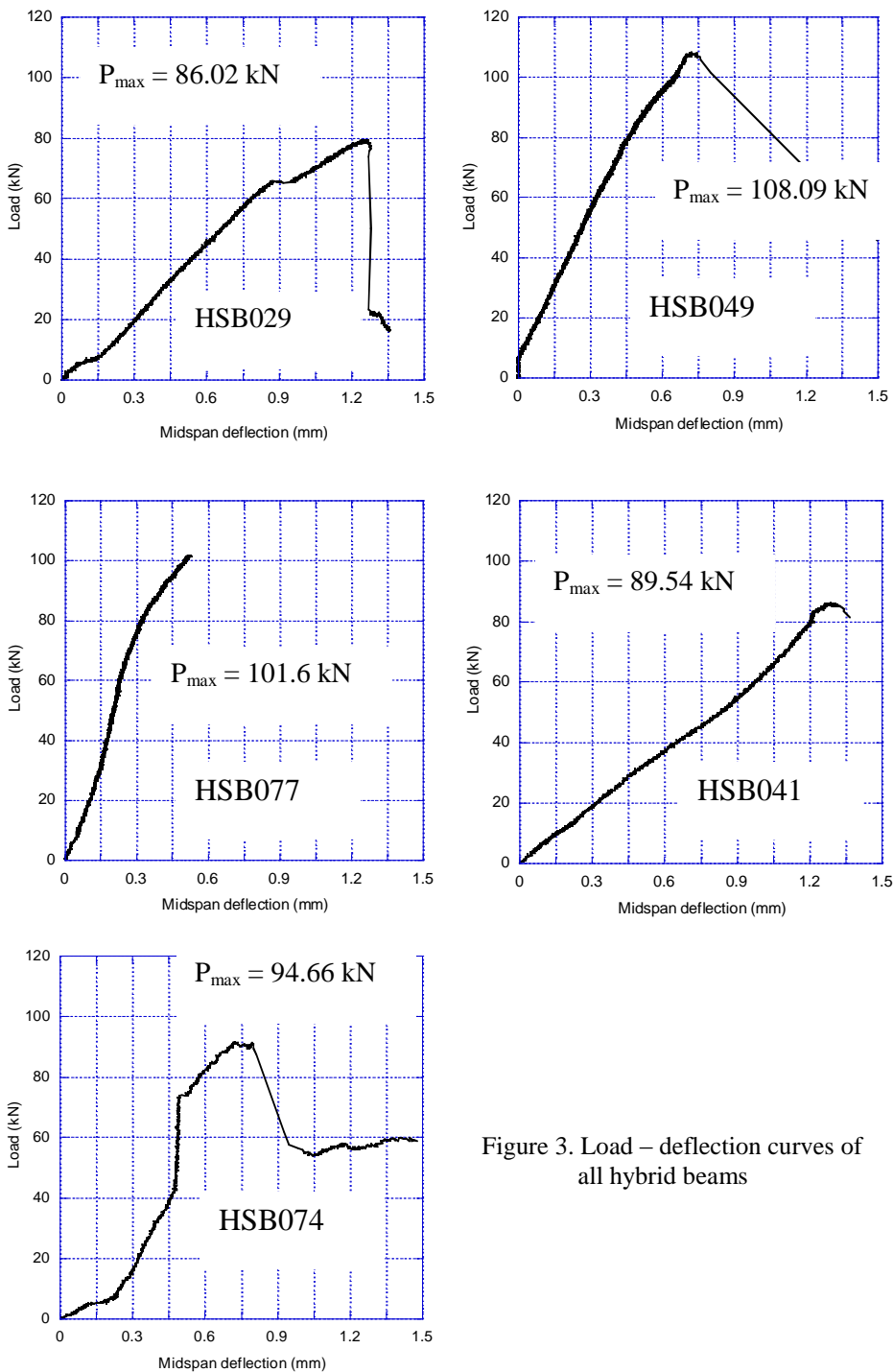
Figure 3. Load – deflection curves of all hybrid beams

When the reinforcement was placed differently (Table 4 and Figure 1c) in the cross-section, even though the value of the longitudinal reinforcement ratio changed from 0.29% to 0.41%, the ultimate load did not change significantly, 86.02 kN to 89.54 kN, respectively. Even for the slightly similar value of ρ, a different load carrying capacity was obtained, as it can be seen from Figure 3 for the following two pairs of specimens: HSB049 (2 bars, Φ8 diameter) versus HSB041 (3 bars, Φ6 diameter) and HSB077 (2 bars, Φ10 diameter) versus HSB071 (3 bars, Φ8 diameter). The main conclusion that can be drawn from these observations is that the arrangement of the longitudinal reinforcement on the cross-section of the composite hybrid beams plays an important role on the carrying capacity of the specimens.

It can also be observed that the midspan deflections corresponding to the peak loads for the specimens with similar longitudinal reinforcement ratios but different arrangements of the bars in the cross-section (HSB049 vs. HSB041 and HSB077 vs. HSB071) are almost the same. Based on the previous observations it can be said that the arrangement of the reinforcement on the cross-section has an important influence both on the load carrying capacity and on the maximum midspan deflection of the beams.

3.3. Finite element analysis

A finite element nonlinear analysis was performed using the LUSAS program. The high strength concrete and the polymer concrete were modeled using linear plane stress elements. The reinforcement was considered as bar type with embedded functions in the plane stress elements. The complete bonding between the reinforcement and the polymer concrete was considered during the initial stages of the simulation.

The material properties and characteristics were determined experimentally and considered in the numerical analysis.

Figure 4 presents the distribution of the tensile strains of the HSB077 beam. The red area in Figure 4 signifies the location of the maximum tensile stresses that lead to the formation of the flexural crack. This is in accordance to the observed behavior of the beam during the experimental stage.

Figure 5 shows the comparison between the load-deflection curve obtained from the experiment and given by the FEM analysis using LUSAS software for the HSB077 beam. It can be observed that there is quite a good agreement between the experiment and the analysis, even though the numerical model showed a slightly larger initial flexural stiffness and peak midspan deflection.

The ultimate load of the HSB077 recorded during the experiment was 101.6 kN. The value for the same load obtained from the analysis was $P_{max}^{FEM} = 101.58$ kN. There is a very good estimation of the beam carrying capacity by using the FEM analysis. However, further study should be conducted in order to improve the numerical model, especially in terms of the initial stiffness.

4. CONCLUSIONS

Both experimental tests and numerical simulations were used to investigate the flexural behavior of hybrid reinforced concrete beam. Based on the analysis of the obtained results the following conclusions can be drawn.
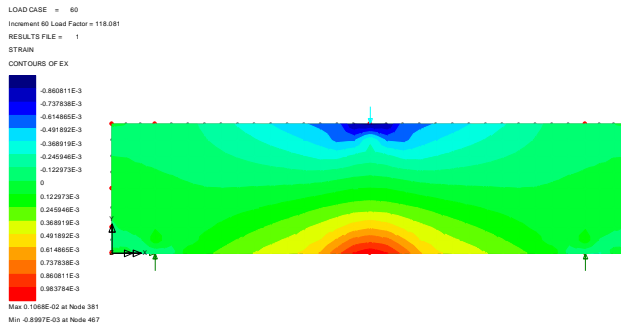
Figure 4. Tensile strains distribution for HSB077 (FEM analysis)
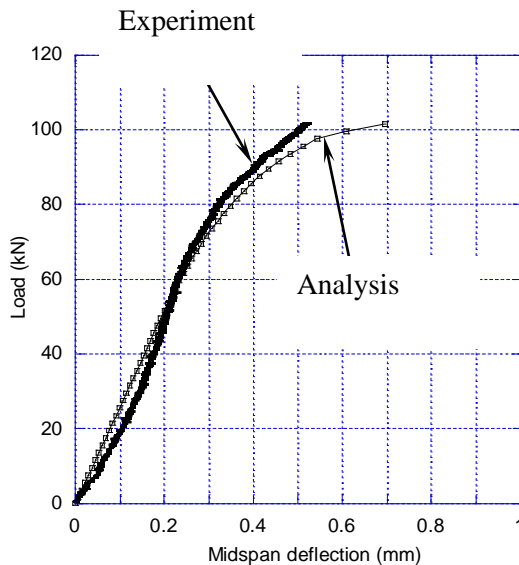
Figure 5. Load-deflection curves for HSB077 (experiment and analysis)

The contribution of the longitudinal reinforcement to the peak resisted load is negligible once a certain value of ρ is attained. The midspan deflection corresponding to the peak load decreases with the increase in the longitudinal reinforcement ratio. This observation is strongly related to the initial stiffness of the specimens with the same arrangement of the reinforcing bars on the cross-section.

The arrangement of the reinforcement on the cross-section has an important influence both on the load carrying capacity and on the maximum midspan deflection of the beams.

The FEM analysis results are in good agreement with the experimental results. However, further study is necessary to improve the numerical model mainly in considering all the factors that influence the initial stiffness of the hybrid beams.

References

1. Snell, L. M., Gillepsie, H. A. and Nelson, R. Y., Polymer concrete and its potential in construction industry, Proceedings of the Oklahoma Academy of Science, Vol. 52, pp. 160 – 162, 1972.
2. American Concrete Institute (ACI 548), Polymer – Modified Concrete Report (3R-03), Farmington Hills, U.S.A., 2003.
3. Rao, V. V. L. K., Aggregate mixture for least void content for use in polymer concrete, Journal of Cement, Concrete and Aggregates, No. 15, pp. 97 – 103, 1993.
4. Park, D. C., Ahn, J. C., Oh, S. G., Song, H. C. and Noguchi, T., Drying effect of polymer-modified cement for patch-repaired mortar on constraint stress, Construction and Building Materials, No. 23, pp. 434 – 447, 2009.
5. Gao, J. M., Qian, C. X., Wang, B. and Morino, K., Experimental study on
6. properties of polymer-modified cement mortars with silica fume, Cement and Concrete Research, No. 32, pp. 41 – 45, 2002.
7. Kreis, R., Polymer concrete – a progressive building material, International Polymer Science and Technology, No. 18, pp. 69 – 74, 1991.
8. Fowler, D. W., Polymers in concrete – a vision for the 21st century, Cement and Concrete Composites, No. 21, pp. 449 – 452, 1999.
9. Dinelli, G., Belz, G., Majorana, C. E. and Schrefler, B. A., Experimental investigation on the use of fly ash for lightweight precast structural elements, Materials and Structures, No. 29, pp. 632 – 638, 1996.
10. Kovler, K., Radiological constraints of using building materials and industrial by-products in concstreuction, Construction and Building Materials, No. 23, pp. 246 – 253, 2009.

Seismic Response of Buildings Subjected to the Bending Phenomena

Mihaela Anechitei[1], Doina Stefan[2] Violeta-Elena Chitan[3]

[1] *Faculty of Civil Engineering, Iasi, Romania*
[2] *Faculty of Civil Engineering, Iasi, Romania*
[3] *Faculty of Civil Engineering, Iasi, Romania*

Summary

A significant problem for the computation of structures subjected to dynamic loads is represented by the assessment of the horizontal loads on the vertical elements of the structure. This aspect can be complicated in accordance with the adopted constructive system. The present codes provide regularity restrictions in order to reduce the consequences of the bending earthquake effect. In this paper a comparison between seismic design requirements depending on the structural regularity is presented

KEYWORDS: *bending phenomenon, accidental eccentricity, energy dissipation, structural regularity, dynamic response.*

1. INTRODUCTION

The need to know the structures behavior under bending strain and to accurately determine its dynamic response represents the main priority in modern design [1].

A major issue in designing and calculating buildings capable to withstand lateral forces is the distribution of horizontal lateral forces upon vertical structural elements. This issue can become extremely complicated, depending on the adopted design.

Seismic design has to follow fairly regularly structure achievement, so that the inertia forces due to the mass have to be transmitted directly to the foundation [1]. Then, when is necessary an irregular shape, structural regularity may be obtained by subdividing the entire structure by seismic joints into dynamically independent units. To relieve supplementary efforts due to structure non regularity, behavior models and scripts will be used to asses if the structure can't be subdivided. To allow a more favorable redistribution of the action effects and widespread energy dissipation across

the entire structure, not only structure has to be symmetrical but the structural elements have to be as symmetrical as possible.

Horizontal seismic motion is a bi-directional phenomenon and thus the structure has to possess lateral rigidity and resistance at horizontal actions in any direction. Unbraced frame structures (with rigid joints), braced frame structures (with articulated joints) and structural walls (figure 1a-c) are typical systems to undertake lateral forces.

The other lateral force resisting systems impose architectural restriction excepting unbraced frame with rigid joints, so in consequence there are limitations in respect to the plan distribution. Moreover, generally, the gravitational force resisting systems are more economic then the lateral force resisting systems. Hence, a typical structure will contain systems to take over both, gravitational and horizontal forces (figure 1d) [2].
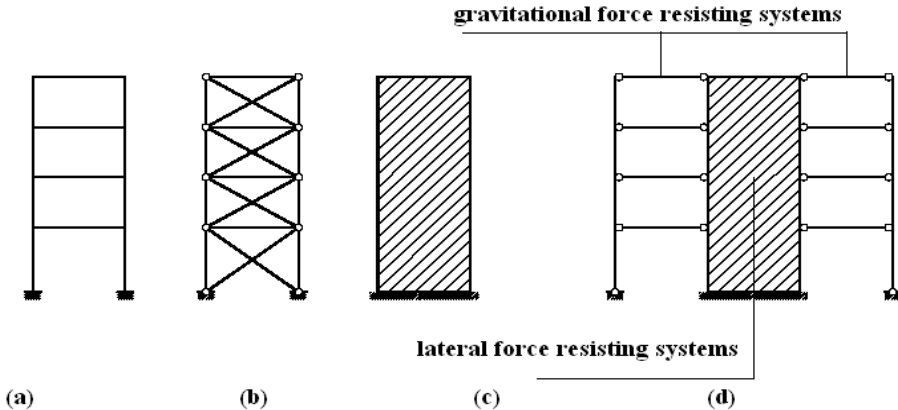
Figure 1. The lateral force resisting systems: (a) – braced frame with rigid joints; (b) – centric braced frames; (c) – structural walls; (d) – combined system.

Besides lateral resistance and stiffness, structures should possess an adequate torsional resistance and stiffness [3]. Torsional flexible structures lead to higher deformations and efforts in peripheric structure elements, as well as non uniform deformations and effort distribution in structural elements. According to the above statements, arrangements where the main seismic load carrying elements are distributed closer to the periphery of the structure present clear benefits (figure 2).
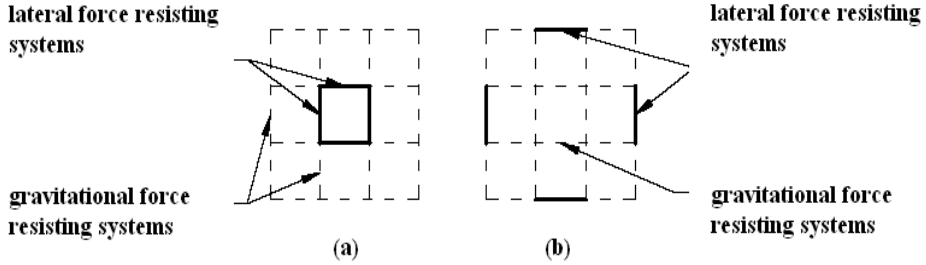
Figure 2. Structure with the same number of lateral resisting elements:
(a)– susceptibly for torsion; (b)– with increased rigidity and resistance to torsion

To ensure a small difference between the structure centre of rigidity (CR) and the centre of mass (CM), disposal of the lateral force resisting systems has to be symmetrical as possible. Seismic forces are inertia forces and their resultant acts in the centre of mass while the structure reaction act in the centre of rigidity. Uniform slab translation due to the action of lateral seismic forces is induced when the centre of mass does not coincide with centre of rigidity (figure 3a). A slab rotational component will exist, beside translational component, if between the centre of mass and the centre of rigidity an eccentricity exists (figure 3b). This effect leads to larger displacements on the flexible side (Δ_{2x} in figure 3b) compared to the rigid side (Δ_{1x} in figure 3b) along the direction of applied forces. In addition translational components will appear perpendicular to the direction of the applied seismic force (Δ_{1y} și Δ_{2y}). This eccentricity it may occur due to either non-uniformity in the rigidity distribution or non-uniformity in the mass distribution.
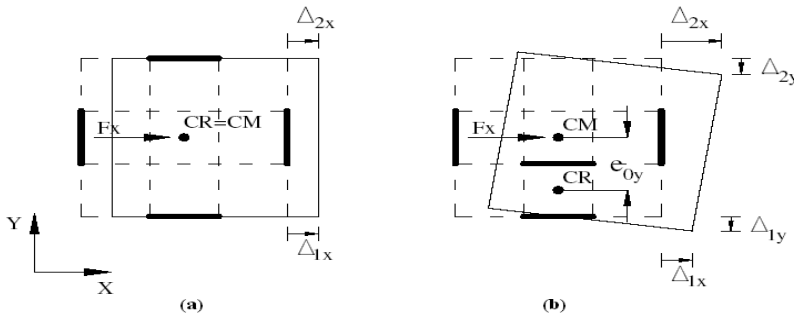
Figure 3. Structure plan with the lateral force resisting systems symmetrical arranged (a)
and with nonsymmetrical arrangement (b)

In a structure properly designed to take over seismic forces the slab has to be able to satisfy the following requirements:
- inertia forces sampling and their transmission to vertical structural elements;
- to behave like a horizontal diaphragm, ensuring that the vertical elements engage independently into taking over the horizontal seismic forces [3].

The seismic design of slabs with irregular shapes and with big voids and the design of slabs belonging to irregular structures (without horizontal and/or vertical regularity), will be based on design models able to show in a sufficient manner the behavior of the elements during an earthquake. A plate loaded on its plane can be, according to the case, assimilated to a deep-beam or truss ("strut-and-tie" model), recommended for the cases of slabs with large voids (figure 4). The model has to be chosen so that the system diagonals do not intersect the voids.
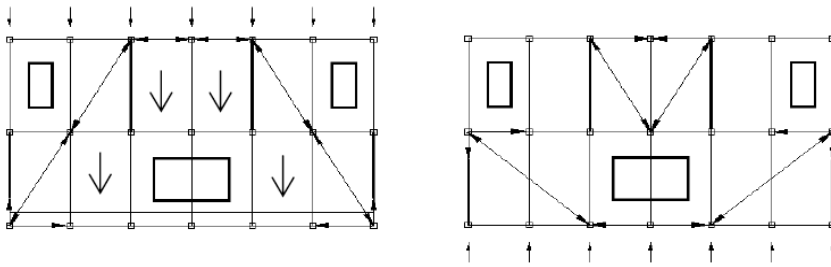
Figure 4. Structural model

The load carrying system consists of the gravitational force resisting systems and the lateral force resisting systems (figure 1). The horizontal diaphragm effect of the plate ensures seismic forces transmission to the lateral forces resisting systems and also ensure structure spatial co-operation. The horizontal diaphragm effect of the plate is useful in the case of structures with irregular plan shape and for case when the lateral force resisting system has different rigidities along the orthogonal directions of the structure. To ensure the horizontal diaphragm effect of the plate the slabs must fulfill stiffness and strength requirements.

In figure 5 the horizontal diaphragm effect of the plate effect on lateral deformations of the structure is presented. When a rigid slab ensures the connection between a peripheric rigid frame (taking over lateral forces) and an interior flexible frame (taking over gravitational forces), the seismic forces is assumed to be proportional to the frame rigidity. In this way the

seismic forces are taken over mainly by the rigid frame, and the rigid slab ensures equal deformations of rigid and flexible frames.
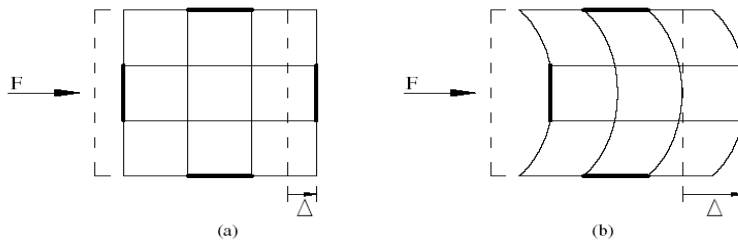
Figure 5. Structure deformations with rigid slab (a) and with flexible slab (b)

When dealing with a case of flexible slab (figure 5b), the rigid and the flexible frame system take the seismic forces in an independent manner. The value of the forces is proportional with each frame mass. In this case, because of a bigger mass and less rigidity the interior flexible frames develop larger deformations that the rigid ones, which involve higher structural and non-structural damage.

2. GENERAL CRITERIA FOR STRUCTURAL REGULARITY WITH RESPECT TO SELECTION OF STRUCTURAL DESIGN MODEL

For the purpose of seismic design, structures are classified into being regular or non-regular. In accordance with this classification one chooses [4]:
- the structural model, which can be either a simplified planar model or a spatial model;
- the analysis type, which can be either a simplified response spectrum analysis (lateral force procedure) or a modal one;
- the value of the behavior factor q, which should be decreased for structures with non-regular shape in elevation.

With regard to the implications of structural regularity on analysis and design, separate considerations are given to the regularity characteristics of the structure in plan and in elevation.

Table 1. Model and method of structural calculus

Case	Regularity		Allowed simplification		Behavior
	Plan	Elevation	Model	Linear elastic analyses	Linear elastic analyses
1	Yes	Yes	Plan	Equivalent lateral force*	Reference value
2	Yes	No	Plan	Modal	Decreased
3	No	Yes	Spatial	Modal	Reference
4	No	No	Spatial	Modal	Decreased

Note: *- Only if structure's height is smaller than 30m and the fundamental period of vibration is smaller than 1,5s;
- The selected model and method of structural calculus corresponded to the level of minimal calculus.

2.1. Structural regularity/ irregularity in plan

Eurocode 8 defines the following criteria in order to consider a structure regular in plan [5]:
- with respect to lateral rigidity, resistance and mass distribution, the structure should be approximately symmetrical in plan with respect to the orthogonal directions;
- the plan configuration should be compact, with regular contours; if the structure present setbacks (re-entrant corners or edge recesses), the sum of the dimension of the setbacks does not have to exceed 25% of the structure dimension in that direction;
- the in-plan rigidity of the slabs must be sufficiently large in comparison with the lateral stiffness of the vertical structural elements, so that the deformation of the slab should have a small effect on the distribution of the forces among the vertical structural elements;
- maximum displacement, determined at an extremity, must not exceed the average displacement of structure extremities with more than 20%, seismic force being applied with normalized eccentricity;
- the slenderness $\lambda = L_{max}/L_{min}$ of the structure should be not higher than 4, where L_{max} and L_{min} are respectively the largest and smallest in plan dimension of the structure, measured along the orthogonal directions.

The Romanian design code P100/2006 anticipates the first three restrictions like Eurocode8 and more [4]:
- at the second restriction, structure should be considerate regular in plan, setbacks case, this does not affect slab plan rigidity and differences between slab contour and slab convex polygonal envelope does not exceed 15% of the slab area;
- structure limit reduction should be realized only on the bearing element;
- maximum displacement determined at an extremity should not be higher than 1,35 of both structure extremities displacement;
- at each level and for each direction of analysis x and y, the structural eccentricity e_o and the torsional radius r should be in accordance with the two conditions below, which are expressed for the direction of analysis y:

$$e_{0x} < 0.30\, r_x$$
$$e_{0y} < 0.30\, r_y$$

(2)

where:
- e_{0x}, e_{0y} are the distances between the centre of stiffness and the centre of mass, measured along the x direction, which is normal to the direction of analysis considered, respectively on y direction;
- r_x, r_y are the square root of the ratio of the torsional stiffness to the lateral stiffness in x direction, respectively in y direction ("torsional radius").

2.2. Structural regularity/ irregularity in elevation

Eurocode 8 sets the following criteria that all the structures must satisfy in order to be considered regulate in elevation [5]:
- structural system must be monotone along the vertical direction without variations from the foundation level up to the top level of the structure. If the structure present setbacks on the height this must not exceed 20% of the dimension of the inferior level;
- both the lateral stiffness and the mass of the individual storey must remain constant or reduce gradually, without sudden changes, from the base to the top of structure;
- for gradual setbacks preserving axial symmetry, the setback at any slab should not be greater than 20 % of the previous plan dimension in the direction of the setback (figure 6a and figure 6b);
- for a single setback within the lower 15 % of the total height of the main structural system, the setback should not be greater than 50 % of the previous plan dimension (figure 6c);

- if the setbacks do not preserve symmetry, on each face the sum of the setbacks each storey should not be greater than 30 % of the plan dimension at the ground slab above the foundation or above the top of a rigid basement, and the individual setbacks should not be greater than 10 % of the previous plan dimension (figure 6d).
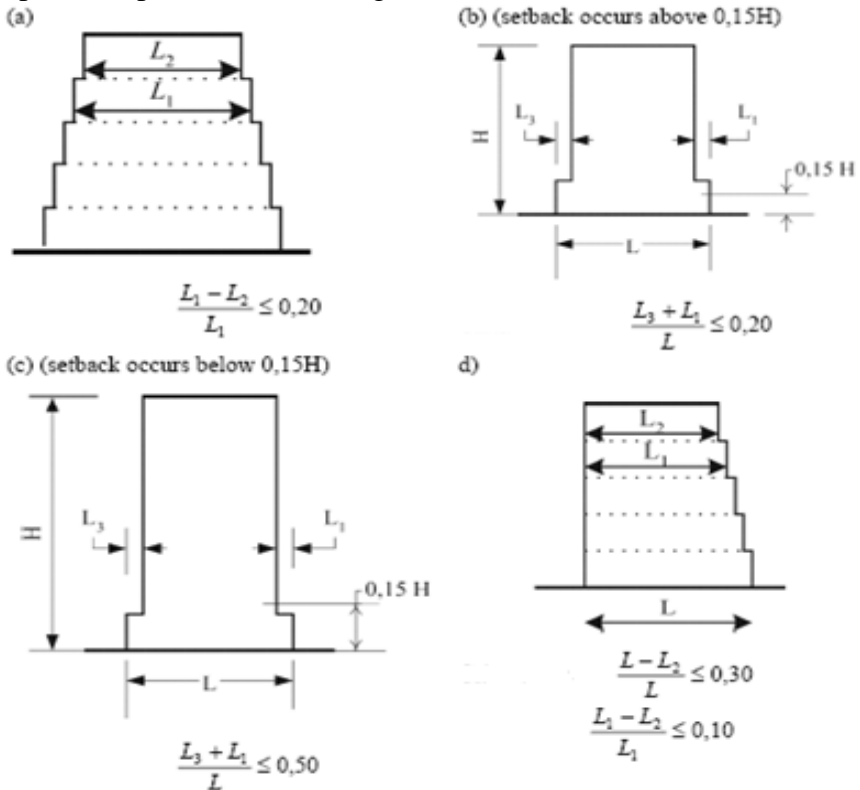
Figure 6. Criteria for regularity in elevation

The Romanian code provisions P100/2006 for regularity in elevation are [4]:
- the structure does not present reduction of lateral rigidity higher than 30% of inferior or superior level;
- the structure does not present reduction of lateral resistance higher than 20% of inferior or superior level;
- if the dimensions of structural elements are reduced from the base to the top of structure, the rigidity and resistance variation have to be uniform without any sudden reduction from the base level to the top one;

- the mass has to be uniformly distributed, so that the differences between the storey mass and adjacent storey do not exceed 50%.

3. CONCLUSIONS

Although the design requirements require the achievement of regular structures in plan and elevation, there are various causes (functionality, esthetics, economy, configuration of available land) out of which results buildings with structural and mass dissymmetry.

The bending phenomenon is one of the most common causes for structure failure during major earthquakes due to sudden change of regularity, rigidity and resistance of structural elements. These sudden changes occur at planar as well as elevated level, leading to large values of ductility requirement thus, the necessity to improve the strength of structure's component elements.

Therefore, the structure and/or the structural elements should be as regular shaped as possible also, strive for a uniform distribution of masses and loads in order to limit the occurrence of bending phenomenon as much as possible.

References

1. Enache R., *Răspunsul seismic torsional generat de cutremurele vrâncene*, Ed. Matrix rom., Bucuresti 2008.
2. Negoiţă Al., Pop I., s.a., Inginerie *seismică*, Ed. Didactică si Pedagogică, Bucuresti 1985.
3. Duan X., Chandler A., *Torsional Coupling Effects in the Inelastic Seismic Response of Structures in Europe*, Proceedings of the 9-th European Conference on Earthquake Engineering, Vol. 1, Moscova, 1990.
4. P100-1/2006, *Normativ pentru proiectarea antiseismică a construcţiilor de locuinţe, social-culturale, agozootehnice si industriale*.
5. Eurocode 8-1998, *Design of structures for earthquake resistance*.

Mihaela Anechitei, Ph.D., The "Gheorghe Asachi" Technical University of Iaşi, Faculty of Civil Engineering, B-dul Mangeron 43, Iaşi, Romania, email: mihaelaanechitei@ce.tuiasi.ro

Doina Stefan, Prof. dr. eng. "Gh. Asachi" Technical University of Iasi, Faculty of Civil Engineering, B-dul Mangeron 43, Iasi, Romania, email: dstefan@ce.tuiasi.ro

Violeta-Elena Chitan, Lector dr. eng., "Gh. Asachi" Technical University of Iasi, Faculty of Civil Engineering, B-dul Mangeron 43, Iasi, Romania, email: chitanvioleta@yahoo.com

Robot helps us to rehabilitate an Over Pass in Resita

Adrian Bota[1], Dorian Bota[2] Alexandra Bota[3]

[1] *Civil Engineering Faculty, "Politehnica" University of Timisoara, 300223, Ramania*
[2] *S.C. APECC S.R.L, Timisoara, 300133, Ramania*
[3] *S.C. ALDOR S.R.L, Timisoara, 300133, Ramania*

Summary

The over pass to be rehabilitated is situated in the northern part of the city Resita and passes the switch yard for railways and the Barzava river.

The substructure of the over pass, consisting of two spans situated on the left bank of the Barzava river, is under passed by a junction arm for the access on the over pass.

In the winter of 2007 an over gauged transport has heavily hit the three monolith reinforced concrete girders of the superstructure.

In spite of the significant damages, the superstructure has kept its bearing capacity needed for a light traffic with a maximum load of 3,5 t.

The paper presents the damages of the superstructure and also the rehabilitation solutions, which involve the adjustment of the geometry of the under passing junction arm as well.

KEYWORDS: Over pass rehabilitation, Reinforced concrete, Lifting system, Road geometry adjustment

1. GENERAL ASPECTS

The over pass over the switch yard for railways afferent the station Resita North, situated in the city Resita, assures the connection between the national road 58B Resita – Voiteni and 58 Resita – Caransebes [2]. In addition to this, the over pass facilitates the connection between the Lunca Barzavei neighbourhood in the north of the city and the anchient and industrialized part situated in the south (Fig. 1).

As an entirety the over pass consists of two parallel structures, the first one, situated in the North, executed in 1965 as a monolith reinforced concrete solution, and the second one, situated in the south, executed in 1989 in prestressed precasted

concrete solution. Both structures of the over pass were dimensioned for the loading class E.

Figure 1. Lateral view towards the first hit beam

The initial structure consists of three sections:
- one section from the west part, curbed, assures the access towards Timisoara;
- the second sections from the west part, also curbed, provides the access towards Resita South but also the passing over of the junction arm afferent the direction Timisoara-Caransebes;
- the third section is streight and assures the passing over the switch yard of the railway.

The execution of the new structures in 1989 allowed the increase of the gauge up to 4 traffic lanes an the emplacement of the tramway in a separate track. The older structure, from 1965, is aimed only for vehicle and pedestrian trafic.

The superstructure build as a frame affected by the intervention works, consists of two spans of each 22 m, simply beared on the marginal infrastructures, pier and abutment, and has fixed ends on the central pier (frame knot).

The total width of the over pass is 12,80 m and includes the carriage way of 8,20 m, a footway of 2,60 m on the right side and a safety area of 2,00 m on the left side, next to the tramway.

The cross section has three girders out of monolith reinforced concrete having an interax distance of 4,00 m. The girders are 1,80 m high. The spatial compound effect of the bridge deck is assured by 3 cross beams situated in the field and the ones from the bearing sections.

The degraded structure of the over pass is passing the junction arm between the national road 58B Resita - Voiteni and 58 Resita - Caransebes.

This road bears all kind of traffic gauge, in the direction Resita – Timisoara, respectively Timisoara – Caransebes via Resita.

The way has asphalt coating with disleveled border stones having a width of 7,00 m for two traffic lanes.

It has to be pointed out that the inferior gauge of the over pass is only 4,20 m, fact that is against the effective standards, which foresee a hight of 5,00 m. In this situation accidents, which could affect the integrity of the over pass structure, can occure.

2. **DEGRADATIONS AND THEIR CAUSES**

Subchapter title uses ".08a Subchapter" style, Times New Roman font, 12 points, line space single, alignment left, 18 points before and 6 points after. A left tab is placed at 8 mm and the hanging is also at 8 mm.

In the first decade of December 2007 an over gauged transport has under passed the over pass. The restriction for the maximum height of 4,20 m established when entering the under passing junction arm, was not considered and the impact was followed by the heavy degradation of the three reinforced concrete beams, in the central area of the marginal span, between the current cross beams.
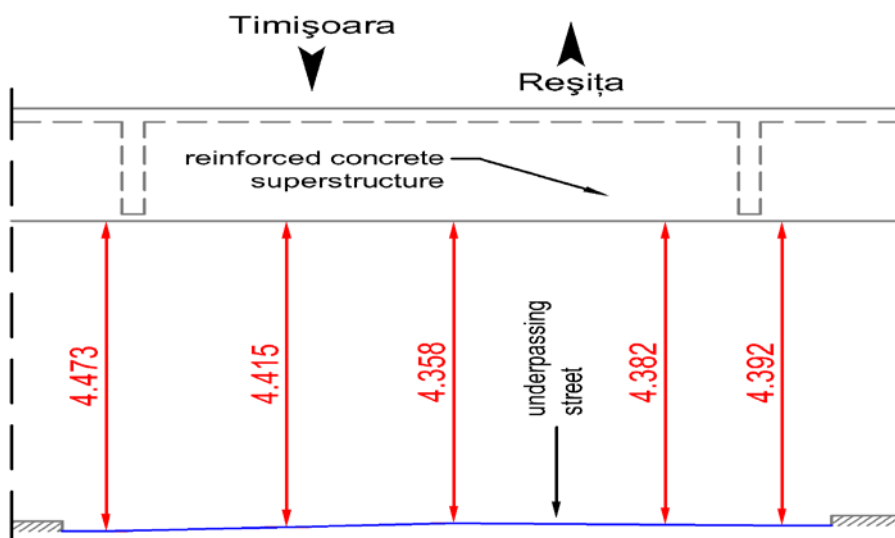
Figure 2. The vertical gauge under the first hit beam

In order to clarify the causes which lead to the mentioned degradation, measurements for the vertical gauge were made by using electronic devices with laser [1]. These measurements were carried out in 3 sections in the over pass area: under the steel gauge restriction device, under beam 1 (from Timisoara) and under beam 3 (from Resita).

It is notable that from chronologically point of view, the impact occurred as follows: beam 1, beam 2, beam 3 [1]. Thus first was beam 1 hit having the minimum vertical gauge 4,358 m, with 0,158 m higher than the restriction height of 4,200 m (Fig. 2).

The girders of the span on the abutment side show important degradations of the concrete in the core and the flanges, respectively of the resistance reinforcement, with disrupted and deformed bars, some of these having a seriously diminished section (Fig. 3, 4 and 5).

Figure 3. Beam 1

Figure 4. Beam 2 (central beam)

Figure 5. Beam 3

Due to this degradations, on about 40% of the reinforcement can not be counted anymore, fact that leads to a proportional diminishing of the bearing capacity of the over pass. It was estimated that the reserve of bearing capacity is satisfactory only for vehicles with a maximum load of 3,5 t. Therefore a tonage restriction was imposed in order to keep the traffic for light vehicles.

3. REMEDIAL SOLUTIONS

In order to establish the optimal rehabilitation solution, the structure was expertized and two posibilities were considered:
- rehabilitation of the structure;
- replacing the existing structure.

Considering the fact that the replacing solution would mean intervention works at the bearing areas, which would had to be adapted to the designed cross section, and also the alteration of the intermediate pier beam (a highly complex operation), the option was to bring the structure to an adequate bearing capacity. This solution is advantageous as structural concrete is of good quality, C25/30 [2] (Fig. 6).

Figure 6. Concrete test rods from the superstructure

Considering opting for the replacing of the existing structure the following situation is reached:

- ▪ on the same traffic direction there will be two different structure types, as rebuilding the structure in a monolith solution is technicaly an obsolete aspect;
- ▪ the over pass will have three structures types with very distinct ages (1965, 1989 respectively 2009) which would request specific maintenance works.

Nevertheless bouth solutions impose the lowering of the grade line in order to obtain an appropriate gauge under the over pass, according to the standards in use.

For the rehabilitation of the degraded part of the over pass, three technological solutions were considered:

- a) external prestressing applied on the affected girders, solution which was considered unfitting as the structure is realized with curbed girders having a

radius of about 170 m; this leads to horizontal efforts aferent the longitudinal prestressing phenomen;

b) consolidation with carbon fibres apllied on the lower flange of the girders, solution which would not provided sufficient security of the consolidated area due to the unappropriate vertical gauge of the under passing street;

c) renewing of the degraded reinforcement by replacing the affected bars with new ones connected with the existing bars in the area where the concrete was not destroyed.

The third solution was retained as being the most convenient considering the execution and the behaviour of the structure.

The solution requests that, at the moment of the intervention, the efforts in the damaged reinforcement should be reduced close to zero. Only this way the new reinforcement will be active after the concreting similar to the existent reinforcement.

In order to bring the mounted reinfocement in a effort status similar to the one of the existing bars, the temperature of the new reinforcement will be modified, which will lead to the expansion of the bars before welding and to their contraction when cooling down and therefore to the stressing of the bars.

For an important diminishing of the unit stress in the reinforcement in the affected area, the bridge deck will be supported provisionaly with steel tubes. On these tubes hydraulic jacks will be mounted which will be used to modify the anti-gravitational loads upon the structure and therefore the stress state [3] (Fig. 7).
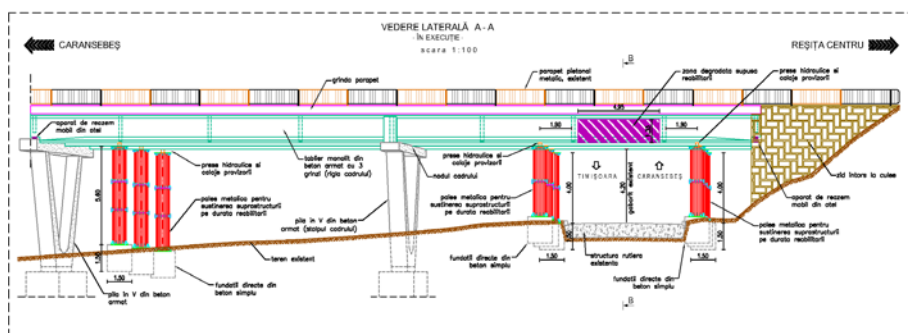
Figure 7. Provisional support of the structure

Due to the characteristics of the frame structure, additionally supports for the superstructure were necessary also in the unaffected span. In this way the loading level in the frame elements was maintained at a maximum value comparable to the one the structure was initially designed for (permanent load + special vehicles V80 convoy) (Fig. 8).
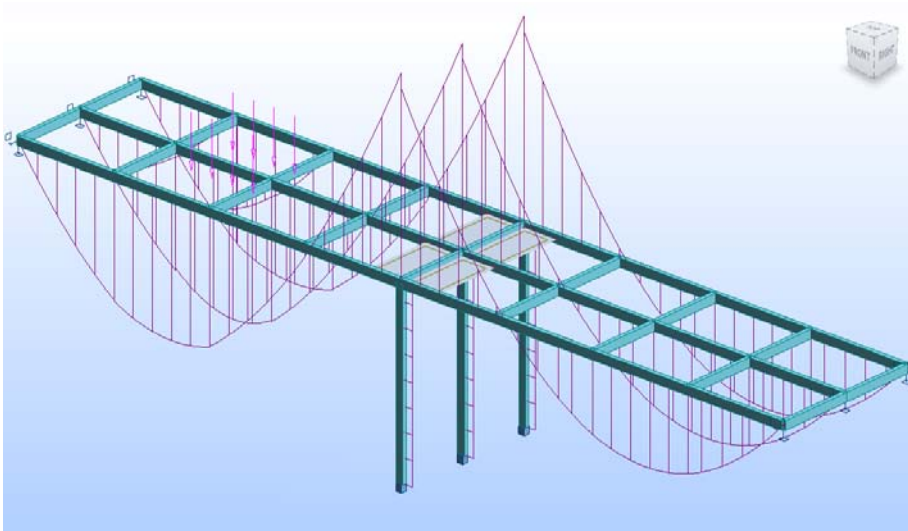
Figure 8. Bending moment from permanent load + V80 convoy

The principle of superpositioning the effects made possible to find a load combination in the 3 supporting lines with jacks, which lead to a minimal load value in the degraded area and to acceptable values in the other characteristic sections (lower than the loads the structure was designed at) (Fig. 9 and 10).
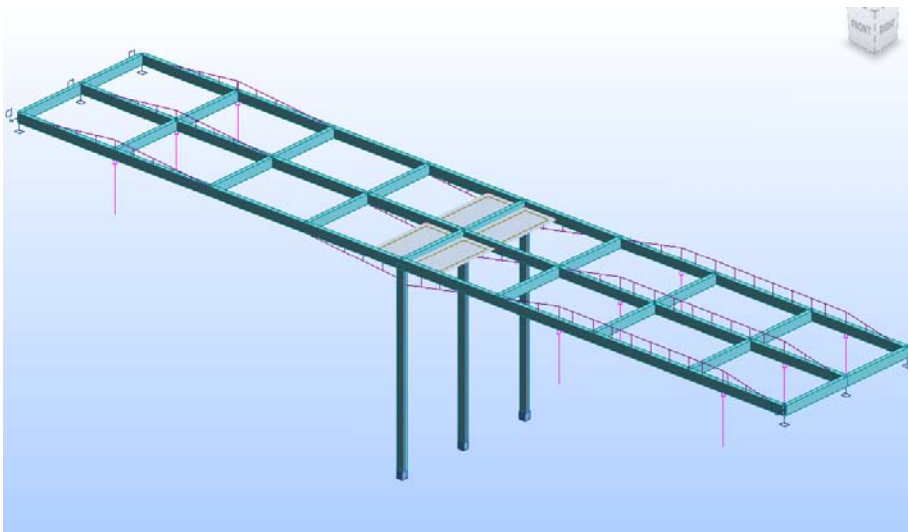
Figure 9. Bending moment from aditionally loading from the hydraulic jacks
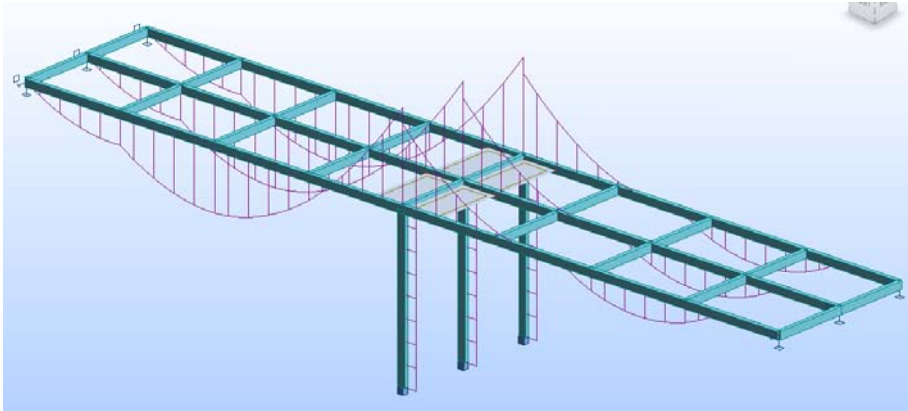
Figure 10. Bending moment from aditionally loading from the hydraulic jacks and permanent load

Thus the replacing works of the degraded reinforcement can be carried out at 23% of the load afferent the permanent loading (Fig. 11).

	K x	M max [kNm] in point 20/100				M max [kNm] in point 8/100			
		girder G1 TM		girder G2		girder G1 TM		girder G2	
		in use	in rehab.	in use	in rehab.	in use	in rehab.	in use	in rehab.
Structure		1206	1206	1210	1210	731	731	735	735
Dead load		1166	1166	1166	1166	714	714	713	713
S+D+2A30		2372		2376		1445		1448	
S+D+V80		2518		2507		1498		1499	
jacks line 1	**4.5**		-794		-794		-1121		-1121
jacks line 2	**4**		-976		-976		-359		-359
jacks line 3	**4**		139		139		51		51
demolition G1			-118		-57		-43		-30
demolition G2			-59		-88		-32		-28
demolition G3			-22		-57		-14		-30
TOTAL			542		544		-72		-69
			23%		23%				

Figure 11. The optimum value of the aditionally loading from the hydraulic jacks

After the renewal of the degraded reinforcement, the core and the flange of each girder will be reconcreted.

When the rehabilitation works are finished, the provisionaly steel tubes will be removed together with the afferent foundations.

The works will be finished by modifying the geometry of the under passing street aiming to provide an appropriate vertical gauge (Fig, 12).

Works for the renewal of the sewage respectively for the street lighting will also be executed [3].
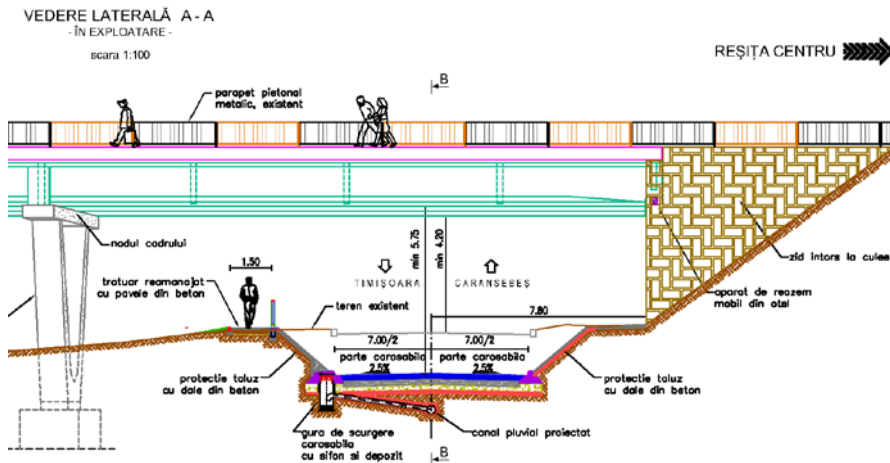
Figure 12. The designed under passing street

4   CONCLUSIONS

By carrying out de rehabilitation works, the following objectives are reached:
- ▪ bringing of the bearing capacity of the over pass at the level of the loading class E;
- ▪ keeping the structural assembly of the over pass as a monolith reinforced concrete structure;
- ▪ obtaining an appropriate vertical gauge under the over pass for a street with 2 traffic lanes and footway;
- ▪ providing all safety conditions for the traffic development on and under the over pass.

References

1. ***   *Raport de determinare a gabaritului la Pasajul Reşiţa Nord, SC ALDOR SRL Timisoara-RO, Contr. 102G/2008.* (in Romanian)
2. *** *Expertiză tehnică – Pasaj rutier Triaj – Lunca Bârzavei, Reşiţa, SC ALDOR SRL Timisoara-RO, Contr. 102E/2008.* (in Romanian)
3. *** *DALI - Pasaj rutier Triaj – Lunca Bârzavei, Reşiţa, SC ALDOR SRL Timisoara-RO, Contr. 132/2008.* (in Romanian)

Practical Utilization Findings of Concretes with Gypsum-Free Cements at Building of Concrete Pavements and Landing Ground

Jiri Brozovsky[1] and Jiri Brozovsky, Jr.[2]

[1] *Institute of Building Materials and Components , Faculty of Civil Engineering, Brno University of Technology, 602 00Brno, Czech Republic*
[2] *Department of Building Mechanics, Faculty of Civil Engineering, VSB-Technical University of Ostrava, 708 33 Ostrava, Czech Republic*

Summary

The paper describes research findings and observations concerning practical application of concretes based on gypsum-free cements. Concretes made of gypsum-free cements feature short processing time and high initial strength over 1 to 3 days. Also, the article analyzes chosen factors impacting to fresh/hardened concrete – to begin with influence of mineralogical composition of aggregates, impact of water-cement ratio to initial setting time of fresh concrete as well as impact of water-cement ratio to concrete initial strength. The paper presents confrontation of concrete strengths using standard Portland cement with the same of concrete based on gypsum-free cement. Furthermore, described is experience in applied application of concretes based on gypsum-free cements. In view of short processing time as to concretes based on gypsum-free cements i.e. 25 to 50 minutes as a rule, these concretes are optimal in particular for small volume constructions or repair works requiring putting into operation as soon as possible as from casting, e.g. cement-concrete road carpets.

KEYWORDS: concrete, sclerometer, strength, analysis.

1. INTRODUCTION

There are different methods of how to reach initial high concrete strength values; one of them is utilization of special cements inclusively Portland gypsum free cements, i.e. those in which setting regulator – the gypsum – is replaced by another system of setting regulation. In the Czech Republic, manufactures have produced gypsum free cements (GFC) with specific surface of $400 – 600$ m^2/kg and setting regulation system Na_2CO_3 + additives based on sulphite extracts. An advantage of such cements was a high strength at the age of 1 to 3 days, which enabled producing of concretes with high initial strength. To reach a proper consistence

of fresh concrete, no plasticisation additives were necessary, as the gypsum free cement setting regulation system had a strong plasticisation effect due to sulphite extracts.

Such concretes, above all, have been used for slab constructions, most frequently for repairs of cement-concrete roads and airport runways.

This paper summarizes the research knowledge and practical experience in connection with application of the concretes using Portland gypsum free cements.

2. DEMANDS ON PARAMETERS OF GYPSUM FREE CEMENTS AND CONCRETES USING GFC

As concretes containing gypsum free cements have been used above all for repairs of roads and airport runways, which should be serviceable in a possibly short time after the repair, this precondition is reflected in demands on parameters of gypsum free cements and concretes produced by using thereof.

2.1 Gypsum Free Cement – Specification and Demands on Features

Typical features of gypsum free cement are:

- – Short initial setting

- – Short lag between starting and end point of setting

- – High initial strength at the age of 1 to 3 days

The demands on parameters are shown in Table 1.

Table 1. Požadavky na vlastnosti bezsádrovcového cementu

Regulation system of setting time for cement		$0,5 - 0,6\%$ KORTAN FN + $1,8\%$ Na_2CO_3 of clincer weight	
Property		Unit	Desired Value
Specific Surface		m^2/kg	>425
Initial Setting Time		min	> 25
Period of Setting		min	< 90
Compression Strength	4 h	MPa	≥ 2
	24 h		≥ 35
	3 days		≥ 45
	7 days		≥ 50
	28 days		≥ 55

Property		Unit	Desired Value
Flexural Strength	4 h	MPa	≥ 0.25
	24 h		≥ 6.0
	3 days		≥ 7.0
	7 days		≥ 7.5
	28 days		≥ 9.0

2.2 Concrete Using Gypsum Free Cement – Specification and Demands on Features

The concrete based on gypsum free cement represents an alternative material usable for repair of cement-concrete roads, namely for local repair as well as for total replacing of the single slabs.

Demands on concrete parameters for repair and renewal of cement-concrete roads are shown in Table 2. There are two different concrete types in relation to the slab thickness to be repaired:

- Mortar – aggregates, grain size $D_{max} < 8$ mm as a maximum. Recommended for slab repair thickness between 0.01 and 0.05 m. The values of compression and tensile strength have been measured on specimens (baby squares 0.04 x 0.04 x 0.16 m) in accordance with CSN EN 196-1.

- Concrete – aggregates, grain size $D_{max} \in (8; 32$ mm). Recommended for slab repair thickness > 0.05 m. The strength values have been measured on specimens in accordance with CSN EN 12390-3, resp. CSN EN 12390-5.

Table 2: Demands on Composites Using Gypsum Free Cements

Parameter		Unit	Motrar	Concrete
Initial Setting Time		min	≥ 20	≥ 40
Sample		m	0.4.x 0.04 x 016	0.1 x 0.1 x 0.4
Compression Strength	3 days	MPa	≥ 45	≥ 30
Flexural Strength	3 days	MPa	$\geq 5,0$	$\geq 4,0$
Concrete Surface Scaling	7 days	g/m^2	≤ 1000 afret 75 cykles	
	28 days		≤ 1000 after 100 cykles	

3. FRESH CONCRETE STARTING POINT OF SETTING

BSPC concretes may be characterized as composites with short starting point of setting. However, the main problem of utilization thereof is, to ensure an adequate

time of processing. The research results and pieces of knowledge based on practical application have shown that fresh concrete using GFC (GFC-FC) starting point of setting is influenced especially by:

- Gypsum free binder features (granulation finesse, number of additives regulating the starting point of setting, clinker chemical composition);
- Mineralogical and chemical composition of the compact natural aggregates;
- Cement-water ratio (W/C).

3.1. Mineralogical Composition of Aggregates

The foregone research has shown a solid evidence of greywacke mineralogical composition influence on the GFC-FC starting point of setting. Upon greywacke selection, the exploited aggregates should be preferred; sands with high content in quartz should be used; sands with high content in feldspar are not convenient. The type of used coarse aggregates has not any distinguished influence on the hardened concrete strength.

3.2. Cement-Water Ratio

The starting point of fresh concrete setting delays in dependence on the cement-water ratio increase. However, this fact, above all, negatively influences initial strength values of the concrete hardening.

3.3. Supposed Starting Point of Fresh Concrete Setting

On the base of test results [1, 2], an empiric relation (1) for an informative fresh concrete starting point of setting IST_{FC} derived from the cement slurry starting point of setting IST_{CP} was calculated as follows:

$$IST_{CP} = a.IST_{FC} \quad \text{pro W/C} \leq 0.40 \quad a \in (0.4;0.6) \tag{1}$$

4. STRENGTH OF CONCRETE USING GYPSUM FREE CEMENT

4.1. Concrete Strength Influenced by Cement-Water Ratio

- The Cement-Water Ratio (W/C) mostly influences compression strength and tensile strength under flexure of the concrete at the age of 1 day.

- A W/C value of 0.38 as a minimum is necessary for reaching high initial strength values with concrete of the age of 1 – 3 days. Any exceeding values will result in an aqueous deceleration accompanied with a retard of strengthening process.
- Concentration of setting regulator admixtures (0.5; 0.6 % KORTAN FN + 1.8 % Na_2CO_3 of the clinker weight) enables it to reach the supposed high initial strength values of BSPC-B with regard to the recommended W/C value.
- KORTAN FN additive having besides retardation ability also strong plasticization effects enables processes reaching to 20 – 150 mm cone shrinkage under the low W/C values.

Graphs in Figures 1 and 2 illustrate the W/C impact on GFC using concrete.
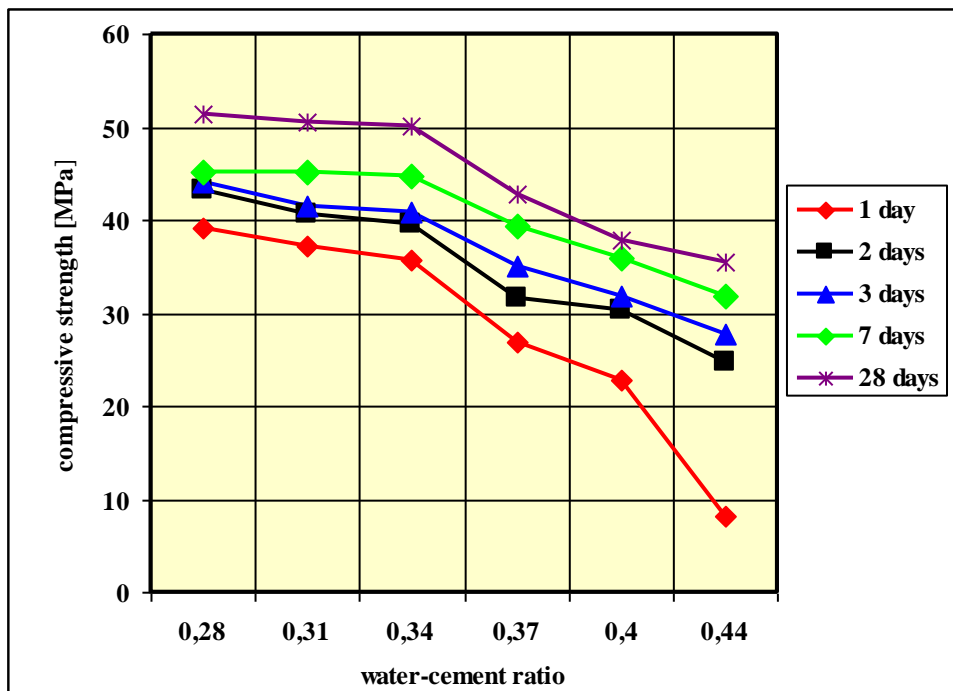
Figure 1: W/C Impact on GFC-C Compression Strength
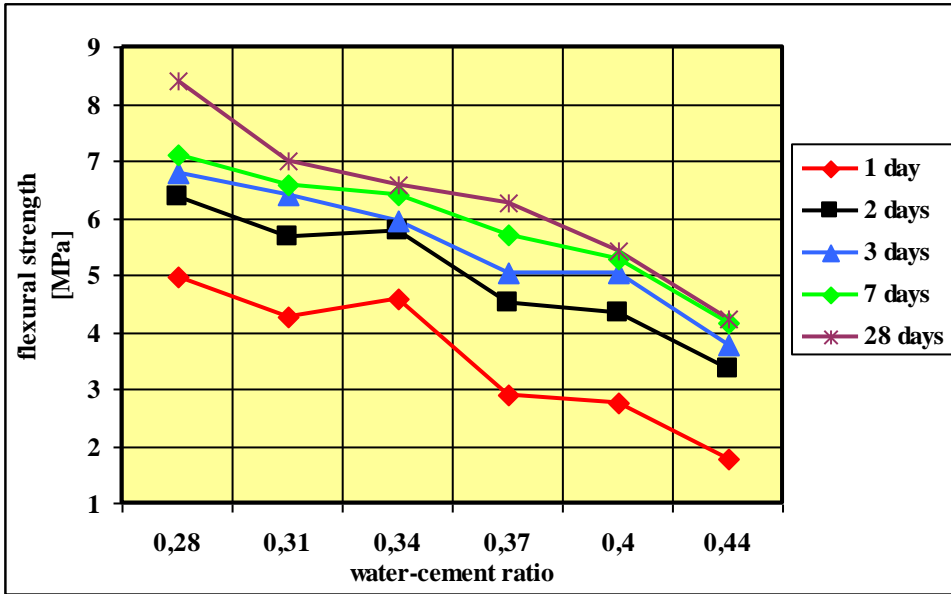
Figure 2: W/C Impact on GFC-C Tensile Strength under Flexure

4.2 GFC Using Concrete Strength Progression in Time

GFC-C compression strength progression in time in comparison with strength progression of concrete using a normal Portland cement is graphically demonstrated in the Figure 3. To generalize the results, the compression strength absolute values are given in % - 100%; the concrete age is 28 days. For concretes using normal Portland cements, the compression strength was calculated from the relation 2 as per the CSN 73 1201,

$$f_{c,cu,t} = f_{c,cu,28}\left(\frac{1.36t}{t+10}\right)$$ (2)

where:
$f_{c,cu,t}$ – concrete cube strength at the age of "t" days,
$f_{c,cu,28}$ – concrete cube strength at the age of 28 days,
t – age of concrete for which the strength has been determined.

The GFC-C compression strength and tensile strength under flexure progression in time is shown in the Figure 5. The strength of concrete at the age of 3 days is considered as 100%. An evaluation of 1 day strength values has shown that at this age, BSRVC-B compression strength has been distinctively influenced by cement-

water ratio. It is not efficient to produce concretes with W/C > 0.38, as an exceeded value of W/C > 0.38 causes deceleration of hydration process and retardation of the concrete strength growth.
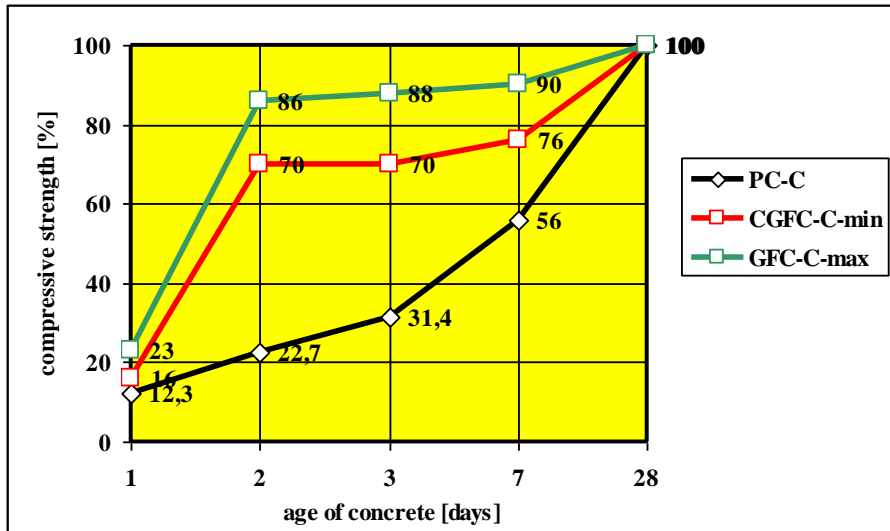
Figure 3: GFC-C Compression Strength Progression Depending on Time in Comparison with Concrete Using Standard Portland Cement
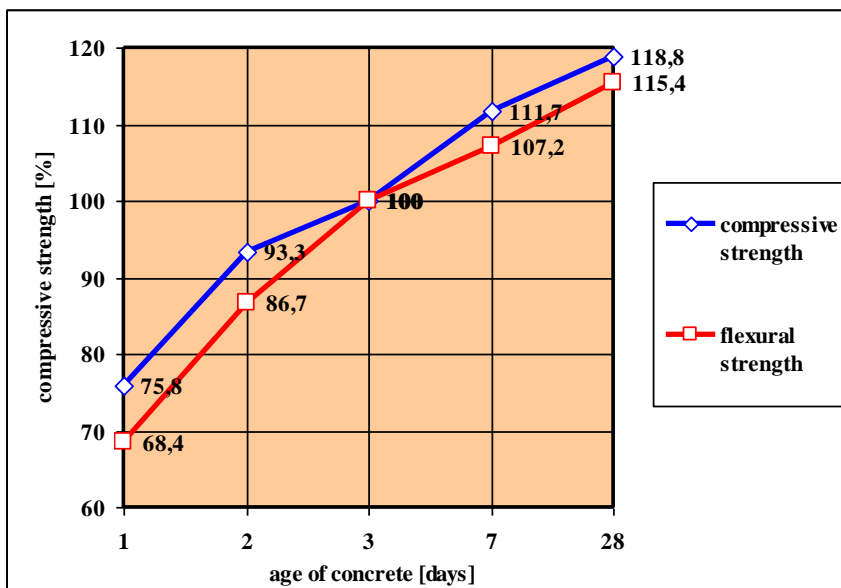
Figure 4: GFC-C Compression Strength and Tensile Strength under Flexure Progression in Time

5. CONCRETE SURFACE RESISTANCE TO ALTERNATIONS OF FROST AND THAWING AND IMPACTS OF DEFROSTING CHEMICALS

This feature is very important in relation to concretes used for cement-concrete road and airport surfaces, which need to be treated with defrosting chemicals in winter, in order to ensure negotiability. Such testing lies in cyclic freeze and defrosting of a concrete sample dipped in a 5 % NaCl solution.

A waste volume (in g/m^2) as a consequence of the damaged surface scaling is an evaluation parameter for the concrete resistance to frost and thawing.

Concretes using gypsum free cements have shown scaling waste values of 220 to 620 g/m^2 after 100 test cycles. The mentioned values are valid for concretes free of aeration additives.

Concretes using gypsum free cements are, so to say, highly resistant to frost and defrosting chemicals.

6. PIECES OF KNOWLEDGE BASED ON PRACTICAL APPLICATION

Following pieces of experience are available due to the application of concretes using gypsum free cements in repairs of cement-concrete roads and airport runways:

- GFC-C using is limited by relatively short-time starting point of fresh concrete setting, i.e. by the period necessary for manufacturing, transportation and processing. The variation starting point coefficient of setting was ca 20%, however, the demanded starting point of setting was not reached in all cases. The necessary starting point of setting in duration of 40 minutes as a minimum brought about certain troubles at concreting. The lag of ca 5 – 10 minutes between the fresh concrete starting and end points of setting was too short.

- A utilization of such concretes is recommendable in cases supposing a high strength at the age of 3 days as a maximum. For constructions demanding high strength values after 7 days or more, the concretes using standard Portland cements and corresponding admixtures are more convenient.

- Concretes using gypsum free cement are suitable for small-volume-concreting, when the concrete is produced on the building site directly,

whereas a concrete mixer batch covers a complete concreting of one element.

- A voluminous concreting, i.e. placing of more mixer batches into one element, proved to be very complicated.

- Upon GFC-C manufacturing, the fixed water portion is to be kept, otherwise a water overdose results in diminution of strength values, especially of those regarding the starting point of setting.

7. CONCLUSION

The results of research and experience from practical application have confirmed a suitability of concretes using gypsum free cements, especially for repairs of cement-concrete roads.

At the age of 2-3 days, concretes using gypsum free cements do reach strength values comparable with those of the concretes at the age of 28 days using standard Portland cement. The 28-days-strength-values of both concrete types are comparable.

GFC-C utilization is limited by relatively short-time starting point of fresh concrete, i.e. by the period necessary for manufacturing, transportation and processing.

A rigorous keeping of recommendation for concrete components, especially for water admixture is very important.

Acknowledgements

References

1. Drochytka R.: et al. Progressive Building Materials with Utilization of Secondary Raw Materials and their Impact on Structures Durability. but, *Final report of the project VVZ CEZ MSM: 0021630511, Brno 2008*. Brozovsky J.: Subtask 3 (in Czech).
2. Brozovsky, J. Investigation of the utilization and preparation of concretes with highly early strength values, Military academy Brno, 1994, (in Czech),
3. Brozovsky, J., Brozovsky, J. jr. : Concrete with gypsum free cement – basic characteristics *In : The Intenational Symposium on Non – Traditional Cement & Concrete*, Brno, Czech Republic, 2002

4. Bydzovsky, J., Brozovsky, J. : Проектирование состава бетонов на безгипсовом портландцементе. *Современный научный вестник*, 2007, No. 17(25), p. 90-97, ISSN 1561-6886.

5. Brozovsky, J. Martinec, P. : Concrete based on gypsum free cements: surface resistance to cyclic de-icing, defrosting and chemical substances. *In 9TH International Conference Modern Building Materials, Structures and Techniques*, Vol. I, Selected papers, ed. Vilnius Gediminas technical University, Vilnius, Lithuania, 2007 p. 29-33 (Vol. 1), ISBN 978-9955-28-201-3

6. Brozovsky, J., Brozovsky, J. jr., Bydzovsky, J. : Влияние состава заполнителя и толщины цементного теста на расход цемента в бетонах на безгипсовом портландцементе. In *VI – я Международная научно-практическая Интернет – конференция „Состояние современной строительной науки – 2008»,* ed. Сб. науч. Трудов – Полтава : Полтавский ЦНТЭИ и журнал Бетон и железобетон в Украине, Poltava, Ucraine, 2008, pp. 26-30

A configuration of seismic energy dissipation system for stiff structures

Horatiu Alin Mociran[1], Eugen Panţel[1]

[1]*Faculty of Civil Engineering, Technical University, Cluj-Napoca, 400027, Romania*

Summary

The aim of the paper is to assess the efficiency of viscous fluid dampers with toggle bracing mechanism in reducing the seismic response of rigid steel frame structures.

A five story, three bay rigid steel frame was chosen for this study as a reference frame. The structure was then equipped with linear fluid viscous dampers, installed with the toggle brace configuration in the central bay of the building.

The dampers were sized to provide 15%, 25% and 35% of critical damping in the fundamental mode.

The numerical results (peak story shear, peak interstory drift and peak lateral floor acceleration) show that the proposed device is usefulness in enhancing the seismic response of stiff structure.

KEYWORDS: toggle brace system, viscous damper, damping ratio, time history.

1. INTRODUCTION

Conventionally, structures have been designed to resist seismic excitations through a combination of strength, deformability, and energy absorbtion. These structures may deform well beyond the elastic limit in a severe earthquake. They may remain intact only due to their ability to deform inelastically, as this deformation results in increased flexibility and energy dissipation. Unfortunately, this deformation also results in local damage to the structure, as the structure itself must absorb much of the earthquake input energy. It is ironic that the prevention of the devastating effects from earthquakes, including structural damage, is frequently attained by allowing certain structural damage.

Damping is one of many methods that have been proposed for allowing a structure to achieve optimal performance when is subjected to an earthquake [1], [2]. The level of damping in a conventional elastic structure is very low, and hence the amount of enrgy dissipated during transient disturbances is also very low.

Viscous dampers are often placed in diagonal or chevron configuration, however such geometric configurations leads to device displacements that are less or equal

to the interstory drift [3], [4]. Interstory displacements are small in the case of stiff structure. Small device displacement involves large damper force and expensive damper [5]. Viscous dampers are ideally suited for flexible structures. The toggle brace system overcomes this problem by using the lever principle to amplify interstory drift at damper level and consequently reduced the damper force (reduced damper size and cost) [6].

2. DESCRIPTION OF STRUCTURE, VISCOUS DAMPERS AND INPUT GROUND MOTION

2.1. The structures

A five story, three bay steel frame building was chosen for this investigation as a reference frame. The structure was then modified by the addition of fluid viscous dampers (Figure 1) to improve the seismic performance, with no attempt made to redesign the main frame elements.
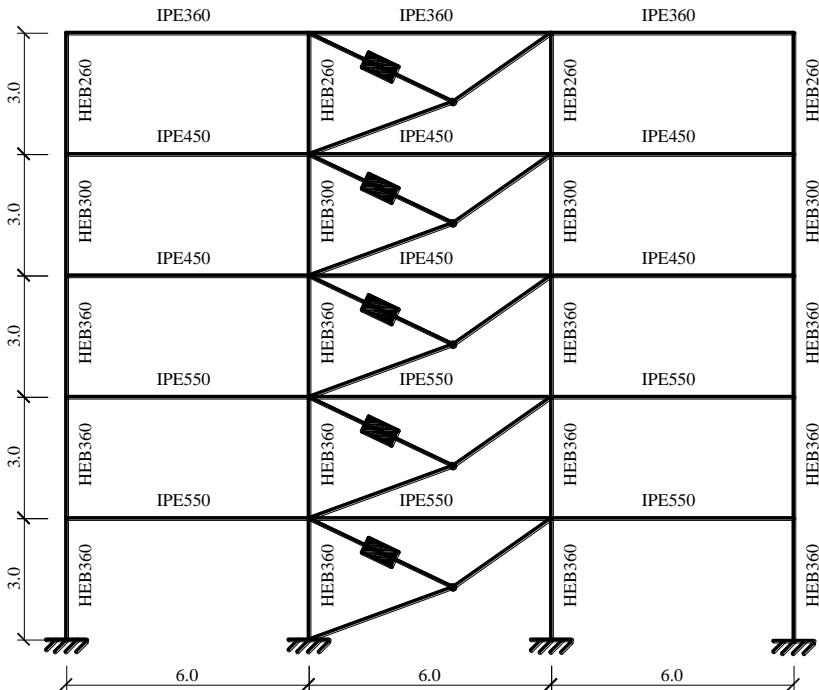
Figure 1. Elevation view of steel frame with viscous dampers

2.2. The viscous dampers

Five linear viscous dampers (Figure 2) will be installed in the central bay of the building. It is assumed that all dampers have identical properties. The dampers will be installed with a toggle brace configuration. The inherent damping ratio of the structure is assumed to be 5%, and the total effective damping ratio of the whole system is designed as equivalent to 15%, 25% and 35% of critical damping for the first mode.
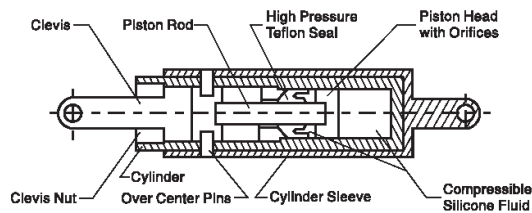
Figure 2. TAYLOR DEVICES Viscous Damper

The damping cofficient of each damper is c=97.51kN-sec/m for the case of a damping ratio of 15%, c=195.02kN-sec/m for a damping ratio of 25% and c=292.53kN-sec/m for a damping ratio of 30%. In this example, the linear effective stiffness is set to zero so that pure damping behavior is achieved.

2.3. Input ground motion

The nonlinear time history analysis was performed using the 1977 Vrancea earthquake record (N-S component) with the maximum peak acceleration of 0,198g (Figure 3).
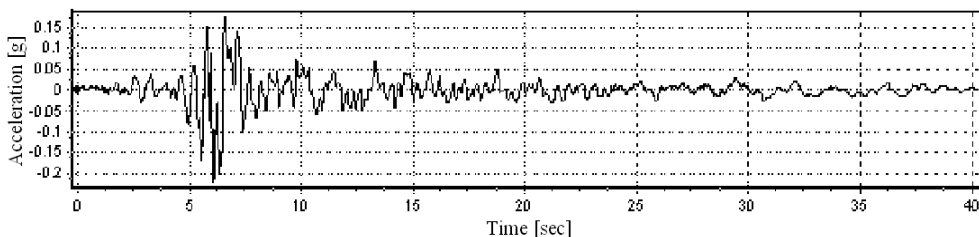
Figure 3. Ground acceleration for 1977 Vrancea Earthquake

3. NUMERICAL RESULTS AND DISCUSSIONS

The time history results are presented and discussed. Comparisons are made of estimated peak story shear, peak interstory drift and peak floor acceleration.

3.1. Peak story shear

The peak story shear $\left(F_{\max}\right)$ are given as a fraction of the total frame weight $\left(W = 2589.84 kN\right)$. Table 1 compares the values obtained for the four cases.

As expected, best performance is achieved for a damping ratio of 35%, although the case of 25% damping ratio produces important response reduction. It should be mentioned that these results apply for an elastic structural system.

Peak story shear profiles are presented in Figure 4.
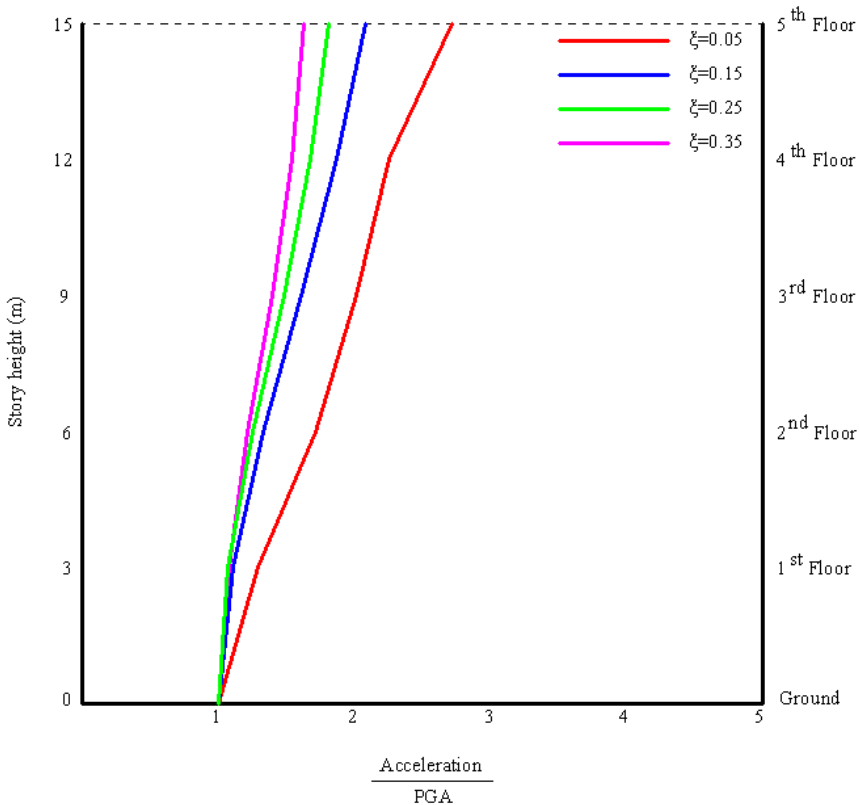
Figure 4. Peak story shear/total weight profile for Vrancea 1977 earthquake

Table 1. Peak story shear/weight results

Floor	$\xi = 0.05$	$\xi = 0.15$		$\xi = 0.25$		$\xi = 0.35$	
	$\dfrac{F_{max}}{W}$	$\dfrac{F_{max}}{W}$	Reduction ratio (%)	$\dfrac{F_{max}}{W}$	Reduction ratio (%)	$\dfrac{F_{max}}{W}$	Reduction ratio (%)
5	0.106	0.066	37.736	0.059	44.339	0.054	49.057
4	0.192	0.132	31.250	0.118	38.542	0.108	43.750
3	0.263	0.197	25.095	0.177	32.670	0.163	38.023
2	0.325	0.263	19.076	0.236	27.385	0.217	33.231
1	0.375	0.329	12.267	0.295	21.333	0.271	27.733

3.2. Peak interstory drift

A comparison of peak interstory drift $\left(d_r^{max}\right)$ responses of the frame structure with and without viscous dampers is shown in Table 2. The obtained results indicate that the maximum interstory drift values were reduced in proportion to the amount of damping supplied in the structure.

Figure 5 shows peak interstory drift profiles for the analysed cases.
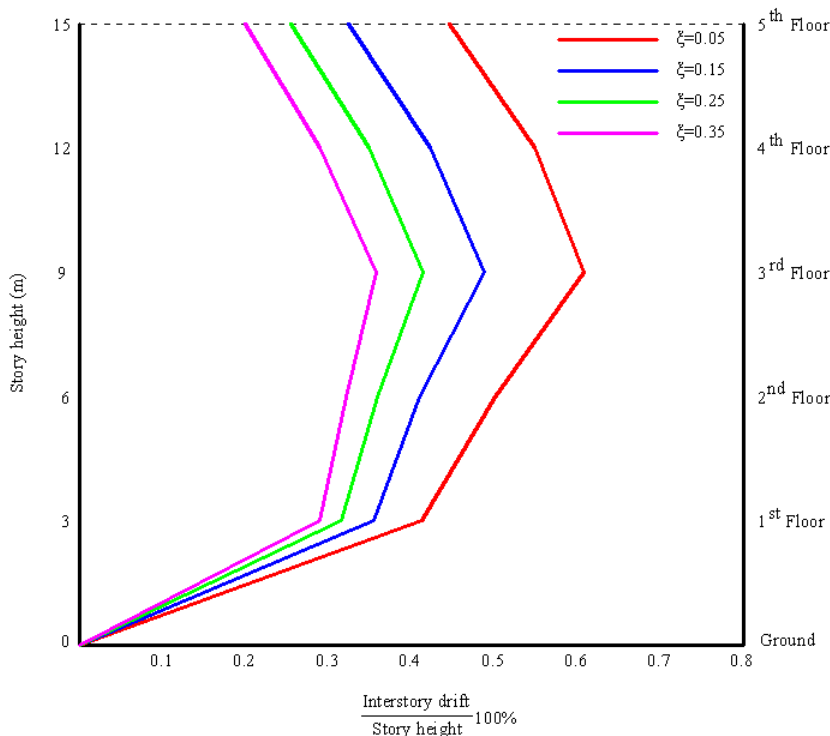
Figure 5. Peak interstory drift/height for Vrancea 1977 earthquake

Table 2. Peak interstory drift/height results

Floor	$\xi = 0.05$	$\xi = 0.15$		$\xi = 0.25$		$\xi = 0.35$	
	$\dfrac{d_r^{\max}}{h}$	$\dfrac{d_r^{\max}}{h}$	Reduction ratio (%)	$\dfrac{d_r^{\max}}{h}$	Reduction ratio (%)	$\dfrac{d_r^{\max}}{h}$	Reduction ratio (%)
5	0.768	0.373	51.432	0.282	63.281	0.206	73.177
4	0.705	0.482	31.631	0.396	43.830	0.317	55.035
3	0.621	0.547	11.916	0.471	24.155	0.398	35.910
2	0.513	0.448	12.670	0.405	21.053	0.362	29.435
1	0.420	0.387	7.857	0.359	14.524	0.333	20.714

3.3. Peak lateral floor acceleration

This parameter is almost never taking into account in the design process, because it requires a time history analyses to obtain it. From the damageability perspective it is the measure that impacts damage to the ceiling and lights, electrical and mechanical equipment, elevators and the building contents.

Table 3 compares maximum lateral floor accelerations $\left(a_{\max}\right)$ normalized by peak ground acceleration (PGA) for the analyzed cases. Reductions of up to 39.92% and 33.32% in the peak values of accelerations were obtained for damping ratios of 35% and 25% (Figure 6).

Table 3. Peak lateral acceleration/PGA results

Floor	$\xi = 0.05$	$\xi = 0.15$		$\xi = 0.25$		$\xi = 0.35$	
	$\dfrac{a_{\max}}{PGA}$	$\dfrac{a_{\max}}{PGA}$	Reduction ratio (%)	$\dfrac{a_{\max}}{PGA}$	Reduction ratio (%)	$\dfrac{a_{\max}}{PGA}$	Reduction ratio (%)
5	2.713	2.082	23.258	1.809	33.321	1.630	39.919
4	2.260	1.864	17.522	1.677	25.796	1.545	31.637
3	2.017	1.604	20.476	1.482	26.524	1.400	30.590
2	1.715	1.325	22.740	1.254	26.880	1.212	29.329
1	1.294	1.102	14.838	1.071	17.233	1.075	16.924
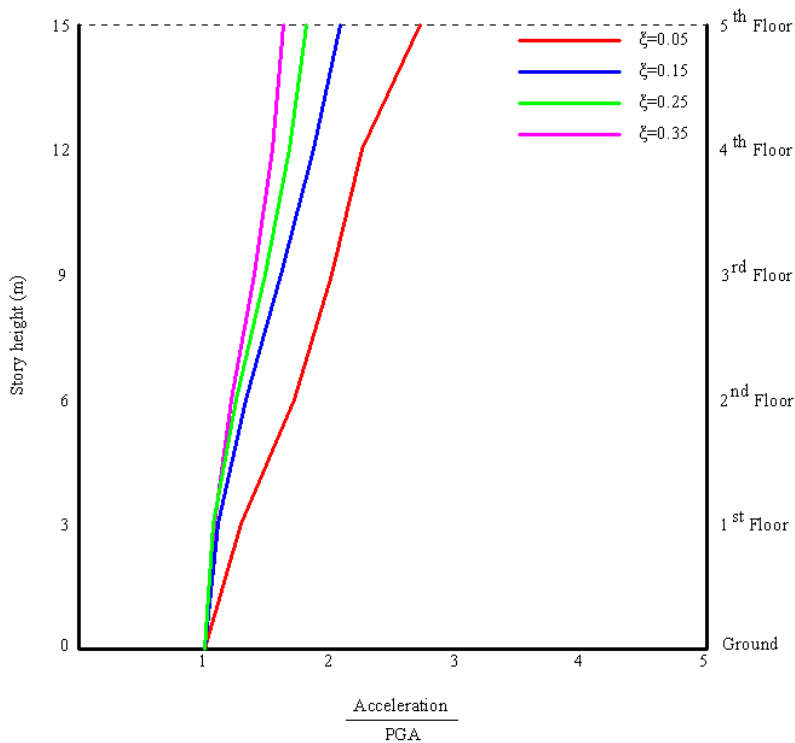
Figure 6. Peak lateral acceleration/PGA profile for Vrancea 1977 earthquake

4. CONCLUSIONS

The paper studies the seismic response of stiff frame structure fitted with viscous dampers installed in a toggle brace configuration, for different damping ratios. The toggle brace system utilizes the lever principle to magnify frame interstory drifts at the damper level and consequently reduce the required damper force.

The time history results show that story shears, interstory drifts and lateraral floor accelerations were reduced significantly in proportion to the amount of damping supplied in the structure [7].

The toggle brace system will facilitate the use of viscous dampers in stiff frame structures.

References

1. Soong, T. T., Spencer J.R., Supplemental energy dissipation: state – of - the - art and state – of - the - practice, *Engineering Structures*, vol. 24, 2002.
2. Christopoulos, C., Filiatrault, A., *Principles of Passive Supplemental Damping and Seismic Isolation*, IUSS Press, Pavia, 2006.
3. Hwang, J. S., Huang Y. N, Huang Y. H., Analytical and experimental study of toggle – brace – damper systems, *Journal of Structural Engineering*, vol. 131, issue 7, 2005.
4. Sundiata M., Parametric study on the effectiveness of the toggle brace damper, *http://mase.wustl.edu/wusceel/reujat/2002/marcelin.pdf*
5. Ribakov, Y., Reinhorn A. M., Design of amplified structural damping using optimal consideration, *Journal of Structural Engineering*, vol. 131, issue 10, 2003.
6. Constantinou, M.C., et al., Toggle brace damper seismic energy dissipation system, *Journal of Structural Engineering*, vol. 127, issue 2, 2001.
7. Mociran, H. A., Stan A. D., The influence of damping ratios on eathquake response of steel frame structures, *Computational Civil Engineering*, Iaşi, 2008.

Thermal technical properties of insulation materials made from easy renewable row sources

Jiri Zach[1], Jitka Hroudova[2]

[1,2] *Department of Technology of Building Materials and Elements, University of Technology, Brno, 60200, Czech Republic*

Summary

The paper presents the results of research focused on heat technical properties of insulating materials from easily renewable organic raw materials, especially from insulations based on technical hemp and other possible raw material sources from agriculture (flax, jute) which can be potentially used for the production of heat insulation. Within the scope of research a study was elaborated with the aim to verify, whether the heat technical properties of above mentioned materials are comparable with the properties of classical heat insulating materials such as polystyrene foam or mineral wool. It can be even assumed that from the standpoint of some specific properties the newly developed materials will dispose with better properties. Within the scope of research first of all the effect of moisture was followed up on the heat technical properties of these materials.

KEYWORDS: insulation materials, thermal conductivity, organics materials, technical hemp.

1. INTRODUCTION

At present we are continually fighting with problems concerning the quantity of crude oil resources which are the mostly used raw material in the production of cellular plastics insulations.

The basic advantage of organic raw materials is in comparison with other raw materials their theoretically inexhaustible production. This fact has advantages, such as the low production costs of raw materials processing with subsequent manufacture of products, further the generally low ecological burden and the easy recycling of materials after exhaustion of their service life. Another serious reason of the fact that the heat insulations based on organic fibers gain still larger popularity in recent years, are the positive properties of these materials in the field of natural moisture accumulation, high diffuse openness.

2. MOISTURE INFLUENCE

The moisture has markedly effects at the heat technical properties of building materials. The most cellular building materials contain under normal conditions a certain percentage of moisture even in the dry state. The quantity of this moisture depends on the porous system of the material, on the relative humidity of the surrounding and on the temperature. The most important material properties influencing the moisture are the properties of the porous system (form, size, openness and distribution of pores). The moisture propagation in the construction takes place chiefly by the diffusion of water vapour and by capillary conduction. The moisture transfer takes place from the place with higher moisture in the place with lower moisture (in the direction of moisture drop or of the water vapour partial pressure drop).

The equivalent value of the heat conduction coefficient of the building material depends on its moisture therefore it is necessary in the course of real calculations to consider the immediate moisture of the building material in the construction and its steady moisture during the use of the construction. The part of the standard heat technical calculation of building structures is their evaluation in the light of water vapour diffusion and condensation, with respect to the change of the building material heat technical properties.

The elevated moisture of the material in the structure can come from different sources. The moisture of the building material can be differentiated according to its origin as: the moisture formed during the manufacture, the technological moisture, the rainfall moisture, the soil moisture and the process moisture.

3. BEHAVIORS OF BUILDING MATERIALS AFTER BUILD IN TO THE CONSTRUCTION

Owing to the moisture electric field is generated in building materials. It is caused by the different mobility of the solved salts and by the different pH values. The electric field is a strong degrading factor in particular of metallic components built in the building structures.

The water or the moisture has a very high degrading effect both at he building material and at the building structure as a whole. The effect of water causes the corrosion of the frame structure and changes of some important building material properties.

The degrading changes caused by water effect can be *reversible* i.e. after the decrease of moisture the original properties of the material (construction) are recovered, and *irreversible,* when permanent damage of the building structure is

caused by the effect of water and moisture even after the subsequent decrease of moisture.

3.1 Dependence thermal conductivity on moisture content

The equivalent value of the thermal conductivity of building materials is very close connected with the moisture content. The thermal conductivity λ [W.m^{-1}K^{-1}] of the wet material is determined by the thermal conductivity of the solid matrix, of fluid phases, of gaseous phases and their quantity, by phase changes and by the spatial distribution of phases. Thermal conductivity value increases in general with the rising moisture content of material.

Thermal conductivity of the totally dry, porous material can be simply expressed by the following equation:

$$\lambda_{dry} = \lambda_{mat} \cdot (1 - P) + \lambda_{vzd} \cdot P$$

(1)

λ_{dry} thermal conductivity of dry material [W·m^{-1}·K^{-1}],

λ_{mat} thermal conductivity of the solid material (matrix) without pores [W·m^{-1}·K^{-1}],

λ_{vzd} thermal conductivity of air [W·m^{-1}·K^{-1}],

P porosity [-].

In the case of material with moisture content, the air pores are gradually filled by water. The increase of thermal conductivity is in the area of low (hygroscopic) humidity sharper. In the area of higher humidity the intensity of the heat conduction coefficient grow, usually decreases in dependence on the increase of the moisture content.

Thermal conductivity of the wet material can be simply expressed in dependence on moisture content by relations bellow:

a) Area of low moisture content (hygroscopic moisture), $\lambda_{(w)}$:

If we consider the heat bridges, which exist in the air-dry material under normal conditions by the effect of continual smallest pores filling still by moisture w_{min} (see above) and the boundary hydroscopic moisture of the material $w_{h,max}$, we obtain for the thermal conductivity of the material $\lambda_{(w)}$ [W.m^{-1}.K^{-1}] the following relation:

$$\lambda_{(w)} = \lambda_{mat(u,\varepsilon)} \cdot (1-P) + \lambda_{vody} \cdot (w - w_{min}) + \lambda_{vzd} \cdot (P - w) \tag{2}$$

$$\lambda_{mat(w,\varepsilon)} = \cfrac{1}{\cfrac{1}{\lambda_{mat(w)}} + \cfrac{3\,\varepsilon\left(1 - \cfrac{w}{w_{min}}\right)}{\lambda_{vzd}\,(1-P)}} \tag{3}$$

$$\lambda_{mat(w)} = \cfrac{1}{\cfrac{1}{\lambda_{mat}} + \cfrac{w - w_{min}}{\lambda_{vody}} + \cfrac{w_{h\,max} - w}{\lambda_{vzd}}} \tag{4}$$

$$\varepsilon = \frac{1 - 2\upsilon}{E_m\, V_m} \int_{p_{c1}}^{0} \frac{w(p_c)}{w_{sat}} \tag{5}$$

υ poisson constant [-],

E_m modulus of elasticity [Pa],

p_c capillary pressure [Pa],

V_m matrix volume in the volume of material [-],

w moisture of the material [-],

w_{sat} moisture of the material after saturation by moisture (in saturated state) [-],

$\lambda_{mat\,(w,\varepsilon)}$ thermal conductivity of the material matrix, respecting material volume changes by the effect of its moisture content [W.m^{-1}.K^{-1}].

b) Area of high moisture content (outside of hygroscopic moisture area), $\lambda_{(w)}$

After reaching the maximum of hygroscopic moisture $w_{h\,max}$ the capillary system is filled by moisture and the parallel system expressing thermal conductivity is modified by the zigzag effect of the with moisture unevenly filled capillary system. This effect can be quantified by the introduction of the uniformity factor R. This factor can be determined on the basis of the porous system structural parameters. The following relation is valid in general (Meng 1994):

$$R = P_{rel}^{FD} \qquad (6)$$

P_{rel} relative porosity [-]

FD factor of the porous system dimensions[-]

The factor of the porous system dimensions is defined (Meng 1994):

$$FD = \frac{\Delta \log P}{\Delta \log r} \qquad (7)$$

In the area of similarity f, we can use for the calculation the relation:

$$R_f = w_f^{FD} \qquad (8)$$

The final value of the humid material heat conduction coefficient $\lambda_{(w)}$ [W.m^{-1}.K^{-1}] , behind the area of hygroscopic moisture can be expressed:

$$\lambda_{(w)} = \lambda_{mat(u)} \cdot (1-P) + \lambda_{vody} \cdot \sum_f w_f \ R_f + \lambda_{vzd} \cdot (P-w) \qquad (9)$$

f number of considered porous fractions, w_f . R_f is the autocorrelation function expressing the deviation of real pores from the parallel capillaries arrangement in the ideal model.

3.2 Dependence thermal conductivity on density

The heat conduction coefficient of the insulating material depends on the volume weight. In the case of materials with very low volume weight $\rho_v \leq 100$ kg.m^{-3} the situation is somewhat complicated. The heat conduction coefficient decreases with the increasing volume weight in the area with low volume weight, because the heat transfer by convection and radiation is limited in the porous structure of the material. After reaching the optimal volume weight, when the heat conduction

reaches its minimum, the heat conduction begins gradually to increase with the volume weight increasing. This effect is caused by the increase of heat transfer by conduction through the material structure of the insulating material.

4. REVIEW OF RESULTS

Samples of heat insulating materials obtained directly from organic raw materials in agricultural production were used for laboratory measurements. In the concrete it concerned samples of technical hemp, flax and jute.

In the scope of research 8 samples were tested, they are presented in table 1.

Table 1. Review of basic properties of testing samples (dry stage)

Sample	Material source	a [m]	b [m]	h [m]	ρ_v [kg.m^{-3}]
1.1	juta	0,3	0,3	0,076192	24,4
2.1	len	0,3	0,3	0,076271	29,6
3.1	konopí	0,3	0,3	0,076875	29,0
4.1	konopí	0,3	0,3	0,069171	30,4
5.1	konopí	0,3	0,3	0,065265	53,0
6.1	konopí	0,3	0,3	0,02936	33,5
7.1	konopí	0,3	0,3	0,009552	102,5
8.1	konopí	0,3	0,3	0,038395	80,9

Comment: a, b, h – size of sample, ρ_v - density

The test samples were conditioned at the temperature +23°C in media with different relative humidity in order to determine their sorption characteristics. The quantity of moisture which was accepted by given materials into their structure depends on the relative air moisture, on the temperature and on structure of these materials.

The test samples were stored in below mentioned media, with the following parameters:

- *dry environment* – relative humidity 0 % a temperature +23°C (samples was dry to constant weight),

- *normal environment* – relative humidity 50 % a temperature +23°C,

- *wet environment* – relative humidity 80 % a temperature +23°C.

The quantity of moisture accepted by the test samples into their structure you will find in table 2. The measured values are presented in the form of the sorption

isothermal line. The determination of the sorption isothermal line was realized at the temperature + 23°C. The humidity by weight of test samples was measured at the relative humidity 50 % and 80 %. The results of measurements are presented in the following table 2 and figure 1.

Table 2. Review of dependence of moisture content on relative humidity (environment temperature +23°C)

φ [%]	Sample 1 w_m [%]	Sample 2 w_m [%]	Sample 3 w_m [%]	Sample 4 w_m [%]	Sample 5 w_m [%]	Sample 6 w_m [%]	Sample 7 w_m [%]	Sample 8 w_m [%]
0	0	0	0	0	0	0	0	0
50	6,52	6,73	6,08	5,18	5,23	5,20	4,83	5,30
80	12,57	12,90	11,62	11,32	9,86	9,93	10,07	10,44
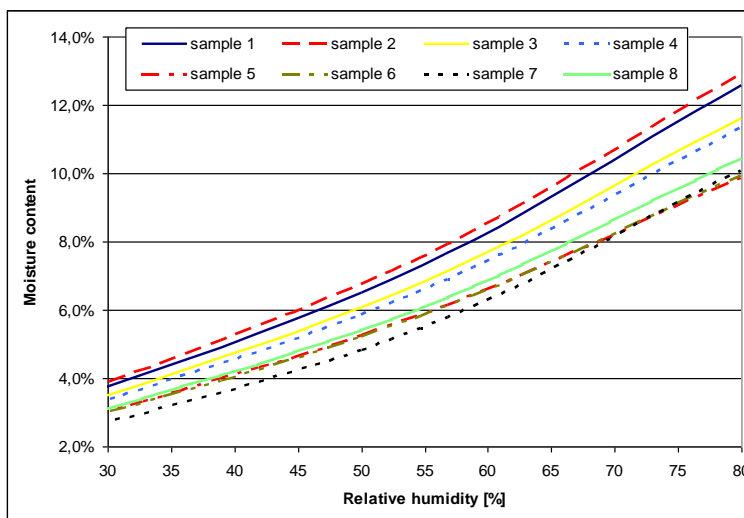
Figure 1. Samples moisture course in dependence on humidity (environment temperature +23°C)

On the base of presented results we can generally state that the moisture of the test samples increases with the increase of the air relative humidity. The highest content of moisture by weight showed the flax sample 2, and on the contrary the smallest content of moisture by weight had the sample 5.

Further the heat conduction coefficient was determined in dependence on the humidity of the surrounding in which the test samples were stored. The determination of the heat conduction was measured by the stationary desk method at the temperature +10°C and at the temperature drop 10°C.

Table 3. Review of measured values of thermal conductivity and moisture content in
dependence on relative humidity (environment temperature +23°C)

Vzorek	φ [%]	0	50	80
1	w_m [%]	0	6,52	12,57
	λ [W.K^{-1}.m^{-1}]	0,0469	0,0482	0,0538
2	w_m [%]	0	6,73	12,90
	λ [W.K^{-1}.m^{-1}]	0,0431	0,0442	0,0537
3	w_m [%]	0	6,08	11,62
	λ [W.K^{-1}.m^{-1}]	0,0485	0,0500	0,0584
4	w_m [%]	0	5,184	11,32
	λ [W.K^{-1}.m^{-1}]	0,0474	0,0488	0,0582
5	w_m [%]	0	5,23	9,86
	λ [W.K^{-1}.m^{-1}]	0,0407	0,0419	0,0502
6	w_m [%]	0	5,20	9,93
	λ [W.K^{-1}.m^{-1}]	0,0429	0,0441	0,0477
7	w_m [%]	0	4,83	10,07
	λ [W.K^{-1}.m^{-1}]	0,0467	0,0482	0,0508
8	w_m [%]	0	5,30	10,44
	λ [W.K^{-1}.m^{-1}]	0,0395	0,0405	0,0452
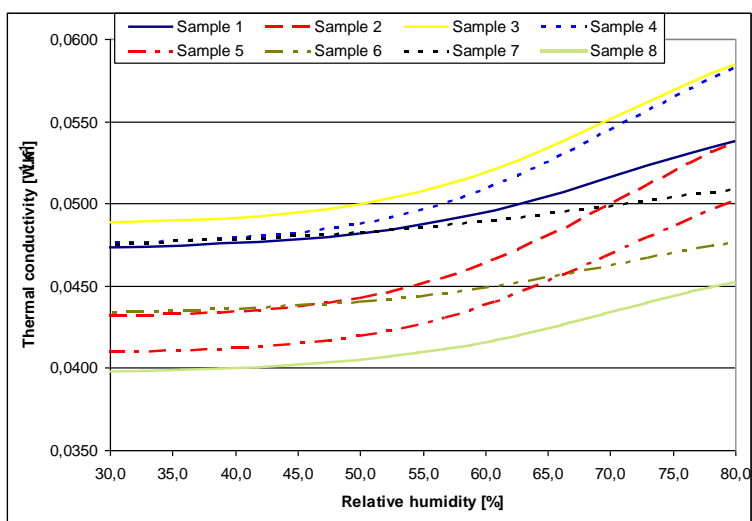
Figure 2. Dependence of thermal conductivity on relative humidity (environment
temperature +23°C)

The presented dependences show that the greatest moisture sensitivity had the
samples no.2, 4 and 5.
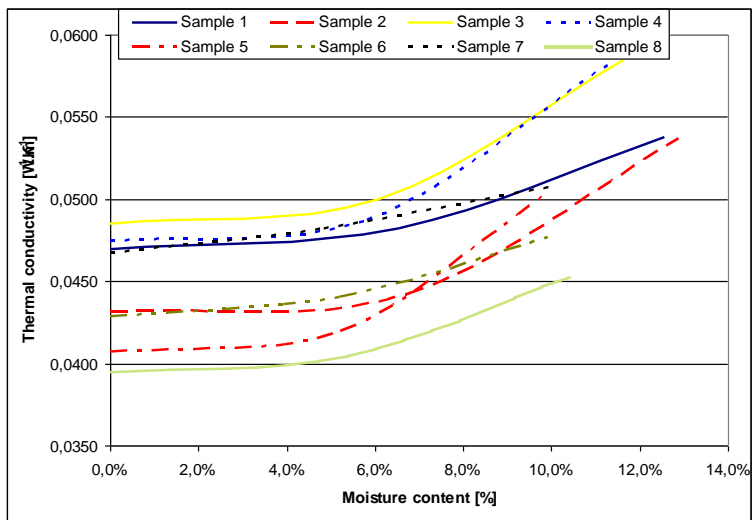
Figure 3. Dependence thermal conductivity on moisture content (environment temperature +23°C)

5. CONCLUSION

According to the above mentioned dependences we can state, that the tested organic materials are sensible to the humidity of the medium in which they are situated and in which they are built in. However when these materials are not in direct contact with liquid water and are not exposed to surroundings with the partial water pressure higher than 1500 Pa (23°C, 50% RH), they show no significant deterioration of heat insulating properties.

For prediction of behavior of thermal insulating materials is very important to know dependence on the thermal conductivity on ambient humidity. This property can be one from most important properties from point of view of selection of optimal material for special realization of building construction.

References

1. EN ISO 12571 Hygrothermal performance of building materials and products - Determination of hygroscopic sorption properties.
2. A. Korjenic, J. Dreyer, S. Stastnik, J. Zach, Warmedammsysteme aus Recyclingmaterialien und ihre thermisch-hygrischen Eigenschaften, 12th Symposium fot Building Physics, Dresden 2007, ISBN 978-3-86005-564-9

Analysis of Compressive Strenghts of Concrete Determined by Different Types of Sclerometers

Jiri Brozovsky

Institute of Building Materials and Components , Faculty of Civil Engineering, Brno University of Technology, 602 00Brno, Czech Republic

Summary

One of the way of finding out the surface of concrete in construction are impact hammers in building practise the most widespread resilient impact hammers of Schmidt system. Sometimes there are also used nonnorm impact hammers for exmaple Masek impact hammer and Ciganek prong. By teoretical we can suppose that for same surrfaces will be at same trial place found same values of surfaces, but this presumption wasn't confirmed yet. In case of nonconfirmed tests of concrete it's needed to use only one type of impact hammer. For searching more accurate results is needed to make accurates tests of concrete, everytime for concretes which are more than 1year old and for using different types of impact hammers for classification the surface of construction.

KEYWORDS: concrete, strength, impact hammer.

1. INTRODUCTION

Non-destructive testing methods, most frequently the hardness test methods, have been used for operative compression strength measuring of concrete, already built-in in construction. Building industry currently uses hardness drop testers of Schmidt system. The processing methods are described in international standard ISO/DIS 8045, European standard EN 12504-2 and in many a national standards, such as CSN 73 1373; ASTM C 805; BS 1881, part 202; NFP 18-417 or JGJ/ T 23-2001. Sometimes, the concrete strength has been measured by means of non-standard methods. In the Czech Republic, we do often use pickaxe tools, concretely the Mašek or Cigánek pointed hammers.

For results of concrete strength measuring by sclerometers, a theoretical assumption should be valid, according to which concrete testing by different hardness test methods at a place should bring about the same values, i.e. when evaluating all the results based on calibration relations for the given test methods, the values of concrete compression strength should be equal. To verify plausibility

of this assumption, we have done an analysis of compression strength values measured by Schmidt impact hammers, types N / L and by Mašek pointed hammer.

The paper deals with analysis of test results, gained by trial of strength done on load-bearing structures; the age of concrete ranged between 25 and 30 years. The package contained 502 values for Schmidt hammers of both types and 90 values for Mašek pointed hammer.

2. DESCRIPTION OF THE USED TEST DEVICES

The text below specifies basic characterization of the used sclerometers, namely of the Schmidt hammers, types N / L, and of the Mašek pointed hammer.

2.1 Mechanic Hardness Drop Tester, Schmidt System

Strength measuring by a hardness drop tester is based on resilient punch rebound from the tested concrete surface resulting in determining of the rebound value.

- The Schmidt impact hammer, type N, gives blow energy of 2.25 J; according to the manufacturer's information, it enables compression strength measuring in the range of 10 – 70 MPa; the ČSN 731373 specifies it as a device, suitable for testing of structures with thickness of 100 mm as a minimum.

- The Schmidt impact hammer, type L, gives blow energy of 0.75 J; according to the manufacturer's information, it enables compression strength measuring in the range of 10 – 70 MPa; the ČSN 731373 specifies it as a device, suitable for testing of structures with thickness of 60 mm as a minimum.

The Schmidt impact hammer is depicted in Figure 1.

2.2.1 Process of Measuring and Evaluation of Test Results

- Test surface: firstly, the dry test surface was rubbed in order to reach smoothness and flatness and to make visible the aggregates grains. 8 trials of rebound measuring on each test surface were done in order to reach at least 5 valid values.
- Calibration relations concrete strength determining: CSN 73 1373 specifies different positions for each type of Schmidt impact hammer in dependence on the calibration relations. The Tables 1 and 2 show concrete compression strength in relation to the detected rebound values. The values are valid for current concrete at the age of 14-56 days, using natural compact aggregates.

− <u>Evaluation of test results</u>: Concrete compression strength f_{be} with not guaranteed accuracy was determined on the base of common calibration relation valid for the given Schmidt impact hammer type according to the ČSN 731373, whereas the sclerometer position was taken into account.

− <u>Correction coefficients</u>: For older concretes, the strength value has been reduced by a α_t coefficient in the range between 0.95 and 0.90. Regarding the concretes at the age of above one year, the α_t coefficient value amounts to 0.90 which, however, does not correspond to the reality. For the concretes at the age of 10 − 30 years, this coefficient value moves between 0.5 and 0. 65 as a rule. There is also an intention to introduce a coefficient expressing or reflecting the concrete condition. In order to gain plausible concrete strength values, it is necessary to do so called „nail down" tests, whereas the selected places have been subjected to non-destructive tests and consequently, specimens in the form of core wells have been sampled for determining of précised coefficient in compliance with the CSN 73 1370.

Key:
1 Impact Plunger
2 Test surface
3 Housing
4 Rider with guide rod
5 Not used
6 Push button, complete
7 Hammer guide bar
8 Guide disk
9 Cap (for models L and LR red)
10 Two-part ring
11 Rear Cover (for models L and LR red)
12 Compression spring
13 Pawl
14 Hammer mass: 14.1 model N, 14.2 model L
15 Retaining spring
16 Impact spring
17 Guide sleeve
18 Felt washer
19 Plexiglas window
20 Trip screw
21 Lock nut
22 Pin
23 Pawl spring

Figure 1: Schmidt Impact Hammer, Types N/ L (Spring of Information: www.proceq.com)

Table 1: Compression Strength Values f_{be} Based on Rebound R of Schmidt Impact Hammers, Types N/L (CSN 73 1373)

Rebound Number	Impact Hammer – type N			Impact Hammer – type L		
	horizon-tally	vertical-ly down	vertical-ly up	horizon-tally	vertical-ly down	vertical-ly up
14				9	14	
15				10	15	
16				12	17	
17				13	18	
18				15	20	
19				16	21	9
20				18	23	10
21				19	24	11
22				21	25	13
23				22	27	14
24		19		23	28	16
25	16	21		25	30	18
26	18	22		26	32	19
27	19	24		28	33	21
28	21	26	14	30	35	22
29	22	27	15	31	36	24
30	24	29	17	33	38	25
32	27	32	20	36	41	29
33	28	33	21	38	43	30
35	32	37	25	41	46	34
36	33	39	26	43	48	36
37	35	40	28	44	49	37
39	39	44	32	48	52	41
40	41	46	34	49	54	43
41	42	47	35	51	56	45
42	44	49	37	53	57	46
43	46	51	39	54	59	48
45	50	54	43	58	62	52
46	52	56	45	60	64	54
47	53	58	47			56
48	55	60	49			57
49	57	62	51			
50	59	64	52			
51	61		54			
52	63		56			
53			58			
54			60			
55			62			

2.2 Mašek Pointed Hammer

The sense of the test is, to detect the depth of pointed hammer penetration into the concrete under the consideration of defined number of strokes and the tool weight. Both, the relevant pointed hammer form and size are shown in Figure 2.

The concrete strength determination follows from the depth of pointed hammer penetration, whereas 20 strokes by the tool in the weight of 2 kg from a distance of 700 mm or 500 mm have been performed.

3 valid measure tests were done in the selected place, whereas the depth of pointed hammer penetration might not differ by more than 20 % in the average.

The concrete compression strength with not guaranteed accuracy for stroke travel of 700 resp. 500 mm is to be reckoned from the common calibration relations (1) and (2):

– *Stroke Travel* of 700 mm

$$f_{be} = 456,4h^{-0,99346} \quad h \in \{120; 18 \text{ [mm]}\} \quad f_{be} \in \{4; 25\} \text{ [MPa]} \tag{1}$$

– *Stroke Travel* of 500 mm

$$f_{be} = 88,4 - 4,6865h + 0,06478h^2 \quad h \in \{40;11\}[\text{mm}] \quad f_{be} \in \{4;48\} \text{ [MPa]} \tag{2}$$

kde :
f_{be} - pevnost betonu v tlaku s nezaručenou přesností
h - hloubka vniku špičáku do betonu

Při provádění zkoušek byl aplikován postup s dráhou úderu 500mm, z důvodu prostorových omezení zkoušených konstrukcí.
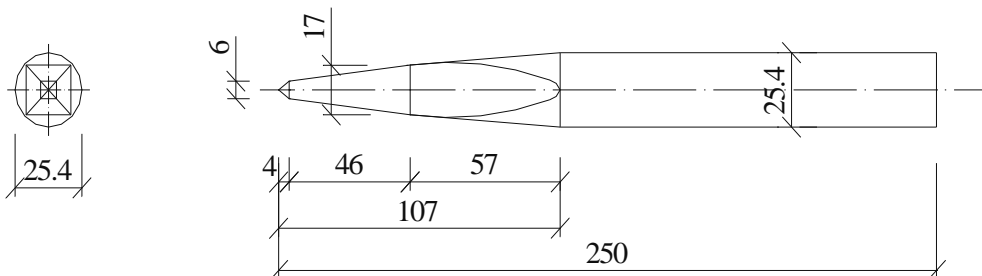
Figure 2: Mašek Pointed Hammer, Form and Size

3. COMPARISON OF CONCRETE COMPRESSION STRENGTH VALUES MEASURED BY DIFFERENT SCLEROMETER TYPES

The comparison is based on results of non-destructive test methods. 502 values gained by measuring in the selected place by means of each Schmidt hammer type were available to be compared with 90 values gained by application of Mašek pointed hammer in the same place of testing.

The f_{be} compression strength values gained from non-destructive testing parameter under the consideration of common calibration relation for the given sclerometer have been compared. For this comparison, the Schmidt impact hammer, type N, was preferred, as this hammer is most frequently used in the building industry.

Coherence between compression strength values based on the tests by Schmidt impact hammers, types N / L, is shown in the Figure 3. Comparison of testing by Schmidt impact hammer, type N, with Mašek pickaxe is shown in the Figure 4; the results having followed from tests by Schmidt impact hammer, type L, and by Mašek pointed hammer are compared in the Figure 5.

Figure 6 shows a comparison of concrete strength values reckoned from the gained relations in dependence on the theory.
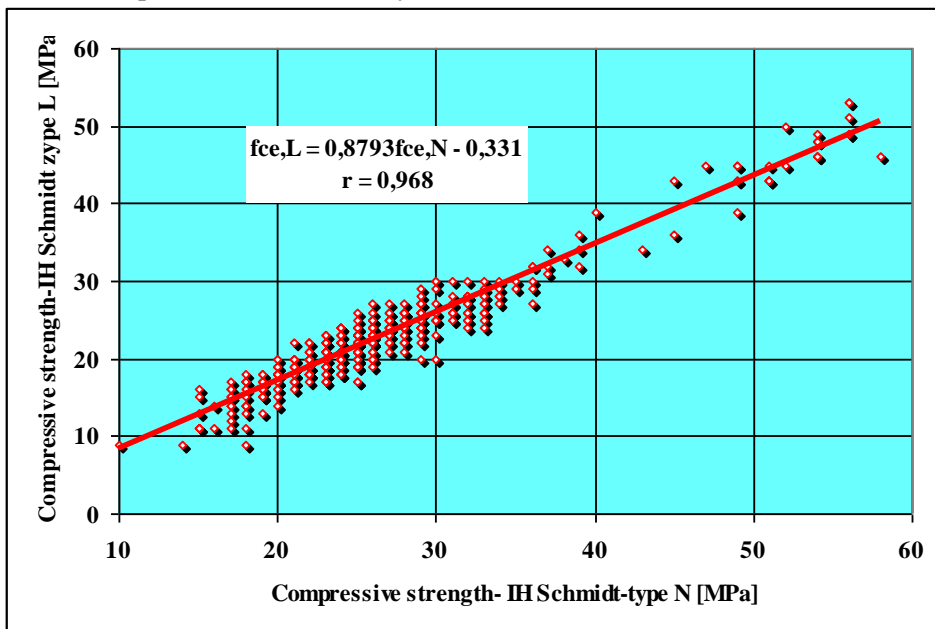
Figure 3: Coherence between f_{be} Compression Strength Values of Non-Guaranteed Accuracy and Values Gained by Schmidt Impact Hammers, Types N/L
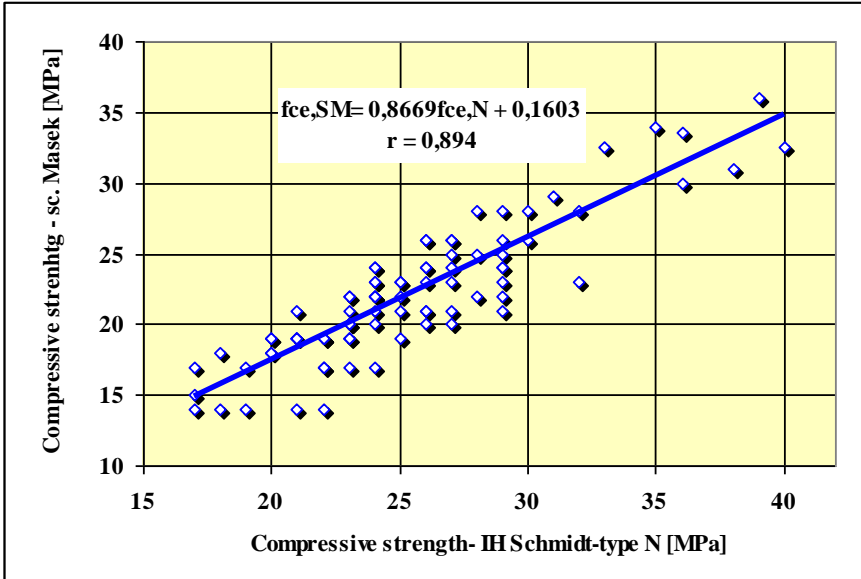
Figure 4: Coherence between f_{be} Compression Strength Values of Non-Guaranteed Accuracy and Values Gained by Schmidt Impact Hammer, Type N, and by Mašek Pointed Hammer
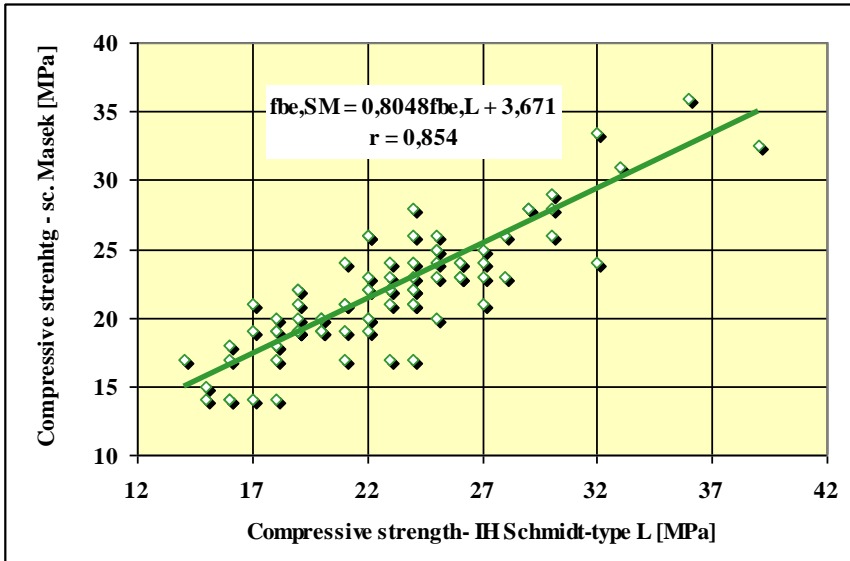
Figure 5: Coherence between f_{be} Compression Strength Values of Non-Guaranteed Accuracy and Values Gained by Schmidt Impact Hammer, Type L, and by Mašek Pointed Hammer
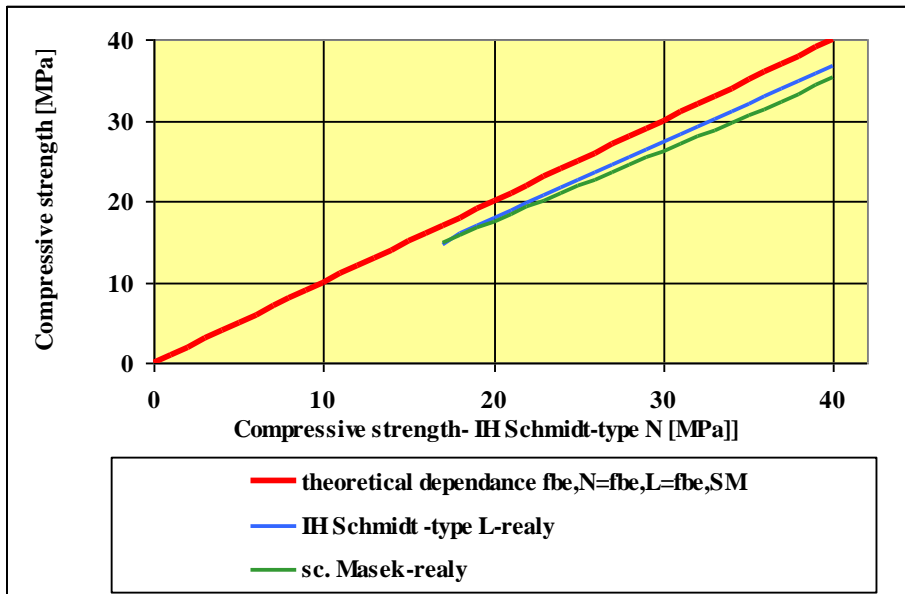
Figure 6: Comparison of f_{be} Compression Strength Values Gained by Schmidt Impact Hammer, Type L, with Results of Mašek Pointed Hammer Testing
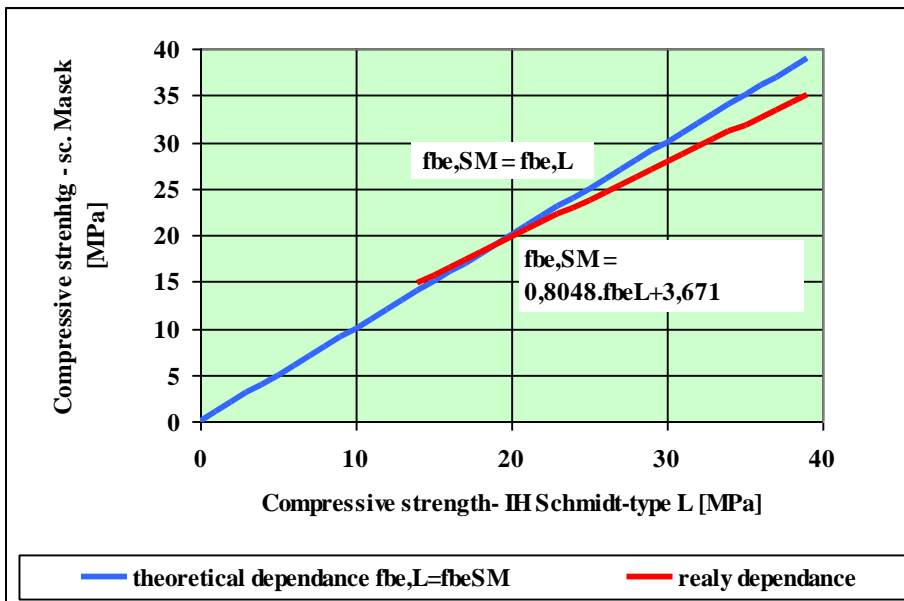
Figure 7: Comparison of f_{be} Compression Strength Values Gained by Schmidt Impact Hammer, Type N, with Results of Mašek Pointed Hammer Testing

4. CONCLUSION

With respect to the analysed results of measured concrete strength values gained by using of different sclerometer types, we may claim,

- That, a conformity of the concrete strength values gained on the base of measuring by different sclerometer types in the same place with evaluation of the same according to the common calibration relation for the given method has not been vindicated.

- There is a high correlation degree between the strength values gained by means of Schmidt impact hammers, types N/L, or by Mašek pointed hammer. The Figure 6 shows that 98 % of strength values based on measuring by Schmidt impact hammer, type L, undergo by 0.6 MPa the values traced by Schmidt impact hammer, type N, and 99 % of strength values measured by Mašek pointed hammer are lower by 0.9 MPa in comparison with the same strength values measured by Schmidt impact hammer, type N.

- Comparing the results of measuring by Schmidt impact hammer, type L, with those of Mašek pointed hammer, the top strength values of 18 MPa are sinking consequently (the deviation is expressed in an absolute value ranging between 0 and 8 MPa), see the Fig. 7. It is recommendable, to use always one and a single type of sclerometer in order to measure the concrete strength within a construction. This rule may be avoided, when a usage of more sclerometer types is necessary, e.g. for the ground that parameters of non-destructive testing lie beyond the measured common calibration relation to be interpreted as the test results.

- An accuracy coefficient should always be set in order to fix the most précised values of concrete strengths (see the proceedings specified in CSN 73 1370). The coefficient is always to be set for concretes at the age of above 1 year.

- In case that different sclerometer types are used for the tests, it is always necessary to quote accuracy coefficients relating to each method.

- The Mašek pointed hammer is recommendable for testing of concrete strength up to 12 MPa.

Acknowledgements

References

1. Drochytka R.: et al. Progressive Building Materials with Utilization of Secondary Raw Materials and their Impact on Structures Durability. but, *Final report of the project VVZ CEZ MSM: 0021630511, Brno 2008*. Brozovsky J.: Subtask 3 (in Czech).
2. Brožovský, J.; MAtějka, O.; Martinec, P. Concrete Interlocking Paving Blocks Compression strenght Determination Using Non-Destructive Methods. *The e-Journal of Nondestructive Testing,* 2007, roč. 12, č. 4, s. 91-97. ISSN: 1435-4934.
3. Brožovský, J., Fojtík, T. , Brožovský, J., jr. Built-in Concretes Made with Gypsum Free Cements: Compression Strength Determination Using Nondestructive Testing Methods. In *The Third International Conference on Structural Engineering, Mechanics and Computation*, Cape Town, South Africa, 2007, ed. A. Zingoni, Millpress Science Publishers, Rotterdam The Netherlands, p. 1554-1559, ISBN 978 90 5966 057 1
4. Brožovský, J., Zach, J. , Brožovský, J., jr. Gypsum free cements and concretes made with them: strength determination using nondestructive testing methods. In *IV Conferencia Panamericana for Non destructive Testing*, Buenos Aires, Argentina, 2007, Primera edición, Asociación Argentina de Ensayos No Destructivos y Estructurales, p. 1-9, (paper №2), ISBN 978-987-23957-0-4
5. EN 12504-2: Testing of Concrete in Structures – Part 2: Non-Destructive Testing - Determination of Rebound Number
6. CSN 73 1370: Non-Destructive Testing of Concrete: Common Regulation.
7. CSN 73 1373: Testing of Concrete by Hardness Testing Methods.
8. ISO/DIS 8045: Concrete, hardened -Determination of rebound number
9. ASTM C 805-97: Standard Test Method for Rebound Number of Hardened Concrete
10. BS 1881, part 202: Testing concrete. Recommendations for surface hardness testing by rebound hammer
11. NFP 18-417: Bétons – Mesure de la dureté de surface au sclérométre
12. JGJ/ T 23-2001: Technical Specification for Inspection of Concrete Compressive Strength by Rebound Method

Numerical modeling method for dynamic behaviour of masonry towers

Jerzy Szołomicki[1]

[1]Departmen of Civil Engineering, Wrocław Universityof Technology, Wrocław, 50-370, Poland

Summary

Dynamic behaviour model is essential to the reliability evaluation and restoration structure of historical masonry towers. In this paper author developed the identification techniques and the main influence factors on the dynamic behaviour of historical masonry towers. Besides sensitivity analysis and model updating criteria are discussed.

KEYWORDS: Historical masonry towers, dynamic behaviour, computational simulations.

1. INTRODUCTION

Historical masonry towers were built long time ago, often suffered various natural disasters and damages, and most of them had been repaired. Therefore most towers have following common characteristics: construction type, non-uniform materials and coexistence of various damage conditions. Since the structural parameters affect directly the dynamic behaviour of historical masonry towers, the dimension, construction detail, damage condition and variation degree should be surveyed carefully and defined reasonably for a good analytical model to be developed.

The techniques of structural identification, and in particular those of modal parameters of linear or linearised models, represent an important tool for analysing existing structures. In fact, synthetic information on damage occurred to towers can be obtained comparing the value of such modal parameters. First of all natural frequencies and damping coefficients, before and after the seismic event.

According to the principle of dynamics, the motion equation of an historical tower can be expressed as follows:

$$[K]\{x\}+[C]\{\dot{x}\}+[M]\{\ddot{x}\}=-[M]\{1\}\ddot{x}_0, \tag{1}$$

where $\{x\}, \{\dot{x}\}, \{\ddot{x}\}$ are the structural nodal displacement, velocity and acceleration vectors, respectively. $[K], [C], [M]$ are respectively, structural stiffness, damping, and mass matrices, $\ddot{x}$ is the ground acceleration.

Taking:

$$[C] = \alpha[M] + \beta[K], \tag{2}$$

if Rayleigh damping is adopted, the mass [M] and stiffness [K] are the main factors to influence dynamic behaviour of the structure.

2. IDENTIFICATION OF MODEL PARAMETERS

The extraction of model parameters from ambient vibration data was carried out by using two different procedures: Peak picking method and Frequency domain decomposition. Both methods are based on the evaluation of the spectral matrix in the frequency domain:

$$G(f) = E\left[A(f)A^H(f)\right]. \tag{3}$$

The Peak picking method leads to reliable results provided that the basic assumptions of low damping and well-separated modes are satisfied. For a lightly damped structure subjected to a white-noise random excitation, both auto-spectral densities and cross-spectral densities reach a local maximum at the frequencies corresponding to the system normal modes. For well-separated modes, the spectral matrix can be approximated in the neighborhood of a resonant frequency f_r by:

$$G(f_r) \approx \alpha_r \varphi_r \varphi_r^H, \tag{4}$$

where: α_r depends on the damping ratio, the natural frequency, the modal participation factor and the excitation spectra. In the present application of the Peak picking method, natural frequencies were identified from resonant peaks in the auto-spectral densities and in the amplitude of cross-spectral densities, for which the cross-spectral phases are 0 or π. The mode shapes were obtained from the amplitude of square-root auto-spectral densities curves while cross spectral densities phases were used to determine directions of relative motion.

The Frequency domain decomposition approach is based on the singular value decomposition of the spectral matrix at each frequency:

$$G(f) = U(f) \sum(f) U^H(f), \tag{5}$$

where: the diagonal matrix $\sum$ collects the real positive singular values in descending order and U is a complex matrix containing the singular vectors as

columns. If only one mode is important at a certain frequency f_r, the spectral matrix can be approximated by a rank-one matrix and can be decomposed as:

$$G(f_r) \approx \sigma_1(f_r) u(f_r) u_1^H(f_r). \tag{6}$$

The first singular value $\sigma_1(f)$ at each frequency represents the strength of the dominating vibration mode at that frequency while the corresponding singular vector $u_1(f)$ contains the mode shape.

3. MODEL UPDATING

Due to the uncertainty of structural parameters of the historical masonry tower, dynamic characteristics predicted by the analytical model often differ from field measurements. The proper reference criteria should be provided for the structural parameters identification in the model updating. From the field testing we can obtain the first n order modal parameters of a structure with N degrees of freedom.

For example, natural frequencies:

$$\lfloor \omega_T^2 \rfloor = diag(\omega_1^2, \omega_2^2, ..., \omega_n^2), \tag{7}$$

and mode shape:

$$[\phi_T] = diag[\{\phi_1\}, \{\phi_2\}, ...\{\phi_n\}]. \tag{8}$$

Generally, $\lfloor \omega_T^2 \rfloor$ measured from the field test is accurate. On the other hand, $[M_A]$ obtained from structural analysis is comparatively accurate but $[K_A]$ is less close to the actual values. To improve the effect of the model updating, the sensitivity system should be constructed for selection of the structural parameters firstly. Besides, taking the fast analysis advantage of LUSAS program, the conventional trial-error method also can be used to simplify the model updating procedure.

4. SENSITIVITY OF DYNAMIC BEHAVIOUR FOR STRUCTURAL PARAMETER ADJUSTMENT

The sensitivity-based model updating procedure and the correlative researches are helpful for the construction of the sensitivity system of historical masonry towers.

Suppose the structural parameters such as mass, stiffness, geometric dimensions and material characteristics described as p_i (i=1, 2,…,n) and the eigenvalues are

considered as derivative functions of structural parameters, the dynamic characteristics of the towers can be expressed as $F=F(p_1, p_2, ..., p_n)$. Then the sensitivity of F to structural parameter p_i is $S_{F_{p_i}} = \partial F(p_1, p_2, ...p_n)/\partial p_i$, and the bigger the absolute value of $S_{F_{p_i}}$, the more the sensitivity of model characteristic to structural parameter p_i.

According to the structural dynamics, the γ-order eigenvalue λ_γ and eigenvector $\phi^{(\gamma)}$, should satisfy:

$$([k] - \lambda_r[M])\phi^{(r)} = 0. \tag{9}$$

By solving the above formula's partial derivative to the i-parameter, the sensitivity of eigenvalue can be obtained:

$$\lambda_{ri} = \phi^{(r)T}([K]_i - \lambda_r[M]_i)\phi^{(r)}. \tag{10}$$

And the sensitivity of the eigenvector is:

$$\phi_j^{(r)T} = \sum_{\substack{k=1 \\ k \neq r}}^{n} \frac{-\phi^{(r)T}([k]_j - \lambda_r[M]_j)\phi^{(r)}}{\lambda_k - \lambda_r}\phi^{(k)} - \frac{1}{2}\phi^{(r)T}[M]_j\phi^{(r)}\phi^{(r)}. \tag{11}$$

Taking the stiffness parameter of structure as main study object, the sensitivity of the γ-order eigenvalue and eigenvector of stiffness k_{ij}, are respectively:

$$\frac{\partial \lambda_r}{\partial k_{ij}} = \phi_{ir}\phi_{jr}, \tag{12}$$

$$\frac{\partial \phi^{(r)}}{\partial k_{ij}} = \sum_{\substack{k=1 \\ k \neq r}}^{n} \frac{-\phi_{ik}\phi_{jr}}{\lambda_k - \lambda_r}\phi^{(k)} - \frac{1}{2}\phi_{ir}\phi_{jr}\phi^{(r)}. \tag{13}$$

5. CONCLUSIONS

The integrated modeling method for the dynamic behaviour takes advantage of ambient vibration technique and finite element analysis, which can obtain not only the synthesis dynamic response of the whole structure but also the contributions of individual factors such as connections, restraints and damage conditions.

References

1. Binda, L. et al. The collapse of the Civic Tower of Pavia: a survey of the materials and structure. *Masonry International,* vol. 20(6): p. 11-20, 1992.
2. Gentile, C. et al. Dynamic investigation of a historic masonry bell tower. *Proc. 6th International Masonry Conference,* 2002.
3. Mottershead, J.E., Friswell, M.I. Model updating in structural dynamics: a survey. *J. Sound and Vibration,* vol. 167: p. 347-375, 1993.
4. Katafygiotis, L.S., Mickelborough, N.C., Yuen, K.V. Statistical identification of structural modal parameters using ambient response data. *Proceedings 3rd International Conference on Computational Stochastic Mechanics*, p. 93-102, Greece, 1998.
5. Zhang Dewen, Zhang Lingmi. Matrix transformation method for updating dynamic model. *AIAA Journal*, vol. 30(5): p. 1440-1443, 1992.

Consideration Regarding the Dynamic Mechanical System Identification

Doina Stefan[1], Violeta-Elena Chitan[2], Gabriela Covatariu[3]

[1] *Faculty of Civil Engineering, Iasi, Romania*
[2] *Faculty of Civil Engineering, Iasi, Romania*
[3] *Faculty of Civil Engineering, Iasi, Romania*

Summary:

In the continuous effort to improve knowledge on the dynamic behavior of a building, the trend is towards the study of a building's behavior having as starting point the tests carried out on site. Tests on site are the current trend in studying buildings behavior. This approach provides the means to:
- Verify structure's quality;
- Verify its security level in real operational conditions;
- Validate existing analytical models of behavior;
- Verify assumptions made on a priori to predict structures response;
- Gain knowledge to improve sizing methods;
- Developing new models of behavior.

The accuracy of modal parameters - frequency and eigenform of vibration own - depend on the precision, which can be measured by the frequency response function (FRF), hence the critical importance of how the excitement of the structure to vibration amplitudes maintain as close to the operating level in all areas of interest have.

Developed techniques for identifying the frequencies and forms its own specific structures using a ***single excitation, excitation concurrent multi-point excitation in several consecutive points***. These methods involve performing iterative process leading to the possibility of automation.

KEYWORDS: *modal parameters, single excitation, frequency response function, parameters identification.*

1. INTRODUCTION

In the continuous effort to improve knowledge on the dynamic behavior of a building, the trend is towards the study of a building's behavior having as

starting point the tests carried out on site. This approach method provides means to:

- ***Assess (verify) quality of structure and its level of security in real operational conditions (real-life situation), the validation of analytical models*** of existing behavior and a priori assumptions made for the structure prediction of response;

- ***Accumulate knowledge necessary to improve methods of sizing*** and justified development of new models of behavior.

Studies on identification of dynamic structures are particularly present at international level and relatively little addressed in our country.

Identifying dynamic involves a combination of basic concepts of systems theory, structural theory models, mathematical statistics, and estimation theory with practical elements of experimental tests, measurement techniques, capture and automatic processing of experimental data.

Special emphasis is currently on deployment and development of techniques for identifying systems for studying the dynamic-seismic behavior of buildings, to optimize the design of new structures and/or safety of the structures damaged by earthquakes, by strengthening and redesign.

A traditional definition of system identification is given by *L.A Zadeh (1962) as* ***"the determination, on the basis of input and output, of a system within a specified class of systems, to which the system under test is equivalent"***.

Thus, identifying a system raises several issues:
- Identifying the system type;
- Nature of the characteristics, which needs to be identified;
- A source of data on the system response;
- Source of data regarding actions upon which the operation of identification is carried out.

Problem identification can have two main aspects:
A. Parameters identification – when analytical expression of the mathematical model is known and the coefficient involved unknown (unknown coefficient values).
B. Total or global identification – no information or a priori information is insufficient to allow a mathematical representation.

Identification of dynamic structures can be defined as: a set of techniques that allow determination of physical parameters that occur in the equations describing the behavior of structures subjected to dynamic – seismic actions.

These techniques have been developed due to difficulties encountered in accurately assessing the rigidity, damping and mass of real-size structure.

For experimental determination of dynamic characteristics one of the following methods may be applied:
i.) Methods of identification using known excitability factors (active method;)
ii.) Methods of identification using size excitation of the normal functioning of the system (passive methods).

The accuracy of modal parameters – frequency and own types of vibration - depend on the precision which can be measured by the frequency response function hence, the critical importance of structure's excitement in order to maintain the vibration amplitudes close to the operating level in all areas of interest.

Generally a process of identification includes:
1) *Choosing the model and its structure*
Generally, the construction of a model goes through the following steps:
- Choosing a model structure based on physical knowledge;
- Determining parameters from the available data (estimation of parameters);
- Checking and testing the model (diagnostic test).
2) *Choosing the comparation criteria* - approximation to model the properties consistent with the actual real structure is expressed by minimizing a *criterion function;*
3) *Estimation and correction parameters.*

Determination of parameters can be performed either by *estimation theory* or by *optimizing parameter.* In general, choosing an algorithm to adjust unknown parameters, which are used to evaluate them so that the identification criterion should be minimized.

Modifying the structure of the model using the criterion function to be minimized does handling identification systems as a problem of optimization. Identification using parametric estimation can be obtained by applying statistical theory to verify the operating parameters of the structure.

The parameters that define the response of a structure can be:
 - *Measurable parameters (observed)* can be determined by direct measurements on actual structure (the coefficients of flexibility matrix, eigenform, functions in response frequency)

 - *Abstract parameters (intuitively)* that can be obtain by the properties of materials (the stiffness, damping and inertia matrix elements).

Troubleshooting estimate parameters can be done in two ways:
- **Using explicit mathematical equations** resulting directly with a set of numerical quantities, such as coefficients of differential equations, their eigenfrequencies, damping factors;
- *Using a method of correcting (adjustment) model*, which assumes implementation of a model whose parameters are ordered in such way so that the model's characteristic is similar to the system in a sense established beforehand.

Application procedure for correction of the model calculation by estimation theory experimental data is the following assumptions and general considerations:
- *The corresponding dynamic structure is linear-elastic or linearization in a given field, invariant with respect to time;*
- *Dynamic model structure is determined in the sense that is known initially through physical parameters - mechanical structure of (*the inertia, stiffness and damping matrix*);*
- *Experimental model is excited by deterministic signals, the recording and processing are considered and disturbance quantities entry.*

Correction procedures can be distinguished by two phases:
i.) The location/detection errors;
ii.) Error correction.

Stage localization/detection of errors is the most difficult. The difficulties arising due to the following reasons:
- there is a lack of experimental data
- perceived incompatibility, usually between the experimental and analytical model studies on the sizes and dimensions
- the different distribution of systematic errors in the analytical and experimental model.

The main objective of the methodology for correction of dynamic models used to study the structure can be defined as a process for "*refining*" an existing analytical model.

Corrected model should reproduce the following:
- the modal proprieties in points which the experimental measurements were done;
- frequency response function, obtained experimentally;

- In the modal properties that have not made measurements;
- frequency response function, obtained analytically only;
- correct representation of model's connection.

2. PROCESSES IDENTIFICATION OF SYSTEMS WITH 1DOF

The simplest method of identification is based on analysis dynamic response of the system with 1 DOF.

A dynamic test is based on the measurement of several quantities of excitation forces applied to the structure. Measurement of excitation force and response in a number of points in the whole area of frequencies is sufficient to describe the behavior of the structure.

The result can be measured in travel, speed or acceleration and the different terms used for the ratio of response and action. Frequency response function is the complex spectrum of the output (response) and excitation spectrum:

$$H(\,j\omega\,)=\frac{U(\,j\omega\,)}{F(\,j\omega\,)} \qquad (1)$$

where: $U(j\omega)$ is the response spectrum, $F(j\omega)$ is the excitation spectrum, $H(j\omega)$ is the transfer function (FRF).

Have been developed various methods of identification systems based on 1DOF response functions used (accelerated, mobility, inertance). So, using accelerated have developed:
- method of peak amplitude;
- method of lagging (phase difference, trail behind) diagram;
- actual component diagram method of admittance;
- polar diagram method of admittance.

3. METHODS OF IDENTIFICATION DYNAMICS OF SYSTEMS WITH NDOF

These techniques used to identify NDOF systems have been developed due to the difficulties encountered in assessing the exact rigidities, damping and mass. The main challenge is to determine the characteristics represented by

the mass (M), damping (C) and stiffness (K) matrices which are not directly measurable in measurable quantities such as frequency, modal shapes, and dampings.

Testing large structures complex takes place in two phases:
Phase I – determining the number of coarse eigenmodes vibration and their resonance frequencies using a single jigger;
Phase II – of the isolated modes by a proper distribution of a number of jiggers along the structure. a match structure and excitation forces from vibrations, thus only interested in how to be dominant excited.

For large structures, with numerous links and disproportional damping and non-linear effects, disproportional near modes are frequent and not only prevents localization frequencies for the identified modes and modal shapes for a fixed jigger position may not coincide with those established in other positions of the jigger.

3.1 Identification of modal frequencies and shapes using a single harmonic excitation

A linear and elastic structure excited by a sinusoidal force will respond directly proportional to the force excitation and has the same frequency.

Measurement of excitation force and response in a number of points on the range frequency is sufficient to describe the behavior of structure.

Were developed following methods of identification using a single excitation:
- method of peak amplitude;
- Kennedy and Pancu method;
- modal connections method (Raney and Hawlett).

3.2 Identification of linear systems excited harmonic simultaneously in several points

A complex structure vibrating simultaneously in several ways. For a correct analysis of the unwanted modes must be eliminated.

To excite a structure in one of the main vibration distribution of forces should be shaped:

$$\{F\} = (\omega_i^2 - \theta^2)[M]\{Y_i\} + \theta[C]\{Y_i\} \qquad (2)$$

Since the purpose of excitation with more jiggers is not only a way to excite interest but also to eliminate the contribution of modes outside the resonance should be noted that outside the resonance can not be undone if all jiggers are placed in unexpected mode nodes.

Methods developed for matching excitation forces from jiggers are:
- method's DECK;
- method's CLERC;
- method's L.M.A.;
- method's ASHER;
- modal adjustment method.

3.3 Identification methods using harmonic excitation in several consecutive points

These methods are considered as "methods of excitation at a point" because it used only one spark drawer which is moved successively to different points of the structure. Current methods using consecutive excitation are:
- independent force methods (Trail – Nash);
- independent overcharge methods.

4. CONCLUSIONS

Tests on site are the current trend in studying buildings behavior. This approach provides the means to:
- Verify structure's quality
- Verify its security level in real operational conditions
- Validate existing analytical models of behavior
- Verify assumptions made on a priori to predict structures response
- Gain knowledge to improve sizing methods
- Developing new models of behavior.

The accuracy of modal parameters - frequency and eigenform of vibration own – depend on the precision, which can be measured by the frequency response function (FRF), hence the critical importance of how the excitement of the structure to vibration amplitudes maintain as close to the operating level in all areas of interest have.

Developed techniques for identifying the frequencies and forms its own specific structures using a *single excitation, excitation concurrent multi-*

point excitation in several consecutive points. These methods involve performing iterative process leading to the possibility of automation.

Depending on the identifying system, the results can be used for:
- verification and validation of analytical models and their correction;
- creation of dynamic models to represent the real structure;
- determination of sizes that are not directly measurable (the inertia matrix M, damping matrix C, the stiffness matrix K) to measurable quantities (frequencies, modal shapes, damping);
- to provide the structural changes;
- predict behavior by calculating the complex structure by using hybrid method consisting in the decomposition structure in sub structures which may determinate the experimental actual characteristics;
- determination by calculating the response to other excitations or more simultaneous excitations based to the measured response for a particular type of excitation.

Some applications in other areas of identifying and estimating the parameters are listed below:
1. In air and automotive industries to determine:
- aerodynamic coefficients;
- the speed of vibration of the surface of an aircraft or missile;
- vibration modes damping depending on the frequency;
- characteristics of dynamic tire – train;
- the dynamic characteristics of landing gear and car suspension;
- dynamic characteristics of turboreactors, turboprops, pistons moving alternative, etc.

2. In process industries (chemistry, fuels, materials) to determine:
- rheological and dynamic characteristics of the material undergoes deformation or leakage;
- the characteristics of combustion processes;
- dynamic parameters of the instruments, transducers, and components of the adjustment processes etc.

Miscellaneous:
- determining the dynamic parameters of biological populations;
- determining the characteristics of systems for which you made predictions that the economic dynamic;
- determining the dynamic characteristics of the human operator on various devices;

- determining the dynamic characteristics of the human or animal body function.

References

1. Eykhoff P., *Identificarea sistemelor* (*System Identifications*), Ed.Tehnica, Bucuresti, 1977.
2. Kecman V., *System Identification Using Modular Neural Network With Improved Learning*, the International Workshop NICROSP 96, Venice, pp.40-48, IEEE Computer Society Press, 1996.
3. Ljung L., *System Identification, Theory for the User*, PTR Printice Hall, Engkewood Cliffs, New Jersey, USA, 1987.
4. Natke H.G., *Application of System Identification in Engineering, CISM*, Courses and Lectures, 1988.
5. Stefan D., *Identificarea dinamică si seismică a structurilor si echipamentelor industriale*, Ed. Tehnica, Stiintifica l si Didactica CERMI, Iasi, 2003.
6. Zadeh L.A., *Teoria sistemelor* (*System Theory*), Ed.Tehnica, Bucuresti, 1982.

Doina Stefan, Prof.dr. eng. "Gh. Asachi" Technical University of Iasi, Faculty of Civil Engineering, B-dul Mangeron 43, Iasi, Romania, email: dstefan@ce.tuiasi.ro

Violeta-Elena Chitan, Lector dr. eng., "Gh. Asachi" Technical University of Iasi, Faculty of Civil Engineering, B-dul Mangeron 43, Iasi, Romania, email: chitanvioleta@yahoo.com

Gabriela Covatariu, Ph.D. eng., "Gh. Asachi" Technical University of Iasi, Faculty of Civil Engineering, B-dul Mangeron 43, Iasi, Romania, email:covagab@yahoo.com

Durability of sintered materials modified by alternative silicate filling agents

Tomáš Melichar[1]

[1]*Faculty of civil engineering, Institute of Technology of Building Materials and Components, Brno University of Technology, Brno, 602 00, Czech Republic, melichar.t@fce.vutbr.cz*

Summary

The issues contained in the study are focused mainly on the durability of glass-based sintered materials for whose production alternative silicate filling agents were used. These sources are waste glass gravel from collected coloured container glass, disassembled TV screens and, last but not least, so-called secondary energy products, i.e. mainly fluid fly-ash and blast-furnace slag. It is generally known that currently fluid fly-ash is not being used as a secondary raw material much. The same applies to the above-mentioned raw glass. I focused mainly on the frost impact on the strength features of sintered materials using both crystalline and amorphous silicate filling agents. I drew up 19 formulas in total. Two sets of test samples consisting of five specimens were made for each formula. The above-mentioned analyses of the samples were carried out and subsequently assessed. I found out that amorphous filling agents had a positive effect on the durability features of the produced materials, whereas secondary products had a negative effect. Therefore, crystalline substances do not seem to be suitable for production of glass-silicates considering their strength features in terms of durability which is stated in this study.

KEYWORDS: durability, bending strength, alternative sources, silicates, glass, waste, recycling, strength

1. INTRODUCTION

Many publications, patents, production technologies, etc. concerning waste production and its subsequent utilization in the form of secondary raw materials based on various researches and experiments have been made. The area of production of building materials and elements is not an exception, on the contrary, with respect to the large volumes of various materials being produced and related waste and consumed energy sources, the effort to utilize secondary raw materials has become one of the primary targets. Because of the current world crisis consumption of secondary raw materials has partially dropped down in some industrial areas and primary sources are being used again. But we can expect that it

is just a temporary effect which should not last long. One of the intensively discussed secondary raw materials in terms of its optimum utilization is raw glass from collected coloured bottles. With respect to its features, i.e. significantly variable chemical composition, this raw glass is not being fully utilized which you can see not only in the Czech Republic but also throughout the EU. Another interesting raw material in terms of its utilization is glass from ordinary TV screens and computer monitors. Increased production of waste, or more precisely electro-waste, which includes TV screens and computer monitors, depends on new technologies which are, thanks to their progressiveness, more lucrative for most consumers. They are mainly LCD-based products and plasma screens which currently have a significant share in the market compared to ordinary screens. An important criterion for the effort to utilize old, useless screens is mainly the fact that they contain some toxic substances. Some recycling lines have been solving the problems how to remove these substances but some harmful elements are contained right in glass matrices and, therefore, they cannot be removed effectively or, more precisely, elimination of these substances is possible but with high economic costs which would probably lead to disappearance of these technologies in practice. Therefore, there is an option to use raw glass directly in specific building materials. One of the ways how to effectively use the above-mentioned secondary raw materials is e.g. production of glass-silicate materials. They are already being used in the building industry in different ways. Thanks to their excellent features you can see them in various types of buildings. Glass-silicate materials are designed mainly for surface treatment of walls and floors. Production of these materials consists in a heat treatment of granulated batches of glass, other substances and admixtures and their subsequent mechanical processing to the required form.

2. EXPERIMENTAL PART

2.1. Formulas

At the beginning I drew up a basic material batch according to my practical experience on whose basis I determined the input raw glass – borosilicate glass – and the temperature regime of the production process. In this way I made reference samples whose features were compared with the features of samples which had been modified in a certain way. In that year I modified the composition of the batch in the following three ways:

- correction of the grain size composition,
- correction of the raw material batch composition,

- modification of the temperature regime.

I used four types of secondary raw materials in total. The features of the samples made of them were compared with the reference samples produced on the basis of the practical findings. Three test specimens (whose dimensions were approx. 65 × 25 × 130 mm) were made for each formula within the research. The following symbols were used for marking the test specimens:

- RE – reference raw glass,

- CR – screen raw glass (a mixture of funnel screens)

- CO – recycled coloured container glass,

- SLX – finely ground blast-furnace slag (X – a number representing the share of the secondary raw material from the original batch in percents),

- FAX – fluid fly-ash (X - a number representing the share of the secondary raw material from the original batch in percents).

The other numbers used for marking the samples represent the maximum temperature of isothermal persistence in the course of the production process and the granulated batch fractions (only raw glass; fly-ash and slag were very fine).

2.2. Analysis of the input raw materials

Within the research I carried out several appropriate analyses of the input raw materials first. The chemical composition of the raw materials described in the following table is important in order to find out their features at increased temperatures. There is a significant difference in the content of particular elements of recycled glass and the other raw materials.

Table 1. Chemical analysis of secondary raw materials

Component	Sample			
	CR	CO	FA	SL
SiO_2	66.79	69.79	25.49	30.25
Al_2O_3	4.21	1.80	24.65	5.42
Fe_2O_3	0.28	0.40	7.09	1.12
BaO	10.7	0.30	-	-
CaO	0.28	9.92	22.61	36.95
MgO	0.11	2.17	0.64	6.31
Na_2O	7.57	12.2	0.6	0.37
K_2O	6.91	0.97	0.38	0.56
PbO	0.91	-	-	-
SrO	0.25	-	-	-
TiO_2	0.04	-	5.35	-
LiO_2	0.38	-	-	-

MnO	-	0.03	0.043	-
Cr$_2$O$_3$	-	0.074	-	-
ZrO$_2$	-	0.02	-	-
Organic compounds	-	0.50	-	-
SO$_3$	-	-	15.82	1.75
P$_2$O$_5$	-	-	0.32	-

2.3. Durability and strength parameters

In accordance with the normative documents concerning ceramic facing elements and in connection with the previous phases I focused on determination of some basic features by means of which I checked the influence of the substitution of the primary raw materials used for production of glass-silicate materials on their final parameters. Namely it was a study of the influence of cyclic freezing and de-freezing (ČSN EN ISO 10545-12) of these materials on the final strength parameters (ČSN EN ISO 10545-4). The following chart shows a comparison of the average strength values before and after the frost test (100 cycles) with the exception of the test specimens produced using fluid fly-ash. The samples were examined only visually.
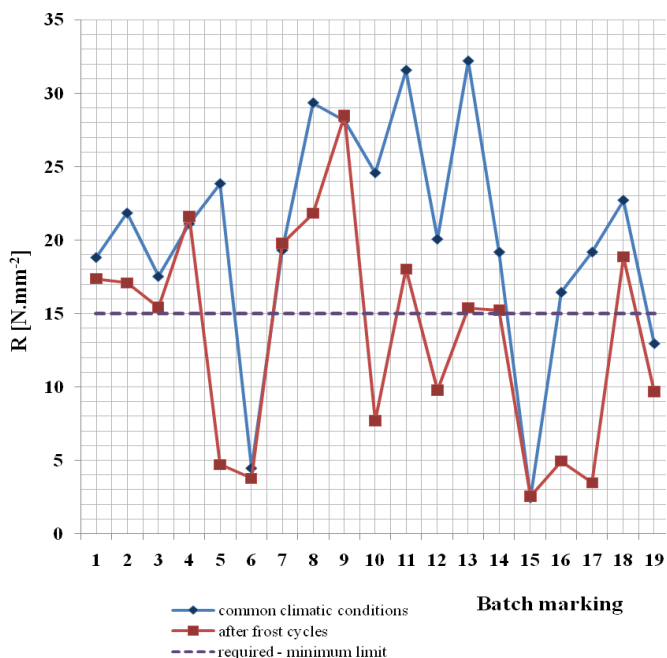
Figure 1. Bending strength comparing before and after frost cycles

Table 2. Explanation of batch marking

1. RE 900 0-6	11. CR 800 1-8
2. RE 960 0-6	12. CR 800 4-8
3. RE 1050 0-6	13. CR 960 0-8
4. CR 700 0-1	14. CO 800 0-4
5. CR 700 0-8	15. CO 800 2-16
6. CR 700 4-8	16. CO 960 2-16
7. CR 750 0-8	17. CO 1050 2-16
8. CR 775 0-8	18. SL2,5
9. CR 800 0-8	19. SL5,0
10. CR 800 1-4	

The graphic assessment of the values shows dependence on the applied secondary raw material as well as on its volume and the related grain size and the maximum temperature of isothermal persistence during the production process. One of the important criteria for assessment of glass-silicate products designed for wall facing and floor paving used for both interiors and exteriors is their appearance. Therefore, I also carried out a visual assessment of their appearance which is documented in the photographs below.
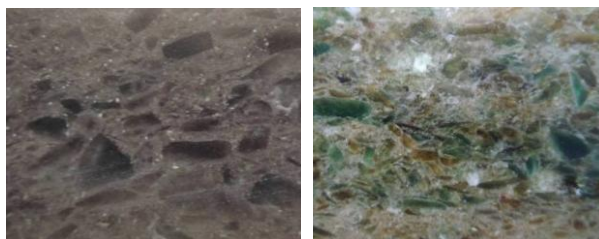
Figure 2, 3. Structure of the samples made of screen raw glass – CR 750 0-8 (left) and coloured container raw glass – CO 800 0-4 (right)

Figure 4, 5. Structure of the sample made of reference raw glass and an admixture of fluid fly-ash – FA5.0 (left) and an admixture of finely ground slag – SL5.0 (right)

3. CONCLUSIONS

At the conclusion I can state that I checked the modification option for the composition of the batch of glass-silicate materials using four types of secondary raw materials and one of them was found absolutely unsuitable (i.e. fluid fly-ash – these samples were falling apart when removed from the moulds). Regarding screen raw glass, coloured container raw glass and finely ground blast-furnace slag I reached very good, comparable and in some cases better strength parameters than in the reference samples with appropriately chosen grain size composition, optimum dosing and temperature regime. The visual assessment obviously shows that secondary raw materials do not have any significant effect on the appearance of the structure of the final products but it is necessary to pay attention to purity of these raw materials which plays an important role there. The results also show resistance of glass-silicate materials to frost which is, in terms of their utilization in exteriors under our ordinary climatic conditions, very important. I have also found out that there are no significant negative changes in the strength features, with the exception of the test samples produced using a coloured container recycled material with coarse fraction. Therefore, it is obvious that glass-silicate facing (or paving) materials containing secondary raw materials may be a future solution how to reduce consumption of primary mineral resources and energy which will have a positive effect mainly on the environment. The above-mentioned facts show the need of a further extensive research in order to check the other parameters influencing utilization of sintered glass materials.

References

1. FANDERLIK, I.: *Silica glass and its application*, Elsevier Amsterdam, 1991
2. MATOUŠEK, J. *Anorganické nekovové materiály*, VŠCHT v Praze, 1992
3. Lingart, Y. *Imitation of natural material tiling using waste glass*, Glass Technol. 39 (2) (1998) 42–43.
4. N. Menad, Cathode ray tube recycling, Resources Conserv. Recycling 26 (1999) 143–154
5. ČSN EN ISO 10545-4 Ceramic tiles – Part 4: Determination of modulus of rupture and breaking strength
6. ČSN EN ISO 10545-12 Ceramic tiles – Part 12: Determination of frost resistance

The Influence of The Glazing Area on the Opaque Area, at a Wall having a Window

Ioan Moga[1], Ligia Moga[2]

[1]*Physics of Constructions, Faculty of Civil Constructions, University of Cluj-Napoca, Cluj-Napoca, 400027,Romania*
[2] *Physics of Constructions, Faculty of Civil Constructions, University of Cluj-Napoca, Cluj-Napoca, 400027,Romania*

Summary

The resistance structure of the building forms linear thermal bridges in the building envelope elements. The intersection of those linear thermal bridges is forming thermal bridges having a spatial geometry. Thermal bridges are zones with the highest thermal permeability and temperatures having minimum values on the surface of the building envelope.

The objective of the paper is to establish in an accurate manner the thermal transmittance of an element of the building envelope and the minimum temperatures that arise on the surface of the building envelope, taking into consideration the presence of the thermal spatial bridges formed at the intersection of the linear thermal bridges.

KEYWORDS: Energy economics, Mathematical modelling, Simulation, Heat transfer, Dynamic modelling.

1. INTRODUCTION

The continuous rise of the energy price for heating the dwelling houses is a permanent concern of designers, researchers, and specialists in the field of thermal insulating of buildings and for energy savings during their exploitation life.

For a better knowing of the real phenomenon of the flows that are passing through the elements of the building envelope, the determination of the spatial temperature fields is imposed, with the help of some specific calculus programs based on which, the energetic performance of the building is determined. Since 1978 our research collective is interested and preoccupied in elaborating those types of programs. Using these types of programs, energetic efficient constructive solutions were elaborated for the elements of the building envelope used for constructing new buildings. For the existing fund of buildings, the elaborated calculus programs were used for determining the energetic performances, with the purpose of

energetic certifying of the building and for the analyses of the energetic solutions of energetic rehabilitation.

From the package of thermal - energetic calculus programs of buildings, the most used is the „CIMPSPAT" program that establishes the temperature spatial field in steady state regime, for elements having a complex formation.

From the many studied cases by our research collective, the paper presents just a part of the studies made. The study refers to 2 types of walls, an opaque wall and a wall having a window, non-insulated and insulated with expanded polystyrene in 4 variants of insulating, respectively 5 cm, 10 cm, 15 cm and 20 cm. The thermal insulation of the building on the exterior surface of the wall is turned on the embrasures of the window hole, up to the window frame with a thickness of 4m.

We limited in presenting the results for the energetic behavior of the 2 types of walls, without approaching in this paper the complex problem of superficial temperatures and the risk of condense, for avoiding the mould appearance

2. METHODOLOGY AND RESULTS

2.1. The work method

The thermal flows and the superficial temperatures are determined based on the spatial temperature fields established on a 3D spatial geometric model, in accordance with the methodology presented in Norm *EN ISO 10211/1:2005 "Thermal bridges in building construction-Calculation of heat flows and surface temperatures-Part 1:General Methods"*, using calculus methods of class A. For the calculus of the thermal flows and the superficial temperatures the used calculus methods are similar, but are not identical implying different contour conditions.

For determining the thermal flows and the superficial temperatures the calculus program CIMPSPAT 2008 variant (initial variant 1980), is used. The program establishes the spatial temperature field in steady state regime for elements having complex formation, using the high preciseness method of the thermal balance, in each node of the calculus network. The number of the digitization network on the 3 directions, the number of the materials having different physical characteristics and the number for conditions to limit is unlimited. The equations number of the energy balance is influenced by the computer capacity. The programming language used for the calculus program has developed from Fortran to Pascal and up to Delphi 7, having inserted the calculus modules in C++ language.

Based on the temperature field determined in the calculus network nodes and the thermal flows in the nodes from the surfaces of the element are determined. The

mathematical modeling of the spatial heat transfer phenomena in stationary thermal regime is given by the equations with second order partial derivatives with limit conditions, having the next formula:

$$\frac{\partial}{\partial x}\left[\lambda(x,y,z)\cdot\frac{\partial\theta(x,y,z)}{\partial x}\right]+\frac{\partial}{\partial y}\left[\lambda(x,y,z)\cdot\frac{\partial\theta(x,y,z)}{\partial y}\right]+\frac{\partial}{\partial z}\left[\lambda(x,y,z)\cdot\frac{\partial\theta(x,y,z)}{\partial z}\right]=0$$

(1)

The iterative calculus of the equations system obtained by writing the energy balance in the network nodes is considered finalized, when the flows on the interior and exterior surface are in equilibrium, which means that the sum of the flows that enter and exit through the surfaces of the elements is lower than a given precision. Usually the precision is ε=0.001 W for the current construction elements and a higher precision for the envelope elements that contain thermal bridges with higher thermal conductivities (metallic elements).
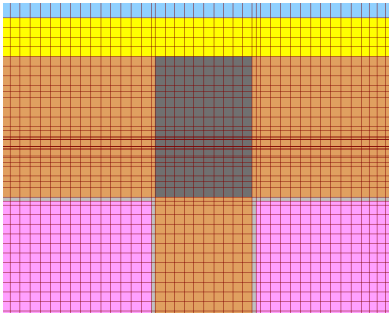
a.) the intersection of walls   b.) the window under the lintel
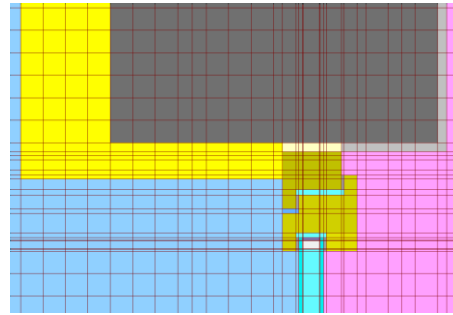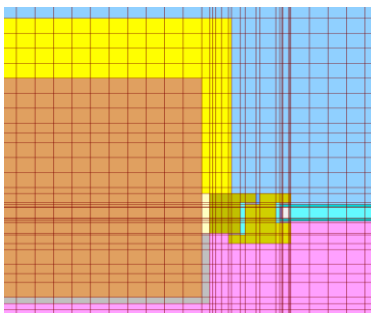
c.) window – wall joining   d.) the sash of the window
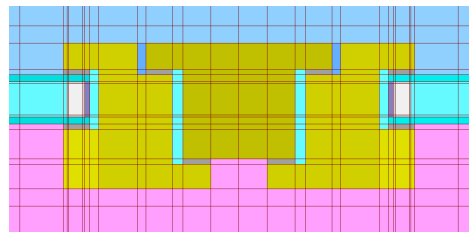
Figure 1. Details for the spatial network of digitization

The spatial geometric model, contained between the cutting planes was divided with the help of some sectional planes to form the orthogonal temperature field design network. The calculus network placed automatically by the calculus program having steps covering between 10 and maximum 25 mm on all directions, taking into consideration the stipulations of 5th chapter "The Building Modeling" from the EN ISO 10211-1:1995 norm. For an accurate evaluation of the heat losses in the room, the cutting planes were placed at about 1 meter in the interior of the room and about 50 centimeters in the opposite rooms.

Because of the limited space, in the paper is presented the thermal performance of one of the frequent solutions used in making the buildings in Romania. The solution is a full brick masonry wall of 36,5 cm thick, presented in two constructive solutions of realization (without window and with window), before and after thermal rehabilitation. The climatic conditions were considered the ones from the IIIrd climatic zone, were our city lies, which mean an exterior air temperature of -18°C.
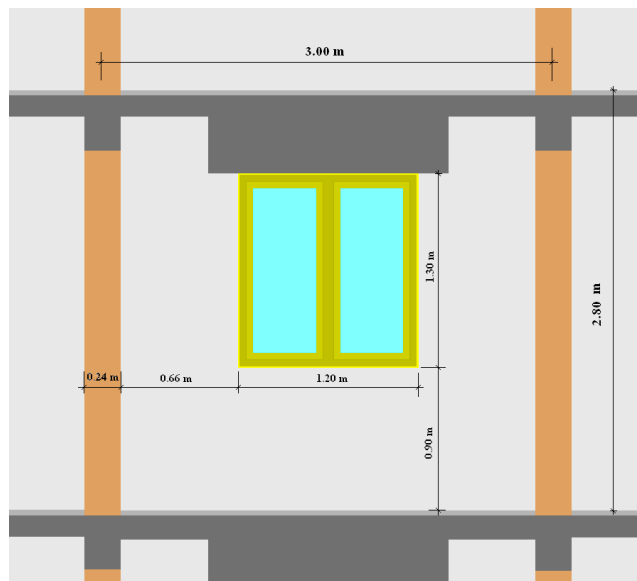
Figure 2. The geometric dimensions of the wall having a window

The analyzed element has the following geometrical dimensions:

- the thickness of the standard solid brick masonry is d=36.5 cm.
- the flooring thickness is 14 cm.
- the wall plaster layer is 1 cm thick inside and 2 cm thick outside.

- The additional thermal insulation on the external side of the wall was taken for four variants of thicknesses: 5 cm, 10 cm, 15 cm, 20 cm. Over the thermal insulation material a plaster of 5 mm reinforced with glass fiber net, was applied.

The opaque wall, having an interaxis dimension of 3 m and a height of 2,80 m, has a total surface of 8,40 m^2. For the variant of the wall having a window, the total surface of the wall is of 8,40 m^2, from which the opaque surface is of 6,89 m^2 and the surface of the window of 1,51 m^2. The dimensions of the window hole are 1,20 x 1,30. For this type of window placed in the hole with the named dimensions, using the calculus relation (1) from the Norm EN ISO 10077/1:2000, the thermal transmittance of the window will be U_{wn}=1,676 W/m^2K.

For the thermal characteristics of the glazing surface, the calculus thermal conductivities λ_c [W/(m·K)] and the normal emissivity coefficients of the surfaces ε_n of the materials used for making the window, were those in Annex D of Norm 10077/2:2003. The equivalent thermal conductivity λ_{ech} of the air from the cavities of the window framework, are determined by taking into consideration the thermal flow through conduction, convection and radiation, depending on the cavity geometry and of the emittance characteristics of the surfaces that delimitates it. For the non-ventilated cavities, few ventilated and ventilated the procedure from point 6 of the norm 10077/2:2003 was taken into consideration. The next values from the norm were taken into consideration: $U_{g,n}$=1.3 W/(m^2·K), $U_{f,n}$=1.36 W/(m^2·K), the bi-dimensional thermal coupling coefficient L^{2D}_n=0.481 W/(m·K) and the linear thermal transfer coefficient of the aluminum element of spacing ψ_n=0.084 W/(m·K)

The design heat conductivities of the building materials used for our study are as follows:

- standard solid brick masonry, of ρ = 1800 kg/m^3 and λ = 0.80 W/(m·K);

- cement and lime mortar plaster, of ρ = 1700 kg/m^3 and λ = 0.87 W/(m·K);

- reinforced concrete of ρ = 2500 kg/m^3 and λ = 2.00 W/(m·K);

- thermo-insulating material cellular polystyrene of ρ = 20 kg/m^3 and λ = 0.044 W/(m·K)

2.2. Analysis of the obtained results

The results obtained by using the calculus program, are presented under numerical and graphical form, respectively under isothermal shapes. The results were obtained from the study made on two constructive solutions of walls, respectively a full wall and the wall having a window.

In the case of the full wall, from comparing the obtained results in the four solutions of wall thermal insulating, with the results obtained in the case on non-

insulated wall, a decrease of the heat flow is observed, respectively of the thermal transmittance from 31%- for the case of 5 cm insulation, to 10 %- in the case of 20cm insulation.

Table 1. Numerical results for the opaque wall

Total for the element	The insulation degree				
	Non insulated	Insulated			
		5 cm	10 cm	15 cm	20 cm
Φ_o [W]	644.66	195.90	115.09	81.31	63.01
R_o [m^{2}K/W]	0.495	1.629	2.773	3.926	5.066
U_o [W/ m^{2}K]	2.019	0.614	0.361	0.255	0.197
%	100	30	18	13	10

For the wall having a window hole is observed that the distribution of the total heat flow from the wall between the opaque area and the glazing area for the opaque area, will decrease along with the increase of the protection degree from 82%- for the case of the non insulated wall to 20%- for the case of the insulated wall with 20 cm. For the glazing area the total heat flow rises from 18 % - in the case of the insulated wall up to 60 % - the case of the non insulated wall. The thermal transmittance will reduce along with the rise of the thermal insulation degree, form the insulated case with 5 cm up to the insulated case with 20 cm.

Comparing the values for the thermal transmittance of this type of window, determined based on the calculus relation from the norm 10077/ 1,2, with the values of the thermal transmittance determined based on the spatial calculus of the temperature field, differences are observed up to 41 % in the case of the non insulated wall, and of 28- 29% in the four variants of rehabilitation.

The calculus relations foreseen in the 10077/ 1,2 norm are not taking into consideration the areas with high thermal permeabilities of the window, represented by the punctual thermal bridges which are formed at the intersection of the linear thermal bridges, represented by frames and spacers at the corners of the window and at the contact between the sash and the frame of the window. This can be observed in the way the isothermal surfaces are arranged on the surface of the glass and on the surface of the window frame as seen in figure number 4, for the case of the insulated wall.

Table 2 . Numerical results for the wall having a window hole

		Non insulated	Insulated			
			5 cm	10 cm	15 cm	20 cm
The opaque area of the wall	Φ_o [W]	609.25	174.40	123.80	97.45	83.09
	Φ_o/Φ_{tot} [%]	82	58	50	44	40
	R_o [(m^{2}K)/W]	0.429	1.501	2.115	2.687	3.150
	U_o [W/ (m^{2}K)]	2.327	0.666	0.473	0.372	0.317
The glazing area	Φ_v/Φ_{tot} [W]	136.09	124.44	123.74	123.04	122.95
	%	18	42	49	56	60
	R_v [(m^{2}K)/W]	0.422	0.461	0.464	0.467	0.467
	U_w [W/(m^{2}K)]	2.370	2.168	2.155	2.144	2.142
	U_w/U_n [%]	1.41	1.29	1.29	1.28	1.28
Total for the element	Φ_T [W]	745.34	298.84	247.54	220.48	206.04
	%	100	100	100	100	100
	R_T [(m^{2}K)/W]	0.428	1.068	1.289	1.448	1.549
	U_T [W/ (m^{2}K)]	2.335	0.936	0.776	0.691	0.646
	%	100	40	33	30	28

Header note: the "Insulated" label spans the 5 cm, 10 cm, 15 cm, 20 cm columns, under the overall heading "The insulation degree".

If the results obtained for the full wall are compared with the results obtained for the wall having a window, a rise of the thermal transmittance is observed because

of the presence of the window, with 16% for the case of non insulated wall and 228% for the case of insulated wall with 20 cm (table 3).

Table 3 . Comparative numerical results for the full wall- wall having a window hole

Total for the element	The insulation degree				
	Non insulated	Insulated			
		5 cm	10 cm	15 cm	20 cm
U_o [W/(m^2K)]	2.019	0.614	0.361	0.255	0.197
U_T [W/ (m^2K)]	2.335	0.936	0.776	0.691	0.646
$(U_T- U_0)/ U_0$ [%]	16	52	115	171	228
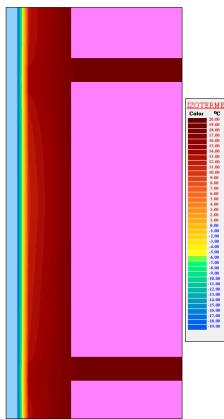
a.) vertical section - full wall   b.) vertical section through the window
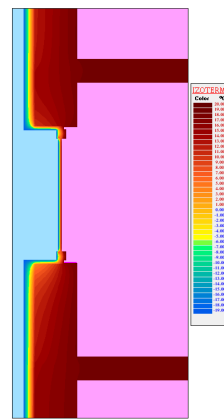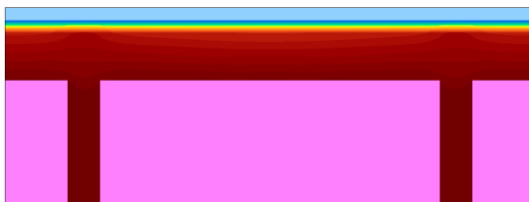
c.) horizontal section - full wall   d.) horizontal section through the window
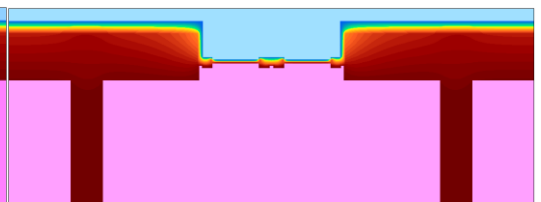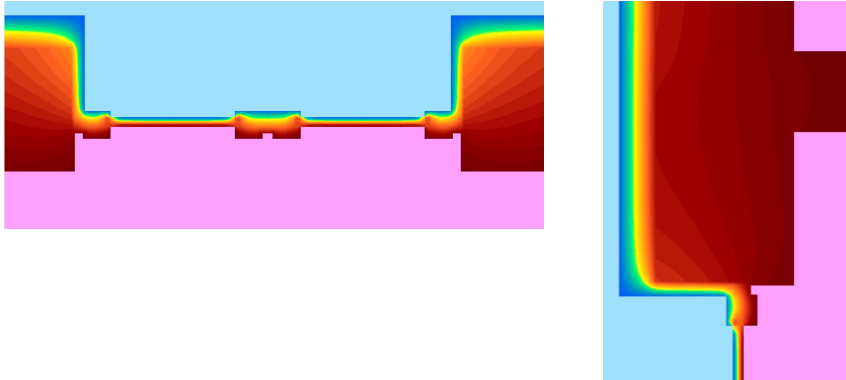
e.) detail for the glazing area in horizontal and vertical section

Figure 3. Graphical results (isothermal curves)
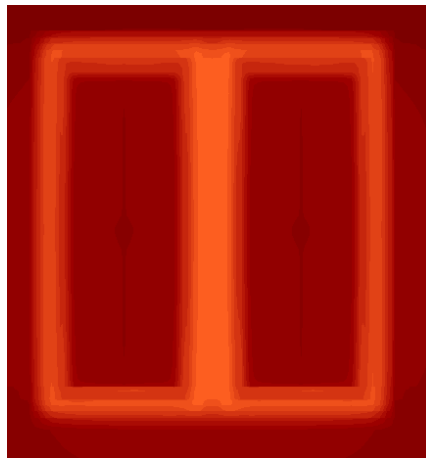
Figure 4. The disposal of the isothermal curves on the frame and the surface of the window glass

3. CONCLUSIONS

From the researches made by our research collective and from the results presented in the paper, the minimum thickness for the thermal insulation for the buildings placed in Romania is of 10 cm thick, equivalent for polystyrene. If the aim is to place the buildings in a superior energetic class, the thickness of the thermal

insulation layer has to be of minimum 15 cm thick, equivalent for polystyrene, thickness of the thermal insulation layer that started to be used in the current practice of thermal rehabilitation of the existing buildings in our town.

Figure 5. Building from Cluj- Napoca town in the process of rehabilitation with 15 cm of polystyrene EPS

The calculus program is useful for the accurate evaluation of the heat losses through the elements of the building envelope, for the accurate determination of the necessary heat for the building and for the correct dimensioning of the installations for heating and ventilating a building. The calculus program "CIMPSPAT" represents a valuable instrument for establishing the energetic performances of the envelope elements for the existing buildings in real conditions of exploitation and for designing new types of elements for the building envelope with direct and favorable effects on energy economics in building exploitation and for reducing the pollution emissions in the atmosphere.

The program is easy to use because of its libraries, offering accurate results in a useful time.

References

1. EN ISO 13789-99 *Thermal performance of buildings – Specific transmission heat loss – Calculation method.*
2. SR EN ISO 10211/1-98 *Thermal bridges in constructions – Heat flows and surface temperatures – Part 1: General calculation methods.*
3. EN ISO 10077-2:2003 *Thermal performance of windows doors and shutters- Calculation of thermal transmittance- Part 2: General method.*

4. DIRECTIVE 2002/91/CE DU PARLEMENT EUROPÉEN ET DU CONSEIL du 16 décembre 2002 sur la performance énergétique des bâtiments / The Directive 2002/91/EC of the European Parliament and of the Council of 16 December 2002 on the energy performance of the buildings.

5. Moga, L.and Moga, I. (2008): *Applications of the Calculus Program "Spatial Glazing" for Windows*, Nordic Symposium on Building Physics NSB 2008, Technical University of Denmark, Copenhagen 16- 18 June 2008, pp.87- 95.

6. Moga, L.and Moga, I. (2008): *Simulation of the Spatial Thermal Transfer through Windows- Spatial Thermal Transfer Coefficient Calculus-* (Extended Abstract), BauSIM 2008, Universitat Kassel, Germany- Kassel 8- 10 September 2008.

7. Andreica, H.-A.and Moga, L. 2008 : *The economic and ecological consequences of the thermal protection degree of building,* The International Conference "CONSTRUCTII 2008", Faculty of Civil Constructions, Technical University of Cluj- Napoca, 9- 10 May 2008

The Influence of Local Damage upon the Behavior of Reinforced Concrete Frame Structures

Oana Mihaela Ioniţă[1], Mihai Budescu[2], Nicolae Ţăranu[3], Silvia Rominu[4], George Ţăranu[5], Cătălin Banu[6]

[1]*Department of Civil and Industrial Engineering, "Gh. Asachi" T.U. from Iasi, Iasi, 700050, Romania*
[2]*Department of Structural Mechanics, "Gh. Asachi" T.U. from Iasi, Iasi, 700050, Romania*
[3]*Department of Civil and Industrial Engineering, "Gh. Asachi" T.U. from Iasi, Iasi, 700050, Romania*
[4]*Department of Civil Engineering, University "Politehnica", Timisoara, 300223, Romania*
[5]*Department of Structural Mechanics, "Gh. Asachi" T.U. from Iasi, Iasi, 700050, Romania*
[6]*Department of Civil and Industrial Engineering, "Gh. Asachi" T.U. from Iasi, Iasi, 700050, Romania*

Summary

Improvements in structural analysis and knowledge of materials over the last decades have led engineers to build structures that are structurally more efficient than in the past. This leads increasingly to extending the constituent materials to the limit of their operational envelope. The result is that modern structures don't have the strength reserve that was inherent in older structures engineered by empirical knowledge and instinct, and hence attention must be given for the way in which they will perform when subjected to abnormal loads.

From an analytical point of view, a progressive collapse is a structural failure that is initiated by localized structural damage and subsequently develops, as a chain reaction, into a failure that involves a major portion of the structural system. The residual structure is forced to seek alternative load paths in order to redistribute the load applied to it. As a result, other elements may fail causing further load redistribution. This process might continue until the structure can find equilibrium by finding stable alternative load paths.

The subject of this paper is the numerical analysis of reinforced concrete frame structures and the damage assessment of partially collapsed structures.

KEYWORDS: abnormal loads, robustness of structures, damage assessment, disproportionate failure, progressive collapse.

1. INTRODUCTION

Providing safety of a structure is one of the main aims of design. In traditional design it is achieved by designing structural components against specified limit states. However, as showed the Ronan Point collapse in UK in 1968, when a gas explosion in one of flats on the 18-th floor of a 22-

storey residential building caused the failure of an entire section of the building [1], this approach is not sufficient. The approach does not exclude the risk of local damage to a structure due to accidental events (e.g., gas or bomb explosion, vehicle impact, gross errors in design, construction or utilization) that can occur during service life of the structure. While probability of occurrence of such events for ordinary structures is low [2], and therefore, they are not considered explicitly in design, their effect on structural safety becomes significant if the structure is not robust, that is when some local damage can trigger a chain reaction of failures causing collapse of the whole structure or of a major part of it, the so called progressive collapse.

The 1995 bombing of the Alfred P. Murrah Federal Building in Oklahoma City, the bombing of the US Embassies in Nairobi and Dar-Es-Salaam in 1998, and the collapse of the World Trade Center Towers in New York and a portion of the Pentagon in Washington due to the terrorist attack on September 11, 2001, drew renewed attention to the problem of reducing the risk of progressive collapse. Current efforts are aimed at the development of explicit design methods for reducing the potential of progressive collapse for new and existing structures [3].

It is recognized that different structures should possess different levels of robustness, which depend on their occupancy, type and size, exposure and other characteristics. Therefore, another new development is to categorize structures, which would require different levels of robustness, using a risk and consequence approach [4]. In this context, reliability analysis of undamaged and/or damaged structures is necessary, which would require probabilistic models of normal and accidental loads and materials properties under static and dynamic conditions [5].

2. ROBUSTNESS OF STRUCTURES

Robustness is a property, the description of which varies so much with context that it is difficult to put order into its manifold aspects, relationships and ramifications.

Robustness is the property of systems that enables them to survive unforeseen or unusual circumstances without undue damage or loss of function. It has become a requirement expressed in modern building codes, mostly without much advice as to how it can be achieved. Engineering has developed some approaches based on traditional practice as well as recent insight. However, knowledge about robustness remains scattered and ambiguous, making it difficult to apply to many specific

cases. Robustness provides a measure of structural safety beyond traditional codified design rules.

The design of a system, being it natural or an artificial one, is typically oriented towards normal use, more precisely towards circumstances which must or can be anticipated to exist during the intended working life of the system. Limiting the design to this may however leave it vulnerable to the effects of events that were not included in the set of anticipated circumstances. These effects can be of very diverse character and may be related to the features that were anticipated in the design but for an unanticipated intensity, or that may not be of a description altogether foreign to the design circumstances [6].

Related to the life span of a building, robustness can represent the preserving of the integrity of the component elements properties, starting with the framing system (which also includes the infrastructure), closings, finishes and ending with the installations.

Robustness must not be understood as an over dimensioning of the elements but as the capacity of the system of adapting without damages to current actions and with minimum shortcomings to the extraordinary ones.

If we refer to the framing system of a building, the robustness has to provide it with the capacity of keeping its integrity to current actions and to not reach collapse in the case of extraordinary actions. When the extraordinary action is the seismic load, robustness must also include the dissipating capacity of the induced energy by ductility, through the capacity of the structural system to form plastic hinges in sensed zones even from the design phase. This means the capacity of the structure of accommodating to an unfavorable situation.

In order to say something rational and consistent on the property of robustness, some basic concepts must be described and clarified as far as possible – although a strict definition in the sense of a reduction onto other, well-known concepts may just be out of reach. One of the concepts foremost in need of this clarification relates to the issue of progressive collapse [6].

3. TYPICAL ASPECTS OF A ROBUSTNESS ASSESSMENT

A robustness assessment involves the following aspects:
- A *system* must be identified and clearly defined.
- *Specific system objectives* must be identified: system robustness relates to certain desirable system objectives (features, characteristics or properties).
- Specific *disturbances* such as hazards, internal or external influences, abnormal, deliberate or unexpected circumstances, or any other trigger events must be identified.

- *Robustness analysis:* this analysis focuses on the overall effect (consequences) of the specific disturbances (Step 3) as they affect the system objectives (Step 2).
- *Persistence:* any measures or indicators of robustness used to rank system robustness must be such that they assign high "marks" to:
  - the persistence of the system objectives subject to the specific disturbances, or;
  - a low and acceptable effect on the system objectives as a result of the disturbances.

The above process can be applied to any system (and its identified features) and to specific disturbances when none of these are subject to uncertainty. The robustness analyses are in fact entirely deterministic. However, in structural applications, the system, the system response, the cause-effect relationships, the hazards and the consequences are usually subject to considerable uncertainty. Therefore it is necessary to consider an additional element in the vulnerability assessment:

- *Risk*: the assessment of robustness must account for all uncertainties associated with system assumptions (Step 1), system objectives (Step 2), the occurrence of disturbances or hazards (Step 3), and model uncertainties involved in the system consequence analysis (Step 4) [7].
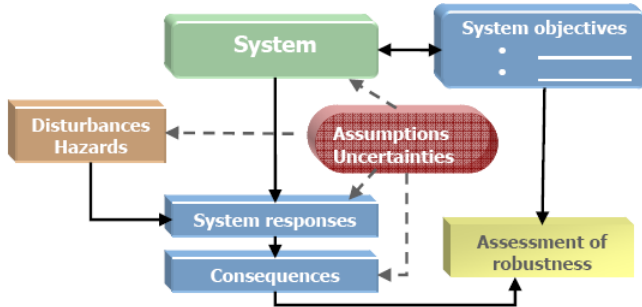
Figure 1. Schematic of the process of assessing robustness [7]

4. PROGRESSIVE COLLAPSE

A progressive collapse is a catastrophic partial or total structural failure that ensues from an event that causes local structural damage that cannot be absorbed by the inherent continuity and ductility of the structural system. The residual structure is forced to seek alternative load paths in order to redistribute the loads applied to it. As a result other elements may fail causing further load redistribution. Therefore, a local damage or failure initiates a chain reaction of failures that propagates vertically or horizontally through the structural system, leading to an extensive

partial or total collapse. While virtually all structural collapses initiate from local as opposed to system-wide damage (earthquakes being a possible exception), it is generally agreed that the key feature distinguishing progressive collapse is that the resulting damage is disproportionate to the local damage caused by the initiating event. Such collapses can be initiated by many causes, including abnormal loads not normally considered in design (e.g., gas explosions, vehicular collisions, and sabotage), severe fires, extreme environmental effects that stress the building system well beyond the design envelope, human errors in design and construction, and misuse. All buildings are susceptible to progressive collapse in varying degrees [8, 9]. Continuous, highly redundant structures with ductility tend to absorb local damage well. Other systems, such as large panel or bearing wall systems, pre-cast concrete slabs or steel joist floors supported on masonry walls, and any building system that is well tied but lacks ductility are inherently more vulnerable because of the difficulties in providing continuity and ductility in such systems.

Specific design approaches to prevent progressive collapse as a result of abnormal loads have not been standardized. There are a number of reference papers on the subject and some studies leading to techniques that can be employed economically for certain construction types. However, building codes and standards that address the issue invariably treat general structural integrity and progressive collapse in qualitative rather than quantitative terms. This is due, in part, to the elusive nature of the definition of general structural integrity and the countless ways by which resistance to progressive collapse can be achieved. Moreover, the lack of quantitative provisions results from the difficulty that the engineering profession has encountered in defining specific events or initial conditions for which progressive collapse resistance should be considered, or the tolerable damage state of a building system that has restrained a progressive collapse successfully. Finally, there is the question of what is acceptable risk? No building system can be engineered and constructed to be absolutely risk-free in the presence of numerous sources of uncertainties that arise in the building process or from potential failure-initiating events. Building codes and standards provide tools for structural engineers to manage risk in the public interest. Of course, code provisions address the risks in building performance as the code and standard-writers have understood and confronted them at particular points in time. The renewed interest in abnormal loads, progressive collapse, and the associated hazards and risks is now taking place in a context that is very different from that historical understanding. Provisions for progressive collapse-resistant design have yet to be identified in terms of either performance level or risk [2].

5. CASE STUDY

In this first phase of the research activity there have been studied five different reinforced concrete frame structures, namely: a planar frame with two spans and four spatial frames having also two spans, but different number of bays (one bay, two bays, three bays and four bays). All the structures have four storeys above the ground level, each 3.00m high. The load bearing system of the structures consists of reinforced concrete columns and beams. The characteristic strength of the concrete is 20MPa. The load applied to the structures was a dead load of $10kN/m^2$.

First, the planar frame structure has been modeled and the structural static analysis has been carried out using the Autodesk Robot Structural Analysis 2010 system. Then, starting from this model the spatial frame structures were modeled by adding progressively one bay.

In Figure 2 are shown the planar frame structure and three of the spatial frame structures with one bay, two bays and with four bays.

a.   c.
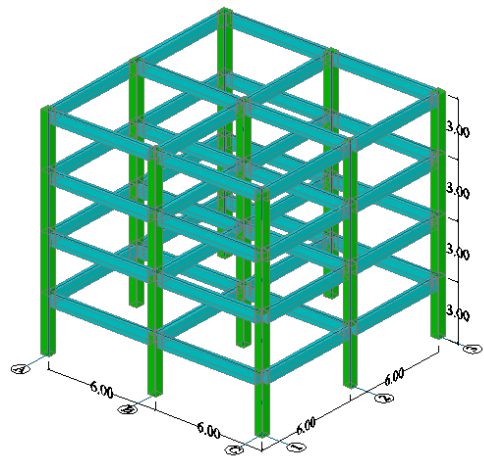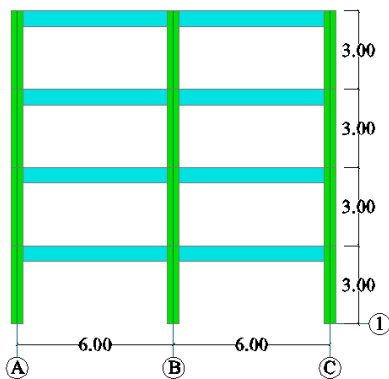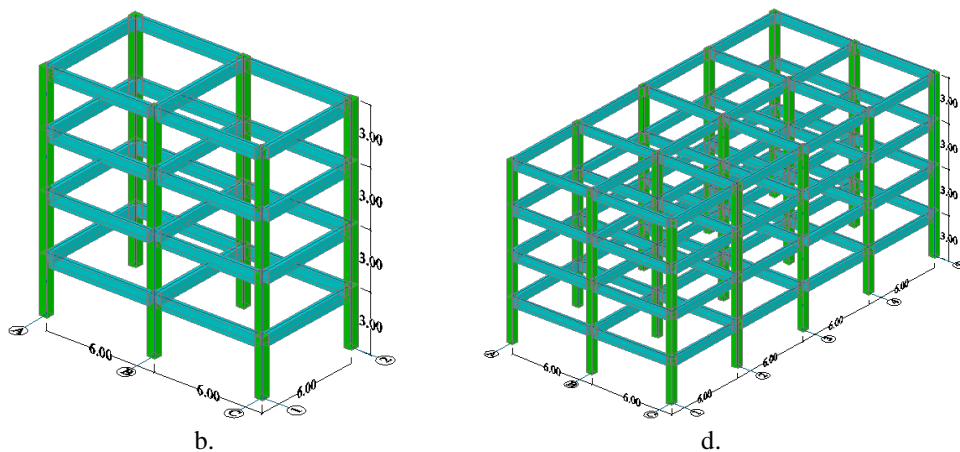
Figure 2. Studied frame structures. (a) Planar frame, (b) Spatial frame with one bay,
(c) Spatial frame with two bays, (d) Spatial frame with four bays

The aim of the analysis was to simulate the local damage of the central column from the first floor of the structures due to an impact loading and then to evaluate the damage state of the structures. It has to be noted that the central column from the first floor wasn't totally removed from the structures. Instead of this, the stiffness of the column was progressively reduced from 100% to 10%.

At each step of stiffness reduction the evolution of the bending moments of the beams along the axis no.1 and of the axial force in the central column from the intersection of the axis no.1 with "B" axis on each floor were recorded. The main interest was to evaluate the compound spatial effect between the initial transversal frame and the longitudinal structural elements progressively added to the structure.

The influence of the local damage from the first floor of the structure upon the load bearing elements from the upper floors was also evaluated. The values of the bending moments and of the axial forces were related to the values obtained at the first step of the analysis and the following diagrams were obtained.

In these diagrams M_A and M_B represent the values of the bending moment evaluated at the end sections of the beams and N_{max} represent the maximum value of the axial force at the bottom of the central columns from "B" axis. The numerical indexes refer to the considered storey and the index "c" refers to the value of the effort at the current step of the analysis.
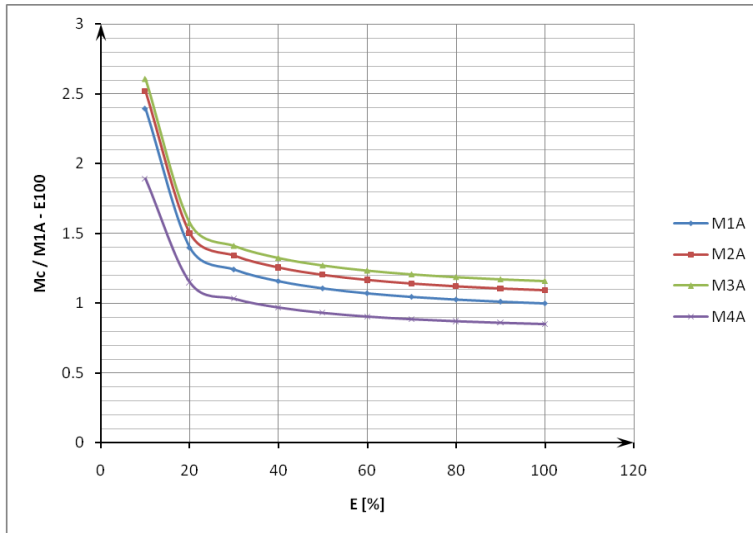
Figure 3. Bending moments M_A on each storey of the planar frame structure
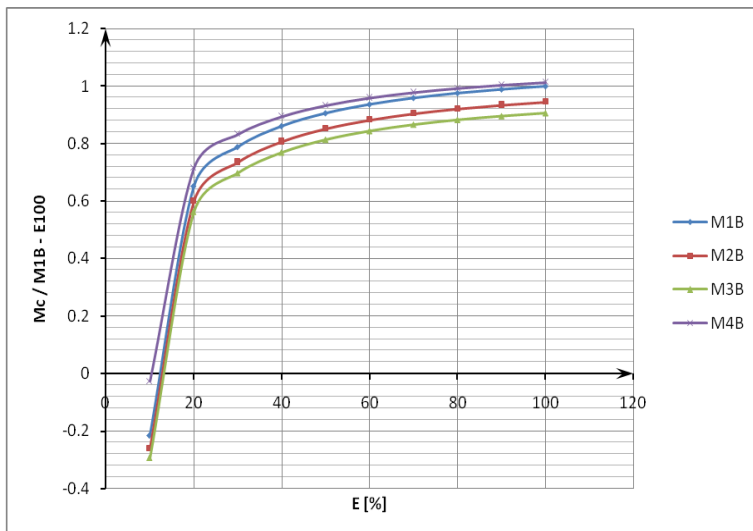
Figure 4. Bending moments M_B on each storey of the planar frame structure
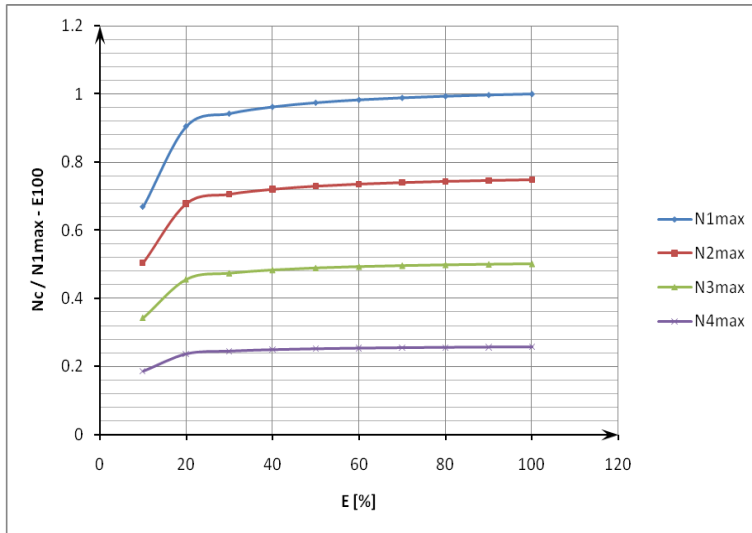
Figure 5. Axial force N_{max} on each storey of the planar frame structure
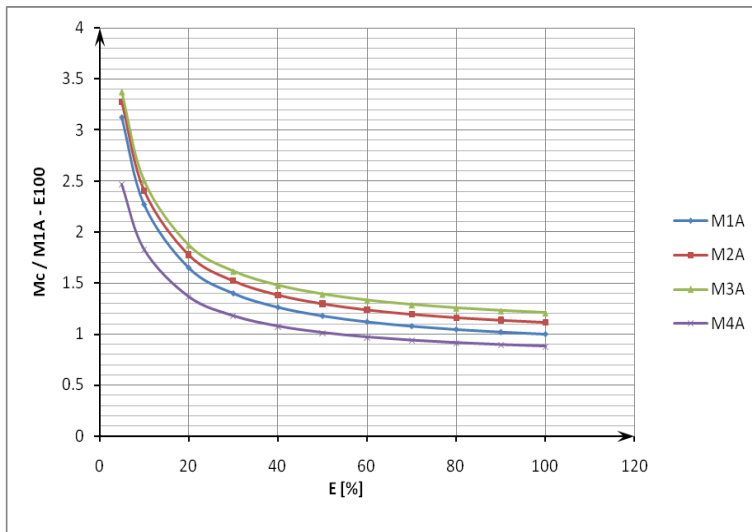
Figure 6. Bending moments M_A on each storey of the spatial frame structure with two bays
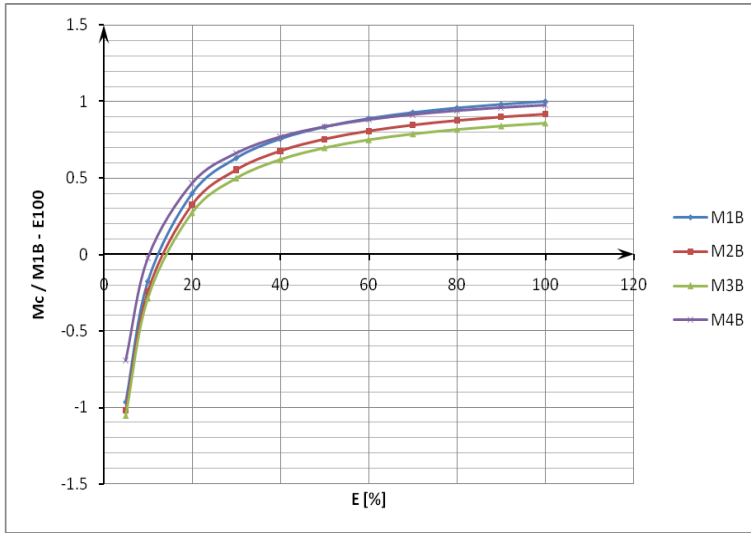
Figure 7. Bending moments M_B on each storey of the spatial frame structure with two bays
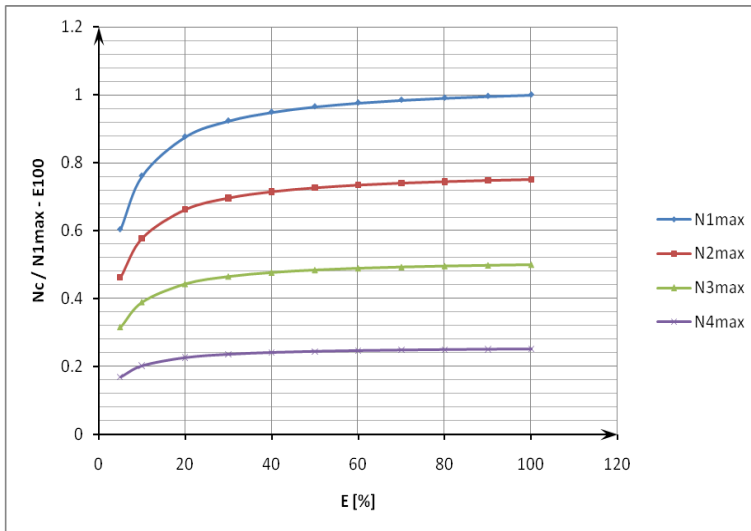
Figure 8. Axial force N_{max} on each storey of the spatial frame structure with two bays

As it can be seen from the previous diagrams, the structural elements from the upper floors are affected in the same proportion, the effort curves developed for each storey having almost the same shape. An inflection point in the evolution of the efforts appears in the case of planar frame structure when the stiffness of the

central column is reduced at 30% and in the case of spatial frame structure it appears when the stiffness is reduced at 20%.

Both in the case of planar frame structure and in the case of spatial frame structures, when the stiffness of the central column is reduced to 10%, the absolute values of bending moment on the beams, M_A, increase suddenly and the bending moment, M_B, becomes positive.

In order to relieve more precisely the influence of the spatial effect upon the evolution of the efforts from the structure, the following diagrams have been drawn. The efforts evaluated in the case of planar frame structure were compared with those resulted in the case of spatial frame structures. As it can be seen from the following three figures, the behavior of the frame structure is improved when the longitudinal frames are added.

Based on these results, one may conclude that the analysis of the planar frame structures is not as precise and relevant for the real situation as the analysis of the spatial frame structures. Only the analysis of the planar frame structures has to be avoided and the compound effect of the spatial frame structures has to be taken into account.
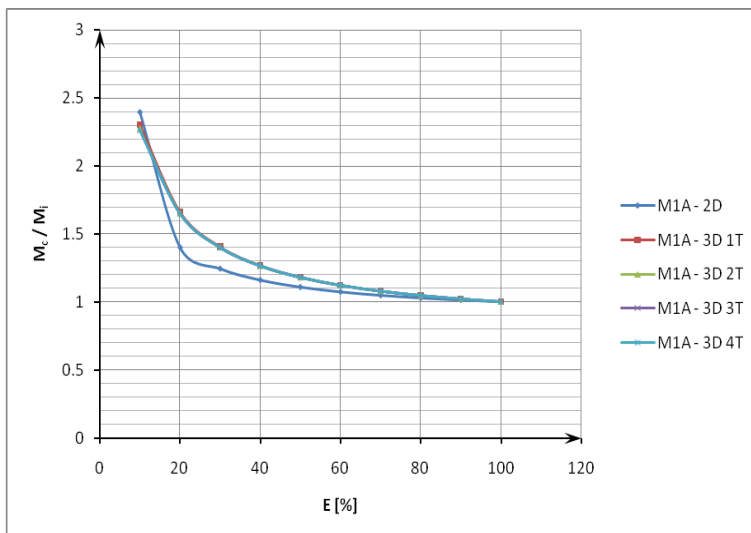
Figure 9. Bending moments (M_A) on the beams from the first floor
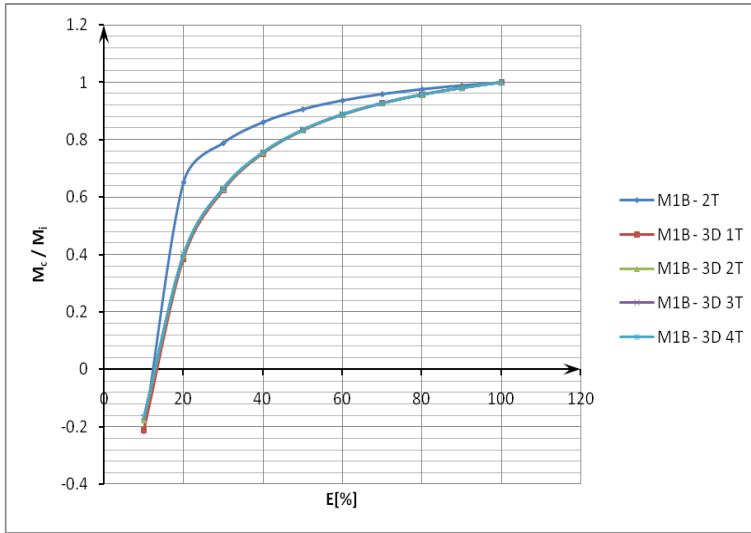
Figure 10. Bending moments (M_B) on the beams from the first floor
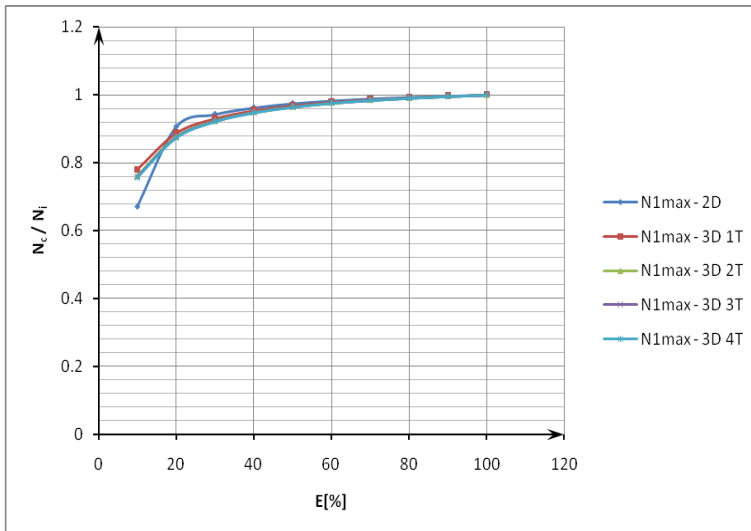
Figure 11. Axial force (N_{max}) in the columns from the first floor

6. CONCLUSIONS

The prediction of possible progressive collapse under specific conditions may provide very important information that could be used to control or prevent progressive collapse. It is now clear that abnormal loadings must be taken into account when designing structures. Abnormal load events could arise from a

number of sources: gas explosion, confined dust or vapor conflagration, machine malfunction, high explosive effects, missile impact etc. However, to date, no adequate tools exist that can perform a progressive collapse analysis with acceptable reliability. Therefore, in the design phase, it is very important to predict the behavior of possible progressive collapse, as accurately as possible, for the various abnormal loads that should be considered.

One should be able to define a desired stable state of a partially damaged or partially collapsed structure for various abnormal loads and local damage combinations. Such collapsed cases and the damage evolution rate should be determined. Since the building after a partial collapse might be still exposed to a next phase of collapse, the residual capacity of a partially collapsed structure will determine its robustness, accordingly. A damaged or partially collapsed structure could be very dangerous without enough information about its expected behavior. The rapid prediction of future behavior, or the next phase of collapse, can increase the safety of both the occupants and rescue personnel.

Considering the results obtained from the present research work, it has to be mentioned the importance of spatial analysis of the structures. Compared to the behavior of the planar frame structure, the behavior of the spatial frame structures was significantly improved. But the number of bays didn't have such a significant influence since the evolution of the efforts in the axis no.1 is almost identical in the four studied cases of spatial frame structures.

It has to be noted that a stiffness reduction under 20% leads to the collapse of the structures.

For some specific types of buildings to which exists the risk of producing local damages it is necessary to assume some scenarios regarding the progressive collapse taking into consideration the necessary local measures for the preventing of global collapse.

The influence of local damage is diminished on the vertical direction with each new level added to the structure, the supplementary levels having a positive effect upon its behavior.

References

1. Griffiths, H., Pugsley, A., Saunders, O., *Report of the Inquiry into the Collapse of Flats at Ronan Point, Canning Town*, Her Majesty's Stationery Office, London, 1968.
2. Ellingwood, B.R., *Load and Resistance Factor Criteria for Progressive Collapse Design*, National Workshop on Prevention of Progressive Collapse in Rosemont, III, Multihazard Mitigation Council of the National Institute of Building Sciences, Washington, D.C, 2002.
3. Val, D.V., Val, E.G., *Robustness of Frame Structures*, IABSE, Structural Engineering International (SEI), vol. 16(2), 2006.
4. Moore, D.B., *The UK and European Regulations for Accidental Actions*, National Workshop on Prevention of Progressive Collapse in Rosemont, III, Multihazard Mitigation Council of the National Institute of Building Sciences, Washington, D.C., 2002.

5. Ellingwood, B.R., Dusenberry, D.O., *Building Design for Abnormal Loads and Progressive Collapse*, Computer-Aided Civil and Infrastructure Engineering 20, 2005.
6. Knoll, F., Vogel, T., *Design for Robustness*, IABSE, Structural Engineering Documents 11, ISBN 978-3-85748-120-8, ETH Zurich, CH-8093 Zurich, Switzerland, 2009.
7. Maes, M.A., Fritzsons, K.E., Glowienka, S., *Risk-based Indicators of Structural System Robustness*, JCSS and IABSE Workshop on Robustness of Structures, ISBN 3-9522686-8-2, BRE, Garston, Watford, UK, 2005.
8. Taylor, D. A., Progressive collapse, *Canadian Journal of Civil Engineering*, vol. 2(4), 1975.
9. Ellingwood, B., Leyendecker, E. V., Approaches for design against progressive collapse, *Journal of the Structural Division*, ASCE, vol. 104, no. 3, 1978.

FEM analysis of masonry-FRP interface

George Taranu[1], Mihai Budescu[1] and Nicolae Taranu[2]

[1]*Department of Structural Mechanics, Faculty of Civil Engineering and Installations, Technical University "Gh. Asachi", Iaşi, 70050, Romania*
[2]*Department of Civil and Industrial Engineering, Faculty of Civil Engineering and Installations, Technical University "Gh. Asachi", Iaşi, 70050, Romania*

Summary

The use of numerical methods for the analysis of masonry structures has been extremely limited due to the large number of influence factors. Due to the high complexity of masonry behaviour, the approach towards the numerical simulation of its structural behaviour has led researchers to develop several constitutive models characterized by different levels of complexity.

In order to solve a given structural problem, several idealizations of material behaviour can be established, each of them being necessarily associated with different degrees of complexity. When dealing with masonry structures, the most common idealizations of material behaviour are elastic behaviour, plastic behaviour and non- linear behaviour.

The aim of this paper is formulation of a numerical simulation hypothesis to study the effect of interface model between Fibre Reinforced Polymer (FRP) and masonry. The hypothesis consists in assigning different stiffness values for the mortar joints. These values simulate the degradations which occur in mortar joints. These lead in obtaining a real structural behaviour. The non linear analysis with finite element method will be used in micro-modelling of a strengthened masonry beam with GFRP at the intrados subjected to vertical load acting in the middle span.

KEYWORDS: non linear analysis, FEM, FRP strengthened masonry beam, micro-modelling interface

1. INTRODUCTION

The numerical modelling of masonry structures through the FEM is a very computationally demanding task because of two different aspects: on the one hand the typological characteristics of masonry buildings do not allow us to refer to

simplified static schemes, on the other hand the mechanical properties of the material lead to a widely non-linear behaviour whose prediction can be very tricky. The calibration of numerical models depends by complete characterization of the material possible after some experiments.

Masonry structures are made of blocks connected by mortar joints. Due to this intrinsic geometrical complexity, which is obviously reflected in the computational effort needed, it is necessary to assume a properly homogenised material and perform the analyses through the finite element method (FEM), when the global behaviour of an entire structure is investigated. On the contrary, when a single structural element is being studied, the actual distribution of blocks and joints can be accounted for [1]. In the next chapters an analysis of a masonry arch in micro-modelling will be presented.

2. THE DIFFERENT MODELLING APROACHES FOR MASONRY

2.1. Theories and methods for modelling masonry

In order to solve a given structural problem, several idealizations of material behaviour can be established, each of them being necessarily associated with different degrees of complexity. Naturally, different types of constitutive models (i.e. different descriptions of the material behaviour, associated with different idealizations of the geometry, such as two- or three-dimensional description), originate a sequence, or hierarchy, of models, which allow the analysis to include more complex response effects as well as more costly solutions.

When dealing with masonry structures, the most common idealizations of material behaviour are elastic behaviour, plastic behaviour and non- linear behaviour. These different idealizations are schematically represented in Figure 1, where each idealization is represented by a typical general load-displacement diagram [2].

By adopting a non- linear analysis instead of a linear analysis, a more comprehensive insight into the structural response can be obtained, with a higher cost, both in terms of necessary input data and required knowledge of the analyst. In the following, a brief description concerning the three idealizations referred to above is given and the most relevant issues are discussed.

2.2.1. Linear elastic behaviour
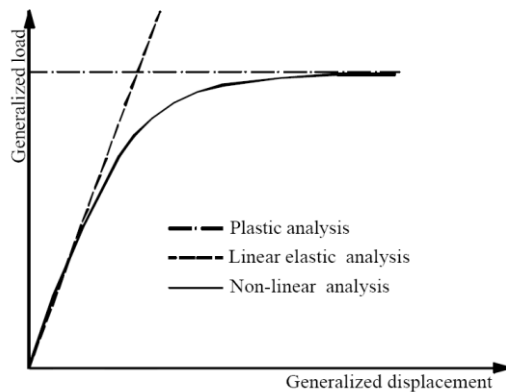
Figure 1. General load-displacement diagrams of a structural analysis.

The linear elastic analysis is the procedure usually followed in structural analysis, where the material is considered to exhibit an infinite linear elastic behaviour, both in compression and tension.

In the case of masonry structures, where joints possess relatively low tensile strength, or even no-tensile strength in the case of dry joints, cracks arise at low stress levels and, therefore, the assumption of elastic behaviour is quite debatable.

In general, linear elastic analyses are not appropriate for ancient constructions [3]. However, in a first stage of analysis, the hypothesis of linear elastic behaviour can be of great help to the analyst. Linear analysis requires little input data, being less demanding, in terms of computer resources and engineering time used, when compared with non-linear methods. Moreover, for materials with tensile strength, linear analysis can provide a reasonable description of the process leading to the crack pattern.

2.2.2 Plastic behaviour

Plastic analysis, or limit analysis, is concerned with the evaluation of the maximum load that a structure can sustain (limit load). The assumption of plastic behaviour implies that, on one hand, the maximum load is obtained at failure and, on the other hand, the material should possess a ductile behaviour. Apparently, this last requirement seems to be unrealizable since the plastic deformations may exceed the ductility of the masonry. However, the limited ductility în compression does not play a relevant role as collapses, except in the case of columns, are generally related to the low tensile strength [3]. Thus, the assumption of a zero tensile strength renders the method of plastic analysis as adequate for the analysis of masonry structures.

The limit analysis theory is an analytical approach aiming to determine the value of the limit multiplier (LM) to be applied to a given load case in order to cause the failure of a structure, considering a rigid-perfectly plastic behaviour. It was initially developed to study the plastic behaviour of steel structures. The application to masonry structures has been initiated by Drucker and Kooharian. [4], [5], [6].

To be helpful in the framework of masonry structures, the limit analysis theory is based on three fundamental assumptions:

- the compressive strength of the constitutive material is supposed to be infinite. In the reality, the commonly used building materials are strong enough to avoid the occurrence of crushing as failure mode.
- the tensile strength of the constitutive material is supposed to be zero. In the reality, the commonly used building materials present some (limited) tensile strength but the joints between the blocks constitute weak planes: the global tensile strength is then based on the negligible value of mortar bond.
- the sliding between blocks along an interface is supposed to be impossible. In the reality, such sliding appears sometimes but seldom observed: the joint inclination is usually correctly chosen with regard to the orientation of the resultant force.

2.2.3 Non-linear behaviour

Non-linear analysis is the most powerful method of analysis, the only one able to trace the complete structural response of a structure from the elastic range, through cracking and crushing, up to failure. The existence of mortar or dry joints, generally the weakest link in a masonry assemblage and characterized by a marked non- linear behaviour, induces a nonlinear response on masonry structures, even for moderate loads, e.g. serviceability loads. Therefore, non-linear behaviour, being the most complete method of numerical analysis, appears as the most adequate approach to be used in numerical simulations of masonry structures. Its use depends on which objectives are required from the analysis. If the sought information can be attained using a simpler method, which turns out to be less expensive or more in agreement with the expertise of the analyst, then its use is advised.

Several non-linear constitutive models have been developed for the analysis of masonry structures. The most popular theories used to formulate consistent constitutive models are plasticity and continuum damage mechanics, generally based on a phenomenological approach, i.e. the constitutive model is directly based on the observed features from experimental tests.

The first approach addressed here is the theory of plasticity. The first scientific work concerning plasticity goes back to Tresca's memoir in 1864 on the maximum shear stress criterion, [9]. Basically, the plasticity theory attempts to replicate the dislocations of the material, being the plastic material behaviour characterized by

the occurrence of permanent deformations. Initially developed for ductile materials, nowadays plasticity is extensively used for other materials such as soils, concrete and masonry. A number of non-linear models based on the plasticity theory aiming at the study of masonry structures have been developed in recent years, both for continuum and discontinuum approaches [10], [11], [12], [13], [14].

3. FEM ANALYSIS OF A STRENGTHENED MASONRY BEAM

3.1 Model parameters

The model proposed to be analyzed is composed by common brick 240x115x60mm and 10 mm mortar joint. The section outcome has 115 x 240 mm. The span of the beam is 600 mm. The constitutive model is presented in figure 2. The program used to calculate the model was ANSYS WORKBENCH Multiphysics. Brick and mortar was considered solids and their properties are defined in table 1. A vertical load in the middle of the span was applied. Both supports are hinged.
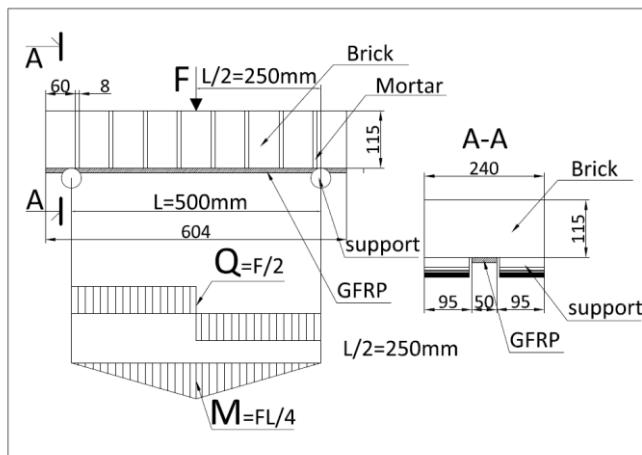
Figure 2. Loading schema of the model analyzed

3.2 Material parameters

All structural material properties were considered linear elastic. Different values of Young's Modulus were given to mortar between 10000 MPa and 1000 MPa.

Table 1. Model materials properties

Material	Young's modulus (MPa)	Poisson's ratio	Density (kg/m³)	Tensile ultimate strength (MPa)	Compressive ultimate strength (MPa)
GFRP	77000	0.28	2600	1500	-
Brick	18000	0.20	1900	-	20
Mortar 1	10000	0.18	2100	-	8
Mortar 2	9000	0.18	2100	-	8
Mortar 3	8000	0.18	2100	-	8
Mortar 4	7000	0.18	2100	-	8
Mortar 5	6000	0.18	2100	-	8
Mortar 6	5000	0.18	2100	-	8
Mortar 7	4000	0.18	2100	-	8
Mortar 8	3000	0.18	2100	-	8
Mortar 9	2000	0.18	2100	-	8
Mortar 10	1000	0.18	2100	-	8
Mortar 11	500	0.18	2100	-	8

3.3 Model geometry and mesh definition

All mortar joint and all brick was defined by solid element which was sketch in Autocad. The sketch was exported with an Acis extension file so that make possible import in ANSYS Design Modeler. After the file was imported material properties was assigned to each solid, and an appropriate mesh method was choose. The model has 25 solid parts, 18687 finite elements and 99554 nodes. These steps are illustrated in figure 3.

(a)   (b)
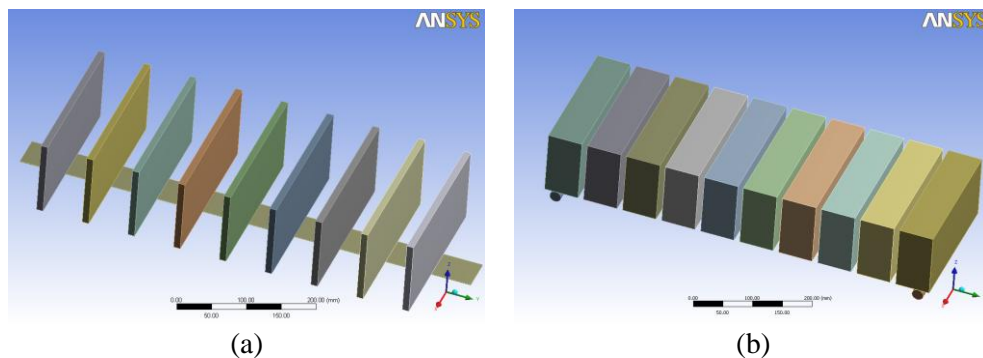
Figure 3. Geometrical models of a) – mortar joints and GFRP strip; b) – bricks

The force applied had 60 kN and was kept constant at each step of E modulus. The duration of each analysis was approximately 20 minutes. After each analysis the material properties of mortar was changed.

(a) (b)
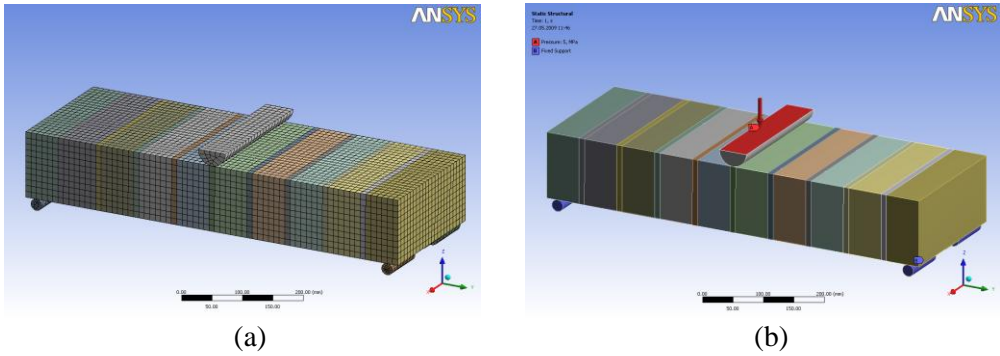
Figure 4. Structural environment analysis: a) –brick type mesh definition; b) – loading schema

3.4 Analysis results

(a) (b)
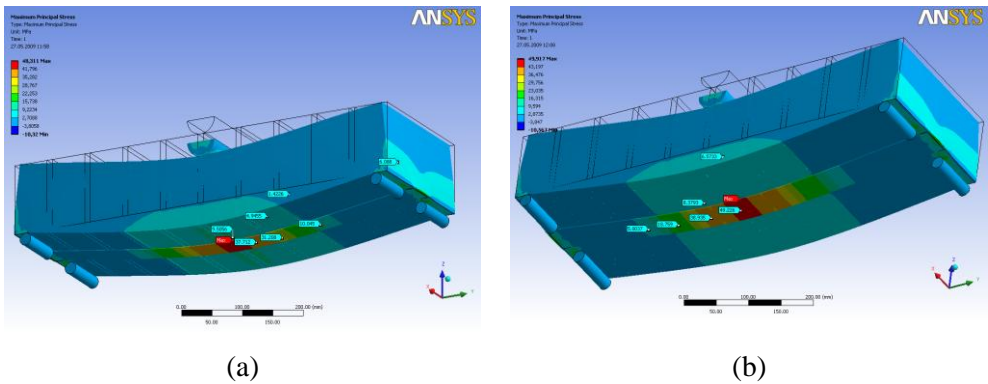
Figure 5. Maximum principal stress: a) – Mortar 1; b) –Mortar 2

(a) (b)
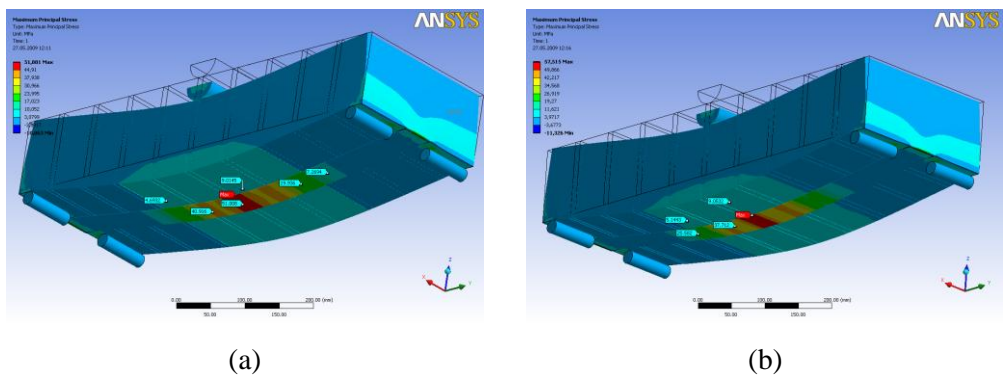
Figure 6. Maximum principal stress: a) – Mortar 3; b) –Mortar 5
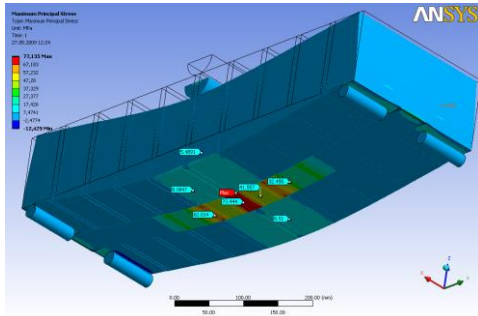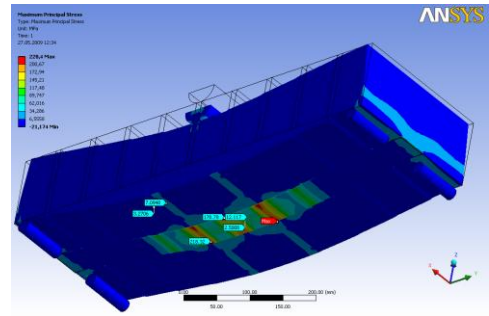
(a)   (b)

Figure 7. Maximum principal stress: a) – Mortar 8; b) –Mortar 11
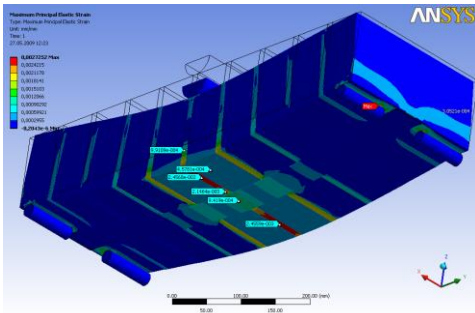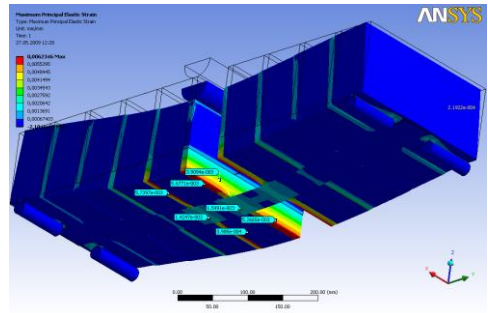
(a)   (b)

Figure 8. Maximum principal elastic strain: a) – Mortar 8; b) Mortar 10
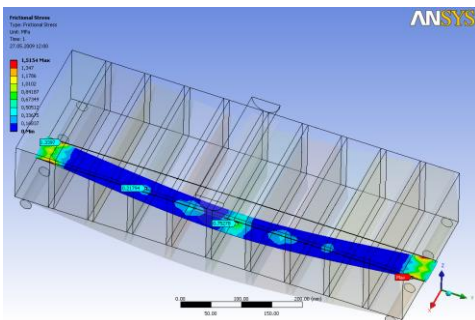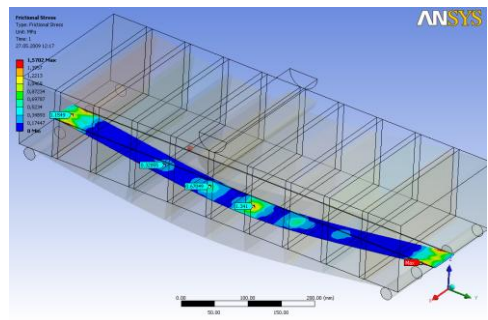
(a)   (b)

Figure 9. Frictional stress on the GFRP strip side: a) – Mortar 1; b) – Mortar 5

(a)　　　　　　　　　　　　　　　　　(b)
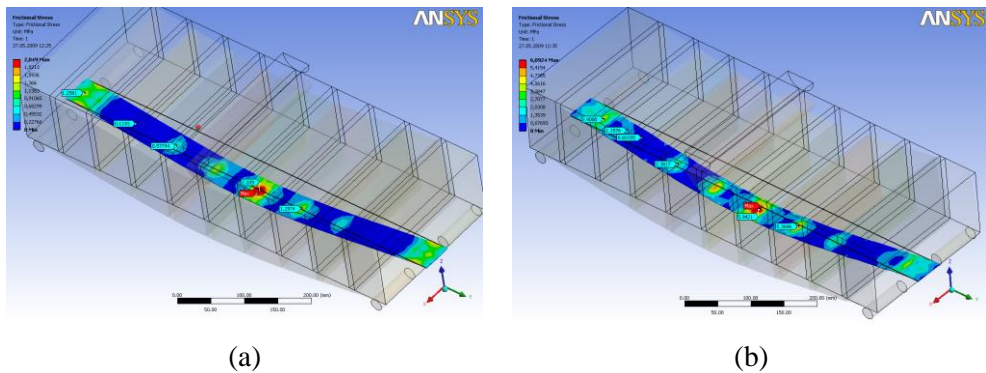
Figure 10. Frictional stress on the GFRP strip side: a) – Mortar 8; b) – Mortar 11

(a)　　　　　　　　　　　　　　　　　(b)
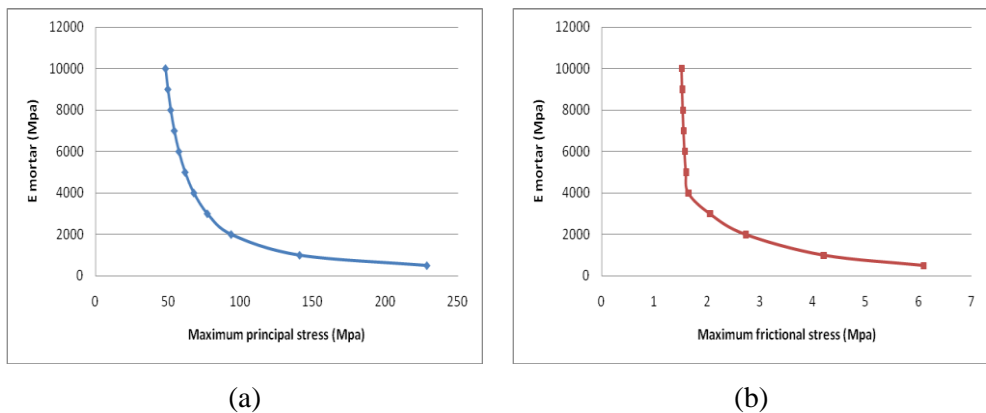
Figure 10. Relation between stiffness and stress: a) – E modulus vs. Maximum principal stress
8; b) – E modulus vs. Maximum frictional stress

3. CONCLUSIONS

The presented results of this research are encouraging but they are only preliminary. The problem of interface (contact) between brick and mortar is very important. To have better results in a micro modelling structural analysis with FEM is necessary to introduce more conditions between elements e.g friction coefficients, shear strength, and others. It is necessary that this kind of analysis to be developed and compared with experimental programs. Another type of analysis could be done if the joint mortars are considered in model as an interface between bricks. The finite element method constitutes an efficient tool to investigate specific behaviours of FRP strengthened masonry elements.

The modification of mortar stiffness is an acceptable approximation of real behaviour of these materials because in reality degradation of mortar is the first step in failure of masonry specimen. After mortar joints failure, tensile stresses appear in bricks so the results are damage of masonry. The composite strips has capacity to assume tensile stress if they pull together so the overall capacity of the strengthened masonry is improved. In model analysis presented the results are approaching by real behaviour of these strengthened elements.

References

1. Giordano, A., Mele, E., De Luca., A., *Modelling of historical masonry structures: comparison of different approaches trough a case study*, Engineering Structures 24 (2002) 1057-1069.
2. Oliveira, D., V., *Experimental and numerical analysis of blocky masonry structures under cyclic loading*, PhD Thesis, Escola de Engenharia, Universidade do Minho (2003)
3. Macchi, G., *General methodology. The combined use of experimental and numerical techniques inside a single study. P. Roca et al. (eds): Structural Analysis of Historical Constructions*. CIMNE, Barcelona, pp. 10-23.
4. Heyman J., *The stone skeleton. International Journal Solids Structures*, 2e 1966, pp 49-279, Pergamon Press Ltd, London, Great Britain
5. Save M., *La théorie des charges limites et son application aux maçonneries. Restauration des Ouvrages et des Structures*, 1983, pp 249-279, Presses de l'Ecole Nationale des Ponts et Chaussées, Paris, France
6. Van Parys, L., Lamblin, D., Descamps, T., *Limit analysis of masonry arches compared with numerical and experimental approaches*, Faculté Polytechnique de Mons - Service de Génie Civil & Mécanique des Structures, Belgique
7. Heyman, J., *Mechanical behaviour of arches and vaults. P. Roca et al. (eds): Structural Analysis of Historical Constructions II*. CIMNE, Barcelona, pp. 1-6., 1998
8. Melbourne, C.; Gilbert, M., *Modelling masonry arch bridges. J.W. Bull (eds): Computational Modelling of Masonry, Brickwork and Blockwork Structures*. Saxe-Coburg Publications, UK. 2001
9. Lemaitre J.; Caboche, J.L., *Mécanique des materiaux solides*. Dunod, Paris, 1985
10. Dhanasekar, M.; Page, A.W.; Kleeman, P.W., *The failure of brick masonry under biaxial stresses*. Proc. Instn. Civ. Engrs., Part 2, 79, pp. 295-313. 1985
11. LOFTI, H.R.; SHING, P.B., 1994. Interface model applied to fracture of masonry structures. J. Struct. Eng., ASCE, 120(1), pp. 63-80.
12. Lourenço, P.B.; Rots J.G., 1997. *A multi-surface interface model for the analysis of masonry structures*. J. Eng. Mech., ASCE, 123(7), pp. 660-668.
13. Lourenço, P.B., 1998. *Experimental and numerical issues in the modelling of the mechanical behavior of masonry*. P. Roca et al. (eds): Structural Analysis of Historical Constructio ns II. CIMNE, Barcelona, pp. 57-91.
14. Pegon, P.; Pinto, A.V., 1996. *Seismic study of monumental structures - structural analysis, modelling and definition of experimental model*. Report EUR 16387 EN, JRC, Ispra, Italy.

Diagnostics of masonry structures

Jiri Brozovsky

Institute of Building Materials and Components , Faculty of Civil Engineering, Brno University of Technology, 602 00Brno, Czech Republic

Summary

It is necessary to know exactly the technical state of structures before any masonry rehabilitation works takes place. It means that it is necessary to investigate physical state of particular structure and properties of building materials. Proper technical investigation includes geometric shape of structure, built in materials, state of surface layers, failures and moisture of masonry. Main property of building materials, which is tested, is compressive strength and according to its results it is possible to classify materials to class and make. For diagnosis of masonry structures we exploit mainly visual evaluation, probe testing, nondestructive methods and in some cases also tests on samples taken from the structure. Important role plays also genesis of masonry materials in particular regions. This knowledge allows informative estimation of built-in materials, in case that it is not possible to carry out any tests on these materials.

KEYWORDS: masonry structures, brick, mortar, NDT, diagnostics

1. INTRODUCTION

The use of building structures is generally connected with the monitoring of its technical condition from the point of view of planning its maintenance, repair remediation or change in use. Diagnostics are used for this task. Diagnostics serve to determine and assess defects to the wall structure.

The objective of masonry structure diagnostics is to determine its technical condition prior to repair, reconstruction or change in use of the building and changes to the load on the masonry support structure.

Masonry structure diagnostics determine the condition of the brickwork as a whole and also the basic physical and mechanical characteristics of the imbedded materials which are essential for performing any possible static assessment. The brickwork is a structure made up of pieces of brick material and mortar.

This article describes the methodology used for the masonry structure diagnostics and includes test methods used to determine the monitored parameters. In addition,

there is a brief overview and the parameters of the brick material used in historical buildings (there is data available on there materials than the materials used today).

2. BRICKWORK MATERIALS

The most common brick materials are:

− brickware (solid bricks, perforated bricks and various types of clay block bricks),

− stone for brickwork,

− concrete masonry units,

− autoclaved aerated concrete masonry units,

− calcium silicate masonry units.

Solid bricks were the most common brick materials used for support structures in the Czech Republic up until the 1950s. Later on various types of perforated bricks were used for brick structures e.g. honeycombed brick, various types of perforated bricks (e.g. CD 29, 36, CD 440, CD INA, etc. up to the currently manufactured bricks e.g. POROTHERM, KERATHEM, Citherm etc.). Other products include autoclaved aerated concrete masonry units and most recently of all concrete masonry units.

Mortar is mainly used as binding material for various types of bricks. For older structures the main types of mortar include lime mortar, composition mortar and grout. These would often be made from components directly on the building site, these days there has been marked increase in industrial manufactured brick mortar − dry mix. Mortar made at the site is characterized by a significantly higher variability in its characteristics than dry mortar mixture − characteristics of this mortar are influenced mainly be their preparation but not to the extent as mortar prepared directly on site because only water is added to the dry mix during preparation, the remaining components are combined in the right proportions during the production process.

2.1 Parameters of bricks used between 1870 and 1989

Two documents published at the turn of 19th century have contributed to the development of masonry construction in the present territory of the Czech Republic, namely the Building Regulations of 1787, and the Patent of 1819,

licensing subjects to manufacture bricks. The Patent also established the dimensions of solid bricks to 303 × 145 × 70 mm. In 1864, new Building Regulations were issued, which established the dimensions of bricks to 290 × 140 × 65 mm (in some cases 220 × 105 × 50 mm). These Building Regulations specified also the requirements for strength characteristics of solid bricks. Table 1 below summarizes brick specifications from 1900 to 1989.

Table 1 - Strength parameters of bricks over various manufacturing periods

Regulations of Early 20th Century		Czech Technical Standards of 1931	
Brick Type	Minimum compression strength [MPa]	Brick Type	Minimum compression strength [MPa]
clinker, clinker brick, vitrified brick	30	clinker, clinker brick, vitrified brick, channel brick	60
superior brick	26	hard stock brick	30
common brick	20	tough brick	15
horizontal coring block	17	common brick	7.5
common solid brick	10		
hollow clay block	8		
Czech Technical Standards of 1944			
Brick Type	Minimum compression strength [MPa]	Brick Type	Minimum compression strength [MPa]
clinker	55	facing brick	15
vitrified brick	35	common brick 150	15
hard-burnt brick	25	common brick 100	10
Czech Technical Standards of 1950 - 1989			
Brick Type	Minimum compression strength [MPa]	Brick Type	Minimum compression strength [MPa]
Solid brick P 7, (75), 10 (100), 15(150), 20 (250),25 (250)	7(7,5);10;15;20;25	Perforated bricks CD 290x240x113 (140) 320x240x113(140) 360x240x113 (140), CD INA, IVA, IZA P4, P6, P8, P10, P15, P20 Perforated metric bricks, Honeycombed brick P8, P10, P15, P20	4;6;8;10;15;20 8;10;15;20

3. TYPES OF DIAGNOSTIC PROCEDURES FOR THE
   MASONRY STRUCTURE

Based on the function and extent of the masonry structure diagnostics can be separated into:
a) Preliminary,
b) Detailed,
c) Supplementary.

a) Preliminary diagnostics serve to determine to extent and type of damage to the masonry structure–visual determination is commonly used for the assessment of damage. In certain cases the movement of the most significant cracking is determined in this stage, whereby providing a basis for the planning of more detailed diagnostics.

b) Detailed diagnostics - the objective is to thoroughly document the technical condition of the structure under investigation. The results serve as a basis for specifying the cause of the defects found, for static assessment of the structure and for planning its repair or reconstruction.

Detailed technical investigation of the structure under investigation determines both the type and extent of the damage and the basic physical–mechanical characteristics of the masonry structure materials which are essential in making an assessment or proposing their remediation. Should planning documentation not be available, the necessary dimensions are determined through the elements investigated. Detailed diagnostics include a range of methods:

- Nondestructive (testing of materials in the construction),

- Laboratory (determination of the parameters of the materials from samples taken from the structure),

- Visual (defects in the structure).

 Characteristic areas of structural damage are documented using photographs or video. It is important to plan the extent and choice of test points so that the results the condition of the structure under investigation can be illustrated as well as possible.

 c) Supplementary diagnostics – the objective is to supplement or clarify the information obtained through the detailed technical investigation of the structure. It is used for parts of the structure which were not available during the detailed diagnostics due to operational or other reasons or to clarify the results of the diagnostics in selected parts of the structure in question. The reason for performing supplementary diagnostics can be either to determine uncharacteristic or very diverse values of the parameters evaluated or for defects which were found after

starting the building work and could not be determined during the detailed diagnostics.

3.1 Categorization of masonry structure diagnostics based on content

Masonry structure diagnostics are made up of two basic elements:

a) Assessment of the technical condition of the structure,

b) Determination of the physical and mechanical characteristics of the materials imbedded in the brickwork.

a) Assessment of the technical condition of the structure involves the determination of the:
−   condition of the surface treatment,
−   geometric shape,
−   type of imbedded materials,
−   geometric imperfections in the masonry structure,
−   defects,
−   dampness to the brickwork.

b) Determination of the physical and mechanical characteristics of the materials imbedded in the brickwork involves:
−   compression strength of the brick material,
−   compression strength of the mortar in the bed joint of the brickwork,
−   level of degradation of the aerated concrete (autoclaved aerated concrete masonry units), or breeze (breeze blocks).

3.2 Assessment of the technical condition of the masonry structure

Assessment of the technical condition of the masonry structure involves the following:

a) Determination of the condition of the surface treatment

Painting and plaster work
−   extent, type and probable cause of damage to paint,
−   adhesion strength of the existing paint coating to the plaster using bond tests,
−   thickness of the existing paint coating,
−   establishing the basic parameters of the paint's environment.

Plaster work
−   extent, type and probable cause of damage to plaster work,
−   bond strength of plaster work to the backing by tapping or peel test,
−   thickness of plaster work,

 – specification of the type of plaster work through chemical analysis (additional test of the type of plaster work is not known).

b) Determination of geometric shape

Determined by measuring the characteristic dimensions of the investigated structure, drawing a sketch and adding the required dimensions.

 c) Type of imbedded materials

Determined visually or by boring in the case of structures with surface treatment – after removing the surface treatment.

d) Geometric imperfections of the masonry structure

Determined visually or by measurement (e.g. buckling, deflection) and recorded graphically or on a drawing of the area of occurrence.

e) Defects

The type of defect is determined visually. The extent is determined through measurement. Monitoring of defects depends on their type. The most common defects include:

 – cracking,
 – frost or mechanical damage to the brickwork,
 – leaching of efflorescent salts

Cracking

Cracking characterizes a disturbance to the brick structure in areas (cross section) where the tension exceeds the relevant limit of the local strength of the brickwork. There can be various origins to the cracking in the masonry structure. Examples of cracking in the brickwork are illustrated in figures 1 and 2. Cracking of the local subsidiary masonry structure can be caused by:

 – uneven settlement,
 – excessive strain on the vertical member throughout the cross section or in areas due to changes in load,
 – changes in the stress condition compared to what was planned,
 – lower carrying capacity than what is required,
 – dynamic effects and shaking,
 – disturbance in integrity and deterioration of parts of the cross section caused by dampness, chemical or biological corrosion,
 – interaction with the surrounding structure,
 – heterogeneity or non-homogeneity of the elements, material and construction imperfections.

Figure 1. Cracking in the brickwork   Figure 2. Cracking in the brickwork

Cracking is assessed from the following points of view:
- significance from a static point of view (insignificant, important, critical),
- cause (strength or distortion effects),
- condition of load stress or distortion of the brick elements,
- development of cracking (direct, angular, through the thickness of the brickwork),
- width of gaping.

Method for assessing cracking:
- the structure under investigation is assessed either in its entirety or can be divided into several parts based on static schematics and the occurrence of cracking along with its development and cause are determined.
- in buildings with more than one floor the development and sequence of the cracking in the walls is investigated for each floor separately.
- the layout and direction of cracking is determined visually. They are illustrated schematically in the graphic documentation of the structure under investigation or its parts (their length and gaping). A gauge for determining the width of cracking is illustrated in figure 3.

The movement of cracks (gaping) is monitored by marking the plaster (placing plaster markers in the brickwork in the areas of cracking and monitoring whether cracking occurs in the markers after a certain period of time) or dilatometrically. For dilatometric measurements a metal marker with a defined distance is fixed to the construction through a crack and the distance is measured using a dilatometer

(Ref. Fig 4). Time intervals (e.g. 1x month) are established for monitoring the damage made to the plaster marker or the distance between the measurement points during the dilatometric monitoring.
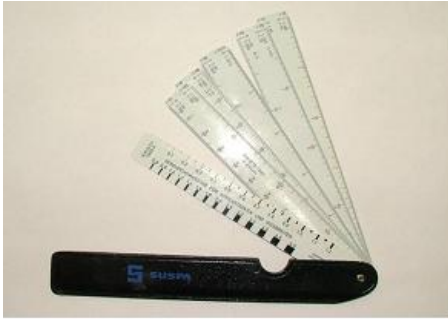
Figure 3. Example of gauge for   Figure 4. Dilatometer for determination
determining the width of cracking   of the movement of cracks

f) Frost or mechanical damage to the brickwork

Determination of the extent of the damage to the brickwork – surface area and depth of the weakened cross-section, cause (adverse characteristics of the material, level of penetration of dampness to the structure). Brickwork affected by frost damage is illustrated in Figure 5.

g) Efflorescence

Efflorescence is the leaching of dissolved salts that were either already contained in the brick or were added afterwards or they were taken up by the penetration of dampness to the brickwork. Efflorescence is generally harmless in relation to the bricks themselves but it can look unsightly because it is capable of penetrating through the plaster – Ref. Fig 6. Qualitative and quantitative determination of the type and concentration of the chemical compounds making the efflorescence using chemical or physical-chemical methods. Assessment of the damage the efflorescence can cause. The extent of the imbedded structure. The level of damage to the masonry structure material.

h) Dampness of the brickwork

Dampness of the brickwork can be specified by two methods:
- Non-destructively – using a moisture meter, or most commonly electrically,
- Destructively – from samples of the brickwork taken from the structure using a gravimetric method based on the technical standards of the given material.

In addition to the values of dampness, its distribution in the construction is also determined. The dampness distribution at depth at a given height level can be determined using gravimetric methods on samples taken from various depths.

Figure 5. Brickwork of perforated bricks showing frost damage

Figure 6. Efflorescence in the brickwork

3.3 Determination of the strength characteristics of the brickwork materials

3.3.1 Destructive tests

Destructive tests are performed on samples of material taken from the structure. Tests are performed based on the procedures codified for the given material in the relevant technical standards. It is difficult to take an intact sample from perforated brickwork in the required amount and no disturb the static stability of the structure.

3.3.2 Nondestructive tests

Nondestructive tests are used to determine the strength of solid bricks and the mortar in the bed joint of the brickwork.

a) Compressive strength of solid brick

Impact hammer methods are used to determine the compressive strength of solid bricks e.g. Schmidt impact hammer, type LB or Waitzmann hammer, in cases where the calibration relationship between the parameters of the nondestructive testing and the compressive strength of the brick are available.

– *Waitzmann hammer*

Waitzmann's scleroscope method counts among impression methods. It is in principle a follow-up of the POLDI hammer designed for steel hardness

determination. It is based on measurement of impression produced by insertion of a punch with defined shape – see Figure 7 – in the inspected material and in a comparison bar with defined strength of 700 MPa. The force for punch insertion is produced by means of a mallet and it is not constant, but depends on the impact force. The non-destructive testing parameter is the ratio β, which is the ratio between the dimple detected on the steel comparison bar and the dimple on the foil put on the tested brick surface. An advantage of the Waitzman's scleroscope in comparison with hardness drop testers is automatic elimination of the impact attenuation.

– *Schmidt impact hammer, types LB*

The Schmidt impact hammer method counts among the rebound methods. The method is based on material hardness determination, in the case in question the hardness of brick crocks. During the test, the hammer punch is hurled with defined energy by means of a spring and the instrument dial indicates the rebound value, which depends on the material hardness - i.e. also on its strength. Schmidt impact hammer, types LB (it is designed for ceramic material testing), has the initial impact energy of 0.735 N.m. Schmidt impact hammer, type LB, is represented in Figure 8.

Figure 7 - Waitzmann Hammer

Figure 8 - Schmidt Impackt Hammer type LB

As an illustration we include calibration relations for determining the compressive strength of solid bricks after testing with a Waitzmann or Schmidt impact hammer, types LB (formula 1 and 2).

Test results for solid bricks from the period 1840 to 1900 by Waitzmann's scleroscope and measurement by Schmidt impact hammers types N was performed on a set of 24 bricks sampled from one object.

– Waitzmann's scleroscope (compressive strength) :

$$f_{bc-W} = 624{,}48\beta^2 - 171{,}8\beta + 16 \quad r = 0.895 \quad \beta \in \{0.2200; \, 0.3700\} \tag{1}$$

– Schmidt impact hammers (compressive strength) :

$$f_{bc-LB} = 1{,}3R - 12 \quad r = 0.93 \tag{2}$$

b) Compression strength of masonry bed mortar

The boring method is used in the Czech Republic - TZUS drill (Figure 9). The principle of the test consists in determining depth of a bore in material at a defined number of revolutions. To ensure reproducibility of results, the drill is equipped with a spring to produce constant thrust of 150N. This device was developed for determination of compression strength of masonry bed mortar and for determination of compression strength of solid burnt bricks inbuilt in masonry. For mortar testing, the number of drill revolutions is 25. The compression strength of mortar is determined from the established depth of bore according to the calibration formula delivered by the device manufacturer (TZUS - Technical and Test Institute for Construction, Prague).

Figure 9. TZUS drill

3.3.2 Determination of the strength classification of the brickwork material

Specification of the strength signs is made pursuant to ISO 13822; solidity characteristics in the structure are calculated as follows. From the individual compression strength values we calculate the mean f_{cx}, standard deviation s_x and

variation coefficient V_x. characteristic compression strength of the brick elements f_{ck} calculated from relation (3) :

$$f_{ck} = f_{cx}(1 - k_n V_x)$$ (3)

Where : k_n – statistical value depending upon the accepted proportion of low results and the number of tests.

4. CONCLUSION

The outputs of the masonry structure diagnostics include:
- extent, level of damage and defects to the brickwork – basis for decision making on the further use or repair to the masonry structure, basis for static calculation or static determination.
- strength characteristics of the brickwork material – for its classification into the relevant strength signs, basis for static calculations.
- geometric shape of the masonry structure - basis for static calculation.
- dampness of the brickwork – basis for specifying damp-proofing measures.

Acknowledgements

References

1. Brozovsky, J., Zach,J., Brozovsky,J., jr. Non-destructive testing of solid brick compression strength in structures. The e-Journal of Nondestructive Testing, 2007, vol. 12, No 11, pp. 1-9, ISSN 1435-4934.
2. Brozovsky, J., Zach,J., Brozovsky,J., jr. Determining the Strength of Solid Burnt Bricks in Historical Structures . The e-Journal of Nondestructive Testing, 2008, vol. 13, No. 9, pp. 1-10. ISSN 1435-4934.
3. Drochytka, R. et al. Progressive Building Materials with Utilization of Secondary Raw Materials and Impact thereof on Structures Durability, Brno University of Technology, Final report to MSM Project 0021630511, Brno, 2007 (In Czech)
4. TZUS s.p. Documentation of the Drill for Testing Strength of Mortar and Bricks in Masonry, Prague, Czech Republic, 1997
5. Vejchoda, J., Brozovsky, J. Diagnostics of Building Structures. Utilisation of Non-Destructive Methods for Testing of Bricks, Report to Project Bet 11/88, Military Academy/VSP, Brno, 1992, pp. 70 (in Czech).

Environmental assessment software for concrete applications

Laura Dumitrescu, Nicolae Taranu

Department of Civil and Industrial Engineering, "Gh. Asachi" Technical University of Iasi, Iasi, 700050, Romania

Summary

Concrete is a versatile material used almost everywhere, from bridges and roads to houses, schools and hospitals. By adopting an environmentally responsible attitude towards the specification, design and construction of civil engineering projects, the undesirable consequences for the world's ecosystems could be minimized.

Life-cycle analysis is a method of assessing the environmental impacts of a product over its projected lifetime, and includes raw materials, material production, design, component production, construction, use, demolition, recycling and re-use. Great effort to develop new LCA methodologies and software has been made in the last two decades.

EcoConcrete is a tool to analyse the environmental performance of European ready mixed and precast concrete products. The software was developed under commission of the European concrete industry associated in a joint project group. The paper presents the structure, operation and functionality of EcoConcrete. A case-study of using EcoConcrete software for the environmental assessment of concrete pavements is also presented.

KEYWORDS: life-cycle assessment, environmental impact, concrete pavement

1. INTRODUCTION

Concrete is one of the most utilized construction materials on the market. The main ingredients in concrete are aggregates (70-80%), cement (10-20%) and water (7-9%). To enhance specific characteristics, chemical admixtures (air-entraining and water-reducing admixtures) can be added. The major impacts associated with concrete are the use of cement – cement production is one of the most energy intensive of all industrial manufacturing processes - and the extraction of raw materials such as virgin aggregates.

Green design and pollution prevention are proactive strategies to minimize the environmental burdens associated with a product or process without compromising functionality. Life cycle assessment (LCA) is an important tool used in pollution prevention and green design efforts. Selection of product design, materials, processes, reuse or recycling strategies, and final disposal options requires careful examination of energy and resource consumption as well as environmental discharges associated with each prevention or design alternative. LCA can show the major environmental problems of a material, product or process. Several LCA software tools have been developed to facilitate the data collection and also the calculation of the inventory results. The exact number of databases is not known, but most of the LCA-software includes initially one of several databases from external sources. Basically there are available two types of databases – extensive general databases which include data on various industrial sectors and smaller databases with data on some specific field [1].

EcoConcrete is a tool which enables the calculation of environmental profiles for ten different European ready mixed and precast concrete products. It was promoted by the "Joint Project Group on the LCA of concrete", composed of the European associations of the different components of concrete. The paper presents the structure, operation and functionality of EcoConcrete, including a case-study of using this software for the environmental assessment of concrete pavements.

2. LIFE CYCLE ASSESSMENT

Life Cycle Assessment (LCA) is a method for analysing and assessing the environmental impact of a material, product or service throughout its entire life cycle, usually from the acquisition of raw materials to final disposal. Traditionally, the main focus in LCA has been on regional and global environmental impacts on the external environment. According to the ISO 14040, the general categories of environmental impacts to be considered in an LCA include resource use, human health, and ecological consequences.

An LCA study consists of four steps (figure 1):
- Defining the goal and scope of the study.
- Making a model of the product life cycle with all the environmental inputs and outputs. This data collection effort is usually referred to as the life cycle inventory (LCI) stage.
- Understanding and evaluating the magnitude and significance of the potential environmental impacts of all inputs and outputs; this is referred to as the life cycle impact assessment (LCIA) phase.
- The interpretation and improvement, in which the findings of either the inventory stage or the impact assessment are combined consistent with the defined scope and goal of the study in order to reach conclusions and recommendations.
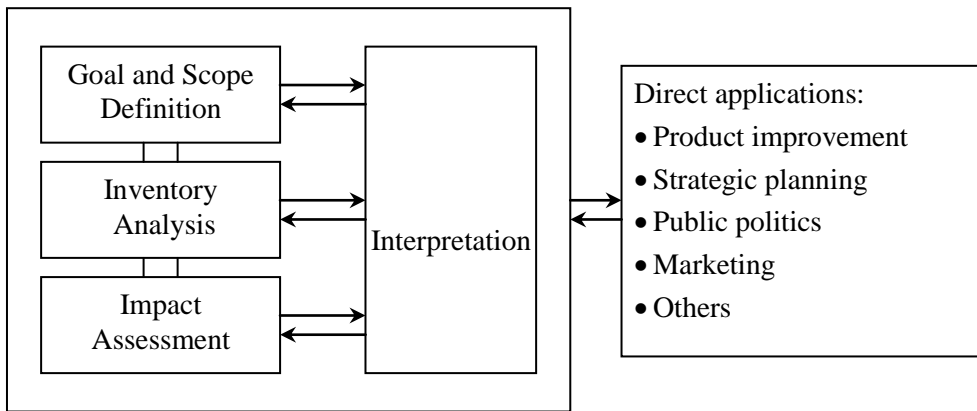
Figure 1. Phases of an LCA

LCA is very complex and time consuming, because the "cradle-to-grave" life cycle always involves numerous stages and activities that give rise to a number of different environmental loadings. To keep the amount of work within reasonable bounds, the assessments must always be limited and efforts must be made to identify the critical stages of the life cycle and those factors responsible for environmental loadings. This requires not only adherence to the basic principles of LCA but also knowledge of the product or activity in question. Great effort to develop new LCA methodologies and software has been made in the last two decades. In the early stages of LCA development, much focus was given to the very detailed and expensive studies. Now, because the most commonly used materials are already included in LCA databases, the trend is towards screening and simplified studies.

One of the most widely used LCA methods is SimaPro, developed by the PRe Consultants company [2]. SimaPro software has a large set of data libraries and also contains a number of impact assessment methods, which are used to calculate

impact assessment results such as: CML 1992, Eco-indicator 95, Ecopoints 97, Eco-indicator 99. Each method contains a number of impact categories; some allow aggregation into a single score, and some do not.

For the specific field of concrete applications, an LCA software tool called EcoConcrete was produced by the joint initiative of five European associations representing the concrete industry or constituents. EcoConcrete, an Excel tool that applies three different LCA methodologies in accordance with the ISO standards to assess the impact of 10 fully-fledged functional units of concrete-based solutions on the environment, was developed in the frame of the EU Thematic Network "European Construction in Service of Society" [3].

3. ECOCONCRETE LCA SOFTWARE TOOL

3.1. Structure of EcoConcrete

EcoConcrete contains two types of datasheets:

- Input datasheets:
    • Product - Select the product of interest;
    • Definition - Define the unit in which the results are expressed;
    • Composition - Define the concrete constituents and transport distances for delivery;
    • Life Cycle - Define the life cycle processes (such as maintenance, replacements and final waste scenario);

- Output datasheets:
    • Overview - Gives an overview of all filled out data related to the functional unit;
    • Main - Shows the environmental performances according to the CML 2000 methodology, the Eco-indicator 1999 methodology or the EDIP methodology.

The data input has the following structure:
    1. Product: choice of the functional unit;
    2. Functional Unit: description of amount, dimensions, service life;
    3. Composition: type and amount of constituents (cement, aggregates, fillers, admixtures, water) and their transport (distance, mode);
    4. Life Cycle: production, transport, construction, maintenance, demolition, recycling and landfill.

EcoConcrete uses life cycle impact assessment (LCIA) data as a basis. This means that the data within EcoConcrete can never be disaggregated to life cycle inventory (LCI) or process data. EcoConcrete assembles an overall LCIA score for a product

based on the separate materials and processes the user selects. The LCIA scores are based on site specific data for products and processes which are averaged and aggregated to arrive to data that can be regarded as representative for Europe.

3.2. Impact assessment methodologies

From different available impact assessment methodologies, EcoConcrete has chosen the following three methods:
- CML 2000 (Centre for environmental sciences, Leiden, NL) methodology;
- Eco-Indicator '99 methodology;
- EDIP (Environmental Design of Industrial Products) methodology.

All three methods comply with the ISO 14042 standard, are operational on European scale, and are still under development. The scientific degrees of the various parts vary and are subject to ongoing improvements.

Differences occur in the number and type of environmental impacts (figure 2), the scientific background, the importance of environmental impacts in different nations, etc.

CML	Eco-Indicator	EDIP
Human toxicity Abiotic depletion Ecotoxicity, fresh water aquatic Ecotoxicity, fresh water sediment Ecotoxicity, terrestrial Acidification Eutrophication Climate change Photo-oxidant formation Ozone depletion Energy Waste (non chemical) Waste (chemical)	**Damage category : Human Health** Carcinogens Resp. organics Resp. inorganics Climate change Radiation Ozone layer **Damage category : Ecosystem Quality** Ecotoxicity Acidification/ Eutrophication Land use **Damage category: Resources** Minerals Fossil fuels	Global warming Ozone depletion Acidification Eutrophication Photochemical smog Ecotoxicity water chronic Ecotoxicity water acute Ecotoxicity soil chronic Human toxicity air Human toxicity water Human toxicity soil Bulk waste Hazardous waste Radioactive waste Slags/ashes Resources (all)

Figure 2. Impact categories included in the impact assessment methodologies

3.3. Results

EcoConcrete presents the LCIA results as tables and as graphs.

Graphs represent relative contributions per environmental theme. These themes vary along with the selected methodology. Tables represent absolute values per

environmental theme. Absolute values are available for different materials and life-cycle phases.

Results are given in terms of impact categories, based on both public and confidential inventories (given by the associations involved). It is impossible to disaggregate the results to see the inventories.

3. IMPACT ASSESSMENT OF CONCRETE PAVEMENTS USING ECOCONCRETE SOFTWARE

EcoConcrete software tool has been used for the assessment of the environmental performance of the concrete pavement solutions proposed in the frame of the FP6 EcoLanes project [4]. The input data are based on information collected from the works carried out at the ALT-LIRA testing facility of the Faculty of Civil Engineering and Building Services in Iasi. Two concrete pavement solutions are tested using EcoConcrete software: un-reinforced concrete and steel-reinforced concrete pavement. A breakdown of the component materials in plain concrete is presented in Table 1.

Table 1. Composition of the un-reinforced concrete

Quantities per 1 m^3 of concrete		
Natural aggregates	%	kg
Natural river sand 0 - 4	40	748
Natural river sand 4 - 8	18	337
Chippings 8 - 16	22	411
Chippings 16 - 25	20	374
Total dry aggregates	100	1870
Cement I 42.5 R		350
Water		146
Additive Cementol Zeta T concentrate	0.67	2.3
Additive Cementol ETA S	0.2	0.7
Concrete density, kg/m^3		2369

The functional unit is 1 m^2 pavement and the service life is selected to be 40 years. The pavement thickness is 20 cm. The material supply is made by truck 16 t load and the transport distances are: 200 km for cement, 100 km for non-crushed fine and coarse aggregates, 200 km for crushed coarse aggregates, 200 km for admixtures. The transport distance of concrete to the site is 8 km. No maintenance and replacement works are considered. The end of life scenario is assumed to be demolition with 100% recycling of concrete and the distance of transport to treatment of 50 km. The results of using EcoConcrete software are presented in Table 2 and Figure 3. Three impact indicators – energy consumption, climate

change and acidification - have been selected, for all materials and life-cycle stages
of the 20 cm plain concrete pavement.

Table 2. LCA absolute results for 20 cm un-reinforced concrete pavement

Environmental impact indicator/mp	Energy (MJ)	Climate change (kg CO_2)	Acidification (kg SO_2)
Cement	437.5000	62.8600	0.1281
Aggregates	12.2953	0.6014	0.0044
Admixtures	9.3600	0.4338	0.0048
Reinforcement	0.0000	0.0000	0.0000
Water	0.0205	0.0014	0.0000
Transport Constituents	209.0542	15.7967	0.1358
Fabrication	14.7200	0.7280	0.0048
2. Transport to site	11.7881	0.8907	0.0077
3. Construction	1.5213	0.1149	0.0010
4. Maintenance	0.0000	0.0000	0.0000
5. Demolition	97.1290	6.2542	0.0439
6. End of life scenario	102.1039	6.8417	0.0521
Total	895.4923	94.5228	0.3825
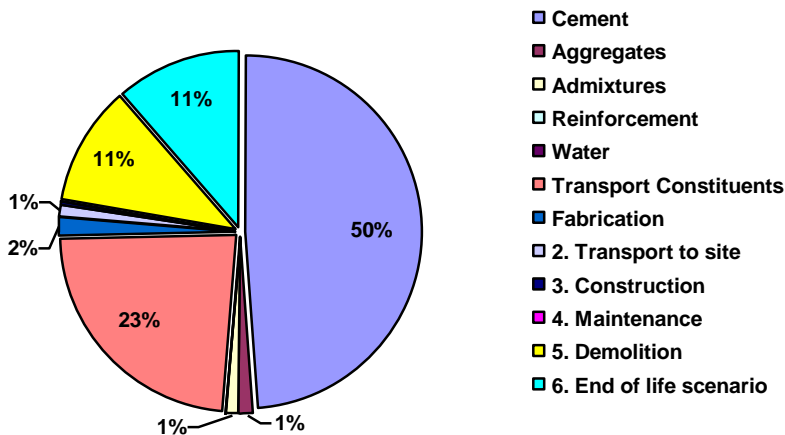
Figure 3. Relative results of energy consumption for 20 cm plain concrete pavement

The main contributor to the total energy consumption is cement (one half),
followed by transport of constituents (23%), demolition and end of life scenario
with 11%.

If a steel reinforcement of 70 kg/m^3 (wire mesh) is considered, transported by truck 16t load from 100 km distance, the energy consumption is 23% greater than in un-reinforced situation (see Table 3 and Figure 4).

Table 3. LCA absolute results for 20 cm steel-reinforced concrete pavement

Environmental impact indicator/mp	Energy (MJ)	Climate change (kg CO_2)	Acidification (kg SO_2)
Cement	437.5000	62.8600	0.1281
Aggregates	12.2953	0.6014	0.0044
Admixtures	9.3600	0.4338	0.0048
Reinforcement	198.8000	10.2900	0.0543
Water	0.0205	0.0014	0.0000
Transport Constituents	213.4082	16.1257	0.1386
Fabrication	14.7200	0.7280	0.0048
2. Transport to site	12.1365	0.9171	0.0079
3. Construction	1.5662	0.1183	0.0010
4. Maintenance	0.0000	0.0000	0.0000
5. Demolition	99.9990	6.4390	0.0452
6. End of life scenario	102.1039	6.8417	0.0521
Total	1101.9096	105.3563	0.4412
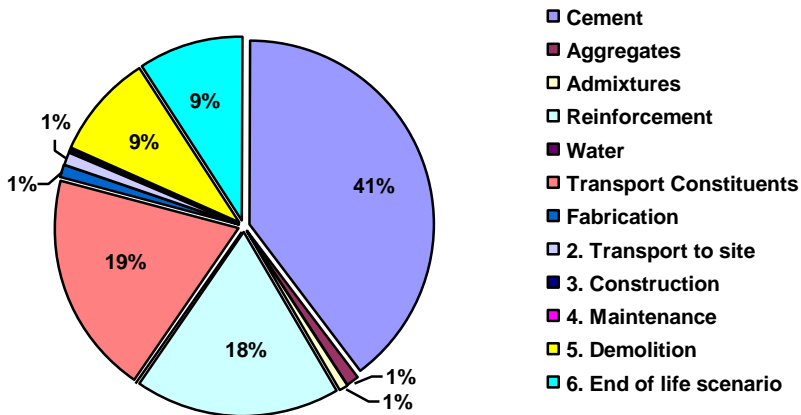
Figure 4. Relative results of energy consumption for 20 cm steel-reinforced concrete pavement

The contribution of cement to the total energy consumption remains the most important, followed by transport of constituents (19%) and steel reinforcement production (18%).

3. CONCLUSIONS

Life cycle assessment provides the more quantitative and scientific basis for promoting life cycle thinking as a key concept. The most important applications are the analysis of the contribution of the life cycle stages to the overall environmental load and the comparison between products for internal or external communications. Basic objective of developing the EcoConcrete LCA tool was to make progress in the assessment and minimisation of the impact of concrete-based products on the environment and to disseminate the results. The data collection is considered representative for Europe, but data are not representative at a national level for all countries. The EcoConcrete LCA software is an understandable and easy to use tool. By using it for the assessment of concrete pavements it is possible to identify the key environmental factors in the life-cycle of pavements and eventual strategies to minimise the environmental impact, such as using low-energy cement or reducing transport distances by choosing local materials.

Acknowledgements

References

1. Koskela, S., Hiltunen, M.R., *A guide to the utilization of LCI/LCA databases for Estonian enterprises*, Finnish Environment Institute, Helsinki, 2004
2. PRe Consultants, SimaPro 7, 2007. Internet site: www.pre.nl
3. ECOserve Network – European Construction in Service of Society, 2007. Internet site: www.eco-serve.net
4. EcoLanes – Economical and sustainable pavement infrastructure for surface transport, 2006-2009. Internet site: ecolanes.shef.ac.uk

Numerical methods for the modelling of interface delamination in composites.

Ruxandra Oltean[1], Nicolae Taranu[1], Ciprian Cozmanciuc[1], Catalin Banu[1], Oana Mihaela Ionita[1]

[1]*Department of Civil Engineering, Gh.Asachi Technical University, Iasi, 700050, Romania*

Summary

Composite materials have been used in structures for centuries. The available software enable us to model composite materials with specialized elements called layered elements, thus we can assign different properties and orientations for the various layers. The failure mechanism discussed in this paper is the interface delamination at the contact surface between two materials. This has motivated considerable research on the failure at the interface.

Interface delamination can be modelled by traditional fracture mechanics methods such as nodal release techniques. Alternatively, we can use techniques that will directly establish the fracture mechanism, by introducing a critical fracture energy that is also the energy required to break apart the interface surface, called cohesive zone model (CZM). In the second part of this paper will be discussed a more recent method to numerically model the delamination, namely discontinuous Galerkin model. This approach offer advantages over the more traditional approach that uses interface elements, as will be discussed in more detail.

KEYWORDS: debonding, interface delamination, composites, cohesive zone model, discontinuous Galerkin model

1. INTRODUCTION

A major failure mode in composite structures is debonding, either between two structural components, or between different layers within a structural part. Conventionally, special interface elements methods are placed a priori between the continuum finite elements to capture debonding at locations where they are expected to emerge. More recently, discretization methods have been proposed, which are more flexible than standard finite element methods, while having the potential to capture propagating debonding cracks in a robust, efficient and accurate manner, two of them being presented in the present paper, meaning cohesive zone model and discontinuous Galerkin method.

Composite materials are somewhat more difficult to model than an isotropic material such as iron or steel. Because each layer may have different orthotropic material properties, extra-care must be exercised when defining the properties and orientations of the various layers. Both fiber and particulate composite materials provide applications in materials science where the multiscale microstructure leads to the need for multiscale modeling. Using this approach, the various aspects of the entire structural problem are considered at different levels of observation, each of them characterized by a well-defined length scale. The different levels at which analyses are carried out, are connected either through length scale transitions, in which the structural behaviour at a given level is homogenised to arrive at mechanical properties at a next higher level [1], or through finite element analyses which are conducted at two levels simultaneously and in which are connected by matching the boundary conditions at both levels [2, 3].

This paper will not focus on the methods for length scale transition or approaches for carrying out multi-level finite element analyses. Instead, we shall focus on so-called meso-level approach, in which delamination is assumed to be the main degrading mechanism. For this purpose, the different levels of analysis – macro, meso and micro – are defined in the context of laminated composite structures. At the meso-level as well as at the micro-level, fracture along internal material boundaries, delamination and debonding, respectively, governs the failure behaviour. Most constitutive relations for such interfaces have in common that a so-called work of separation or fracture energy plays a central role. For this reason the subject of cohesive zone models, which are equipped with such a material parameter, is included in the discussion.

At the meso-level, the plies are modelled as continua and can either be assumed to behave linearly elastically or can be degraded according to a damage law, and are discretised using standard finite elements – while the delamination is modelled in a discrete manner using special interface elements [4, 5]. Generalised plane strain elements are often used to model free-edge delamination [6], while stacks of solid or shell elements and interface elements are applicable to cases of delamination near holes or other cases where a three-dimensional modelling is necessary [3, 7].

2. COHESIVE ZONE MODEL

Recently, the concept of cohesive zones has received revived interest and the cohesive zone modelling (CZM) approach has emerged as a powerful analytical tool for nonlinear fracture processes. This type of model has been widely used for studying the so-called quasi-brittle fracture process zone, which arises prior to complete fracture in, e.g., concrete materials and macromolecular based polymer

materials [8, 9]. Applications to other material systems such as adhesively bonded joints [10, 11], bimaterial interfaces [12], and the dynamic fracture of homogeneous materials [13] have also been very successful. Cohesive zone models have also been used to analyze composite delamination problems. Problems of delamination in the absence of large notches or holes have been studied [14, 15, 16] and also, more pertinently to the present work, in the presence of a notch [17].

CZM involves representing the adhesive bonded interface by a layer of special elements whose constitutive properties describe the traction (or cohesive stress) evolution as the interface is being opened [18]. Thus the core of CZM is the traction-separation law (also called cohesive law) that describes the evolution of interface stresses as functions of interface separations.

2.1. Traction-separation law

The cohesive traction is related to the cohesive separation of the surfaces by a traction-separation law (TS-law). In initially rigid models the cohesive zone is inactive as long as a certain stress level has not been reached. Barenblatt [19] was the first to propose a cohesive zone model for brittle fracture. Another popular model assumes that the cohesive stress remains constant up to a critical separation distance at which it drops down to zero. The second type of model assumes an initially elastic response of the cohesive zone. Most TS-laws of that type follow a similar scheme: the cohesive traction is zero at the beginning of the deformation. With increasing separation, the traction across the cohesive zone reaches maximum, then decreases and eventually vanishes allowing for complete decohesion. Crack growth under increasing external loading occurs when the crack surfaces separate gradually to the point where separation at the crack tip exceeds the critical value Δ_c and the cohesive traction vanishes [20].

In CZM, the potential crack propagation plane or the cleavage plane is idealised as a cohesive zone or cohesive interface and is assumed to support a nominal traction field T (force/unit reference area). This traction field, in general, has components both normal and tangential to the cohesive interface. The mechanical response of the cohesive interface is described through a constitutive law (in terms of a potential function) relating the traction field T with a separation parameter. The constitutive equations are such that, with increasing interfacial separation, the traction across the interface reaches a maximum, decreases and eventually vanishes so that complete decohesion occurs. It should be emphasized here that this constitutive description is a continuum one, and thus does not represent the interaction of two individual atoms across the interface. Also, it does not account for discrete dislocation effects. Consequently, the functional dependence of the traction field on interface separation is not uniquely determined [21].

Typically the cohesive stress increases initially with the opening displacement, reaches a peak and then drops continuously to zero again at a certain critical displacement, as shown in Figure 1, and where the peak cohesive stresses represent the maximum load bearing capability of the adhesive [22].
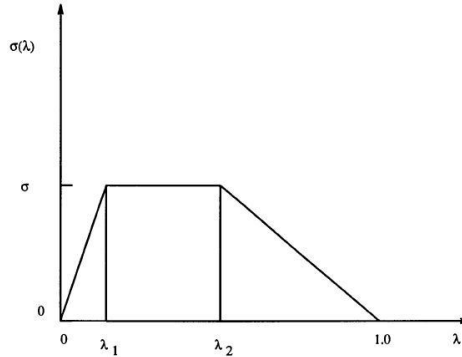
Figure 1. Traction-separation law in cohesive zone model

The TS-law relates the cohesive normal traction N to the normal separation displacement Δ. In principle, TS-laws of any shape can be implemented with little modification. The reason for choosing a TS-law with straight segments is due to the computational costs. An exponential law would require updating the systems matrix continuously. The shape of the law consists of a rising, a constant and a falling segment and is determined by five parameters; the area under the curve defines the fracture energy:

$$\Gamma = 0.50\sigma_{th} \cdot \Delta_c \cdot (1 - \delta_1 + \delta_2) \tag{1}$$

where σ_{th} is the cohesive strength, Δ_c is the crack opening separation above which the cohesive interaction vanishes and δ_1, δ_2 are the shape parameters that define the corners of the trapezoid.

2.2. Interface elements

The interface fracture phenomena play an important role in a number of applications especially in laminated composites. When modelling interface fracture phenomena, the use of discrete approach is advocated to achieve a better representation of the entire fracture process. If failure takes place along well-defined surfaces, a standard way to solve fracture problems with finite element

methods consists of inserting interface elements (or cohesive layers) with zero thickness in the mesh at places where cracking is expected to occur [23, 24].

For interface elements, the interfacial separation is defined as the displacement jump, δ, i.e., the difference of the displacements of the adjacent interface surfaces:

$$\delta = u^{top} - u^{bottom} \tag{2}$$

Note that the definition of the separation is based on local element coordinate system, Figure 2. The normal of the interface is denoted as local direction **n**, and the local tangent direction is denoted as **t**. Thus:

$$\delta_n = n \cdot \delta \tag{3}$$

$$\delta_t = t \cdot \delta \tag{4}$$
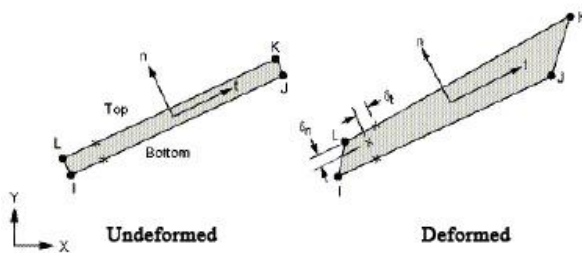
Figure 2. Interface elements

An example where the potential of cohesive-zone models can be exploited fully using conventional discrete interface elements, which is an analysis of delamination in layered composite materials [6]. Since the propagation of delaminations is restricted to the interfaces between the plies, inserting interface elements at these locations permits an exact simulation of the failure mode [3].

3. DISCONTINUOUS GALERKIN MODEL

The discontinuous Galerkin (dG) method is a class of finite element methods, which uses discontinuous, piecewise polynomial spaces for the numerical solution and the test functions. This method has classically been employed for the computation of fluid flow, but more recently, attention has been given to their potential use in solid mechanics, and especially for problems involving cracks [25], or for constitutive models that incorporate spatial gradients [26].

According to Stan [27] the main advantages of the discontinuous Galerkin finite element methods are:

- the shape functions are discontinuous along the element edges;
- the dG methods are locally mass conservative at the element level;
- each element can be thought of as a separate entity (the element topology, the degree of approximation and even the choice of governing equations can vary from element to element and in time over the course of calculation without loss of rigor in the method).

Consider a body that occupies a bounded Lipschitz domain Ω in $\Re^3$ (Figure 3). The continuum problem is governed by the following equations stated in terms of the Cauchy stress:

$$-\nabla \cdot \sigma = b \text{ in } \Omega \tag{5}$$

$$\sigma \cdot n = g_N \text{ on } \partial_N \Omega \tag{6}$$

$$u = g_D \text{ on } \partial_D \Omega \tag{7}$$

where b is the body force, n - the unit vector outward normal to the boundary $\partial\Omega$, g_D and g_N are the boundary conditions applied on the displacement $\partial_D \Omega = \Gamma_D$ and traction $\partial_N \Omega = \Gamma_N$ parts of the boundary, respectively.
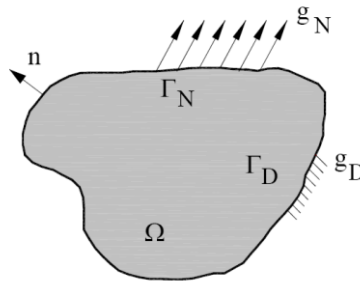
Figure 3. Body with a discontinuity

Let $\Omega_h = \{T\}$ be a shape-regular partition of Ω, where T are finite elements. Let e denote an arbitrary element edge, and $\varepsilon_h = \{e\}$ be the set of all edges. Each element boundary e is shared by two elements T^+ and T^- such that $e = T^+ \cap T^-$, with n^+ being the unit normal vector to T^+ (Figure 4).

We decompose ε_h into three disjoints subsets such that $\varepsilon_h = \varepsilon_I \cup \varepsilon_D \cup \varepsilon_N$, where ε_I is the set of all internal edges, $\varepsilon_I = \{e \in \partial T \setminus \partial\Omega : T \in \Omega_h\}$; ε_D is the set of all element edges on the Dirichlet part of the boundary

$\partial_D\Omega, \varepsilon_D = \{e \subset \partial T \cap \partial_D\Omega : T \in \Omega_h\}$; ε_N is the set of all element edges on the Neuman part of the boundary $\partial_N\Omega, \varepsilon_N = \{e \subset \partial T \cap \partial_N\Omega : T \in \Omega_h\}$.
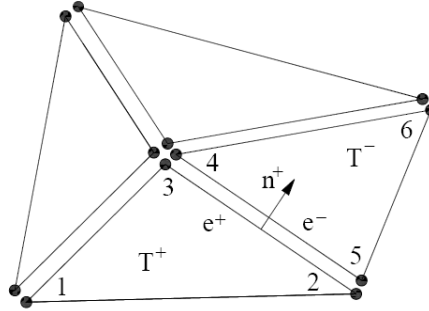
Figure 4. Discontinuous Galerkin mesh

The following approximation space is introduced:

$$V_h = \left\{ \upsilon \in L^2(\Omega) : \upsilon|_T \in P^k(T), \forall T \in \Omega_h \right\} \tag{8}$$

where $P^k(T)$ is the space of polynomials of degree at most k supported on T.

To facilitate construction of a numerical scheme with high order accuracy in the vicinity of discontinuities, we require all discontinuities to lay on the element boundaries.

The stabilized discontinuous Galerkin weak formulation results in the following form: Find $u_h \in V_h$ such that:

$$a(\upsilon_h, u_h) + j(\upsilon_h, u_h) = l(\upsilon_h), \forall \upsilon_h \in V_h$$

in which

$$\begin{aligned}
a(\upsilon_h, u_h) = & (\varepsilon(\upsilon_h), \sigma(u_h))_T - ([\upsilon_h], <\sigma(u_h) \cdot n>)_{\partial_I\Omega_h} \\
& + \alpha(<\Omega(\upsilon_h) \cdot n>, [u_h])_{\partial_I\Omega_h} - (\upsilon_h, \sigma(u_h) \cdot n)_{\partial_D\Omega_h} \\
& + \alpha(\sigma(\upsilon_h) \cdot n, u_h)_{\partial_D\Omega_h}
\end{aligned} \tag{9}$$

$$j(\upsilon_h, u_h) = \left(\frac{\beta}{h_e}[\upsilon_h], [u_h] \right)_{\partial_I\Omega_h} + \left(\frac{\beta}{h_e}\upsilon_h, u_h \right)_{\partial_I\Omega_h} - \left(\frac{\beta}{h_e}\upsilon_h, g_D \right)_{\partial_D\Omega_h} \tag{10}$$

and

$$l(\upsilon_h) = (\upsilon_h, b)_T - (\upsilon_h, g_N)_{\partial_N\Omega_h} + \alpha(\sigma(\upsilon_h) \cdot n, g_D)_{\partial_D\Omega_h} \tag{11}$$

In the above equations β is a positive penalty parameter assumed constant across Ω_h, and h_e denotes the characteristic length of the mesh. The parameter α is either +1, or -1, corresponding to non-symmetric and symmetric interior penalty methods, respectively.

4. CONCLUSIONS

It is worth remarking that, in this paper, a powerful analytical tool for composite delamination was used, namely the cohesive zone model. Normally, delamination is defined as the separation of two plies of a laminated composite, but also delamination can occur exactly at the interface between two phases. Fracture or delamination along the interfaces plays a major role in limiting the toughness and the ductility of the multi-phase materials, such as composites or laminated composite structures. In this concern the interface surfaces of the materials can be modelled using a special set of interface materials or contact elements, and CZM can be used to characterize the constitutive behaviour of the interface.

Another approach, which offers advantages over the more traditional approaches, is the discontinuous Galerkin method that can handle cohesive cracks very naturally. Some of their main advantages are including good stability and consistency, and absence of traction oscillations and spurious reflections. One of the downsides of the dG methods is the computational cost since a loop over the boundaries in the mesh in necessary. Also, an important yet unresolved problem is the automatic selection of the stabilization parameter. However, the presented dG finite element formulation with cohesive models can simplify the computational modeling of failure along well-defined surface.

References

1. Ladevèze, P., Lubineau, G., An enhanced mesomodel for laminates based on micromechanics. *Composites Science and Technology*, 2002, **62:** 533–541.
2. Feyel, F. and Chaboche, J.L., FE^2 multiscale approach for modeling the elastoviscoplastic behaviour of long fibre SiC/Ti composite materials. *Computer Methods in Applied Mechanics and Engineering*, 2000, **183:** 309–330.
3. de Borst, R., Sadowski, T., *Lecture notes on composite materials*, Springer Netherlands, 2008, pp. 38-73
4. Corigliano, A., Formulation, identification and use of interface models in the numerical analysis of composite delamination. *International Journal of Solids and Structures*, 1993, **30:** 2779–2811.
5. Schellekens, J.C.J., de Borst, R., Free edge delamination in carbon-epoxy laminates: a novel numerical/experimental approach. *Composite Structures*, 1994a, **28:** 357–373.
6. Alfano, G., Crisfield, M.A., Finite element interface models for the delamination analysis of laminated composites: mechanical and computational issues. *International Journal for Numerical Methods in Engineering*, 2001, **50:** 1701–1736.
7. Schipperen, J.H.A., Lingen, F.J., Validation of two–dimensional calculations of free edge delamination in laminated composites. *Composite Structures*, 1999, **45:** 233–240.

8. de Borst, R., Fracture in quasi-brittle materials – a review of continuum damage-based approach. *Engineering Fracture Mechanics*, 2002, **69**: 95–112.
9. Elices, M., Guinea, G.V., Gomez, J., Planas, J., The cohesive zone model: Advantages, limitations and challenges. *Engineering Fracture Mechanics*, 2002, **69:** 137–163.
10. Wei, Y., Hutchinson, J.W., Interface strength, work of adhesion and plasticity in the peel test. *International Journal of Fracture*, 1997, **93:** 315–333.
11. Thouless, M.D., Yang, Q.D., Measurement and analysis of the fracture properties of adhesive joints. In: *The Mechanics of Adhesion*. (edited by D.A. Dillard, A.V. Pocious and M. Chaudhury) Elsevier Science, Amsterdam, 2001, pp. 235–271.
12. Tvergaard, V., Hutchinson, J.W., On the toughness of ductile adhesive joints. *Journal of the Mechanics and Physics of Solids*, 1996, **44**: 789–800.
13. Needleman, A., Rosakis, A.J., The effect of bond strength and loading rate on the conditions of governing the attainment of intersonic crack growth along interfaces. *Journal of the Mechanics and Physics of Solids*, 1999, **47**: 2411–2445.
14. Corigliano, A., Formulation, identification and use of interface models in the numerical analysis of composite delamination. *International Journal of Solids and Structures*, 1993, **30:** 2779–2811.
15. de Borst, R., Numerical aspects cohesive-zone models. *Engineering Fracture Mechanics*, 2003, **70**: 1743–1757.
16. de Borst, R. Remmers, J.J.C., Needleman, A., *Computational aspects of cohesive-zone models.15th European Conference on Fracture*, Stockholm, Sweden: European Structural Integrity Society, 2004.
17. Yang, Q., Cox, B., Cohesive models for damage evolution in laminated composites. *International Journal of Fracture,* 2005, **133**: 107-137.
18. Zhou, Z.-Q., Yang, Q.-D., Chen, W.-Q., On the fracture resistance of adhesively jointing structures. *Journal of Zhejiang University SCIENCEA,* 2006, **7(8)**: 1289-1295.
19. Barenblatt, G.I., The mathematical theory of equilibrium cracks in brittle fracture. *Advanced Applied Mechanics*, 1962, **7**: 55–129
20. Broedling, N.C., Hartmaier, A., Gao, H., A combined dislocation-cohesive model for fracture in a confined ductile layer. *International Journal of Fracture*, 2006, **140**: 169-181.
21. Chowdhury, S.R., Narasimhan, R., A cohesive finite element formulation for modelling fracture and delamination in solids. *Sadhana*, vol.25, part 6, 2000, pp.561-587
22. Zhou, Z.-Q., Yang, Q.-D., Chen, W.-Q., On the fracture resistance of adhesively jointing structures. *Journal of Zhejiang university SCIENCEA*, 2006, **7(8)**: 1289-1295
23. Needleman, A., An analysis of decohesion along an imperfect interface. *International Journal of Fracture*, 1990, **42**: 21-40
24. Remmers, J.J.C., de Borst, R., Needleman, A., A cohesive-segments method for the simulation of crack growth. *Computational Mechanics*, 2003, **31**: 69-77
25. Mergheim, J., Kuhl, E. and P. Steinmann, P., A hybrid discontinuous Galerkin/interface method for the computational modelling of failure. *Communications in Numerical Methods in Engineering*, 2004, **20**: 511–519
26. Wells, G.N., Garikipati, K., Molari, L., A discontinuous Galerkin formulation for a strain gradient–dependent damage model. *Computer Methods in Applied Mechanics and Engineering*, 2004, **193:** 3633–3645
27. Stan, F., Discontinuous Galerkin method for interface crack propagation. *The International Journal of Material Forming*, 2008, 1: 1127-1130

Barite Mortar with Fluid Fly Ash as Shielding Material

David Procházka[1], Dalibor Beneš[2]

[1]*Institute of Technology of Building Materials and Components, Brno University of Technology, Brno, 602 00, Czech Republic*
[2]*Institute of Technology of Building Materials and Components, Brno University of Technology, Brno, 602 00, Czech Republic*

Summary

This short article handles about the possibility of utilization of the fluid fly ashes in shielding materials. Because fluid fly ash is a waste and is being produced in large quantity, there is searched for alternatives in its usage. One of possible ways is e.g. its admixing into building materials. This is possible mainly due to chemical composition similarity between fly ash and some building materials. Scores of the time the fly ash is being added to the binder. In this work the fly ash was admixed to calcium hydrate and the resulting mixture was then used as a binder. But firstly it was necessary to ascertain chemical composition of the fluid fly ash and then to compute appropriate relation fly ash:calcium hydrate. After it, the designed binder was used into shielding mortar, which was subsequently tested on X-rays.

KEYWORDS: barite mortar, ionizing radiation shielding

1. INTRODUCTION

Loading of the environment by the human being is big problem todays. The major polluter is still energetic industry, especially burn coal power plants. About 80 % of solid combustion products makes the fly ash. The world-wide ash production (fly ash and bottom ash) is estimated to about 500 Mt/year [1, 2, 3]. The largest producers are China, USA, Russian Federation, India [4]. The most frequent treatment is the waste disposal. But that is discriminating for appropriation of land. But there is also the possibility to add the ash into hydraulic binders, because of its pozzolanic properties (it depends on combustible and burning process quality). Furthermore it can be used as a filler in concrete, e.g. for high performance concrete production. But always it is necessary to watch for its chemical and mineralogical composition. Together with mentioned, there is searched for another exploitation ways. In this paper the ash was tested in a shielding matter.

2. FLUID FLY ASH

For purposes of this work it was used the fluid ash from Hodonín power plant in Czech Republic. As a fuel there is being used lignite (young solid fossil fuel with low heating power). The power plant produces filter ash (granulity 0 – 0,7 mm), dry bed ash (granulity 0 – 1,9 mm) and a stabilisate (mixture of filter ash, bed ash and batch water – it is in point of fact ash mortar; granulity 0,036 – 1,8 mm; it can not be stored). The annual yield of entire ash matter reaches to circa 100 000 tonnes. The price depends on the taken quantity and makes 5 – 30 Kč/t (0,2 – 1,1 euro/t) [5]. The ash attributes determined by the power plant are in the table 1 and 2.

Table 1. Ash matter – Hodonín power plant

		Bed Ash	Filter Ash	Stabilisate
Assesment	Unit		Value	
Ash matter	%	2,70	4,76	3,24
Apparent Density	$kg \cdot m^{-3}$	1014	638	-
Specific Weight	$kg \cdot m^{-3}$	-	2568	-
Total Sulphur Content	%	4,30	4,46	2,30
Specific Activity ^{226}Ra	$Bq \cdot kg^{-1}$	71	163	-
SiO_2	%	28,80	29,00	-
AL_2O_3	%	12,90	14,90	-
CaO	%	26,40	23,00	5,58
K_2O	%	0,58	0,58	-
SO_4	%	-	-	11,69
CO_2	%	-	-	3,82

Table 2. Hodonín ash chemical analysis

Oxid [%]	Filter Ash	Bed Ash
SO_3	7,840	13,400
P_2O_5	0,341	0,142
SiO_2	31,600	30,400
MnO	0,103	0,048
Fe_2O_3	6,640	3,590
MgO	3,720	1,990
Al_2O_3	17,000	13,900
TiO_2	0,541	0,467
CaO	29,400	32,900
Na_2O	0,326	0,258
K_2O	1,170	1,020

Next to the chemical analysis there was done RTG analysis too (see Figure 1,2).
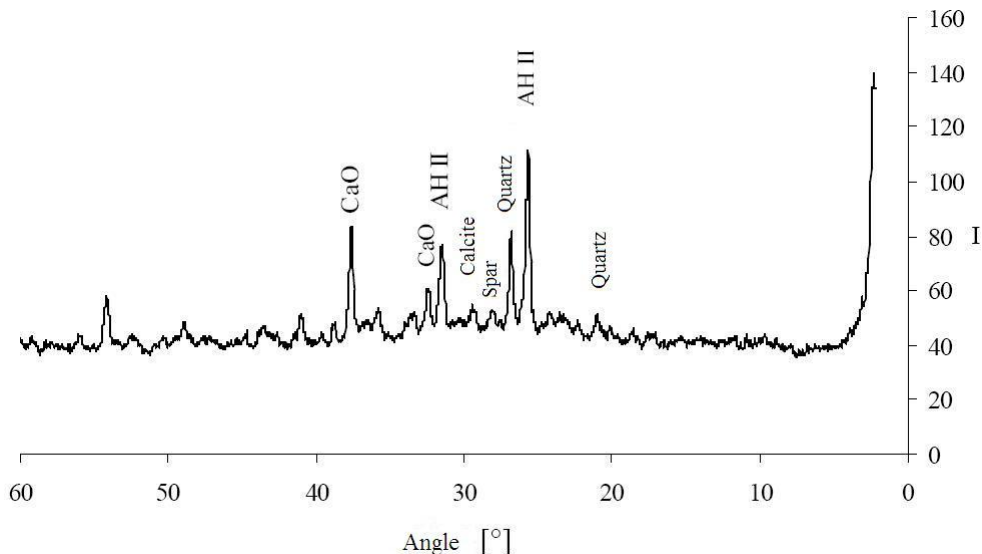
Figure 1. Hodonín filter ash RTG
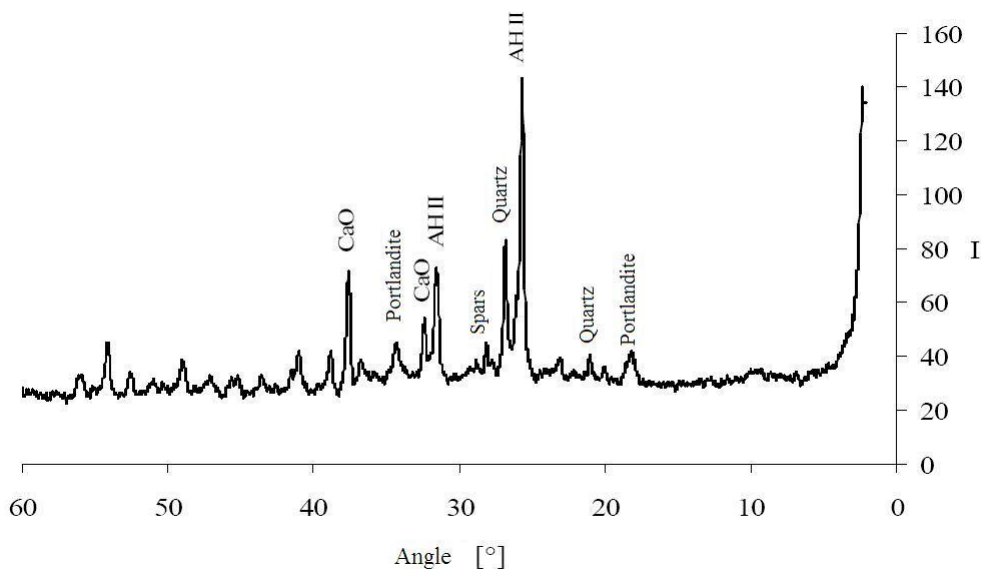
Figure 2. Hodonín bed ash RTG

From the tables 1 and 2 it is evident, that both types of ash are not too different. Because of relative high CaO content, it can be presumed on higher calcite dosage.

As regards to the mineralogy there were identified quartz and spar as rests of combustion, next anhydrite II and calcite as desulfphatation products. After the ash properties verification it was approached to the blended binder design.

3. BLENDED BINDER DESIGN

The blended binder was designed as ash and calcium hydrate mixture according to hydraulic modulus on 1,0 value.

$$M_H = \frac{[CaO]}{[SiO_2] + [Al_2O_3] + [Fe_2O_3]}$$ [-]   (1)

M_H ... hydraulic modulus. It is relation of mass fragments of single hydraulic oxides. The 1,0 value signifies high hydraulic binder.

The dosage relation of ash and calcium hydrate was computed just at this modulus, see table 3.

Table 3. Mixing relation between ash and calcium hydrate

Parameter	Filter Ash	Bed Ash
Ash Content [%]	61,5	61,5
Calcium Hydrate Content [%]	38,5	38,5
Hydraulic Modulus	1,03	0,92
Ash : Calcium Hydrate	1 : 0,625	1 : 0,625

From both ashes and from the calcium hydrate were then prepared trial mixes and proven on shrinkage and strengths. Both mixtures characteristics were nearer more likely to hydraulic binders than to the aerial binders. Even if he had lower strenght values, for research purposes it was used the filter fly ash.

4. SHIELDING MIXTURE DESIGN

At the design it was resulted from already known formula for cement mortar (see Computational Civil Engineering 2008), which was shown itself as viable. As a filler it was used the barite dust. On the ground of its different granulity first several designs were unsatisfactory in comparison with previously used aggregate. The final composition determines table 4.

Table 4. Blended mortar composition

Parameter		Value
Composition [%]	blended binder	12
	barite dust 0-0,063 mm	88
	admixture B	1
	admixture F	0,12
Dry mass Volume weight of the dry mixture in shaked state [kg·m^{-3}]		2 760
Water-cement ratio [-]		0,45
Bulk density of concrete [kg·m^{-3}]	fresh mixture	3 040
	after 28 days of maturing	3 100

After the design it was approached to the testing of technological properties (standardly on prisms 40 x 40 x 160 mm), see table 5.

Table 5. Technological properties

Parameter		Value
Water-cement ratio [-]		0,45
Bending tensile strength [MPa]	after 1 day	0,7
	after 28 days	1,9
Compression strength [MPa]	after 1 day	4,1
	after 28 days	13,3

Relatively low strength values are given by high dose of too fine aggregate – the baryte dusts. The strength values could be possible heigthen e.g. by addition of coarse aggregate and using of superplasticizer. After strength parameters verification it was approached to the final phase of the project – to the findings of shielding abilities.

5. THE SHIELDING PROPERTIES

The ability to shield the ionizing X-ray radiation was checked on tablets 10, 20 ,30, 40, 50 mm and compared with referential lead tablets. The radiaton intensity increased gradually. The results are shown in table 6 and in the figure 3.

Table 6. Shielding ability of barite tablets with blended binder

Voltage U [kV]	Dose rate D [pGy/s]				
	Slab 10 mm	Slab 20 mm	Slab 30 mm	Slab 40 mm	Slab 50 mm
60	18 200	70	48	39	31
80	122 000	240	67	61	56
100	762 000	8 950	791	173	144
135	4 340 000	530 000	80 300	12 700	2 520
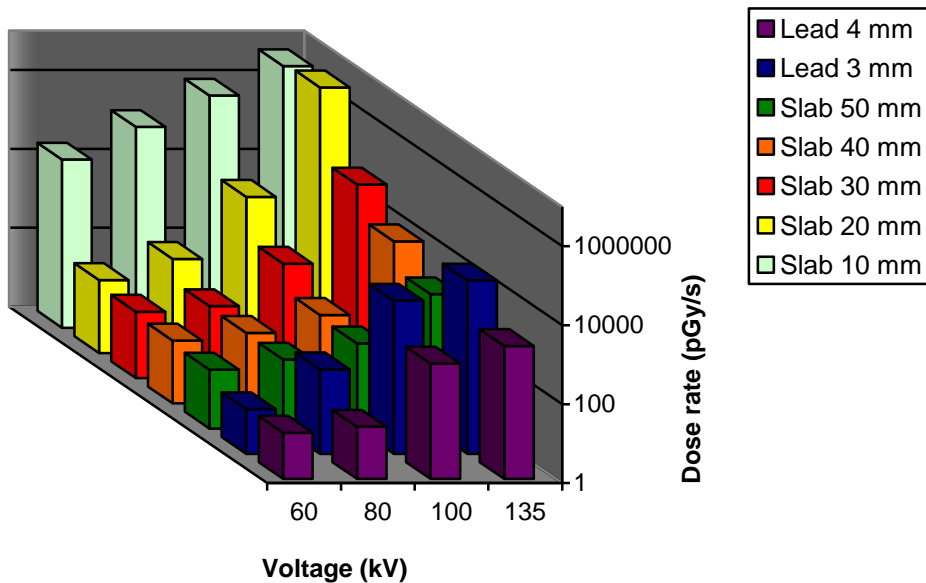
Figure 3. Shielding comparison of barite dust slabs and lead (logarithmic scale)

From the graph it is evident that shielding ability of the barite mixture equalizes to the shielding of 4 mm lead at 50 mm of its own thickness. It is difference around one order. When compared the barite mixture volume weight with the lead density, it is clear that thicker lead must shield more. Seeing that dose input growth exponentially with higher intensity, it is clear that the needed shielding material thickness will be not higher about multiple of density rates, but will increase exponentially too.

CONCLUSION

The performed tests have shown applicability of waste ashes even in so problematic sphere as the ionizing radiation shielding is. Though the ash alone do not administrates to the shielding, the barite is the shielder, he is usable as a bonding component.

Low strength values predestinates the mixture more likely to nonbearing purposes. Yet it is possible to heighten them through formula optimalization and by using of superplasticizer.

If would be compared the shielding of barite dust with blended binder on the one hand and barite sand with cement binder on the other hand (see [6]), the shielding will be higher in case of barite sand say on the ground of higher volume weight. When it is wanted to reach better shielding, the mixture of cement and sand is more suitable to use. On the other side, when there is need to save money, it is possible to use mortar with the barite dusts and blended binder.

Acknowledgements

References

1. Goumans, J. J., van der Sloot, H. A., Aalbers, Th. G., Environmental Aspects of Construction with Waste Materials: *Proceeding[s] of the International Conference on Environmental Implications of Construction Materials and Technology Developments, Maastricht, the Netherlands, 1-3 June 1994, Elsevier Publishing Company, ISBN: 0444818537.*
2. Feuerborn, H.-J., Coal ash utilisation over the world and in Europe, *Workshop on Environmental and Health Aspects of Coal Ash Utilization*, Tel-Aviv, 2005.
3. Reijnders, L., Disposal, uses and treatments of combustion ashes: a review, in: *Resources Conservation and Recycling*, vol. 43, Issue 3, 2005, p. 313-336.
4. Joshi, R. C., Fly ash in concrete: production, properties and uses, Taylor & Francis, 1997, ISBN: 9056995804.
5. *CEZ Hodonín.* [online]. Beton Server – Beton , vše z betonu a vše pro beton v ČR. [cit. 2009-04-20] URL: <http://www.betonserver.cz/cez-hodonin>. (in czech)
6. Procházka, D., Beneš, D. Gamma Radiation Shielding. *Computational Civil Engineering 2008.* Iaşi, România.

Development of core plaster on base fluid fly ash

Dalibor Beneš[1]

[1] *Brno University of Technology, Faculty of Civil Engineering, Department of Technology of Building Materials and Components, Czech Republic*

Summary

This work was expected to examinate the potentialities of fluid fly ashes utilization as hydraulic bonding material in preparation of dry mortar mixtures or more precisely, to examinate presumed potential hydraulic capacities of fluid fly ashes that have been theoretically assumed on the basis of its chemical-mineralogical composition. Tendency work was problems uses of fluid fly ashes at prepare core plaster on base fluid fly ash.

KEYWORDS: fluid fly ash, core plaster

1. INTRODUCTION

This work was expected on development the core plaster on base bind of hydraulic in form dry mortar mixtures. The basic recipes have been design so that: 20 per cent blended hydraulic binder, 80 per cent crushed sand. The blended hydraulic binder was design for three varies batching of fluid fly ash, thus:

– One of weight ratio fluid fly ash plus 1,25 weight ratio of hydrate, in the text as 1,25F

– One of weight ratio fluid fly ash plus 1 weight ratio of hydrate, in the text as 1F

– One of weight ratio fluid fly ash plus 0,83 weight ratio of hydrate, in the text as 0,83F

Like the specimen of reference binder, have been applying mix one of weight ratio of hydrate Mokrá CL 90 and one of weight ratio the Portland cement I 42,5R Rohožník. It was done with 20 per cent weight of dry plaster mix.

– The specimens was testing on technology exams:

– Workable of fresh mortar (diameter range $150 \pm$ mm)

– Assessment of strength in compression and bending tension for time of hydration 3, 7, 14, a 28 days in condition saturate the water vapor

– Assesment of holding to base after 28 days.

Also were assesment watchnig properies of application, namely:

– real demand of water

– time of stupor of core plaster

– stress crak

2. COMPOSION OF DRY MORTARY MIX

Composition of dry mortary mix is show in the consequent tables.

Table 1: Sieve analysis of used fraction

Sieve	fraction 0-0,7 mm	fraction 0,7-1,2 mm	fraction 1,2-2 mm
2	100,0	100	99,2
1,6	100,0	100	90,8
1,25	100,0	100	55,6
1	100,0	99,8	23,6
0,8	100,0	67,2	2,4
0,63	100,0	28,8	0,8
0,315	91,4	1,4	0,4
0,125	70,5	0,6	0,2
0,063	46,4	0,2	0

Table 2: Content of single compounds

Component	Content of component
Binder	20%
Fraction sand 0-0,7mm	25%
Fraction sand 0,7 – 1,2 mm	30%
Fraction sand 1,2 – 2 mm	25%

3. TECHNOLOGIC PROPERTIES

Table 3 including information about technologic properties.

Table 3: Technologic properties of dry mortary mix

Composition of binder/ trace properties		Indication of specimens			
		REF	1,25F	1F	0,83F
PC 42,5 R	[%]	10	11	10	9
Lime hydrate	[%]	10	11	10	9
Fluid fly ash	[%]	0	9	10	11
Norm consistence w*	[-]	0,23	0,26	0,26	0,24
The Strength in [MPa] Compression :					
3 day		1,8	0,5	0,5	0,6
7 days		2,6	1,4	1,8	2,1
14 days		3,0	2,5	3,4	3,1
28 days		3,5	3,1	4,3	4,2
Tensile:					
3 day		1,0	0,5	0,4	0,4
7 days		1,4	0,7	0,9	1,3
14 days		1,4	0,8	1,6	1,8
28 days		1,9	1,5	2,1	2,4
Density [kg/m^3]					
3 day		1980	1910	1930	1890
7 days		1970	1900	1920	1880

* $w = \dfrac{V}{SMS}$ SMS – weight of dry mortary mix   V – weight water

From out comparing of technologic properties of specimen of dry mortar mix resulted that owing to increase of fine shares particle have done to slightly increase the water.

4. APPLICATION PROPERTIES

Bulletin of application properties present table 4.

Table 4: Application properties of specimen plaster

Composition of binder/ trace properties		Indication of specimens			
		REF	1,25F	1F	0,83F
PC 42,5 R	[%]	10	11	10	9
Lime hydrate	[%]	10	11	10	9
Fluid fly ash	[%]	0	9	10	11
Norm consistence w*	[-]	0,23	0,26	0,26	0,24
Time of stupor of core plaster [min]		0:8	0:7	0:10	0:10
Holding to area 7 days [MPa]		0,80	0.15	0,10	0,17
Landing		excellently	excellently	excellently	excellently
Grip		excellently	excellently	excellently	excellently
Creation of rips		finer rips	thicker rips	thicker rips	finer rips

$* \ w = \dfrac{V}{SMS}$ SMS – weight of dry mortary mix   V – weight water

Increase part of fine particle is partly negative express on texture show plaster witch have showed till 24 hours from application finer rips, but unambiguously visible rips, see picture 1. For illustrative were with timing relationship the one year evaluation also plaster prepare at the midyear 2007, which they had similar with have been testing specimens same composition of binder and a very similar composition of extender, see picture 2.

Fig. No. 1: Photo of specimen core plaster

a) Specimen of plaster of referential

b) Specimen of plaster 1,25 F

c) Specimen of plaster 1F

d) Specimen of plaster 0,83 F

Fig. No. 2: Photo of specimen core plaster

a) Specimen of plaster 1,25F year 2007   b) Specimen of plaster 0,83F year 2007
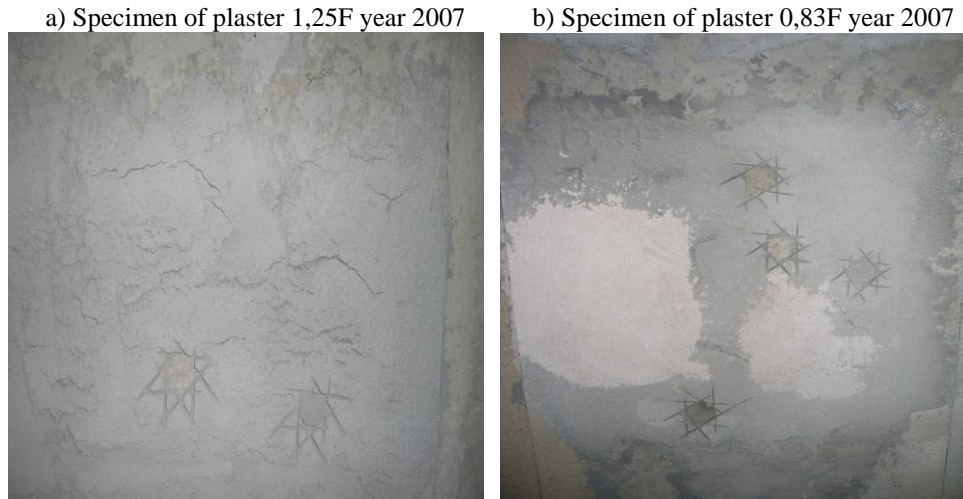
5. CONCLUSION

Plasters preparing for oh these design embody common good technologic properties whereas the best of specimen was with indication 0,83F i.e.: one of weight ratio the fluid fly ash plus 0,83 weight ratio of hydrate. So in the case all testing plasters reach up of strength in compression up to 3MPa till 5MPa, and so may be without problem include in class CS II up until CS IV. These plasters they are have very good technologic properties and simultaneously obtain very good application abilities.

And the conclusion be to say, that depending mix hydraulic lime so present smooth a replacement classic the lime-cement binder attached of industry fabrication dry mortar mixture. This will brought not only economic favoured for the maker, but also will help even cut to up to date ecological load.

Acknowledgements

References

1. CSN 196-1 Methods of testing cement – part 1: Determination of strength
2. VAVŘÍN F.: Mortary, Brno University of Technology, Praha 1980 (in Czech).
3. Drochytka, R. et al., Progressive Building Materials with Utilization of Secondary Raw Materials and Impact thereof on Structures Durability, Brno University of Technology, Final report to MSM Project 0021630511, Brno, 2007 (In Czech)

Numerical simulation of exhaust smoke and hot gases processes in fire for areas/buildings with complex geometry

Dragoş Roşu[1], Dan Diaconu-Şotropa[2]

[1]Faculty of Civil Engineering, "Gh. Asachi" Technical University, Iasi, 700050, Romania
[2] Faculty of Civil Engineering, "Gh. Asachi" Technical University, Iasi, 700050, Romania

Summary

Since the early twentieth century, specialists have conducted experiments over various types of buildings in order to analyse the behaviour during fires. Initially, first tests were carried out on real size models. Over time, these tests became difficult, even impossible, because of increasing complexity of buildings. The explosive evolution of Computer Science field has allowed the development of new software tools for simulation of fire process, generally and also for buildings.

At the beginning of 2000, NIST (National Institute of Standards and Technology – USA) in partnership with some public and private organization from USA and Europe has released an „open source" software, called Fire Dynamic Simulator (FDS), in order to build a computational fluid dynamics (CFD) model of fire-driven fluid flow (heat, smoke emission, hot gases etc.).

This work paper presents a FDS fire simulation for a building with multiple functions/purposes and, also presents the observations based on the analysis of fire expansion in different scenarios.

KEYWORDS: smoke and hot gases evacuation, numerical simulation, FDS, fire, building, parking.

1. INTRODUCTION

Fire safety objective is a major issue during all steps of buildings development starting with designing, execution and continuing with its exploitation. Main standpoints of fires safety are: building stability evaluation for a specified time period; avoidance of initiation and expansion of fire, smoke and hot gases inside the building; limitation of spread fire to adjacent areas; appropriate ways to provide occupants with essential assistance to reach a place of safety or to be rescue; safety for emergency forces.

A very important effect of fire is the emission of heat, smoke and hot gases. Practically, this is demonstrated by the larger number of victims with intoxication than number of victims with fatal burns.

The term complex building refers to high and very high buildings, halls with high capacity (such as conference hall), for various destinations, airports, commercial areas, large spaces for production and storage etc. Also the buildings with underground parking are complex building.

Present work paper, is determined by the impressive increase of the number of investment projects for complex buildings with parking developed in the last years, both international and national level. Fires in these areas are defined by massive emission of heat and smoke, which can expand inside and/or on the front side of building, at the superior levels or to adjacent constructions.

2. NUMERICAL SIMULATION OF SMOKE AND HOT GASES EXHAUST PROCESS

Generally speaking if we consider a building as a system (a set of material elements, human and/or information related to a relationship of interdependence, in a given environment, which meet one or more function specified for ensuring the adequate conditions for conducting one or more activity) then the computing model of system is a representation, in simplified manner, which can provide information (with small precision) about the behaviour of an real system. Numerical simulation of a process conducted in a system often implies, a laborious iterative calculation, performed by specialized computer programs, at the pre-processing entry data and post-processing of results. From the mathematical model is generated a static or dynamic graphical representation (virtual scene), as a powerful tool for analysis.

2.1 Dedicated software for fire modelling and simulations

At this moment, in entire worlds, has been developed a great number of software applications built to analyse the fire as a complex phenomenon, a self-maintained burning with heat transfer, flames and smoke. Now in the scientific domain there is various software specialised in numerical fire simulations which can compute and establish the path smoke and hot gases emissions.

2.1.1. ALOFT-FT^{TM} (A Large Outdoor Fire plume Trajectory model - Flat Terrain)

A computer based model to predict the downwind distribution of smoke particulate and combustion products from large outdoor fires. Measurements and observations at experimental fires have shown that the downwind distribution of smoke is a

complex function of the fire parameters, meteorological conditions and topographic features. To incorporate these features, NIST has developed a fire plume trajectory model that solves the fundamental fluid dynamic equations for the smoke plume and its surroundings. ALOFT-FT is the public domain version of the model for flat terrain using windows based personal computers.

2.1.2 ASET-B (Available Safe Egress Time - BASIC)

A program for calculating the temperature and position of the hot smoke layer in a single room with closed doors and windows. ASET-B is a compact easy to run program which solves the same equations as ASET. The required program inputs are a heat loss fraction, the height of the fire, the room ceiling height, the room floor area, the maximum time for the simulation, and the rate of heat release of the fire. The program outputs are the temperature and thickness of the hot smoke layer as a function of time. ASET-B was written in BASIC by W.D. Walton.

2.1.3 BREAK 1(Available Safe Egress Time - BASIC)

BREAK 1 (Berkeley Algorithm for Breaking Window Glass in a Compartment Fire) is a program which calculates the temperature history of a glass window exposed to user described fire conditions. The calculations are stopped when the glass breaks. The inputs required are the glass thermal conductivity, thermal diffusivity, absorption length, breaking stress, Young's modulus, thermal coefficient of linear expansion, thickness, emissivity, shading thickness, half-width of window, the ambient temperature, numerical parameters and the time histories of flame radiation from the fire, hot layer temperature and emissivity, and heat transfer coefficients. The outputs are temperature history of the glass normal to the glass surface, and the window breakage time. BREAK1 was written in FORTRAN.

2.1.4 CFAST

CFAST is a two-zone fire model used to calculate the evolving distribution of smoke, fire gases and temperature throughout compartments of a building during a fire. These can range from very small containment vessels, on the order of $1m^3$ to large spaces on the order of $1000 \ m^3$.

2.1.5 FPETool

FPETool is a set of engineering equations useful in estimating potential fire hazard and the response of the space and fire protection systems to the developing hazard. This software incorporates an estimate of smoke conditions developing within a room receiving steady-state smoke leakage from an adjacent space. Estimates of human viability resulting from exposure to developing conditions within the room are calculated based upon the smoke temperature and toxicity.

2.2 Fire Dynamics Simulator (FDS)

The software described in this document, Fire Dynamics Simulator (FDS), is a computational fluid dynamics (CFD) model of fire-driven fluid flow. FDS solves numerically a form of the Navier-Stokes equations appropriate for low-speed, thermally-driven flow with an emphasis on smoke and heat transport from fires. FDS is a computer program written in Fortran programming language that reads input data, computes a numerical solution for the governing equations and write its return output data to files. The FDS output files are read by Smokeview, a companion program that produces graphical representations on the computer screen.[2]

The partial derivatives of the conservation equations of mass, momentum and energy are approximated as finite differences, and the solution is updated in time on a three-dimensional, rectilinear grid. Thermal radiation is computed using a finite volume technique on the same grid as the flow solver. The major components of FDS in a brief description are:

Hydrodynamic Model: FDS solves numerically a form of the Navier-Stokes equations appropriate for low-speed, thermally-driven flow with an emphasis on smoke and heat transport from fires;

Combustion Model: For most applications, FDS uses a combustion model based on the mixture fraction concept. The mixture fraction is a conserved scalar quantity that is defined as the fraction of gas at a given point in the flow field that originates as fuel. The reaction of fuel and oxygen is not necessarily instantaneous and complete, and there are several optional schemes that are designed to predict the extent of combustion in under-ventilated spaces;

Radiation Transport: Radiative heat transfer is included in the model via the solution of the radiation transport equation for a gray gas. In a limited number of cases, a wide band model can be used in place of the gray gas model to provide a better spectral accuracy. The radiation equation is solved using a technique similar to a finite volume method for convective transport, thus the name given to it is the Finite Volume Method (FVM). Water droplets can absorb and scatter thermal radiation;

Geometry: FDS approximates the governing equations on one or more rectilinear grids. The user prescribes rectangular obstructions that are forced to conform with the underlying grid;

Boundary Conditions: All solid surfaces are assigned thermal boundary conditions, plus information about the burning behaviour of the material;

Sprinklers and Detectors: The activation of sprinklers and heat and smoke detectors is modelled using fairly simple correlations of thermal inertia for sprinklers and heat detectors, and transport lag for smoke detectors. Sprinkler

sprays are modelled by Lagrangian particles that represent a sampling of the water droplets ejected from the sprinkler. [2]

2.3 FDS fire modelling

The subject of this work paper is to simulate a fire in a complex building developed on three levels, with a public parking at the first level and offices and residential flats at the other two levels. Fire is initiated in a car parked at the semi-basement of building. Principal characteristics of this type of fire are high emission of heat, smoke and hot gases. This FDS simulation will allow us to analyse their expansion outside and on principal front of building through the access car opening.
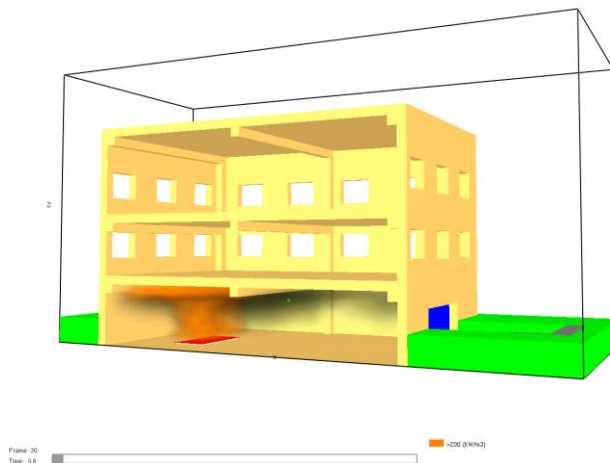
Figure 1.a. Fire point

The building model chosen for simulation is shown in figure 1. The goal of experiment is to analyse the influence of an opening for car access to parking space in the semi-basement of building during a fire. Figure 1 illustrates the forming smoke layer under parking ceiling. [1], [5]
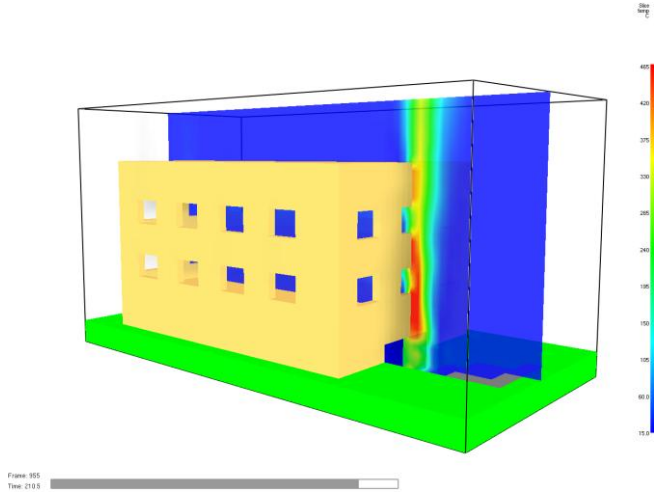
Figure 2. Registered temperatures on longitudinal section

Figure 2 illustrate clearly the spreading on the principal front, of hot gases with temperatures that exceed 450^{0}C. This phenomenon creates favourable conditions for an easily extending of fire through windows from levels above fire-room. [1]
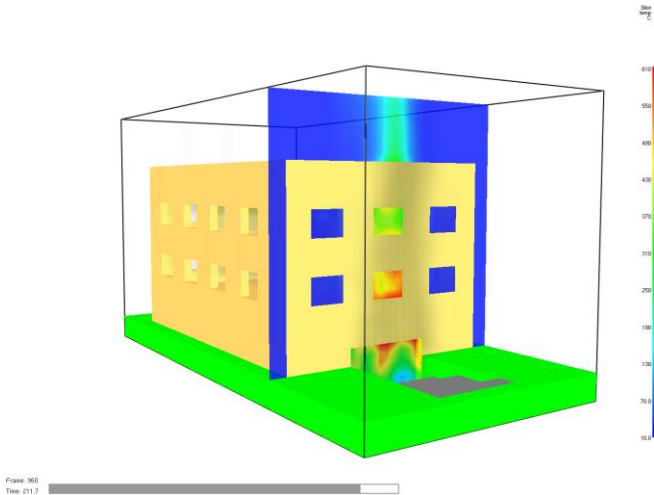
Figure 3. Temperatures –principal front

Highest temperatures are registered on the principal front, especially over opening from the fire-room (see figure 3) and that is the reason why the above first level is the most affected. [1]
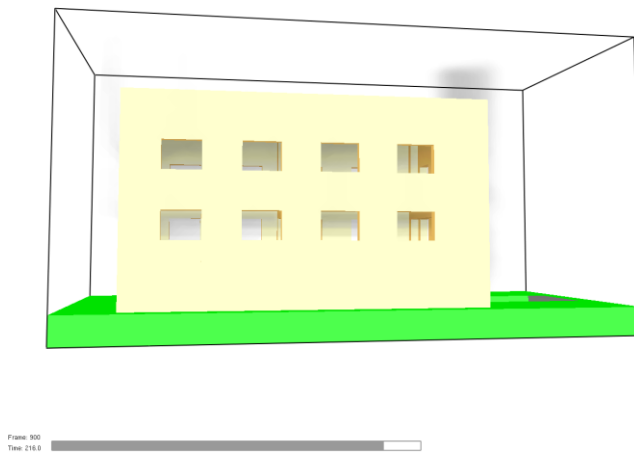
Figure 4. Smoke invasion

In figure 4 the upper levels of building are filled with smoke because the spill plume has became adherent on wall. [1]
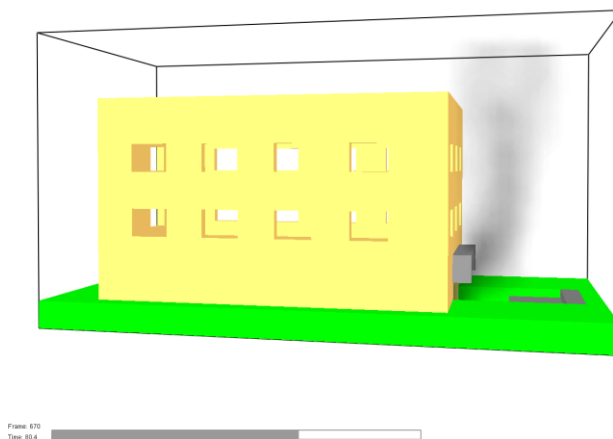
Figure 5. Smoke evacuation for a building with canopy

To remove the adherence characteristic of spill plume the opening from the fire-room was redesigned with a canopy – a concrete element mounted over the opening car access. This, as noted in figure 5, remove the spill plume from the building wall.[1]
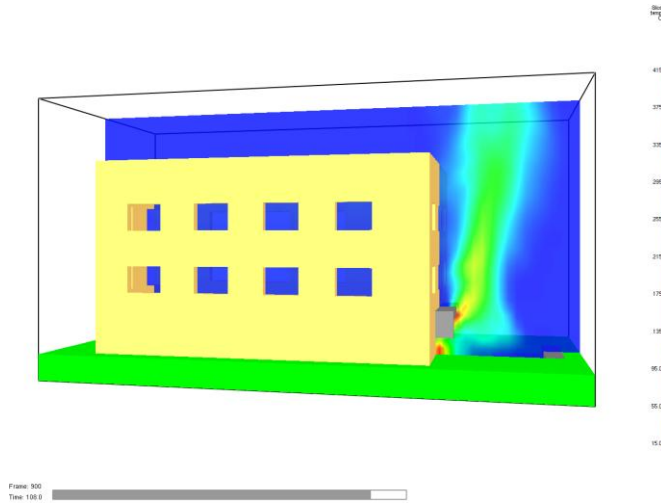
Figure 6. Registered temperatures on longitudinal section of a building with canopy

Figure 6 illustrates that the temperatures of spill plume have not exceeded 300^0C. This time the spill plume has not adhered on the building wall. [1]
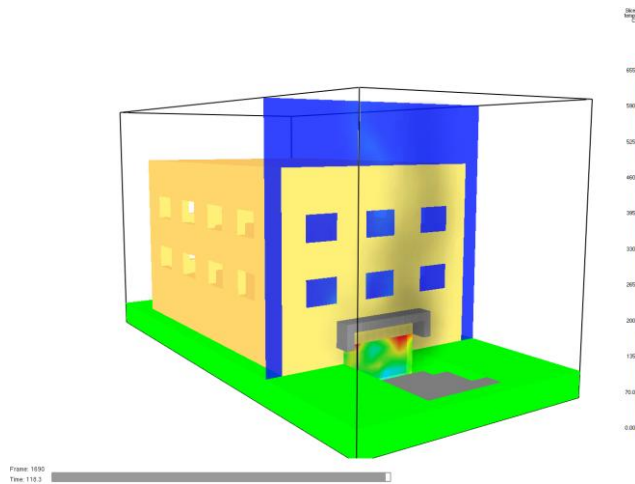
Figura 7. Temperatures –principal front for a building with canopy

On the principal front of building, see figure 7, there are not recorded significant increases in temperature. [1]
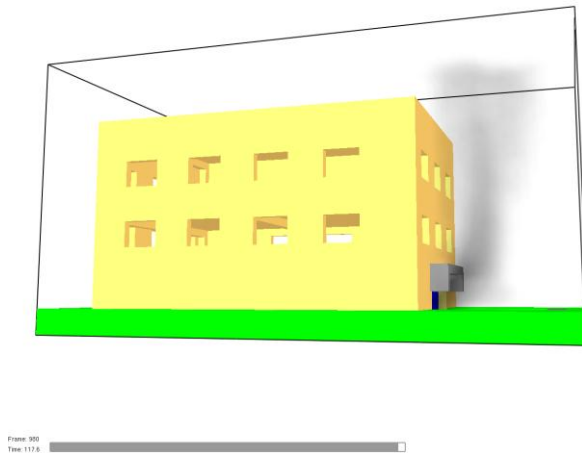
Figure 8. Smoke invasion avoidance

Very important to note is that higher levels of building have not been flooded with smoke. The geometry of canopy may be modified, but its influence over the movement and direction of smoke and hot gases released by fire becomes obviously.[1]

3. CONCLUSIONS

Smoke and hot gases emissions released by the fire represent a particular problem and it may increase due combustible elements used in thermal insulation of buildings (such as polystyrene).

The solution of this problem is routing the spill plume, smoke and thermal flow, so that the upper compartments/levels of building will not be affected. Geometry and dimensions of canopies affect in an essential manner the routing of smoke and hot gases far away from building walls.

Another possible solution would be that higher levels of building above the opening fire-room will not be designed with windows, but unfortunately this solution depends on the purposes of spaces from these levels.

References

1. Forney, G.P., *User's Guide for Smokeview Version 5 – A Tool for Visualizing fire Dynamics Simulation Data*, NIST Special Publication 1017-1, January 2008.
2. McGrattan, K., Hostikka, S., Floyd J, Baum, H., Rehm, R., *Fire Dynamics simulator (Version 5) Technical Reference Guide*, NIST Special Publication 1018-5, January 2008.

3. McGrattan, K., Klein, B., Hostikka, S., Floyd J, *Fire Dynamics simulator (Version 5) User's Guide*, NIST Special Publication 1019-5, January 2008.
4.   ***CEN/TR 12101-5 Smoke and heat control systems - Part 5: *Guidelines on functional recommendations and calculation methods for smoke and heat exhaust ventilation systems*, p. 30-48, 2005.
5. Drysdale, D., *An Introduction to Fire Dynamics*, Second edition, University of Edinburgh, UK, P.296-324, 2008.

Finite Element Analysis of RC beams Reinforced with Fiber Reinforced Polymers Bars

Cătălin Banu[1], Nicolae Ţăranu[2], Ruxandra Oltean[3], Ciprian Cozmanciuc[4], Oana Mihaela Ioniţă[5]

[1]*Department of Civil and Industrial Engineering, "Gh.Asachi" T.U. from Iasi, Iasi, 700050, Romania,*
banu@ce.tuiasi.ro
[2]*Department of Civil and Industrial Engineering, "Gh.Asachi" T.U. from Iasi, Iasi, 700050, Romania,*
taranu@ce.tuiasi.ro
[3]*Department of Civil and Industrial Engineering, "Gh.Asachi" T.U. from Iasi, Iasi, 700050, Romania,*
olteanr@ce.tuiasi.ro
[4]*Department of Civil and Industrial Engineering, "Gh.Asachi" T.U. from Iasi, Iasi, 700050, Romania,*
cozmaniucc@ce.tuiasi.ro
[5]*Department of Civil and Industrial Engineering, "Gh.Asachi" T.U. from Iasi, Iasi, 700050, Romania,*
ionita@ce.tuiasi.ro

Summary

Fiber reinforced polymers (FRP) have been used for many years in the aerospace and automotive industries. In the construction industry they can be used for cladding or for structural elements in a highly aggressive environment. These materials are now becoming popular mostly for the strengthening of existing structures. Fiber reinforced polymers can be convenient compared to steel for a number of reasons. There are a number of advantages in using fiber reinforced polymers. These materials have higher ultimate strength and lower density than steel.

The subject of this paper is the numerical analyses of RC structural elements. The finite element method has been chosen as a basic framework for the analyses. The main aim was to make the most effective use of the algorithms currently available for the numerical non linear analysis and to improve them, where possible, in order to reduce the number of hypothesis conditioning the results. Such results can then support the interpretation of experimental data and can be used to determine quantities that cannot be easily measured in laboratory tests.

The analysis have been carried out by using the finite element code LUSAS, widely used in both the scientific research and the design industry.

KEYWORDS: FRP materials reinforced concrete, internal reinforcement, finite element.

1. INTRODUCTION

The finite element analysis of reinforced concrete structures can be carried out using several models according to the purpose of the research and the size of the control volume relevant for the specific application. For example the analysis could be either used to calculate the deflections on the whole structure under a given loading condition or to investigate the local effects in a particular area of the structure. In the first case we can adopt a model that describes the overall stiffness of the reinforced concrete, either cracked or not, while in the second case we may find convenient to understand where the cracking will occur, how it will develop and to compute the distribution of stresses between concrete and steel and concrete and FRP. In general the overall behavior of a structure can be successfully investigated using structural elements such as beams, shells, trusses.

Their use will limit the computational onus and simplify the definition of the structure. When it comes to investigate a reduced volume from a bigger structure, solid elements combined if necessary with structural elements are more appropriate. This is the case for this analysis as the focus is on what happens within a single structural element.

The main structural material for the systems under investigation is concrete. Concrete gives a defined shape to the structural elements and the loads are, in fact, applied directly to the concrete. The standard and FRP reinforcement, although essential, are auxiliary components. Correct modeling of the nonlinear behavior of concrete is therefore essential. The mechanical behavior of concrete has been investigated worldwide and today there is a general agreement among researchers on its characteristic properties [1, 2, 3, 4, 5, 6, 7, 8, 9, 10, 11, 12]. There are models to describe almost every single mechanical property of the concrete along every kind of load path. The most sophisticated ones include elasto-plastic constitutive laws with complex hardening laws, non-associative flow-rules, post yielding softening.

However these models cannot be easily used within a finite element code and simplified models have been developed to take into account only the particular aspects relevant to each specific application.

A very important aspect in the modeling of RC beams retrofitted with FRP is the representation of the interfacial behavior between the different materials. Correct modeling of the interface FRP/concrete is necessary as slippage occurs between reinforcement and concrete. Moreover slippage is affected by cracking of concrete. To allow the cracks to open it is necessary to model relative displacements between concrete and reinforcement. This is possible by mean of special interface elements or joint elements.

2. FINTE ELEMENT MODELING OF RC BEAMS REINFORCED WITH FRP REINFORCING BARS

For a rational and safe design of any strengthening work an appropriate analysis method is required. The choice of such a method is not uniquely determined and depends largely on the purpose of the analysis. Usually in engineering simple and conservative models are sought. Simple models have two main advantages: the first one is obviously the ease of use, but engineers are also interested in having models not very sensitive to parameters difficult to determine with the required accuracy and reliability.

The intrinsic complexity of structural problems implies that simple models are possible only if strong assumptions are made. This can be done only if there are sufficiently wide experimental grounds to prove that they are acceptable. Also assuming something arbitrarily implies that the model is stripped off of all the features that are deemed not to be relevant in the calculation of the quantities of interest. This means that even though the results calculated are sufficiently accurate the model is not encompassing all the aspects of the physics of the problem and some aspects are missed out or included together with others on an empirical basis. Besides, different models are usually used to calculate different quantities belonging to the same structural element.

As an example, when we calculate the ultimate bending capacity of a section of reinforced concrete we do not bother modeling the behavior of the interface between the reinforcement bars and the concrete assuming perfect adherence. The consequences of this assumption are only taken into account limiting the failure strain of the reinforcement. If we want to calculate spacing and width of cracks we must resort to models including the bond slip behavior at the interface.

If the model is to be used for a more thorough understanding of the structural behavior of the element being analyzed or to carry out a design outside the boundaries of the experimentation validating the simplified models, some of the assumption must be removed and consequently the related aspects included realistically.

As the objective of this work is not the determination of a specific quantity but rather the understanding of how RC structures reinforced with FRP work and what should be included and what not in their analysis, complex and comprehensive models are sought.

In this paper, the modeling of FRP reinforced structures is discussed with a view to defining a model as close as possible to reality, capable of replacing or integrating laboratory testing for the investigation of the structural behavior.

In order to do so, the physical problem is described first. Subsequently the models developed are described. Details of the different features included are given.

2.1 Finite Element Modeling of Reinforced Concrete

Suitable Finite Element models are required for reinforced concrete structures. Herein an overview of typical approaches, their motivations and range of applicability is given to provide background for the adopted models. Within the framework of the finite element method reinforced concrete can be represented either by superimposition of the material models for the constituent parts (i.e., for concrete and for reinforcement), or by a constitutive law for the composite concrete and embedded reinforcement considered as a continuum at the macro level.

Because of their wider range of applicability, models of the first type are more popular.

The finite element method is well suited for superimposition of the material models for the constituent parts of a composite material. Material models of this type can be employed for virtually all kinds of reinforced concrete structures. Depending on the type of problem to be solved, concrete can be represented by solid elements, shell or plate elements, or beam elements.

The reinforcement is modeled either by separate truss or beam elements (discrete representation) or by separate elements of the same type as the concrete elements, which are superimposed on the latter (embedded representation) or by distribution of reinforcement to thin layers of equivalent thickness (distributed representation).

Superimposition of concrete and reinforcement to model reinforced concrete requires constitutive models to account for bond and dowel action on the concrete-reinforcement interface.

Discrete representation of reinforcement allows modeling of bond and dowel action by means of special elements connecting adjacent nodes of concrete and reinforcement elements. The distributed representation and the embedded representation of the reinforcement, however, do not permit the use of bond elements, because the displacements of concrete and reinforcement at the interface are presumed to be the same. Consequently, the effect of bond slip can only be accounted for implicitly by modifying the constitutive relations for concrete or reinforcement.

If reinforced concrete is modeled by a constitutive law for the composite concrete and embedded reinforcement considered as a continuum, the material behavior of reinforced concrete on the macro level is described such as if this composite material was a single material. Constitutive models of this type are essentially based on the results of experimentation on reinforced concrete panels [9], [10], [11], [5]. Since reinforced concrete is treated as a single material, neither the reinforcement nor the reinforcement-concrete interaction needs to be modeled separately. Models of this type are appropriate only if reinforcement is distributed uniformly.

2.1.1 Finite elements for concrete

a)   b)
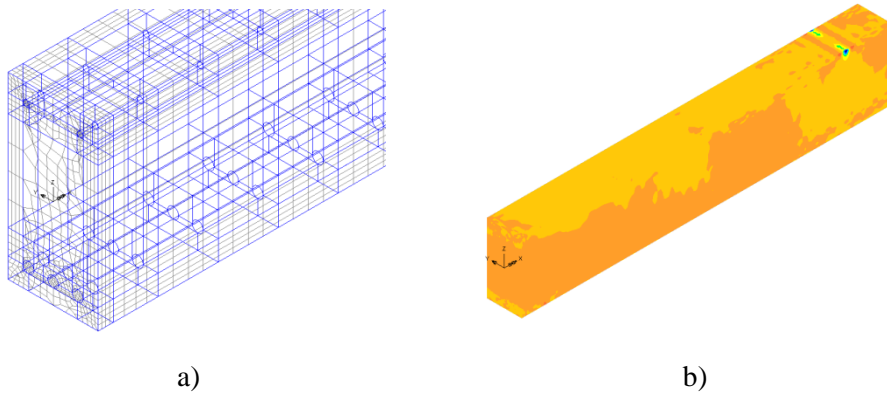
Figure 1. Concrete representation: a) concrete and reinforcement meshing, b) strain distribution in the concrete

Depending on the application a number of finite element types can be used for concrete. These elements can be continuum elements (solids) or structural elements (shells, beams). The above elements are generally of the same type used for any other material. Special mention can be made of multilayered shells or fibber beams in which nonlinear behavior of the main material and inhomogeneities are dealt with by subdividing an element into layers or fibers. Multilayered and fiber elements are not used in this work and therefore are not discussed but provide yet an alternative approach for modeling of reinforcement.

2.1.2 Representation of reinforcement

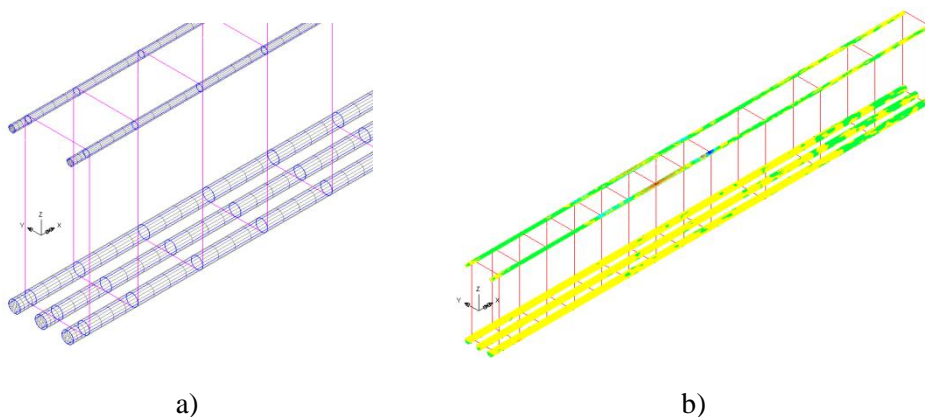a)   b)

Figure 2. Reinforcement representation: a) reinforcement meshing, b) strain distribution in the reinforcement

2.1.2.1 Discrete modeling

Discrete representation of the reinforcement is based on modeling the reinforcing bars as separate elements. Commonly, truss or cable elements are used for this purpose. However, for the investigation of structural details, occasionally two-dimensional or even three-dimensional elements are used. Truss and cable elements do not have rotational degrees of freedom and carry only axial forces.

The material behavior of truss and cable elements is described by means of the one-dimensional constitutive relations. In order to guarantee compatibility of the displacements of the concrete and reinforcement, truss and cable elements must coincide with the boundaries of the concrete elements. The node points of both types of elements must also coincide. Hence, the shape functions for the concrete elements and the truss or cable elements must be of the same order.

For instance, three-dimensional isoparametric trilinear 8-node elements and two dimensional isoparametric bilinear 4-node elements for the representation of concrete are compatible with linear 2-node truss elements for reinforcing steel. Three-dimensional isoparametric quadratic 20-node elements and two-dimensional isoparametric quadratic 8-node elements for the representation of concrete are compatible with quadratic 3- node cable elements for the reinforcing bars.

The location of the reinforcement elements is obviously determined by the layout of the reinforcement. Consequently, the boundaries of the concrete elements must follow the reinforcing bars. Thus, the layout of the reinforcement has a strong influence on the generation of the finite element mesh for a concrete structure.

Commonly, when the overall structural behavior is investigated, coinciding nodes of concrete and reinforcement elements are assigned the same degrees of freedom. Bond slip and dowel action are either disregarded or considered implicitly by modifying the constitutive relations of concrete or reinforcement. However, especially for the investigation of the behavior of structural details, it may be necessary to model bond slip and dowel action more accurately.

For this purpose, different degrees of freedom are assigned to the coinciding nodes of concrete and reinforcement elements. Special interface elements, referred to as bond or contact elements, are employed to connect the different degrees of freedom of coinciding nodes and concrete elements. Simple interface elements connect a single node of a concrete element with a single node of a reinforcement element and are often referred to as joint elements. Such elements are basically nonlinear springs.

a)

b)
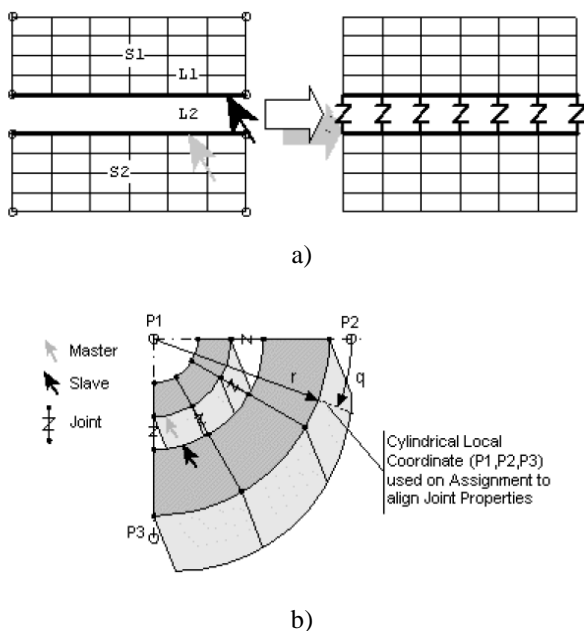
Figure 3. Interface elements: a) 2D interface element (mesh), b) 3D interface element mesh

An alternative to nodal interface elements are continuous interface elements [13]. Such elements are characterized by a continuous concrete-reinforcement interface along the entire length of the reinforcing bars. Compared with nodal interface elements, their performance is better [Keuser 1987, [14]]. Obviously discrete reinforcement elements and continuous interface elements can be combined to reinforcement-interface elements. Such elements allow modeling of the behavior of both the reinforcing bar and the interface. Moreover, if a discrete crack model is used, then the concrete to concrete interface behavior at cracks, governed by aggregate interlock can be modeled by interface elements. Interface elements are also used in this work to model the interface between FRP and concrete.

The main advantage of modeling reinforced concrete by superimposition of concrete and reinforcement elements is the relatively accurate representation of the mechanical behavior of the reinforcement and the interface. The discrete representation is the only way of accounting for bond slips and dowel action directly. Disadvantages of this approach are the great effort required for the discretization of a structure and the significant increase of the number of degrees of freedom. These disadvantages are the consequence of having to consider each reinforcing bar in the finite element mesh. Therefore, discrete modeling of the reinforcement is generally restricted to the analysis of structural details or single structural elements as beams taken in isolation from the remainder of the structure.

It is important to note, as will be recalled later on, that opening of localized cracks can be appropriately modeled only by this approach.

2.1.2.2 Embedded modeling

Separate elements for concrete and reinforcement are also used for the embedded representation. However, this representation of the reinforcement, the same type of elements with the same number of nodes and degrees of freedom and, consequently, the same shape functions are used for the concrete and reinforcement.

Hence, the embedded approach is characterized by incorporating the one-dimensional reinforcing bar into two- or three-dimensional elements Figure 4. The stiffness matrix and the internal force vector of embedded reinforcement elements only contain the contribution of reinforcement bars. They are computed by integration along the curves representing the segments of the reinforcing bars within the respective element. The embedded reinforcement elements are then superimposed on the respective concrete elements. The reinforcement bars do not have to follow the boundaries of the concrete elements. Hence, the embedded representation of the reinforcement allows generating a finite element mesh without taking much care about the layout of the reinforcement. Rather, the reinforcing bars may pass through the concrete elements in an arbitrary manner. Since the reinforcement elements and the concrete elements must be assigned the same degrees of freedom, perfect bond between concrete and reinforcement is obtained. Hence, bond slip and dowel action can only be modeled implicitly by modifying the constitutive relations for concrete or reinforcement. A disadvantage of this type of approach is that special reinforcement elements are required. Such elements may not exist in the available finite element program. Moreover, similar to the discrete approach, each reinforcing bar must be considered when preparing the input for the analysis.
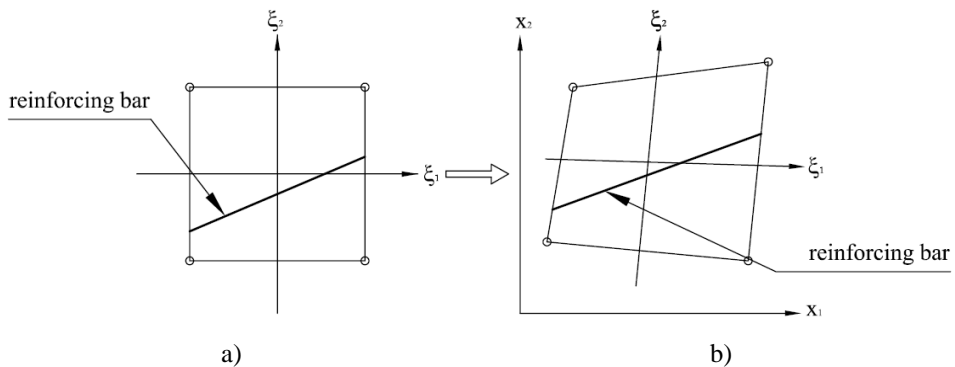

a)   b)

Figure 4. Embedded reinforcement element: a) in the local coordinate system, b) in the global Cartesian coordinate system.

2.1.2.3 Distributed modeling

The distributed modeling of the reinforcement is characterized by smearing reinforcing bars over an element that is superimposed onto the main concrete element. Accordingly, for instance, membrane elements with an eccentricity can be superimposed onto shell elements to model a layer of reinforcement.

The correct area of reinforcement along a unit length section of the structure is obtained assuming an equivalent thickness for the elements. The constitutive equation for such an element with a unidirectional layer of smeared reinforcement is generally referred to the local directions of the element which are parallel and normal to the reinforcing bars.

A combination of the distributed and the embedded representation of the reinforcement is obtained by smearing the reinforcement to thin layers, embedding the smeared layers into elements of the same type as the concrete elements and superimposing these elements on the concrete elements. This approach is convenient, for three-dimensional concrete structures with arbitrarily oriented layers of reinforcement.

Combining concrete and reinforcement within an element requires the assumption of perfect bond between the concrete and the reinforcement layers. Hence, bond slip and dowel action can only be modeled implicitly by modifying the constitutive relations of concrete or reinforcement.

Note that this approach is only appropriate for uniformly distributed reinforcing bars.

Models for consideration of interface behavior were emphasized that the discrete representation of the reinforcing bars allows explicit consideration of bond slip and dowel action by means of special interface elements.

If, on the other hand, the embedded or distributed representation is chosen for the reinforcement, then the interface behavior can only be modeled implicitly by means of appropriate modifications of the constitutive relations for concrete or reinforcement.

The implicit representation of the interface behavior is characterized by an appropriate empirical or theoretical modification of the constitutive laws for the concrete and/or the reinforcement. Especially for the analysis of relatively large structures, where the reinforcement is modeled by the embedded or distributed approach and cracking is taken into account by a smeared crack model, the implicit approach is the only possibility to model the interface behavior.

Aggregate interlock at cracks is considered implicitly by introducing a modified shear modulus into the constitutive relations for concrete. The interface behavior at concrete to reinforcement interfaces, caused by bond slip, is modeled implicitly by relating the tension stiffening effect either to concrete or to reinforcement. Hence, either the constitutive law for the concrete or the one for the reinforcement is modified appropriately.

Concrete related models for consideration of tension stiffening are more popular than reinforcement related models. In concrete related models, tension stiffening is accounted for by replacing the softening branch of the tensile stress-strain diagram for plain concrete, by the respective average stress-average strain diagram for the concrete component of reinforced concrete.

The difference between plain concrete and reinforced concrete is given by the magnitude of the ultimate strain. The values for the ultimate tensile strain of reinforced concrete reported in the literature are characterized by a large scatter. However, as a rule of thumb, the ultimate tensile strain of reinforced concrete can be taken as one order of magnitude larger than the ultimate strain of plain concrete.

If modified constitutive relations for concrete are obtained from the examination (experimental or analytical) of the behavior of a specimen reinforced only in the longitudinal direction and subjected to uniaxial tension the constitutive model must be extended to multiaxial case where cracks are not necessarily orthogonal to the reinforcement.

The simplest possible approach is to apply the modified uniaxial tensile post-peak constitutive law for the concrete to the principal directions of strain without consideration of the layout of the reinforcement.

However, since tension stiffening is caused by bond stresses between the concrete and the reinforcing bars, it is preferable that concrete-related tension stiffening models are referred to the directions of the reinforcement. This can be done considering tension stiffening as a function of the concrete strains in the direction of the reinforcing bars.

Alternatively, a reinforcement-related tension stiffening model can be employed. In this approach the residual tensile load-carrying capacity of cracked concrete is accounted for by a modified stress strain curve for the reinforcement. Consequently, the reinforcement-related tension stiffening model is a priori referred to the directions of the reinforcing bars.

In Figure 5 basic concrete-related (a) and reinforcement-related (b) tension stiffening models are reported. The model was derived on an experimental base [15, 16].

In the figure $\tilde{\varepsilon}$ denotes the average tensile strain, σ_{ts}^C is the average residual tensile stress carried by the concrete and ρ denotes the reinforcement ratio.

If the residual tensile load-carrying capacity of the cracked concrete is related to the reinforcing reinforcement, the additional stresses in the reinforcement $\Delta\sigma_{ts}^S$ is computed from σ_{ts}^C and ρ, i.e., $\Delta\sigma_{ts}^S = \sigma_{ts}^C/\rho$. Hence, the material parameters for the tension stiffening models shown in Figure 5 are σ_{ts}^C, $\tilde{\varepsilon}_{ck}$, $\tilde{\varepsilon}_{ts,A}$, $\tilde{\varepsilon}_{ts,B}$ and $\tilde{\varepsilon}_{ts,C}$.

The experimental results, on which this model is based on, indicated that the tension stiffening mainly depends on the reinforcement ratio and that is practically independent of the angle enclosed by the reinforcement and the cracks (provided the tension stiffening is evaluated in the direction of the reinforcement).

The constitutive law represented in Figure 5 relates to the uniaxial case. When it is generalized to the multiaxial case the direction of the cracks may not be orthogonal to the reinforcement. In this case the strain in the direction of the reinforcement at cracking in lower than $\tilde{\varepsilon}_{ck}$ and can even be negative. For this reason, if the tension stiffening relation above is to be applied in the direction of the reinforcement, it has been proposed to assume that after cracking the initial stress in the concrete, in the direction of the reinforcement, is σ_t^C and the linear branch is omitted. In this approach there is, therefore, a discontinuity of the stresses at the initiation of cracking.
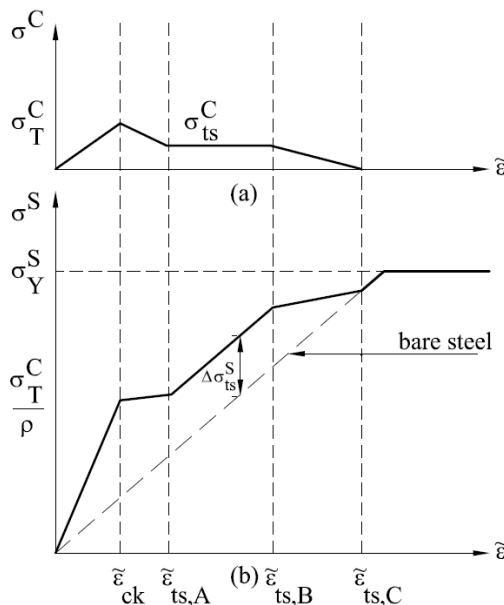
Figure 5: Modeling of tension stiffening by modifying the constitutive laws: a) for concrete, b) for reinforcement

The concrete-related model of Figure 5(a) yields almost the same structural response as the reinforcement-related model (Figure 5(b)), provided it is formulated in terms of the concrete strain in the direction of the reinforcement.

However, if the concrete related model is formulated in terms of the principal tensile strains of the concrete, the stiffening effect vanishes too early. It is also noted that in reinforcement related tension stiffening models, the compressive stresses in the concrete are somewhat overestimated. The reason for this is the neglect of the stress-carrying capacity of the cracked concrete.

The above simple model has been described to introduce the basic principles of the implicit representation of the bond slip behavior. There exist a large number of very refined models for implicit representation of bond slip that are derived on theoretical considerations and incorporated in a number of constitutive laws, proposed for reinforced concrete, featuring the smeared crack concept [5]. These refined models include also other aspects of concrete behavior like, dilatancy; aggregate interlocking, reinforcement dowel action and damage accumulation under cyclic loading. This class of models will be examined in the chapter on crack modeling but the focus will be on aspects other than bond slip behavior.

In the context of the present work, the implicit representation of the bond slip behavior has the relevant shortcoming that it cannot be effectively combined with a discrete cracking approach and it is therefore not used in the applications.

However, the method is appealing for applications to macroscale problems because interface elements do not need to be specified.

3. CONCLUSIONS

From the inspection of the results presented in this section the following conclusive remarks can be drawn:

• the proposed nonlinear numerical model of RC beams reinforced with FRP in flexure is capable of capturing many important aspects of the behavior of these structural systems, up to failure;

• cracking plays a key role in the development of the stresses at the FRP/concrete interface;

• bond-slip between concrete and reinforcement rebars is to be taken into account in order to get accurate results;

References

1. P. Menetrey and K. Willam., Triaxial failure criterion and its generalization. ACI Structural Journal, 92(3):311–317, 1995.
2. G. Etse , R.L. Willam, Fracture energy formulation for inelastic behavior of plain concrete, International journal for numerical methods in engineering ,Vol 120 No 9 1983-2011, 1994.
3. H.G. Kwak, F.C. Filippou., Finite element analysis of reinforced structures under monotonic loads, Structural engineering mechanics and materials, Report No. UCB/SEMM-90/14, Berkeley, 1990.
4. J. Lemaitre, J.L. Chaboche., Mechanics of solid materials, Cambridge University Press, 1994.
5. K. Maekawa, A. Pimanmas, H. Okamura, Non linear mechanics of reinforced concrete, Spon press, 2003.
6. J.G. Teng, W.C. Zhu,C.A. Tang., Mesomechanical model for concrete. Part I: model development, Magazine of Concrete Research, Vol.56, No.6, pp 313-330, 2004.
7. J.G. Teng, W.C. Zhu,C.A. Tang., Mesomechanical model for concrete. Part II: applications, Magazine of Concrete Research, Vol.56, No.6, pp 331-345, 2004.
8. P. Soroushian, K. Choi, and A. Alhamad., Dynamic constitutive behavior of concrete. ACI Structural Journal, 83(2):251–258, 1986.
9. F. Vecchio, M.P. Collins., The response of reinforced concrete to in plane shear and normal stress, Pubblication N. 82-03, Department of civil engineering, University of Toronto, 1982.
10. F. Vecchio, M.P. Collins., The modified compression field theory for reinforced concrete elements subjected to shear, ACI Structural Journal, Vol.3(4), pp. 219-31, 1986.
11. R.G. Selby, F. Vecchio, M.P. Collins., Analysis of reinforced concrete elements subject to shear and axial compression, ACI Structural Journal, Vol.93, No. 3, pp. 572-582, 1996.
12. K.J. Willam, E.P. Warnke, Constitutive models for triaxial behavior of concrete, Int. Ass. for Bridge and Struct. Engng., Seminar on concrete structures subjected to triaxial stresses, Paper III-01, pp. 1-30, Bergamo (Italy), 1974.
13. G. Alfano and M.A. Crisfield. Finite element interface models for the delamination analysis of laminated composites: mechanical and computational issues. International Journal for Numerical Methods in Engineering, 50(7):1701–1736, 2001.
14. M. Keuser, G. Mehlorn., Finite element models for bond problems, Journal of structural engineering, ASCE, Vol.113, No. 10, pp.2160-2173,1987.
15. J. Kolleger, G. Mehlhorn., Material Model for Cracked Reinforced Concrete, IABSE Colloquim on Computational Mechanics of Concrete Structures, Delft, 1987. Report No. 54, pp 63-74.
16. J. Kollegger, G. Mehlhorn., Material model for the analysis of reinforced concrete surface structures, Computational Mechanics, 6:341-357, 1990.

Structural Health Bridge Evaluation with Static and Dynamic Tests

Gheorghiță Boacă[1]

[1]*Facultatea de Construcţii şi Instalaţii , Universitate tehnica „Gh. Asachi" , Iaşi*

Summary

This article describes the norms in force for static and dynamic tests performed on bridge structures.

Because currently on the road began to move very large capacity vehicles and passing speed of 100 km / h, most bridges made with older than 20-30 years to be technical expert to determine they can be left in operation without a major intervention, or if possible intervention to increase bearing capacity, or need a new bridge implementation.

Attempts should be made to new bridges, with a ninth composition, special, or important bridges.

Static load that is subject to a bridge should be on a schedule set to obtain the most adverse effects.

For static tests, road convoys will travel at a speed of max. 5km / h until the characteristic positions, where they will stop and will be stationed until it stabilizes the superstructure.

For dynamic tests, the shares are given by the convoys, they must move at a constant speed. A greater impact can be achieved by creating uneven.

In order to make a comparison between the results of the test data in situ, and the results of calculations is necessary to know the values of actions requiring the bridge and their position on the bridge.

Measurements to be carried out during the tests are compared with values measured in a sleep state, the bridge is loaded with useful actions.

KEYWORDS: bridge, monitoring, test, static, dynamic, technical health

1. INTRODUCTION

Obtaining information it provides a structure such as a bridge, driven by popular uploads necessary to establish the level of service, require testing.

The results obtained from measurements during the tests, compared with the results of the calculation.

Static and dynamic tests are meant to highlight how the bridge behaves uploads acted useful to determine with greater accuracy following:

- Bearing capacity

- Structural stability

- Elastic structure

- Deformations and movements characteristic areas

- Difference from the results of calculation

Attempts should be made to new bridges, with a ninth composition, special, or important bridges.

The tests should be performed and the old bridges if:

- There is an overhaul that changed the original composition

- It would increase traffic, or traffic capacity on the route of a convoy is interposed particular

- To overcome life and need any type of restrictions

- The bridge is of economic importance and / or national high, requiring regular testing program

Actions which are used for the tests

   1.   Static testing:

- Different types of convoys

- Special construction machinery

- Weights

   2.   Dynamic tests

- Different types of convoys

- Vibrating devices

For static tests, road convoys will travel at a speed of max. 5km / h until the characteristic positions, where they will stop and will be stationed until it stabilizes the superstructure.

For dynamic tests, the shares are given by the convoys, they must move at a constant speed. A greater impact can be achieved by creating uneven.

In order to make a comparison between the results of the test data in situ, and the results of calculations is necessary to know the values of actions requiring the bridge and their position on the bridge.

Measurements to be carried out during the tests are compared with values measured in a sleep state, the bridge is loaded with useful actions.

During the tests is envisaged observation of apparatus for measuring and evaluating the values given by them to determine:

- Maximum arrow;

- Movements Basic infrastructure and equipment;

- In the most sought - specific deformations;

- Size and opening cracks in concrete bridges for static tests, and

- Development of maximum arrow;

- The most requested areas - development of specific deformations;

- Development of open cracks in concrete bridges.

Items that are considered to be important for the measurement will be provided with two measuring devices, to make a comparison between the values recorded.

 Devices that are used to make the cercare must:

- Be checked metrology;

- Indicate with precision the appropriate measurement type you made.

2. STATIC TESTS

Static load that is subject to a bridge should be on a schedule set to obtain the most adverse effects.

Value expressing the effectiveness of a test is given by the ratio of the size guardians result of sizing, the useful loadings calculated by different methods S_{stat} and extent of the effort that resulted in charges has undergone bridge S_n.

$$E_{fstat} = \frac{S_{stat}}{S_n}$$

(1)

Depending on the value date of the report, one can say how much the bridge may be subject to traffic requirements or restrictions are necessary.

To consider that the bridge is subjected to static load, should be made a progressive loading can have a single cycle of loading and unloading, or more cycles of loading and unloading.

If a single cycle, the loading is done in steps, up to maximum efficiency and unloading can be accomplished in one step, or in reverse order of loading steps.

If it made more successive cycles of loading and unloading, then cycles will be done in ascending order of their effectiveness.

The test is considered done, when the schemes were carried load test measures were made in the measuring instruments and readings to see how the response of the bridge.

Reading measuring devices is just the opposite of the value stabilizes. It is possible that failure to reach the actions of the sample in the loading position of the scheme you want, to achieve a higher efficiency of load in an intermediate position, which requires a continuous surveillance of the measuring instruments.

Installation of measurement is recommended to be several days before to see the influence of temperature differences. In order not to influence too much the temperature tests are recommended during periods influenced by atmospheric factors condition (temperature, wind, precipitation).

Reading levels indicated by measuring devices is made prior to 1 hours, then 15 min, the start of the test. After the start time of the test are reading the periods of time, indicating the timing of implementation of each scheme of loading, unloading respectively, and stabilizes over the load effects. After removing the load, the readings continue as long as between two successive readings are no differences.

We can consider that a bridge has a corresponding reaction in static tests, if:

- No signs of failure or loss of stability;

- Did not affect the functionality of the bridge;

- Cracks appeared and their behavior falls within the limits imposed by technical rules;

- Maximum arrows f_{el} fall within the limits imposed by technical rules;

- Arrows elastic as compared to the corresponding arrows f_{tot}, is less than the value K_1 of the table.

- The bridges we f_{rem} arrows remaining, compared with the corresponding arrows f_{tot}, is lower than the K_1, given in Table 1.

- For bridges that have been put to action with static efficiency equal to or greater, shall be considered as the ratio of residual f_{rem} arrows, and arrows corresponding f_{tot}

be less than the $\dfrac{K_1}{2}$

- Work unit of maximum demand sections are

Table 1

Construction materials		K		K1	K2
		$E_{fstat} \leq 1,0$	$E_{fstat} \leq 1,2$		
Iron	Welded joints	1,05	1,05	0,10	0,40
	Riveted joints	1,05	1,05	0,15	0,40
Reinforced concrete		1,00	1,10	0,25	0,50
Prestressed concrete		1,05	1,15	0,20	0,45

It should be borne in mind that all the time but will run tests to observe strictly the behavior of the bridge. If irregularities are found in the manifestation of the bridge, stop testing. If the values recorded by measuring instruments falling within normal limits, and the bridge is appropriate behavior can skip to the next stage of loading.

If tests are carried out, other than known and will be executed under a test project.

If you try to bridge the great structure that attempts should be running under a test project, which is specified in the test parameters.

If after carrying out tests shows that the bridge did not fit within the appropriate, shall be required to take immediate action

3. DYNAMIC TEST

Dynamic tests are normally applied only after the static tests were performed and behaved structure within acceptable limits. Like the static tests should be made a careful tracking of all the affected test to stop the test if there is an excess of allowable limits.

Dynamic load test arrangement must achieve a static efficiency at typical sections than 0,7.

To determine the dynamic behavior of the bridge to boot, are used primarily road convoy or rail, which will move in both directions. The test starts with a convoy movement speed of 10 km / h and gradually increased up to speed design.

Measuring devices must be able to take measurements continuously throughout the test. Recording measurements can be analyzed after the test.

Dynamic test provides the following calculation:
- Dynamic coefficient

$$\Psi_{m\breve{a}s} = \frac{f_{din}}{f_{stat}} \text{ or } \Psi_{m\breve{a}s} = \frac{\varepsilon_{din}}{\varepsilon_{stat}}$$

f_{din} - maximum measured in an arrow point, dynamic convoy crossing a certain speed;

f_{din} - measured in the same spot where the arrow was measured f_{din}, the load applied to the same convoy lie in which the f_{din},

ε_{din} - The maximum deflection measured at a specific point, dynamic convoy crossing a certain speed;

ε_{din} - specific deflection measured at the same point where the measured ε_{din}, the static load applied in the same convoy in which the position ε_{din}
- Natural frequency of the bridge;
- The frequency bridge when the action of the sample is measured near the ground;
- Decremented logarithmic of depreciation. Its value is defined as the natural logarithm of the ratio of two successive amplitudes of the same sign, or contained within a period.

Test result gives the maximum speed at which degradation begins to occur, it may make a comparison between the deformation and displacement, or stress can cause the characteristic sections.

4. CONCLUSION

This article describes the norms in force for static and dynamic tests performed on bridge structures.

Because currently on the road began to move very large capacity vehicles and passing speed of 100 km / h, most bridges made with older than 20-30 years to be

technical expert to determine they can be left in operation without a major intervention, or if possible intervention to increase bearing capacity, or need a new bridge implementation.

Technical expertise is based on visual and nondestructive testing, which, possibly for lack of funds, provides only characteristics of the materials. The very few times to make determinations of the bridge behavior under real conditions of exploitation, in stating deformations, displacements, stress, etc. .. However, it is highly unlikely that the tests are being carried out in extreme weather conditions, winter or summer, when the bridge acts such tasks.

References

1. STAS 12504-86, Poduri de cale ferată și șosea. Încercarea suprastructurii.
2. AND 522-06, Instrucțiuni tehnice de pentru stabilirea stării tehnice a unui pod
3. Clough, R.W., Penzien, J., *Dynamics of structures*, McGraw-Hill, New York, 1993.
4. Popescu, I., Tanase, R., Asupra modelării statistice a fenomenului de defectare în cazul podurilor, *Buletinul IPI*, Tomul XLVII, Fasc. 5, 2001. (in Romanian)
5. Comisu C.C. *Integrated monitoring system for improving the durability of the structure of intelligent bridges, research program grant nr. 6345/2005* – Faculty of Civil Engineering of Iasi, CNCSIS, Romania.
6. Comisu C.C., *Mobile lab for dynamic testing and diagnosis of bridges for highways, research program CEEX 309/2006*, Faculty of Civil Engineering of Iasi - CNCSIS, Romania.
7. Chase, Steven B., Dynamic Bridge Substructure Evaluation and Monitoring, *Publicationa no. FHWA-RD-03-089*, September 2005
8. Udd,E., Fiber optic smart structures, Wiley, New York., 1995.
9. Glisic, B., et al., Piles monitoring during the axial compression, pullout and flexure test using fiber optic sensor, 2005
10. Manetti, L., Inaudi, D., Glisic., B., 3-Demon Monitoring Pletform: Examples of applications in structural and geotechnical monitoring projects, 13th FIG, Lisbon, 2008

Steel Bridge Fabrication. Specific Equipment and Machinery. Data Base

Cristian Blejeru[1], Constantin Ionescu[2]

[1]Phd, "Gh. Asachi" Technical University of Iasi, Iasi, 700050, Romania
[2]Professor,Department of Structural Mechanics, "Gh. Asachi" Technical University of Iasi, Iasi,

Summary

The present paper analyses the construction of steel bridges, focusing on steel bridge fabrication process flow and in the same time it deals with specific equipment and machinery. Furthermore, it includes up-to-date steel bridge fabrication methods, in the concept of durable development of these type of structures.

The paper also includes a data base which will correlate the stages of the fabrication process of steel bridge superstructures with specific equipment and machinery, directly or indirectly involved in the process.

KEYWORDS: steel bridge, superstructure, girder, fabrication, erection, data base.

1. STEEL BRIDGE FABRICATION

1.1. Abstracts

Steel bridge superstructure construction, as a component of the structure life cycle, consists of two main processes – fabrication and erection.
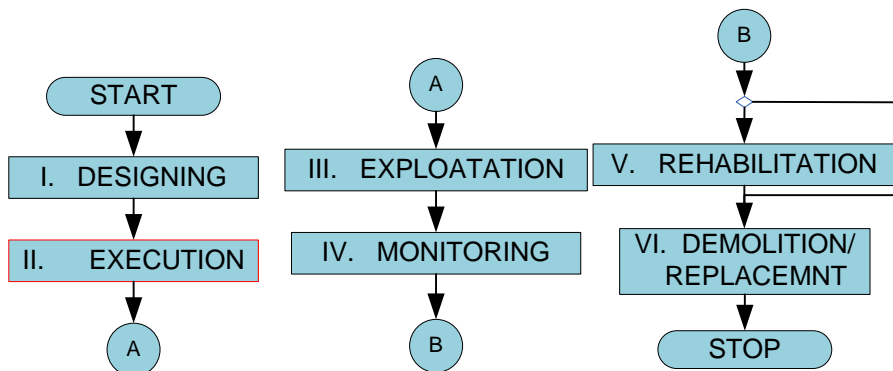

Fig. 1 Life cycle of steel bridge structures [1]

Over time, along with technological developments, in the field of constructions and construction materials, it has been achieved an important progress in fabricating new high performance structures.
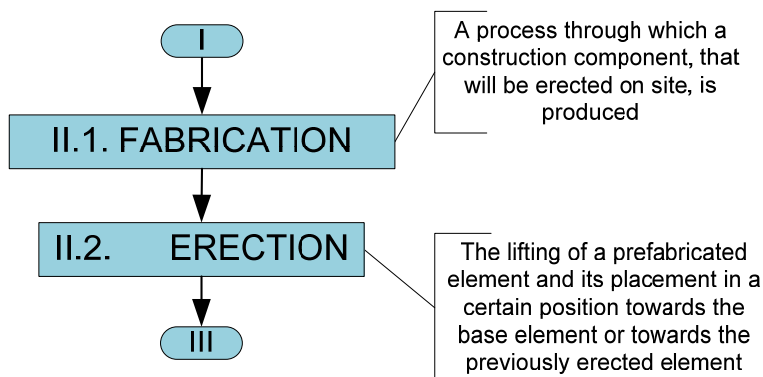
Fig. 2. Steel bridge construction. The stages of the steel bridge construction process.

1.2 The Fabrication of Prefabricated Elements – Fabrication process

Fabrication is a production process, through which are industrially produced construction elements which are going to be erected on sites. The fabrication of prefabricated elements does not belong to the construction field but to the construction materials and metallurgical industry[1].

The fabrication process has borrowed methods which typically belong to the industry and in this way heavy operations have been mechanized. As a result a high quality of products has been obtained and a higher productivity, with implications on the construction time of a steel structure.

The fabrication process involves a number of advanced methods and technologies at every stage (design, construction and materials technology) such as[1]:
- Productivity growth through the typification of superstructure elements during the design stage;
- The correlation of prefabricated elements characteristics (overall dimension, weight, construction joint system) with the erection characteristics (the bearing capacity of transportation vehicles and cranes, selected erection methodes);
- The use of a tight tolerance system, which allows a correct erection, without any further site works;

All the fabrication activities are part of a production process, in which prefabricated elements are transformed into a final product.

I

II.1.1   INPUT DATA

II.1.2   SUPPLAYING WITH MATERIALS AND STORAGE

II.1.3 MATERIALS PREPARATION

II.1.4 CUTTING / PLATE FINISHING

II.1.5 TEMPORARY ASSEMBLY OF THE PREFABRICATED ELEMENT

QUALITY CONTROL   NO

YES

II.1.6   FINAL ASSEMBLY OF THE PREFABRICATED ELEMENT

WELDING QUALITY CONTROL

II.1.7   CORROSION PROTECTION

II.1.8   STORAGE OF PREFABRICATED ELEMENTS

II.1.9 SHIPMENT

II.2

I

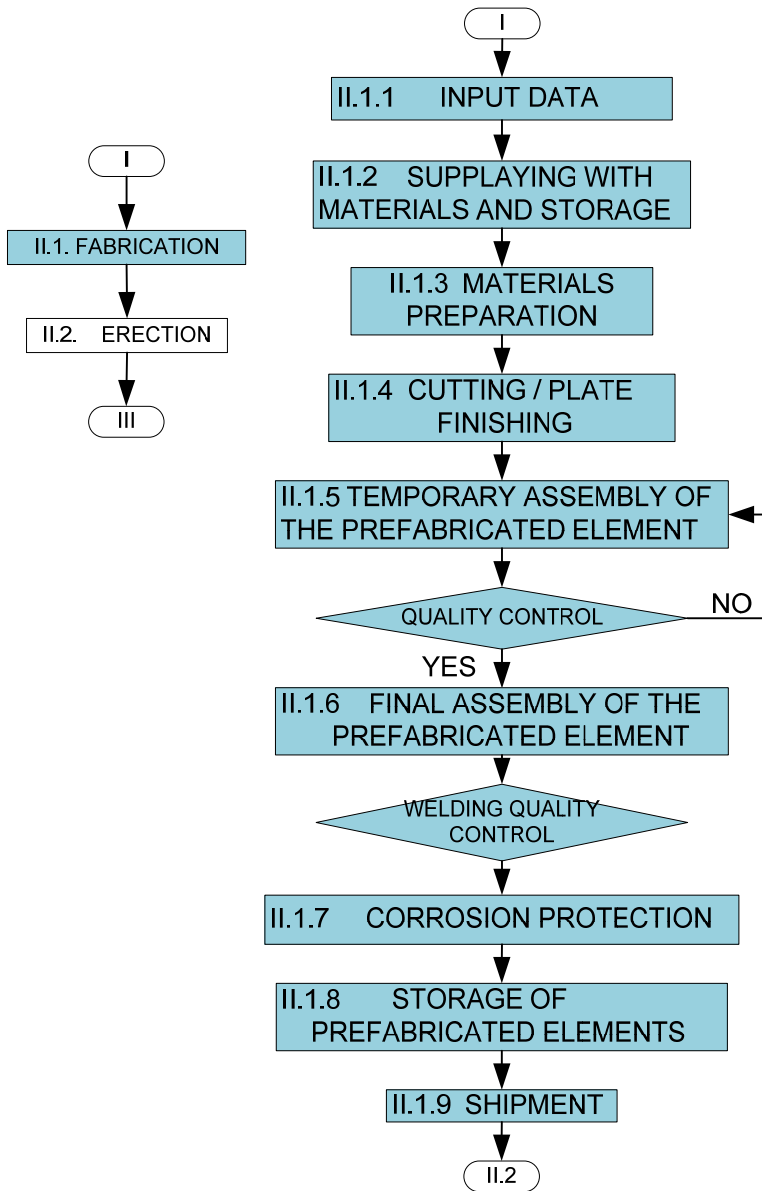II.1. FABRICATION

II.2.   ERECTION

III

Fig.3 The stages of the fabrication process in steel plants

1.3 Prefabricated Elements in Steel Bridge Fabrication

The elements of a steel bridge superstructures are produced in a plant in the form of welded subassemblies. They are erected on site according to the geometric shape of the superstructure through the mounting joints[2].

1.3.1 The mounting Joints of Web Girders

The mounting joints through which all the elements of the cross section are connected, as a result of splicing the girder into sections with lengths and weights limited by transport and handling equipment, are continued through riveting, high resistance screws or welding.

The placement of mounting joints is done taking into consideration the following constraints:
   - The joints section are going to be placed on the girder in the low tension area;
   - The joints sections should be as simple as possible (the girder bottom flange should be as simple as possible);
   - The sections of a structure should be as few as possible;
   - The mounting joints should be placed, if possible, simmetrically on the girder.
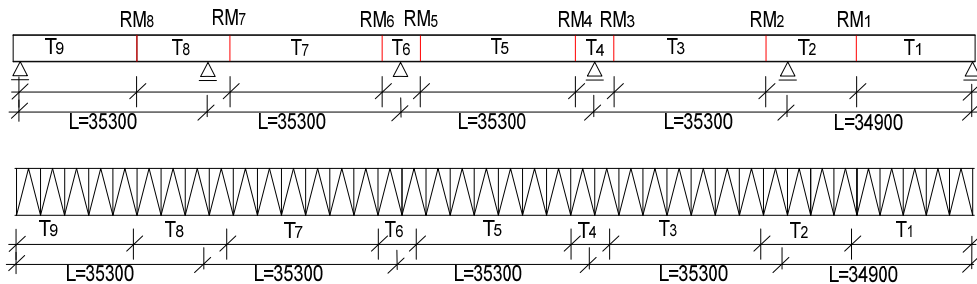
Fig. 4 Mounting joints of a continuous web girder bridge on 5 spans
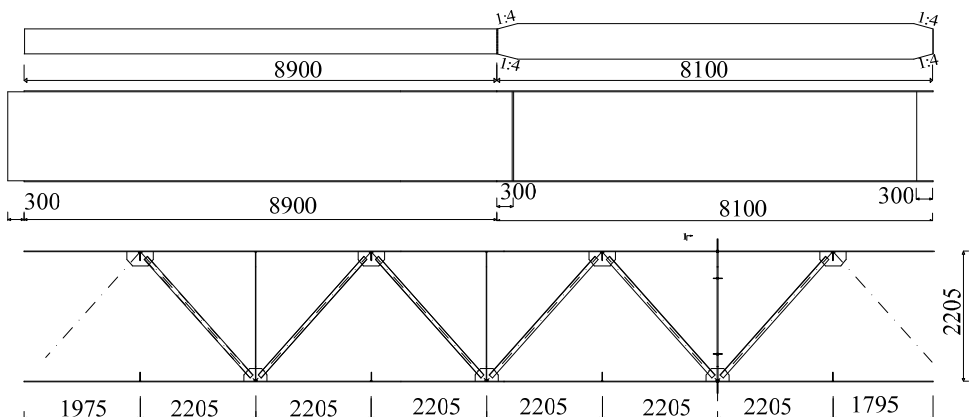
Fig. 5 T8 section details

In the case of the steel bridge shown above, the mounting joints are placed along the main girders, each of the other elements of the deck, the cross beams and the bracing bars, with reduced sizes could be considered independent components of the deck sections; except for the end bracing bars of the section (fig.5), which are erected on site after coupling the mounting joints.

Main girder

Cross beam

2205
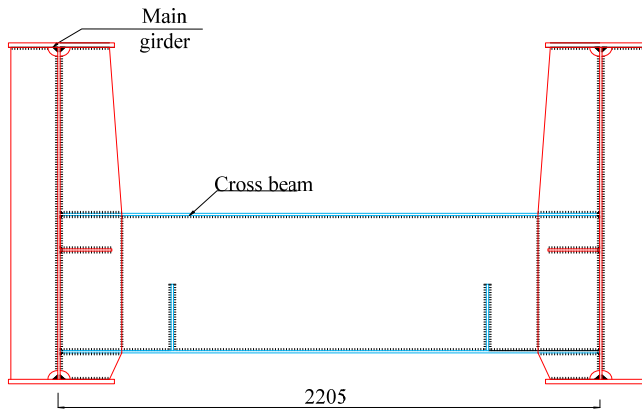
Fig. 6 Steel bridge cross section

Tabel 1. Prefabricated elements of a web girders steel bridge

Prefabricated elements	Constructive shape of the prefabricated elements
Crossbeam	
Girder	
Bracing bar	
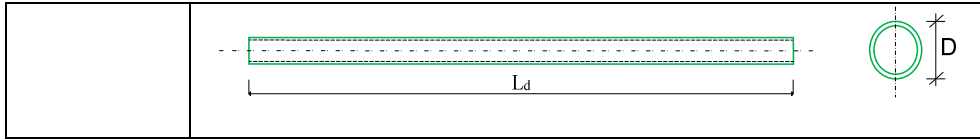
1.3.2 The Mounting Joints of Truss Girders

A road steel bridge with Warren through truss girders will be analysed. The section shape of the superstructure is shown at fig.7.
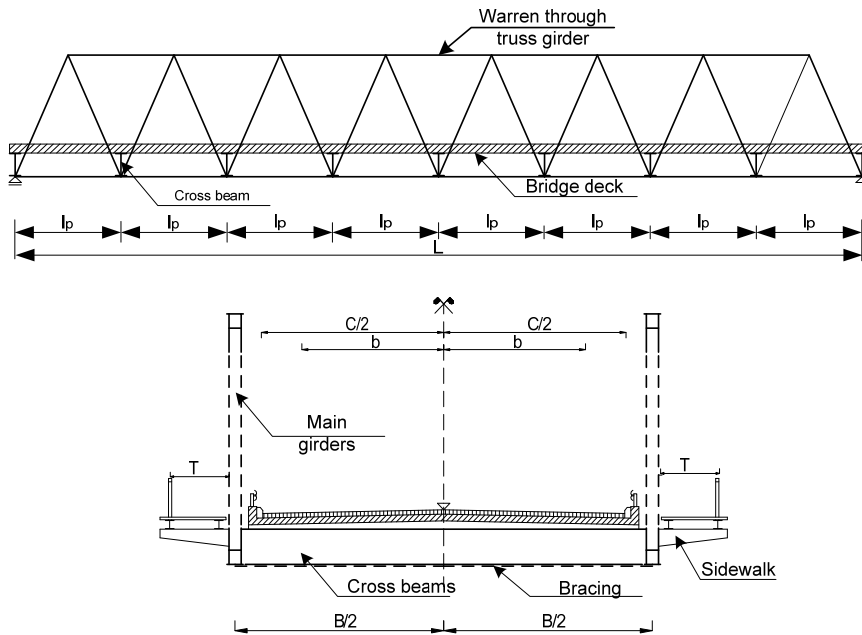
Fig. 7 Road steel bridge with warren through truss girders

The mounting joints are placed only on the truss girders outline, each of the inner bars of the truss girders, verticals and diagonals, are independent elements. The mounting joints are placed taking into consideration the following constraints [2]:
- The mounting joints are placed on the less tensioned bars, outside but in the same time near the truss knots;
- The mounting joints are placed, if possible, simmetrically towards the middle of the truss girders;
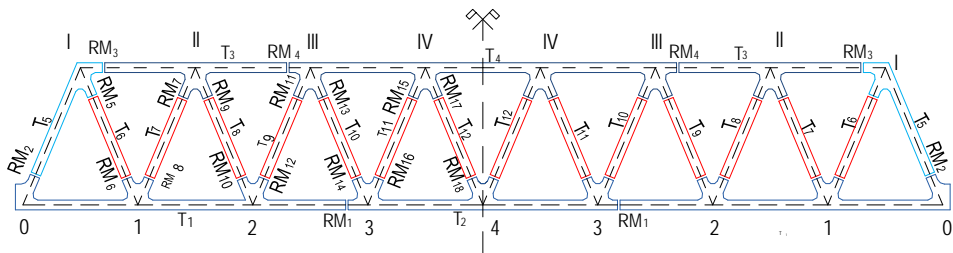
Fig.8 The placement of the mounting joints at a warren through truss girder.[3]
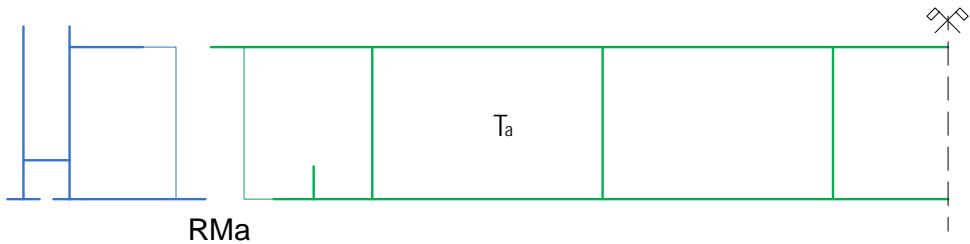
Fig.9 The placement of the mounting joint between the cross beam section and the main girder section

Tabel 1. Prefabricated elements of a warren through truss girder bridge

	Prefabricated element	Constructive shape of the prefabricated elements
1	Warren truss girder section – bottom chord (T_1, T_2)	
2	Warren truss girder section - top chord (T_3, T_4)	

3	Warren truss girder ending diagonals (T_5)	
4	Warren truss girder diagonals ($T_6 \div T_{12}$)	
5	Cross beams (Ta)	
6	Lateral bracing bars(C.O.T.I)	
7	Sidewalk cantilever	
8	Sidewalk longitudinal beam	
9	Sidewalk cover system	

1 0	Pedestrian guardrail	
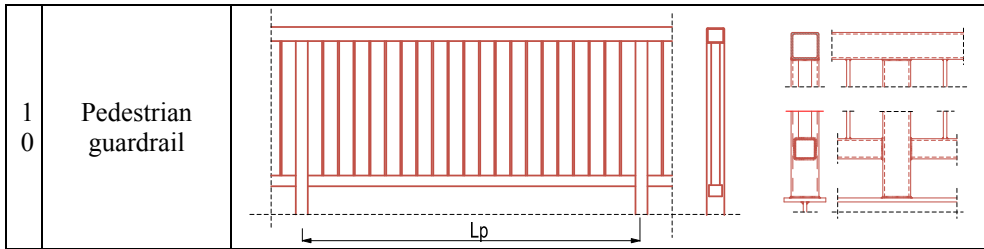
The prefabricated elements of a steel structure are produced in plants according to the design documents, put together by the plant engineers (based on the design sheets and specification made by the structure engineer), consisting of the following:

1. All the operations involved in the fabrication process starting with the cutting of elements and ending with their shipment;
2. The cutting technology;
3. The technological process for each of the subassemblies, which has to ensure for the welded joints the same mechanical characteristics as for the welded material.
4. The preassembling in the plant, the measurement methodology of the allowance limits.

Each plant has its own organisation for the production flows. Therefore in fig. 9 it is shown the organisation of a plant which can manage its own production in two distinct flows:

- ▪ The fabrication of steel bridge;
- ▪ The painting process of steel structures assemblies and subassemblies;
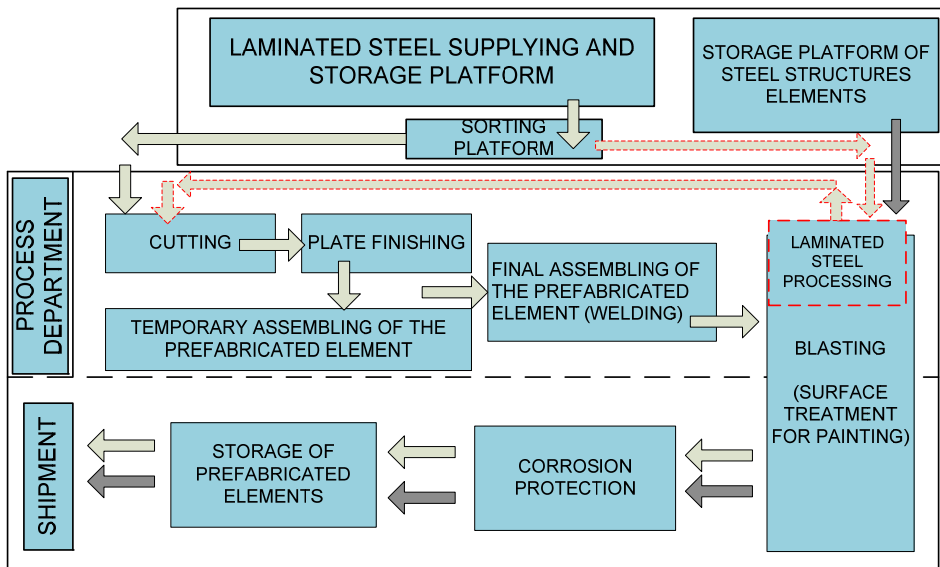
Fig. 10 Plant fabrication process flow [3]

1.4. Prefabricated Elements Erection

The erection process has gained a great deal of importance in the construction industry as the prefabricated elements production is continuously developing.

The erection as a production process, means the final placement of a structure components (prefabricated elements). In this context the erection process has the following characteristics [1]:
- The binding of the erected element;
- The lifting and handling of a prefabricated element and its placement in a certain position towards the base element or towards the previously erected element;
- The coupling of the structure elements in order to avoid relative displacements, resulting in a statically and functionally well-defined whole; The term *erection process* is, generally speaking, connected to the machinery used in this process

```
                                    ┌──────┐
                                    │ II.1 │
                                    └──────┘
                                        │
                                        ▼
                            ┌───────────────────────┐
                            │ II.2.1 DELIVERY TO SITE│
                            └───────────────────────┘
        ┌───┐                           │
        │ I │                           ▼
        └───┘               ┌───────────────────────┐
          │                 │ II.2.2    STORAGE OF   │
          ▼                 │ PREFABRICATED ELEMENTS │
 ┌─────────────────┐        └───────────────────────┘
 │ II.1. FABRICATION│                   │
 └─────────────────┘                    ▼
          │                 ┌───────────────────────┐
          ▼                 │ II.2.3  PREPARING THE  │
 ┌─────────────────┐        │   ERECTION PROCESS     │
 │ II.2.  ERECTION │        └───────────────────────┘
 └─────────────────┘                    │
          │                             ▼
        ┌─────┐             ┌───────────────────────┐
        │ III │             │ II.2.4 LIFTING AND     │
        └─────┘             │     ASSEMBLING         │
                            └───────────────────────┘
                                        │
                                        ▼
                            ┌───────────────────────┐
                            │ II.2.5  TEMPORARY      │
                            │ ASSEMBLING OF THE      │
                            │ PREFABRICATED ELEMENTS │
                            └───────────────────────┘
                                        │
           ┌──────────────┐    NO       ▼
           │2.2.5' ADJUSTING,│◄──── FORM AND POSITION CONTROL
           │   LINING UP    │
           └──────────────┘        YES  │
                   │                    ▼
                   │        ┌───────────────────────┐
                   └───────►│ II.2.6 FINAL ASSEMBLING│◄──┐
                            │ OF THE PREFABRICATED   │   │
                            │      ELEMENTS          │   │
                            └───────────────────────┘   │
                                        │            NO │
                                        ▼               │
                              FIELD CONNECTIONS ─────────┘
                              QUALITY CONTROL
                                   YES  │
                                        ▼
                            ┌───────────────────────┐
                            │ II.2.7  BRIDGE DECK    │
                            │     ERECTION           │
                            └───────────────────────┘
                                        │
                                        ▼
                            ┌───────────────────────┐
                            │ II.2.8  EXECUTION OF   │
                            │ BRIDGE CARRIAGE WAY    │
                            └───────────────────────┘
                                        │
                                        ▼
                            ┌───────────────────────┐
                            │ II.2.9  ACCEPTANCE     │
                            └───────────────────────┘
                                        │
                                        ▼
                                     ┌─────┐
                                     │ III │
                                     └─────┘
```
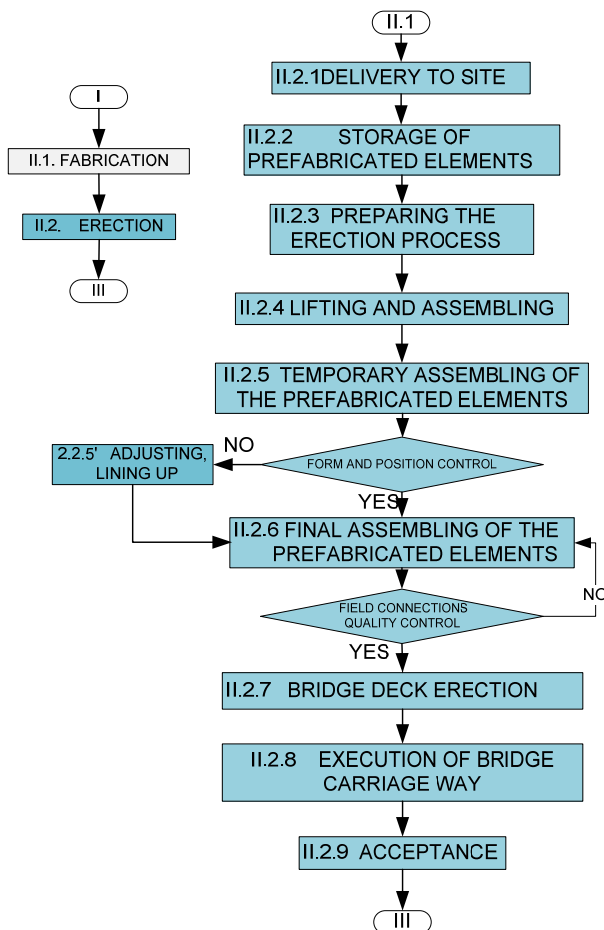
Fig.11. The erection process flow

From all the activities which take place in the production process in order to transform the prefabricated elements into a final construction, the main technological process is the erection. The lifting and handling of the prefabricated elements and their placement in a certain position using a lifting machinery, represents an *erection procedure*.

The erection procedure of a steel bridge superstructure is chosen depending on the site location (topography), access on site, structure complexity and the erector's equipment and machinery. The erection procedure of a structure can be established by the designer in order to be adopted by the erector; in addition, the erection procedure can be established by the erector himself only with the designer's approval.

Over time, there have been found several improvement methods for the machinery performance. Along with the procedures which ensured the safety and productivity of the erection, some procedures have become classic. In Romania the most widely used, taking into account the great number of small and medium span length bridges, are the crane erection procedures.

The lifting of a prefabricated element, in order to be erected in the structure, could be done in several ways, depending on the one hand on the element size, weight and geometry and on the other hand on the crane lifting capacity and location. The easiest lifting procedure of a prefabricated element consists of lifting it with a single crane, using a single cable connected in two points with the lifted element (fig.12).
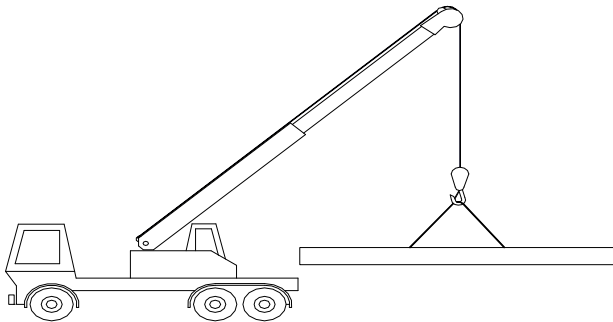
Fig.12 Prefabricated elements erection with a single crane

In a more complex alternative, the lifting of a prefabricated element consists of a multi-point erection frame attached to the member with beam clamps or slings and lifted using multiple cranes attached at different locations along the frame (fig. 13). With both lifting procedures, tag lines attached to the prefabricated element are used for hand guidance to ensure safe placement[4].
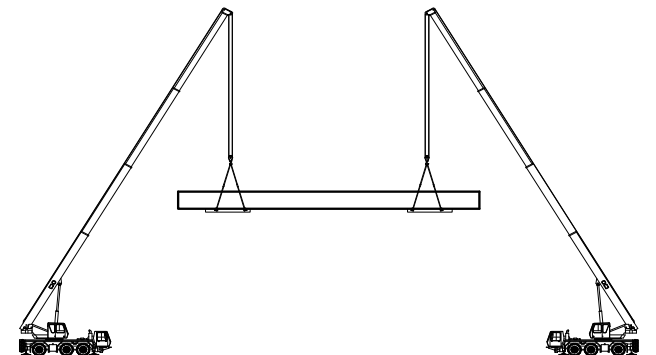
Fig.13 Prefabricated elements erection with two cranes.

2. SPECIFIC EQUIPMENT AND MACHINERY OF THE FABRICATION PROCESS – DATA BASE

2.1. Input Data Analysis and Processing

The input data analysis and processing represents the first stage of a steel bridge fabrication process flow.
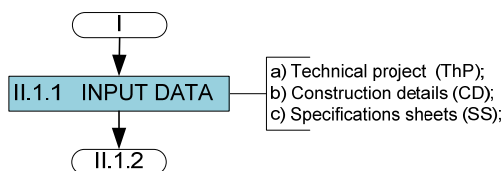
Fig. 14 Input data analysis and processing

This preparation stage begins in the design office of the plant; where the design sheets are made by a specialized company, the design sheets and the bill of materials are checked by the fabricator's design office. The sheets which get to the fabricator (Construction Details – C.D.) must present exactly what is to be fabricated; the dimensions must be clearly marked and must provide all the necessary data for the fabrication. The design office also establishes the fabrication technology, along with all the necessary operations and their characteristics for each construction component.

In addition, the bill of materials are checked here and there are elaborated a series of supplementary documents necessary for ordering materials, cutting the elements, drilling and processing of different pieces.

In case the designer has not elaborated a welding plan, this will be elaborated in the design office, along with the technological welding sheet.

The more complete are the documents elaborated by the design office, the easier will be the supplying, processing and fabrication stages. Also, their quality is thus ensured.
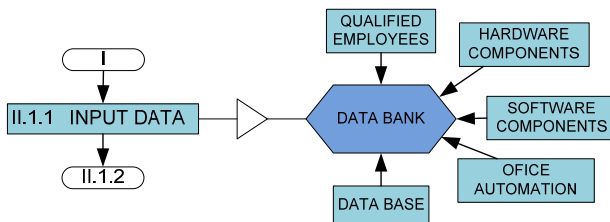
Fig. 15 Specific equipment and machinery for input data analysis and processing

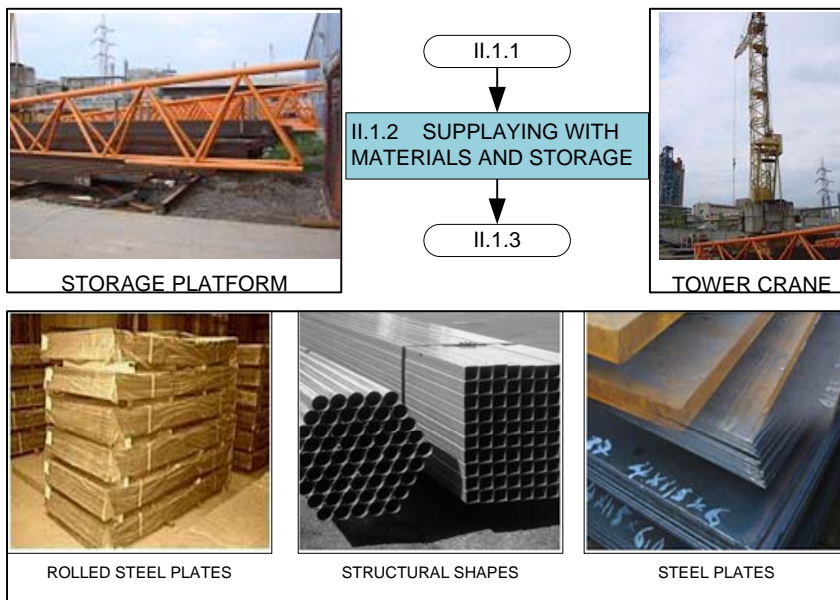## 2. 2. Supplying and Storage

Fig. 16 Material Supplying and Storage

2. 3.Preparation of Materials

When choosing the rolled steel, the quality, condition, appearance and possible lamination flaws must be checked.

The correspondence of the data with the project requirements and standards will be checked according to the serial number printed on the roll steel and to the analysis and mechanical testing report.

The condition of the pieces and possible lamination flaws will be identified by examining both outer sides. The rusty roll steel, soiled with mud, oil or paint will be cleaned before processing.

An ultrasonic check could be performed if it proves necessary and if its technically possible.

The rolled steel which has bigger deformations, must be redressed/flattened out before marking and cutting-off.

The the rolled steel straightening is done under the conditions mentioned by the current prescriptions. Cold straightening is allowed only if the deformations do not exceed the values mentioned by the current rolled steel standards.
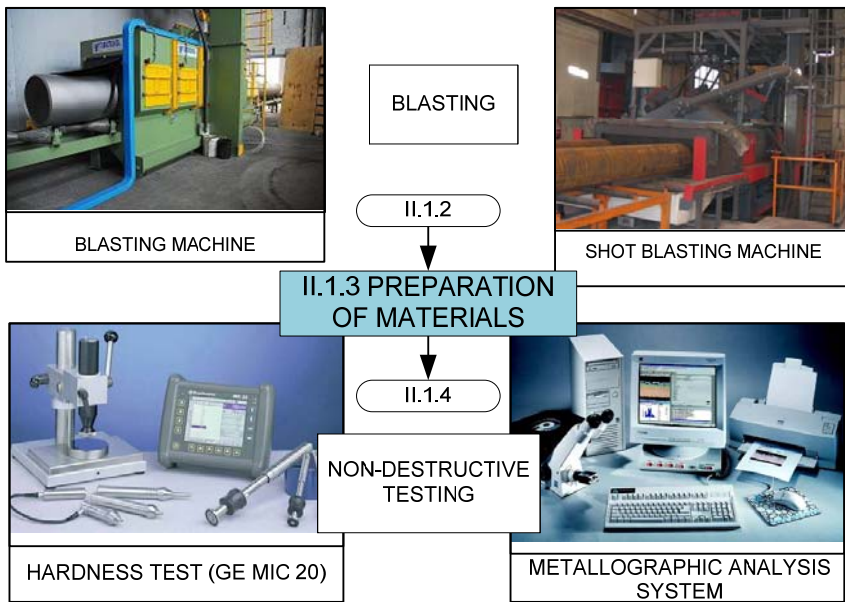
Fig. 17 The preparation of materials

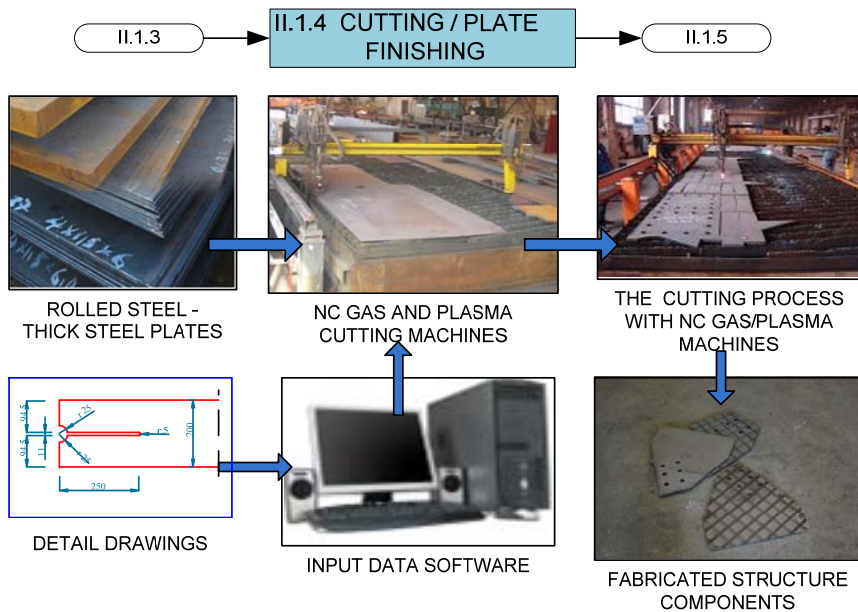## 2. 4. *The Cutting and Plate Finishing*

Fig. 18 The cutting of the prefabricated elements

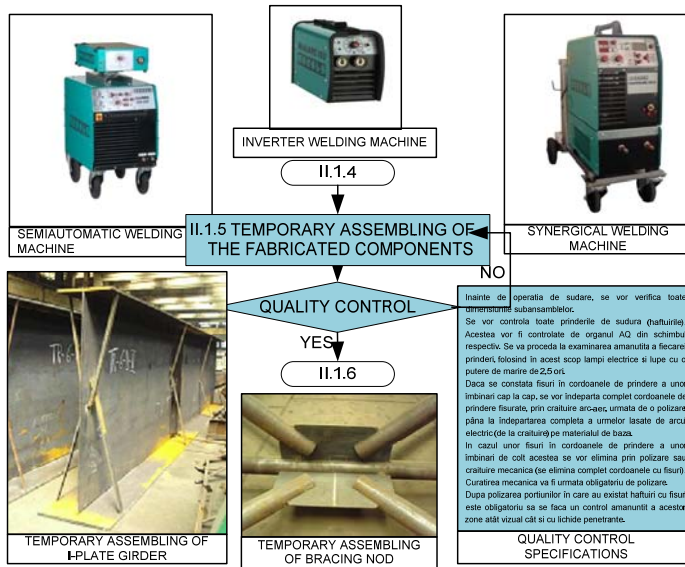## 2. 5. The Temporary Assembling of the Prefabricated Element

Fig. 19 The temporary assembling of the prefabricated elements

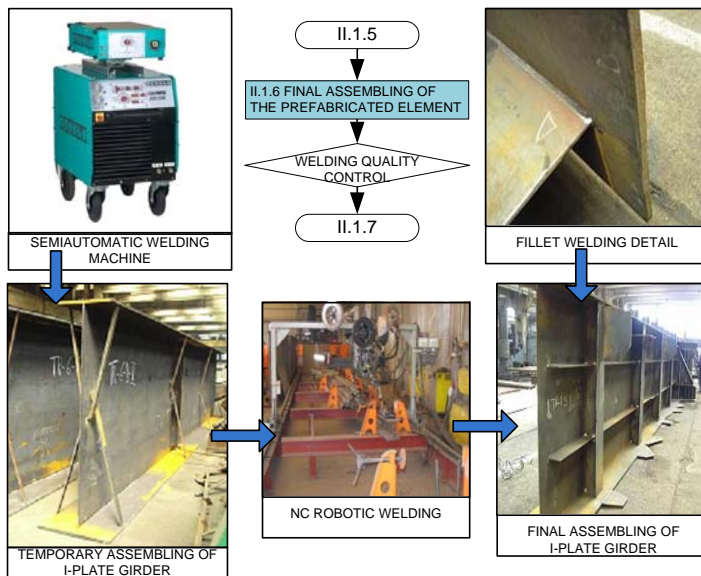## 2. 6. The Final Assembling of the Prefabricated Element

Fig. 20 The Final Assembling of the prefabricated elements

2. 7. Welding Quality Control

Fig. 21 Specific Equipment for Welding Quality Control

2. 8. Anticorrosive Protection of the Prefabricated Elements
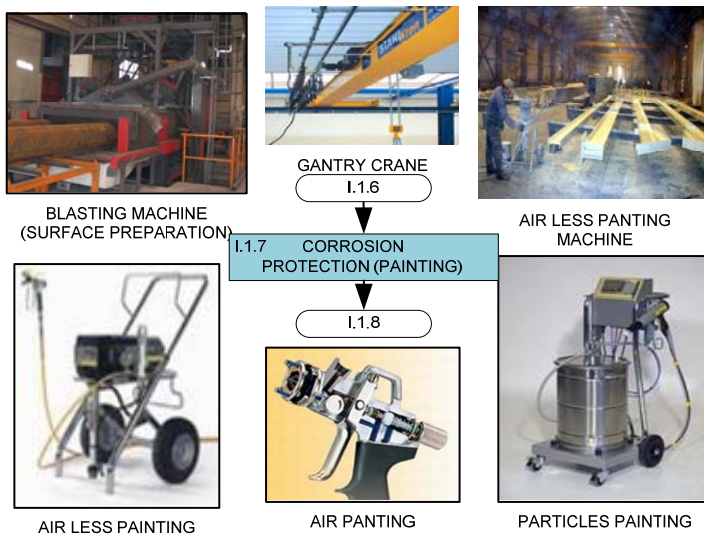

Fig. 22 Anticorrosive protection of the prefabricated elements

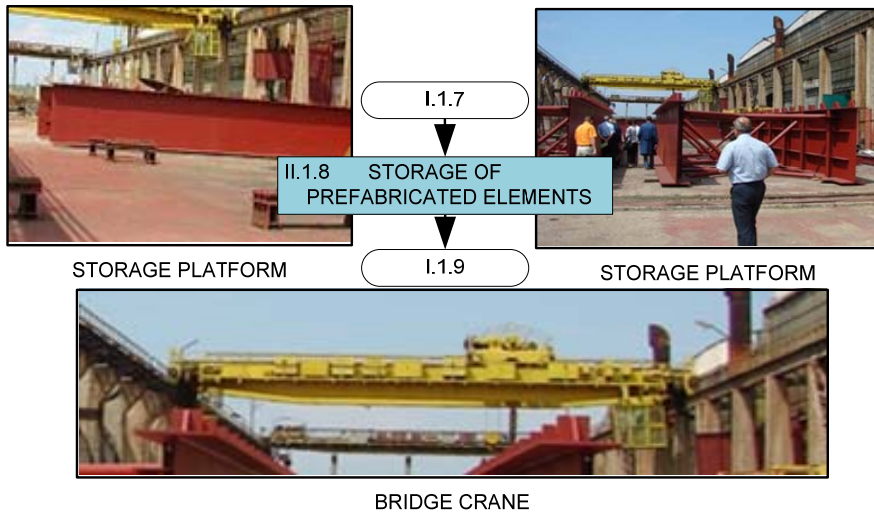## 2. 9. Storage of the Prefabricated Elements

Fig. 23 Storage of the prefabricated elements

2. 10. The Shipment of the Prefabricated Elements

For each prefabricated element which leaves the plant, a quality certificate will be released in order to certify the fact that the subassembly is qualitatively and dimensionally compliant with the project and the specification sheets.

The current regulations state that the erector can accept plant fabricated elements only if they are accompanied by a quality certificate.

The technical control bodies of the erector will check randomly the quality of the plant fabricated pieces and whether the initial project and the current technical regulations are followed.

3. CONCLUSIONS

Quality Control should commence with the designer and continue through the preparation of drawings and material procurement; maintaining the quality during the entire production process will depend heavily on the fabrication details and on the material obtained.

The larger fabricators have their own Quality Control Department, which will create and maintain a QC-manual, describing the method of operation throughout

the fabrication process. The Quality Control Department will liaise with the shop management to make sure that all workers have the skill required for the job on hand and that welders are qualified to undertake the prescribed welding procedures.

Regular checks are necessary to ensure that:
- All materials can be checked against specifications.
- Material is checked for laminations.
- Welding electrodes are identifiable.
- Welding electrodes are stored in the required conditions.
- Welding procedures are being followed.
- Welding is being inspected during the process.
- Identification marks are clear and visible.
- All equipment is maintained correctly.

Close liaison should always be maintained between the QC staff and the Drawing Office.

Concluding summary

- Good design makes efficient use of material and makes proper provisions for tolerances in fabrication and erection;
- Good interaction between shop floor and drawing office is indispensable for economical and efficient fabrication and erection;
- Labour should be used as effectively as possible so that labour costs are minimised. Automatic processes should be used where feasible and appropriate;
- Quality control is essential.

References

1. Rusu, M., *Montarea în construţii*., Editura Tehnică, Bucuresti, 1983.
2. Jantea, C., Varlam, F., *Poduri metalice. Alcatuire si calcul.* , Editura Venus, Iasi, 1996.
3. Popescu, V., *Construţii metalice.,* Editura Tehnică, Bucuresti, 1963.
4. National Steel Bridge Alliance, *steel Bridge Design Handbook. Chapter 13 Design for Constructability,* 2007.

Specific technology and equipment used for construction of concrete bridges

Costel Pleşcan[1], Constantin Ionescu[2], Rodian Scînteie[3] and Paul Brănici [4]

[1] *Department of Structural Mechanics, "Gheorghe Asachi" Technical University from Iasi,700050, România*

[2] *Department of Structural Mechanics, "Gheorghe Asachi" Technical University from Iasi,700050, România*

[3]*Department, University, City, Zip code, Country*

[4] *Department of Structural Mechanics, "Gheorghe Asachi" Technical University from Iasi,700050, România*

Summary

This paper presents the stages of technology to achieve a B.O.R. system, as presented in the article.

First is a brief summary, in the concept of achieving high complexity system "concrete bridge - obstacle crossing-road, indicating the works which are required for each subsystem.

In this work is presented in detail, plant and equipment necessary to achieve concrete bridges. Currently, in our country most of the bridges are made with precast pre-stressed beams, functions of the bridge span the beams type are chosen.

KEYWORDS: concrete bridges, superstructures, precast beams, database.

1. EXECUTION OF CONCRETE BRIDGES

Bridge is defined as a construction that supports a transmission path over the obstacle, leaving a space for ensuring continuity of obstacle crossing.

In the "bridge" construction type B.O.R. cannot be regarded as single element (Figure 1.1), it coexists with the obstacle is crossed (Figure 1.2) and the road that it serves (Figure 1.3).

Accepting the idea that the bridge can be likened to a system achievement construction involves methods and techniques of systems theory, systems engineering, reliability theory and data.

Fig. 1.1. Bridge on NR 28A, km 22+660 .

Fig. 1.2. OBSTACLE- Siret River.

Fig. 1.3. Road NR 28A.

Currently, in Romania is done new bridges on highway under construction, on way of local and national roads that are in rehabilitation, by altering the way, by pass through the belts of cities, by destruction of removing those disasters, especially floods because .

Therefore we find three subsystems with a special importance to achieve the system "B.O.R" as shown in Figure 1.4 .
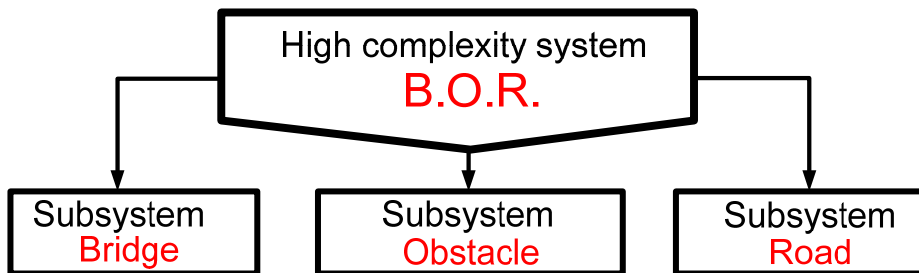

Fig. 1.4. High complexity system „B.O.R."

At the construction of a "bridge", are used machinery and equipment-specific for the works that are presented below:

    a)   Pickling vegetable layers

    b)   Building the foundations

        -    direct foundation

-    suspended foundation

c) Building the grating of the foundation

d) Building the elevation

   -    elevation of pier

   -    elevation of abutment

e) Building the embankments behind the abutment

f) Building the connection beams with the embankment

g) Works in the river bed

   -    work to bed profiling

   -    work with defense and bottom sills

h) Building superstructure

   -    building beams

   -    assembling and transversal linked

   -    building the parapet

i) Building bridge causeway

   -    building support layers, waterproofing and coating of waterproofing

   -     building of sidewalk

   -    building pavement layer on the bridge

   -    assembling parapets

j) Achieving joints

1. BUILDING THE PRECAST FOR REINFORCED CONCRETE BRIDGE

The element that makes the difference from other types of superstructures is the deck, element which is composed mostly of precast beams linked with transverse cross beam.

Achievement of these elements is machined using specific processes to obtain industrial products, respecting the quality requirements, required by current rules. The production process is conducted to achieve a certain flow chart of prefabricated elements (Figure 2.1.).

In the first stage is made the supply of necessary materials: aggregates, cement, fastening iron and additives for concrete (Figure 2.2.), the materials will be stored in designated areas for each material.

Supply with the necessary materials → Building the reinforcing carcasses → Assembly the reinforcing carcasses and the reinforcing fascicle in the form

Preparation of concrete and concreting ← Closing and sealing of the form ← Pretension of the reinforcing fascicle

Hardening of concrete → Cutting the heads of the reinforcing facicles → Storage and delivery to the user
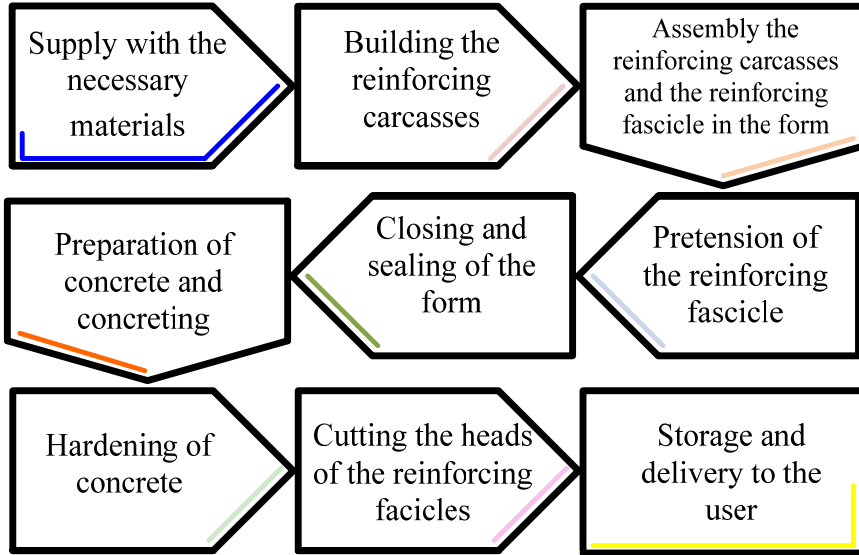
Fig. 2.1. Technological flow of a plant for prefabricated beams

This stage is specific equipment trucks for material transport (Fig. 2.2.b) Rollers (Figure 2.2. A).

Fig.2.2. (a) storage of aggregates, (b) cement storage silos,(c) storage of concrete steel

Prepare the concrete iron to build reinforcing carcasses:

- Straightening, if they are in the coils;
- Cutting, figure2.3. a;
- Shaping, figure 2.3. b;

- Building the stirrups, figure 2.3. c.

Fig.2.3. (a) cutting, (b) shaping,
(c) building the stirrups

Beam reinforcement assembly is made manually (Figure 2.4. A), introduce active reinforcement beams (Figure 2.4. B) expected to be prestressed (Figure 2.4. C).

Fig.2.4. (a) passive reinforcing, (b) active reinforcing,
(c) pretensions equipment bundles

Installation is automatic shuttering in position, which is auctioned hydraulic, (Figure 2.5.).

Fig.2.5. (a) Metal Formwork, (b) fasteners in position,
(c) fasteners of bundles

Transport of aggregates in station of concrete preparation (Figure 2.6.c), is made with conveyor belt (Figure 2.6.) cement supply of concrete station is made with a system of pipes fitted with screw (Figure 2.6.b)

Fig.2.5. (a) conveyor belt, (b) cement pipes for transport,
(c) station for concrete preparation

3. CONCLUSIONS

The advantages of using prefabricated elements are well known in the delivery of construction, with reference here to: greater speed of construction, higher quality, independence from weather conditions, large openings due pre-stress , good behavior in structures with dynamic load , the solutions are economic, aesthetic solutions, ecologic solutions.
To use the most appropriate benefits listed is very important to correctly choose a technical solution since the preliminary phase of the project -bridge design.

In this way we ensure that:

• prefabricated elements are used in an optimal way;

• there is sufficient time available to ensure efficiency of production;

• structure nodes, fixture details and stability of the entire structures are well designed;

•assemblage will be quick.

References

1. SC. SOMACO. SA filiala Roman
2. SC. BUILDCORP. SA filiala Iaşi
3. Revista Drumuri şi Poduri, ISSN 1222-4235
4. Stelian Dorobantu, Utilajul şi tehnologia lucrărilor de căi de comunicaţiei, Bucuresti, Editura Didactică şi Pedagogică, 1995